PROTON ELECTROLYTE MEMBRANES WITH HYBRID MATRIX STRUCTURES FOR ASSEMBLING FUEL CELLS

ZHANG XINHUI

NATIONAL UNIVERSITY OF SINGAPORE

2007

PROTON ELECTROLYTE MEMBRANES WITH HYBRID MATRIX STRUCTURES FOR ASSEMBLING FUEL CELLS

ZHANG XINHUI

(*M. ENG., Beijing University of Chemical Technology*)

A THESIS SUBMITTED

FOR THE DEGREE OF DOCTOR OF PHILOSOPHY

DEPARTMENT OF CHEMICAL & BIOMOLECULAR ENGINEERING

NATIONAL UNIVERSITY OF SINGAPORE

2007

ACKNOWLEDGEMENT

First of all, I genuinely wish to express my deepest appreciation and thanks to my supervisors, Associate Professor Hong Liang and Dr. Liu Zhaolin, for their intellectually-stimulating guidance and invaluable encouragement throughout my candidature as a Ph.D student at the National University of Singapore. Professor Hong's comprehensive knowledge and incisive insight on polymer materials as well as his uncompromising and prudent attitude toward research and insistence on quality works have deeply influenced me and will definitely benefit my future study. His invaluable advice, patience, constant encouragement and painstaking revisions of my manuscripts and this thesis are indispensable to the timely completion of this project. I am also grateful to Dr. Liu Zhaolin. His immense background and experience in electrochemical knowledge of fuel cell technology enabled me to work through many technical problems smoothly.

I would also like to express my gratitude to my colleagues Dr. Tay Soik Wei, Dr. Yin Xiong, Mr. Wang Ke and Mr. Shang Zhenhua for all the handy helps, technical supports, invaluable discussion and suggestions.

I am grateful for the Research Scholarship from the National University of Singapore (NUS) that enables me to pursue my Ph.D. degree. I am also indebted to the Department of Chemical & Biomolecular Engineering of NUS for the research infrastructure support.

Last but not least, this thesis is dedicated to my parents for their great understanding and steadily moral support throughout my Ph.D. program.

TABLE OF CONTENT

SUMMARY

In recent years, development of the science and technology of proton exchange membrane fuel cells (PEMFCs) has been an intense research area, of which the ultimate goal is to reduce our reliance on fossil oil and to cut down carbon dioxide emission in the transportation sector, as well as to enable clean and reliable energy for the portable power generators. As a crucial component of PEMFC, the traditional electrolyte membrane faces the key challenges from the elevated operation temperature and the suitability of liquid fuels such as methanol. Hence, high-performance proton exchange (electrolyte) membranes (PEMs) are in great demand. In this thesis, three types of composite membranes were fabricated by incorporating hybrid nanoparticles into a perlfuorosulfonic acid polymer matrix (i.e. Nafion® resin). These hybrid nanoparticles were prepared by different methods: grafting an oligomeric ionomer layer to an individual silica nanoparticle; or grafting oligomeric chains to a cubic siloxane molecule; or polymerizing vinyl cubic siloxane molecules in the host matrix. In addition to the Nafion-based nano composite membranes, H_3PO_4–doped polybenzimidazole (PBI) membrane was chemically modified as well to generate a novel type of composite matrix. It was obtained through introducing a macromer of unsaturated polyester (UP) into the polymerization system of PBI. As a result, a loosely crosslinked PBI-UP network, which encapsulates pristine H_3PO_4 as the proton conducting phase, was generated. The resulting network offers better anhydrous proton conductivity and stronger mechanical strength than the unmodified counterpart. Based on the membrane fabrications and fuel cell evaluations, the exploration of physicochemical mechanisms that cause changes in

electrochemical behaviors, solvent affinity, and mechanical properties in the different composite membranes in question constitutes the major part of this thesis. In the following paragraphs, the main perspectives and accomplishments of different chapters of this thesis are highlighted respectively.

A special type of microsphere that comprises a silica core and a densely grafted hydrophilic polymer layer was firstly synthesized by heterogeneous atom transfer radical polymerization (ATRP). This heterogeneous ATRP synthesis provides a novel way to confer only low-molecular-weight but closely packing polymer chains, which interpenetrate with the silica network in the outer layer of microspheres. With investigation into its interfacial behaviors and electrochemical properties in the different solution medium, it was found that such core-shell particles with polyelectrolyte chains can exhibit different hydrodynamic volumes in methanol-H_2O mixtures with different ratios and in aqueous solution with different pH values. Most importantly, the polyelectrolyte layer can also offer a strong promoting proton transport.

Such core-shell nano-particles with ionomer chains are considered as valuable materials to be used to modify Nafion matrix. It was found that the low content silica-poly (3-sulfopropyl acrylic acid) (PSSA) core–shell nanoparticles, PSPA-SiO_2, in the membrane matrix of Nafion enhances its performance in PEMFC by boosting the flux of protons and facilitating their transport. From further analysis, this boosting role comes from the fact that each PSPA-SiO_2 particle bears a high density of sulfonic acid groups, and the

facilitating role is attributed to the hydrophilic interactions between PSPA-SiO_2 particles and the sulfonic acid groups of Nafion chains.

In contrast to silica nanoparticles, a new material, polyhedral oligomeric silsesquioxane (POSS), has also been used to modify Nafion matrix since it has well-defined cubic octameric siloxane skeleton (about 1-3 nm in size) with eight organic vertex groups, one or more of which is reactive or polymerizable to pursue the hybrid properties of organic polymer and ceramics. Firstly, vinyl-overhung $Q_8M_8^V$ cubic molecules, 1, 3, 5, 7, 9, 11, 13, 15- octakis (dimethylviylsiloxy) pentacycloc octasiloxane, have been polymerized with Nafion recasting process and the resulting rigid P($Q_8M_8^V$) blocks have also yielded an impact on formatting the Nafion matrix. It was found that the P($Q_8M_8^V$) blocks generated *in-situ* in the Nafion matrix played the blocking role in restricting random extensions of proton conducting channels (PCCs) and promoted ordered assembling of Nafion molecules. As a result, compared with the pristine Nafion membrane, the resultant composite membranes containing P($Q_8M_8^V$) of 5 ~ 15 wt.% manifested obvious improvement on both suppressing methanol permeability and raising power density output of the single direct methanol fuel cell (DMFC).

The other hybrid POSS nanoparticles have been synthesized via grafting polyacrylonitrile short chains to the cubic methacryl-POSS molecules by ATRP. It was observed that by introducing this kind of branched nano particles (*sb*-POSS) into the Nafion matrix in an appropriate amount, a significant enhancement on the performance of Nafion membrane in a direct methanol fuel cell (DMFC) was attained. This revamping role is associated

with the initial clustering of *sb*-POSS particles in the Nafion matrix from their fully dissolved state, which happens when the content of *sb*-POSS is increased to ~5 wt.%. It was found that this conversion brought about constriction to the maximal extent of hydrophilic proton conducting channels in the Nafion matrix according to the analysis by differential scanning calorimetry (DSC). As a result, the composite membrane containing *sb*-POSS of 5 wt.% produced more than double power density output than the native Nafion membrane.

Finally, polybenzimidazole (PBI) was also studied as a host polymer matrix. In this work, unsaturated polyester (UP) macromer was introduced to crosslink PBI blocks and then to achieve reinforcing phosphoric acid (PA) – doped polybenzimidazole (PBI) membrane. Compared with the PA-doped PBI obtained from conventional impregnating method, the resulting membrane not only achieved much better mechanical properties of PBI membrane with a higher PA doping level, but also possessed the desired high-temperature proton conductivity. Furthermore, a promising performance of the membrane in a single H_2 fuel cell was accomplished at 150 ^{o}C without humidifying either electrode.

ABBREVIATIONS

A	exposed area of the membrane (used in Equation 2.3 and 2.4)
ABPBI	poly(2, 5-benzimidazole)
An	acrylonitrile
ATRP	atom transfer radical polymerization
AFC	alkaline fuel cell
Bpy	2, 2′-bipyridyl
C_A	the methanol concentration in the donor compartment (used in Equation 2.3)
C_B	the methanol concentration in the receptor compartment (used in Equation 2.3)
CDMVS	chlorodimethylvinyl-silane
CLPE	cross-linked high-density polyethylene
CTACl	cetyltrimethyl ammonium chloride
D	the diffusion coefficient (used in Equation 2.3 and 2.4)
DMA	Dynamic Mechanical Analysis
DMAc	*N, N'*- dimethylacetamide
DMF	*N, N'*-dimethyl formaide
DMFC	direct methanol fuel cell,
DMPA	α, α-dimethylol propionic acid
DSC	Differential Scanning Calorimetry
E_{cell}	half-cell potential (used in Equation 2.5)
EC	ethylene carbonate

EDS	Energy Dispersive X-ray Spectroscopy
EIS	Electrochemical Impedance Spectroscopy
EMACI	*N, N'*-methyl-(6-hexylcarbamatoethylmethacrylate) imidazolonium bromide
FESEM	Field Emission Scanning Electron Microscopy
FT-IR	Fourier Transform Infrared Spectroscopy
FTIR-ATR	Fourier Transform Infrared- Attenuated Total Reflectance Spectroscopy
GC	Gas Chromatograph
GPC	Gel Permeation Chromatography Analysis
HEMA	2-hydroxyethyl methacrylate
H_2-FC	fuel cell driven by hydrogen gas
HPA	heteropolyacid
i_d	limiting methanol permeation current density measured voltammetrically (used in Equation 2.7)
i_0	current density
I.V.	inherent viscosity
IEC	ion exchange capacity
IEP	isoelectric point
K	partition coefficient between the membrane and the adjacent solution (used in Equation 2.3 and 2.4)
L	thickness of the membrane (used in Equation 2.3, 2.4 and 2.8)
MBA	*N, N'*-methylenebisacrylamide
MCFC	molten carbonate fuel cell
MDP	monododecyl phosphate

MEA	Membrane Electrode Assembly
MSA	methanesulfonic acid
NMR	Nuclear Magnetic Resonance Spectrum
P	power density
PA	phosphoric acid
PAA	poly(acrylic acid)
PAAVS	poly(vinylsulfonic acid/co-acrylic acid)
PAFC	phosphoric acid fuel cell
PAMPS	poly(2-acrylamido-2-methyl-1-propanesulfonic acid)
PATBS	poly(acrylamid tert-butyl sulfonic acid)
PAZO	poly(1-(4-(3-carboxy-4-hydroxyphenylazo benzene sulfonamide)-1,2-ethanediyl, sodium salt)
PBI	poly(2, 2'-(m-phenylene)-5, 5'-bibenzimidazole)
PCC	proton conducting channels
PDDA	poly(diallydimethylammonium chloride)
PEEK	polyether(ether)ketone
PEM	proton exchange membrane
PEMFC	fuel cell includes proton exchange membrane fuel cell
PES	polyethersulfone
PI	polyimide
PMA	phosphomolybdic acid
PPA	poly(phosphoric acid)
PPBP	poly(4-phenoxybenzoyl-1,4-phenylene)
PPQ	polyphenylquinoxanline

PPs	poly(phthalazinones)
POSS	polyhedral oligomeric silsesquioxane
PSSNa	poly(sodium stryrene sulfonate)
PSU	poly(arylene-ether-sulfone)
PTA	phosphotungstic acid
PTFE	poly(tetrafluroroethylene)
PVA	poly(vinyl alcohol)
PVDF	polyvinylidene fluoride
P4VI	poly(4-vinylimidazole)
$Q_8M_8^V$	1, 3, 5, 7, 9, 11, 13, 15- octakis (dimethylviylsiloxy) pentacyclococtasiloxane
R	the resistance of the membrane (used in Equation 2.8)
RH	relative humidity
S	the cross-sectional area of the membrane (used in Equation 2.8)
SAXS	Small Angle X-ray Scattering
Sb-POSS	starburst oligomeric structure
SMA	silicomolybdic acid
SMP-K	3-sulfropopyl methacrylate, potassium salt
SOFC	solid oxide fuel cell
SPA-K	sodium 3-sulfopropylacrylate, potassium salt
SPEEK	sulfonated polyether(ether)ketone
SPEK	sulfonated polyetherketone
SPFP	sulfonated perfluoro-polymer
SPOP	sulfonated poly[bis(phenoxy)phosphazene]

SPSF	sulfonated polysulfone
SSNa	sodium 4-styrenesulfonate
STA	silicotungstic acid
STY	styrene
t	permeation time (used in Equation 2.3 and 2.4)
TEM	Transmission Electron Microscopy
TEOS	tetraethoxysilane
TEVS	triethoxyvinylsilicane
TFA	trifluoroacetic acid
TGA	Thermogravimetric Analyser
T_g	glass transition temperature
THF	tetrahydrofuran
TMAS	tetramethylammonium silicate
UI	2-undecylimidzole
UP	unsaturated polyester
V_B	solution volume of the receptor compartment (used in Equation 2.3 and 2.4)
V_{cell}	cell voltage (used in Equation 2.5)
4VP	4-vinylpyridine
VTF	Vogel-Tamman-Fulcher equation
x_o	molar fraction of methanol in the feed stream (used in Equation 2.7)
X	acid-doping levels
Z’	real component of impedance
Z”	imaginary part of impedance

Greek letters

σ	proton conductivity (used in Equation 2.8)
χ	a lumped term constant (used in Equation 2.6)
η	viscosity of the solution in the solvent (used in Equation 7.3)
η_{an}	anode overpotentials (used in Equation 2.5)
η_{cat}	cathode overpotentials (used in Equation 2.5)
η_0	viscosity of pure solvent (used in Equation 7.3)
η_i	inherent of viscosity (used in Equation 7.4)
η_r	relative viscosity (used in Equation 7.3 and 7.4)
η_{xover}	methanol crossover overpotential (used in Equation 2.5)
η_{ohmic}	ohmic overpotential. (used in Equation 2.5)
ξ	electroosmotic drag coefficient of protons in the membrane (used in Equation 2.7)
ζ	zeta potentials

LIST OF FIGURES

LIST OF TABLES

LIST OF SCHEMES

CHAPTER 1

INTRODUCTION

1.1 General background

A fuel cell is an electrochemical energy conversion device. It produces electricity from external supplies of fuel (on the anode side) and oxidant (on the cathode side) in the presence of an intercalated electrolyte thin layer between the two electrodes. Generally, the fuel flows in and cathodic reaction products flow out while the electrolyte layer remains in the cell to separate the anodic reaction from the cathodic reaction. Fuel cells can operate virtually continuously as long as the necessary flows are maintained. Generally, there are many types of fuel cell available and among the fuel cell options, PEMFC is the most promising option due to the high power density, relatively quick start-up, rapid response to varying loads, as well as low operating temperatures provided by PEMFC and has been developed for transportation applications, as well as for personal devices such as laptops, cell phones and hearing aides and for stationary applications (Gottesfeld et al., 1997) In principle, PEMFC is classified into two subcategories according to fuel-supply. One is fuel cell driven by hydrogen gas (H_2-FC) which uses hydrogen as fuel to transform chemical energy liberated during the electrochemical reaction of hydrogen and oxygen to electrical energy. (Won et al., 2003; Woo et al., 2003 and Boddeker et al., 2001) Presently, for producing H_2-fuel, the most

developed industrial processes are steam reforming and partial oxidation with coal, methane or gasoline. In all of these cases, the CO level coming out of the processor can only be reduced to 50 or 100 ppm. (Pietrogrande and Bezzecheri, 1993) However, CO is a major problem because trace amounts of CO (less than 10 ppm) poison the Pt anode electrode catalyst in the state-of –the-art H_2-FCs operating at 80 ^oC. CO-tolerant electrode catalysts (e.g. Pt-Mo, Pt-Ru) have been developed to enhance CO tolerance, but the problem still exists with these electrocatalysts. In order to alleviate the problem of CO poisoning and to improve the power density of the cell, it would be effective to lift up the operating temperature to above 100 °C. (Savinell et al., 1994; Alberti et al., 2001 and Yang et al., 2001) In addition, higher temperature (> 120 ^oC) operation also reduces system weight, volume and complexity (Li et al., 2003), which increases power density, specific power, and functionality through system and component simplification and enhances the electrode kinetics and the catalytic activity for electrode reactions. (Kreuer, 1997)

The second sub-category of PEMFC is fuel cell driven by methanol (direct methanol fuel cell, DMFC) or ethanol which enables the electrochemical process without the headache of handling hydrogen storage problem. However, two problems accompany with operating DMFC: The first problem is that a significant amount of methanol could easily penetrate across the electrolyte via diffusion to the cathode, known as methanol crossover. This drawback results in the polarization of cathode (Pu et al., 1995 and Burstein et al, 1998) and thus contributes to decreased overall cell efficiency and lifetime. The second problem is that oxidation of methanol ($CH_3OH + H_2O \rightarrow CO_2 + 6H^+ + 6e^-$) on the anode

has a slower kinetics than that of hydrogen because it involves releasing six electrons and therefore consists of several elementary reaction steps.

Such these obstacles for the development of PEMFC are related to the limitations associated with the proton electrolyte membranes usually employed [e.g. Nafion or other types of sulfonated perfluoro-polymer resins]. Therefore, in order to improve the performance of PEMFC from the perspective of cutting down methanol diffusion level through electrolyte, preparation of an applicable membrane that has a significantly lower methanol permeation coefficient (i.e. permeability) than Nafion but maintains the same proton conductivity has been a focus of research. Although there is not a remedy for both methanol crossover and slow anode kinetics, developing a PEM that could retain methanol crossover at the low level required and adequate mechanical stability at elevated temperatures will be also beneficial to accelerating oxidation of methanol on the anode.

An ideal ion exchange membrane fuel cell electrolyte generally includes the following properties: high ionic conductivity, zero electronic conductivity, a substantially low gas permeability, dimensional stability, high mechanical toughness, and low transference of water by conducting ions, high resistance to thermal degradation, as well as chemical stability to oxidation and hydrolysis. Previously, some polymer electrolyte membranes have been traditionally considered as a blend consisting of a hydrophilic polymer and strong inorganic acid, such as poly (ethylene oxide)-H_3PO_4 (Donoso et al., 1988), polyacrylamide-H_2SO_4 (Rodriguez et al., 1993) and branched poly (ethylene imine)–H_2SO_4 (Yoshida et al., 1994). However, the presence of strong inorganic acid in the

polymer matrixes has several disadvantages in potential applications, such as acid-catalyzed polymer degradation and loss of hydrophilic polymer mechanical strength.

Practically, three particular designs could satisfactorily meet the above criteria technically. The first design relies on amphiphilic polymers with the hydrophobic segments constituting a continuous phase to sustain mechanical features while the hydrophilic groups assembling to form the second continuous phase that allows ions to transport. The second design makes use of the polybenzimidazole as an "absorbent" to hold absolute phosphoric acid as the proton conducting channel under nil-humidity level and high temperature. The third design relies on using a robust hydrophobic polymer thin film, over which there are densely arrayed micropores penetrating through the film, as the host matrix. These pores are then filled with a hydrophilic ionic conducting polymer to generate proton conducting channels.

As the model PEM of the first design, sulfonated perfluoro-polymer (SPFP) symbolizes the state-of–the-art of the plastic electrolyte membrane and can satisfy a number of requirements for effective, long-term use in fuel cells. (Eisenberg et al., 1982; Gottesfeld et al., 1997 and Datta et al., 2002) However, SPFP membrane is not able to hold matrix water when the fuel cell's operating temperature is above 100 ^{o}C, which brings about a severe decrease in the proton conductivity of membrane. In addition, SPFP membrane also has very high methanol permeability because it can be swollen by the aqueous solution of methanol. Therefore, it is necessary to modify SPFP membrane to maintain high proton conductivity at elevated temperatures or to reduce its methanol permeability. Some modification methods attempted to add inorganic particle fillers such as SiO_2, TiO_2,

and ZrO_2 into SPFP matrix. Among these approaches, in-situ formation of inorganic fillers which is based on sol-gel reactions within the pores of the membrane is most popular due to the fact that size and distribution of inorganic particles in the SPFP membrane can be well controlled by the concentration of precursors. (Adjemian et al., 2002; Jalani et al., 2005; Xu et al., 2005 and Jiang et al., 2006) However, it should be noted that the modification also lowers markedly the proton conductivity of the membrane owing to introduction of these less proton conductive oxides. Besides this, poor dispersion of these inorganic particles in the membrane owing primarily to the lack of thermodynamic compatibility between the particles and matrix undermines mechanical strength of the membrane. Therefore, it needs to advance the embedding modification method by employing specially tailored particle filler that include conductive functional groups to render SPFP membranes with higher proton conductivity and better mechanical properties.

The second design is performed based on poly(2, 2'-(m-phenylene)-5, 5'-bibenzimidazole) (PBI), a polymer with very strong cohesive energy, extremely high temperature stability, and high chemical resistance. Hence PBI can be made into a fiber with excellent textile and tactile performance. (Wang et al., 1996) Although PBI is not ionic conductive by itself, it is a promising host matrix for some strong oxo-acids due to its imidazole groups and aromatic rings which can be sulfonated. Previously, sulfuric acid has been introduced to dope PBI membrane. (Glipa et al., 1997; Roziere et al., 2001 and Bae et al., 2002), or grafting sulfonate groups directly onto the PBI backbone was the other way to make PBI become proton exchangeable. With the second method, the

degree of sulfonation is an important parameter that directly affects the ion exchange capacity and specific hydration number, and the proton transport properties. A higher degree of sulfonation leads to higher proton conductivity of the membrane but also reduces the mechanical properties of the membrane because it promotes water-uptake capability. In addition, a low decomposition temperature of the sulfonated PBI also limits its application in the high temperature PEMFC. Therefore, as a substitute for sulfonic acid groups, phosphoric acid (H_3PO_4) has been applied to dope PBI membrane due to its higher decomposition temperature. Three different methods have been developed to dope PBI membranes with phosphoric acid (Ma et al., 2004): (1) casting from a solution of polymer in NaOH/ ethanol solution under N_2 environment, followed by washing with water until pH=7, and then doping by immersion in phosphoric acid solution; (2) casting from a solution of 3-5% polymer in *N, N'*- dimethylacetamide (DMAc), followed by evaporation of DMAc, and then doping by immersing in phosphoric acid solution; (3) directly casting from a solution of PBI and H_3PO_4 in a suitable solvent such as trifluoroacetic acid (TFA), followed by evaporation of the solvent and the film is ready for use. Because membranes cast using the DMAc method are stronger and have better mechanical properties than those prepared by the other two methods, most of the membranes reported in the literatures were prepared by the DMAc method (Li et al., 2001; He et al., 2003 and Ma et al., 2004) However, for phosphoric acid doped PBI membrane by the above methods, a very high PA doping level can also deteriorate the mechanical properties of the membrane, especially at temperatures above 100°C even though these membranes have the desirable property of high conductivity. Therefore, an alternative method is necessary. An *in-situ* doping PBI method using polyphosphoric acid

is a possible alternative for fabricating phosphoric acid doped PBI membrane with high proton conductivity and mechanical strength.

Filling porous membranes, as the third design concept of fabricating PEM, is proposed by filling a polymer electrolyte into a porous hydrophobic polymer thin membrane. The strong and rigid film used as the porous substrate can allow the matrix to mechanically prevent any excess swelling of the filling polymer. This would also effectively suppress any fuel crossover through the membrane and reduce the change in area between the dried and wet states of the membrane. On the other hand, the filling polymer having high sulfonic acid content can exhibit high proton conductivity. (Nishimura and Yamaguchi 2004; Kanamura et al., 2005) As a result, the membrane performance for single cell can be optimized by controlling the relationship between its proton conductivity and the fuel permeability.

1.2 Research objectives and scope

The development of high performance proton exchange membranes (PEMs) has been a challenge for PEMFC technology. The main theme of this research project is to pursue restructure the proton conducting channel of the exiting PEMs by creating hybrid nanoparticle fillers or macromer crosslinked network. Four different types of PEMs were fabricated and the physical chemistry of fundamental filler-matrix interactions was explored:

(1) To modify sulfonated perfluoro-polymer (SPFP) membranes via design and synthesis of hybrid nano-particles composed of inorganic core and organic thin graft layer as a specialty filler, and then assess proton conductivity, methanol permeability, mechanical properties, and most importantly single cell performance of the resultant composite membranes.

(2) To reinforce H_3PO_4-doped PBI membrane through crosslinking PBI segments, while they were being grown, by an unsaturated polyester (UP) macromer to form a highly plastic network, which presents a stronger capability to hold dopant H_3PO_4 molecules and largely improved mechanical properties. This membrane targets high-temperature (120-150 ^oC) application under zero humidity condition.

(3) To study the nature of the interactions between hybrid nanoparticles and the host matrix as well as impacts of such interactions on the electrochemical polarization behavior of the modified membranes in PEM fuel cell.

To achieve the above goals, this research project investigated properties and performances of the composite membranes, and the results achieved can be divided into five parts as highlighted below:

(1) Silica microspheres with densely anchored hydrophilic oligomeric chains consisting of conductive copolymer of homopolymer groups were prepared by atom transfer radical polymerization (ATRP). The particular traits of these core-

shell particles including glass transition behaviors of the densely grafted polymer layer, as well as different responses of hydrodynamic volume and zeta potential of the particles to the change in solvating powder and pH values of the dispersion media will be studied. We will also examine how the ionic transport in the designated liquid medium is affected by the solvated particles with a substantially low volume fraction.

(2) Nafion® membranes, as one kind of sulfonated perfluoro-polymer (SPFP) membranes were modified with different content of silica-poly (3-sulfopropyl acrylate acid) (PSPA) core–shell nanoparticles. Their thermal properties and proton conduction behaviors were investigated. Furthermore, single cell performances of modified membranes were compared with that of pure Nafion membrane.

(3) Nafion® membranes were also modified by *in-situ* polymerization of POSS (polyhedral oligomeric silsesquioxane) in the Nafion polymer matrix. Distribution of poly(POSS) in the polymer host matrix was investigated. Furthermore, effects of this distribution on repressing methanol permeation and restructuring proton channels in the membrane matrix were studied.

(4) A novel hybrid structure material, starburst poss-g-acrylonitrile oligomer, was prepared by ATRP with monomer acrylonitrile. Different content of starburst poss-g-acrylonitrile oligomer was embedded in the Nafion polymer matrix. The

proton conduction mechanism of the composite membrane was investigated by Arrhenius plot of membrane proton conductivities as well as membrane structure characterization and thermal analysis.

(5) Unsaturated polyester-reinforcing H_3PO_4-polybenzimidazole membrane which is a PEM for operating at nil matrix humidity condition was developed in this thesis. PBI membrane with unsaturated polyester (UP) as a crosslinker was doped with hydrolysis of polyphosphoric acid. Thermal physical properties of the doped PBI-UP membrane were studied to investigate complexation of phosphoric acid with PBI-polyester and thus mechanism of proton conduction in the membrane was also established.

The four types of hybrid structures obtained by incorporating the nano-particles with dense oligomeric ionomer layer, the starburst oligomeric molecules, the rigid molecular fragments, and the unsaturated polyester crosslinker were introduced into different host matrixes of PEMs respectively. Such PEMs displayed higher proton conductivity, lower methanol permeability and better mechanical properties. Furthermore, they should achieve better single cell performances. It is predicted that they can also be operated for a longer time than the respective homogeneous host PEMs. In addition, studies of proton conduction mechanisms that sustain the revamping effect could also provide some valuable suggestions for development of proton exchange membrane in the future.

CHAPTER 2

LITERATURE REVIEW

2.1 Fuel cells

2.1.1 Introduction

Fuel cells have emerged as one of the most promising technologies for the power source of the future. Though Sir William Grove first introduced the concept of a fuel cell in 1839, the fuel cell research has emerged as a potential field in recent decades. A fuel cell is an electrochemical energy conversion device. The anode provides an interface between the fuel and the electrolyte, catalyses the fuel reaction, and provides a path through which free electrons are conducted to the load via the external circuit. The cathode provides an interface between the oxygen and the electrolyte, catalyses the oxygen reduction reaction, and provides a path through which free electrons are conducted from the load to the electrode via the external circuit. The electrolyte acts as the separator between fuel and oxygen to prevent mixing and therefore, preventing direct combustion. Fuel cells differ from batteries in that they consume reactants, which must be replenished, while batteries store electrical energy chemically in a closed system. Additionally, while the electrodes with in a battery react and change as a battery is charged or discharged, a fuel cell's electrodes are catalytic and relatively stable.

2.1.2 Fuel cell theory

Several processes are involved in the operation of a fuel cell. The processes can be summarized as: gas transfer to the reaction sites, the electrochemical reaction at those sites, the transfer of ions and electrons as well as their combination at the cathode (Fig. 2.1). Gases must diffuse through the electrode leaving behind any impurities which may disrupt the reaction while liquid produced at the surface of the electrolyte, or added through humidification must be either added to the electrolyte for hydration, or drawn away from the reaction sites so as not to block reaction sites based on the concentration gradient between the gas channel (high concentration) and the reaction sites (low concentration).

Two main electrochemical reactions occur in a fuel cell at the anode and cathode respectively.

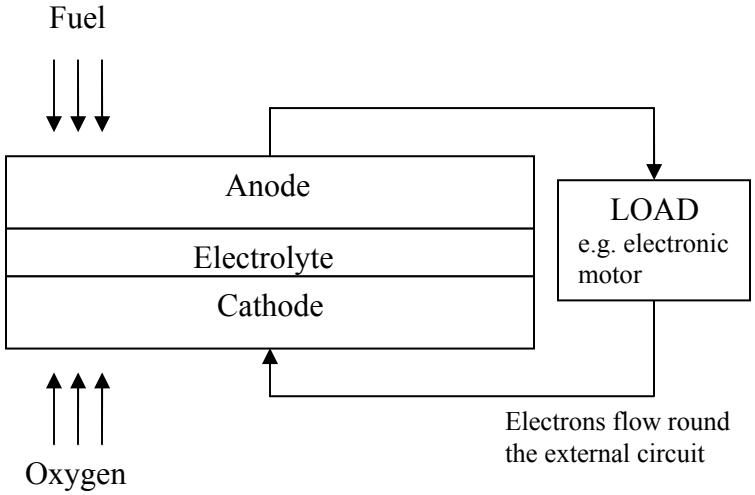

Figure 2.1 Fuel cell diagram

The anode reaction in fuel cells is either direct oxidation of hydrogen, or methanol or indirect oxidation via a reforming step for hydrocarbon fuels. The cathode reaction is oxygen reduction from air in most fuel cells. For hydrogen/oxygen (air) fuel cells, the overall reaction is

$$H_2 + \frac{1}{2} O_2 \rightarrow H_2O \quad \text{with} \quad \Delta G = -237 \text{ kJ/mol}$$

Where ΔG is the change in Gibbs free energy of formation. The product of this reaction is water released at cathode or anode depending on the type of the fuel cell. The theoretical voltage E^0 for an ideal H_2/O_2 fuel cell at standard conditions of 25 ^oC and 1 atmosphere pressure is 1.23 V. The typical operating voltage is about 0.6-0.7 V for high performance fuel cells.

2.1.3 Classification of fuel cells

Fuel cell technologies are named by their electrolyte, as the electrolyte defines the key properties of a fuel cell, particularly the operating temperature. Generally, six distinct types of fuel cells have been developed and applied commercially as shown in the figure 2.2. However, both hydrogen fuel cell (H_2-FC) and direct methanol fuel cell (DMFC) use polymeric proton exchange membrane as electrolyte, so they are two subcategories of proton exchange membrane fuel cell (PEMFC).

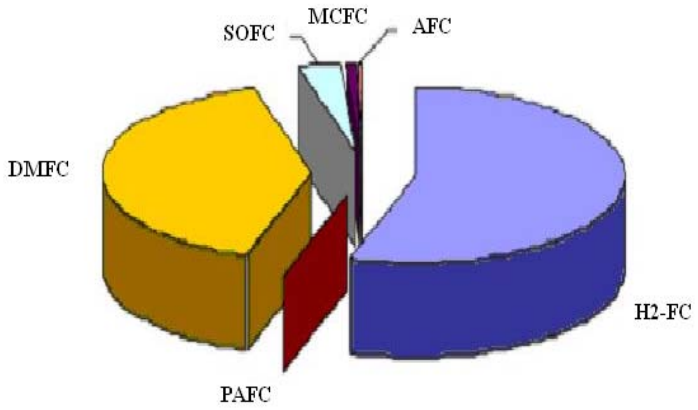

Figure 2.2 Fuel cell distributions

While all five fuel cell types are based upon the same underlying electrochemical principles, they all operate at different temperature regimens, incorporate different materials, and often differ in their fuel tolerance and performance characteristics, as shown on table 2.1.

Table 2.1 Description of Major Fuel cell Types (O'Hayer et al., 2006)

Fuel cell type	**PEMFC**	**PAFC**	**AFC**	**MCFC**	**SOFC**
Electrolyte	Polymer membrane	Liquid H_3PO_4 (Immobilized)	Liquid KOH (Immobilized)	Molten carbonate	Ceramic
Charge carrier	H^+	H^+	OH^-	CO_3^{2-}	O^{2-}
Operating temperature	50-120 ^oC	200 ^oC	60-200 ^oC	650 ^oC	600-1000 ^oC
Catalyst	Platinum	Platinum	Platinum	Nickle	Perovskites (ceramic)
Cell components	Carbon based	Carbon based	Carbon based	Stainless based	Ceramic based
Fuel compatibility	H_2, methanol	H_2	H_2	H_2, CH_4	H_2, CH_4, CO

Among all above fuel cell options, PEMFC is the most promising option due to the high power density, relatively quick start-up, rapid response to varying loads, as well as low operating temperatures provided by PEMFC and has been developed for transportation applications, as well as for personal devices such as laptops, cell phones and hearing aides and for stationary applications. (Gottesfeld et al., 1997) A sign of dominance of PEMFC in recent time is reflected in the number of companies that have sprouted "manufacturing" these units, various demonstration programs, and increased in patents that have appeared. Moreover, the drive for zero emission vehicles has led to great technological strides in the development of PEMFC. (Basu, 2007)

2.2 Proton Exchange Membrane fuel cells (PEMFCs)

The proton exchange membrane fuel cell uses polymeric membrane as the electrolyte and is the best candidate for light-duty vehicles, buildings and much smaller applications.

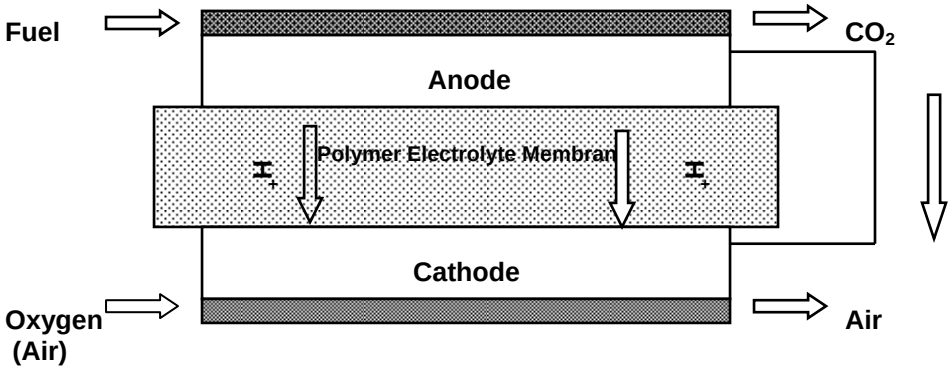

Figure 2.3 Diagram of PEMFC

For H_2-FC, the chemical energy liberated during the electrochemical reaction of hydrogen and oxygen can be transformed to electrical energy, as opposed to the direct combustion of hydrogen and oxygen gases to produce thermal energy.

The oxidation half-cell reaction on the anode:

$$H_2 \rightarrow 2H^+ + 2e^-$$

The newly formed protons permeate through the polymer electrolyte membrane to the cathode side. The electrons travel along an external load circuit to the cathode side of the membrane electrode assembly (MEA), thus creating the current output of the fuel cell.

The reduction half-cell reaction on the cathode:

$$4H^+ + 4e^- + O_2 \rightarrow 2H_2O$$

At the cathode side oxygen molecules react with the protons permeating through the polymer electrolyte membrane and the electrons arriving through the external circuit to form water molecules.

For DMFC, the fuel source, methanols can oxide on a catalyst layer to form carbon dioxide. Water is consumed at the anode and is produced at the cathode. Positive ions (H^+) are transported across the proton exchange membrane to the cathode where they react with oxygen to produce water. Electrons are transported via an external circuit from anode to cathode providing power to external devices.

The half-reactions are:

Anode: $CH_3OH + H_2O \rightarrow CO_2 + 6H^+ + 6e^-$

Cathode: $3/2\ O_2 + 6H^+ + 6e^- \rightarrow 3H_2O$

The primary components of a PEMFC are an ion-conducting electrolyte membrane, a cathode and an anode. The basic cell consists of a proton conducting membrane, such as a perfluorinated sulfonic acid polymer, sandwiched between two platinum impregnated porous carbon electrodes. The other side of the electrodes is made hydrophobic by coating with an appropriate compound, such as Teflon which provides a path for gas diffusion to the catalyst layer (GDL) (Stroh et al., 2001; Gottesfeld et al., 1997; Bevers et al., 1998 and Cha et al., 1999). Together, these three are often referred to as membrane electrode assembly (MEA), of simply a single fuel cell. In the simplest example, a fuel such as hydrogen is brought into the anode compartment and an oxidant, typically oxygen, into the cathode compartment. The other components are gas flow distribution plates for reactants, and mechanical components like end plates, current collectors, gaskets, bolts and nuts. The voltage of a fuel cell is small when drawing a useful current, that is, to produce a useful voltage many cells have to be connected in series. Such a collection of fuel cells in series is known a stack. The most obvious way to do this is to connect the anode plated with the adjacent cathode plate of the next cell with a wire all along the stack. A better method to do this is to use a “bipolar plate” where the entire face of the

anode plate (opposite the gas distribution side) is in contact with the obverse of the cathode plate (Borup et al., 1995; Stroh et al., 2001; Wilson and Busick 2001).

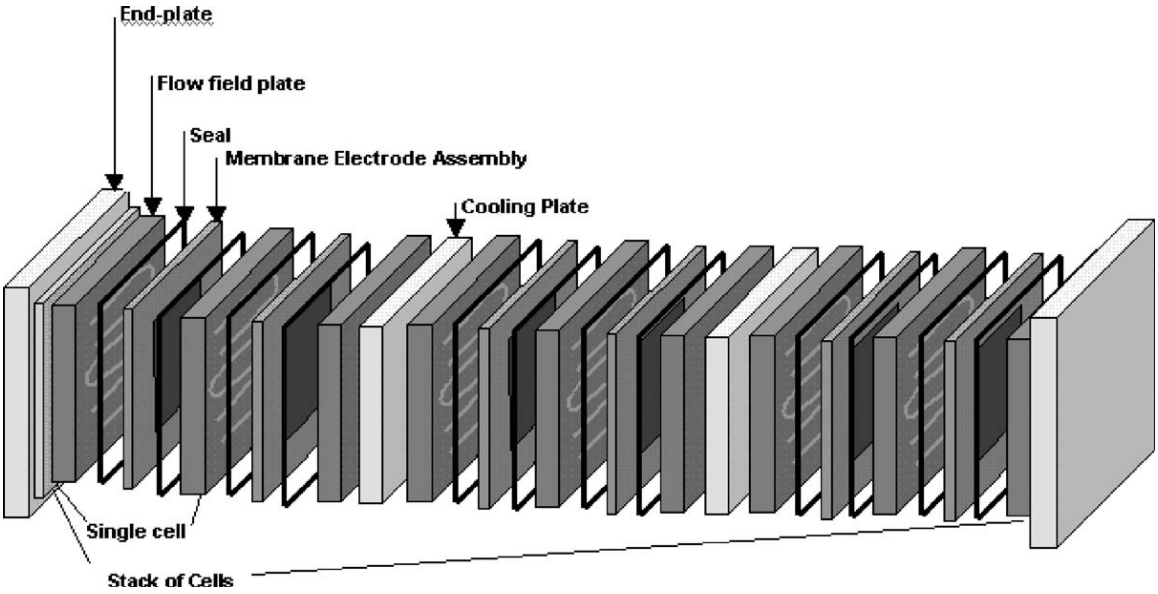

Figure 2.4 PEM fuel cell hardware (Mehta and Cooper, 2003)

Presently there are some technical problems that have to be overcome for the development of PEMFCs. Meanwhile, Tolerance to carbon monoxide (CO) is one important issue, particularly when hydrogen is formed from methanol by steam reforming. Methanol reformatted contains as much as 25% carbon dioxide (CO_2) along with a small amount (1%) of carbon monoxide (CO) for H_2-FC. It has been proven that PEM fuel cell performance drops with a CO concentration of only several parts per million. This is due to the strong chemisorption force of CO onto the catalyst. The other important issue is slow methanol oxidation kinetics and methanol diffusion from the anode to the cathode for DMFC. So in order to counter these problems, one (a binary catalyst) or sometimes

two elements (a ternary catalyst) are added to the base catalyst to form catalyst alloys. Binary and ternary anode catalysts such as Pt-Ru/C, Pt-Mo/C (Bauman et al., 1998), Pt-W/C (Pinheiro et al., 2000), Pt-Ru-W/C (Holleck et al., 1998), Pt-Ru-Al_4 (Denis et al., 1998), and Pt-Re-(MgH_2) (Dodelet et al., 2000) are typically. However, it is difficult that the catalyst alloys are produced as active as possible with reasonable cost to lower CO concentration below the level of 10 ppm and enable so high methanol conversion at the anode that methanol diffusion can be reduced through the electrolyte. Aiming to solve the above problems, this thesis research mainly focuses on fabricating high performance proton exchange membranes (PEMs) applied for both H_2-FC and DMFC. Therefore, in the following part of literature review, (1) development of proton exchange membranes; (2) transport mechanism of PEMs; and (2) characterization methods of PEM performance will be reviewed.

2.3 Proton exchange membranes

In general, PEMFC requires an ion exchange polymer in the form of a continuous pore free sheet. The properties which characterize the ideal ion exchange membrane fuel cell electrolyte will include the following: high ionic conductivity, zero electrical conductivity, low gas permeability, dimensional stability, high mechanical strength, and low transference of water by conducting ions, high resistance to degradation, as well as chemical stability to oxidation and hydrolysis. A number of factors affect the conductivity of the membrane, e.g. ionic size, charge and the solvation. The most highly conducting membrane electrolytes for fuel cell application are those in which the mobile

ion is the hydrogen ion and the solvate is water at saturation. Proton exchange membranes are classified by materials applied for their fabrication into: (1) Sulfonated perfluoro-polymer membranes; (2) Sulfonated thermoplastic polymer membranes; (3) Phospohoric acid doped polybenzimidazole (PBI) membranes; (4) Polybenzimidazole (PBI) composite membranes; and (5) Other polymer membranes.

2.3.1 Perfluorosulfonic acid membranes

Sulfonated perfluoro-polymer and its derivatives (SPFP) symbolize the state-of–the-art of the plastic electrolyte membrane, satisfying in impressive fashion an array of requirements for effective, long-term use in fuel cells. In this ion exchange membrane, the sodium counter-ion can be easily exchanged with other cations by soaking the polymer in an appropriate aqueous electrolyte solution. For commercial materials, structure parameters are shown as the table 2.2. This gives rise to a molecular weight in the range of 100 to 1500 gram of resin (in its dry hydrogen ion form), per one mole of ion exchange sites. (Banerjee et al., and Manley et al., 1996) The commercialized perfluorinated membranes Nafion® series have emerged as standard materials for low-temperature fuel cell applications. (Eisenberg et al., 1982; Gottesfeld et al., 1997 and Datta et al., 2002) No other type of materials could replace Nafion® for decades because of inability to provide high proton conductivity with high chemical and thermal stability.

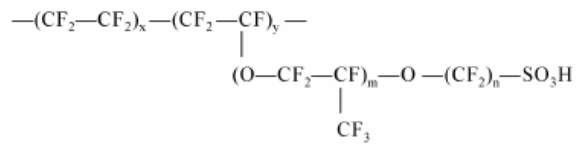

structure parameter	trade name and type	equivalent weight	thickness (μm)
	DuPont		
$m = 1$; $x = 5-13.5$; $n = 2$; $y = 1$	Nafion 120	1200	260
	Nafion 117	1100	175
	Nafion 115	1100	125
	Nafion 112	1100	80
	Asashi Glass		
$m = 0, 1$; $n = 1-5$	Flemion-T	1000	120
	Flemion-S	1000	80
	Flemion-R	1000	50
	Asashi Chemicals		
$m = 0$; $n = 2-5$; $x = 1.5-14$	Aciplex-S	1000–1200	25–100
	Dow Chemical		
$m = 0$; $n = 2$; $x = 3.6-10$	Dow	800	125

Table 2.2 Commercial SPFP membranes by producer (Li et al., 2003)

Sulfonated perfluoro-polymers have the branched chain architecture with sulfonic acid groups locating at the end of sides chains and hence thermoplastic and soluble in several organic polar solvents. It is widely accepted that sizeable ionic clusters scattered in a surrounding of hydrophobic organic medium can also exist in the polymer. By inspecting the change in fluorescence spectroscopy due to the diffusion of heavy cations into the matrix of hydrated Nafion polymers, Lee & Meisel (Lee and Meisel, 1980) have confirmed the existence of inverted misellar structure. Gierke & Hsu (Hsu and Gierke, 1983) considered the clusters to be interconnected by short narrow channels in the hydrated Nafion matrix, as illustrated in Fig. 2.5. The microstructure offers both proton conducting channels (continuous phase) and mechanical framework (dispersed phase), upon which membrane of Nafion polymers exhibit it the dual properties when hydrated.

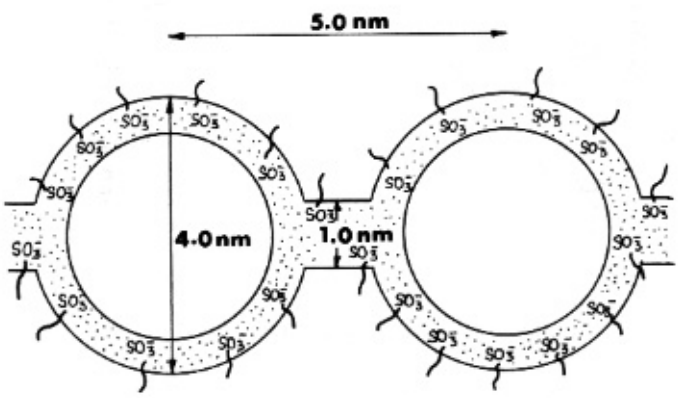

Figure 2.5 Cluster network model for Nafion perflorinated membrane (Hsu and Gierke 1983)

However, Nafion® series are totally not able to hold matrix water when temperature is above 100 °C which decrease the proton conductivity of membranes and have high methanol permeability. Therefore, it is useful to make these membranes have high temperature resistance, low methanol cross-over, greater mechanical and high proton conductivity. Therefore, several recent modification approaches have been used to overcome these problems. Modified Nafion membranes containing inorganic fillers (SiO_2, TiO_2, ZrO_2, and ZrP), hetero-poly-acids, and other polymers have been reported (Mauritz and Moore, 2004; Mauritz and Hassan, 2007).

2.3.1.1 Inorganic oxides

The approaches of synthesizing inorganic modified Nafion membranes include casting a bulk mixture of powder or colloidal state of inorganic with Nafion solution and *in-situ* formation of inorganic particles utilizing the membrane as template. Meanwhile, the advantage of *in-situ* method is that the particle size can be controlled by the concentration

of precursors because the size and dispersion of these solid particles are of utmost importance in final performance of fuel cells. Mostly, the *in-situ* method is based on sol-gel reactions and water within the pores of the membrane. In the recent years, most reports focused on the development of the Nafion/TiO_2, Nafion/SiO_2 and Nafion/ZrO_2 composite membranes which applied $Ti(OPr)_4$ (Sacca et al., 2005 and Jalani et al., 2005), tetraethoxysilane (TEOS) (Adjemian et al., 2002 and Jalani et al., 2005, Xu et al., 2005 and Jiang et al., 2006) and Zirconium (IV) *tert*-butoxide (Jalani et al., 2005) as precursors respectively by an impregnation of Nafion membrane via sol-gel processing of precursor solution or by preparing a recast film in alcohol solution or *N, N'*-dimethylacetammide (DMAc) solution. The introduction of the fillers supplies the composite membrane with a good mechanical and thermal resistance as well as improves the water uptake and IEC values if compared to the commercial Nafion membrane. In addition, the methanol crossover of composite membranes is also reduced obviously. This may be because that the impregnation of the oxide particles into the nanopores of Nafion can prevent the membranes from hydration and lead to the destruction of the pore structure. Yet because the proton conductivity of the composite membranes containing these less proton conductive oxides is markedly lowered compared with that of a pristine Nafion membrane, introducing these inorganic oxides can not always lead to a desired improvement in the performance of the membrane electrode assembly (MEA). In order to enhance conductivity, besides remain membranes' inherent property, some attempts have been reported to introduce some inorganic additives with some kinds of inorganic acid such as sulfonated acid (Rhee et al., 2006 and Zhai et al., 2006) and Heteropolyacid (Shao et al., 2004 and Xu et al., 2005) into Nafion matrix. The nanocomposite

membranes showed higher proton conductivity than composite membranes containing untreated inorganic oxide particles. The relative permeability of methanol through these composite membranes was also reduced in comparison with pristine Nafion membranes. However, from the SEM image, the particle dispersion is not uniform so that the membranes can not be applied for a long term fuel cell operation.

2.3.1.2 Zirconium phosphate

Zirconium phosphate was incorporated into Nafion with the procedure first described by Grot and Rajendran. (Grot and Rajendran, 1999) The treated Nafion membrane was dipped into zirconyl chloride solution for several hours and then immersed in phosphoric acid to form zirconium hydrogen phosphate in the membrane and re-protonate the sulfonate anions to regenerate the acidity of the membrane. The composite membrane revealed a slight reduction of ionic conductivity, a significant improvement of mechanical stability, and increased water retention. The overall efficiency at 130 ^{o}C was increased during DMFC operation because the reduction in the ionic conductivity is overcompensated for by the decrease in methanol crossover. With H_2-FC, the slight reduction in overall efficiency corresponded to the decrease in ionic conductivity. However, they displayed better fuel cell performance than Nafion membrane when the fuel cell was operated at reduced humidity. (Bauer and Willer-Porada, 2006)

2.3.1.3 Heteropolyacid modification

Heteropolyacid (HPA), an inorganic super acid, has two kinds of complex arrangement structure, commonly known as the "Keggin" and "Dowson" structure. (Fig. 2.6) HPA displays different reduced compounds when several electrons are introduced and is also very soluble in water and alcohols. Hence it is interesting to determine whether or not HPA has any effect on Nafion performance in proton electrolyte membrane fuel cell. Nafion-based organic/inorganic composite membranes with different heteropolyacid (HPA) additives have been shown in the above section. In the recent years, many reports have focused on preparing Nafion/HPA composite membranes with different HPAs (phosphotungstic acid (PTA), silicotungstic acid (STA), phosphomolybdic acid (PMA) and silicomolybdic acid (SMA) and different HPA concentrations.

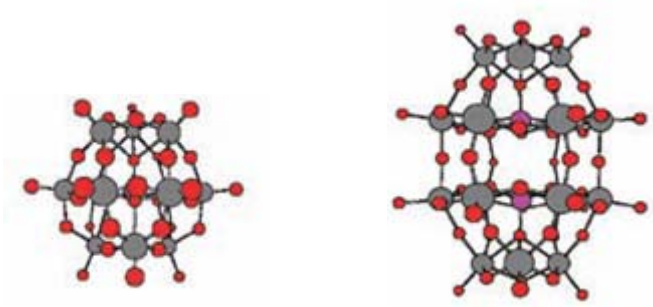

(a) (b)

Figure 2.6 HPA structures: (a) "Keggin" structure, (b) Dawson structure

Tazi et al., (Tazi et al., 2000) developed an inexpensive and novel method of synthesizing cation exchange membranes based on Nafion® 117 solution and silicotungstic acid with

and without thiophene (named NASTATH and NASTA respectively). The water uptake and ionic conductivity of NASTA and NASTATH were compared with those of Nafion® 117. It was shown that the water uptake of the composite membranes at 110 °C was significantly better than that of Nafion® 117 (27 wt.%) at 80 °C and the ionic conductivity of them was found to be significantly higher than that of the Nafion® 117. This is because the introduction of STA in the Nafion® 117 membrane to form the NASTA or NASTATH membranes may increase the number of protonic sites in the membranes. This may improve the membranes' ionic conductivity and water uptake and also explain why stability of these membranes after pretreatment in hot deionized water though STA are soluble in water and alcohols.

Malhotra and Datta (Malhotra and Datta, 1997) first proposed the incorporation of PTA in the Nafion membrane with the objective of serving the dual functions of improving water retention as well as providing additional acidic sites. Thus, they doped Nafion membranes with PTA, and were able to show high fuel cell performance at lower RH and elevated temperature (120 °C). Unfortunately, due to high water solubility, the PTA eventually leaches out from the PEM. Ramani et al. (Ramani et al., 2004) have more recently shown that Nafion-PTA membranes can be stabilized by heat treatment and the leaching of PTA can be reduced. In addition, this research group also evaluated the performance of Nafion/PTA, Nafion/PMA, Nafion/STA and Nafion/SMA at temperatures between 80 °C and 120 °C and under ambient pressure with cathode inlet relative humidities (CIRH) ranging from 100 to 35%.

2.3.1.4 Polymeric multilayer modification

Various multilayer membrane structures have also been investigated with the aim of suppressing methanol crossover. Kim et al. (Kim et al., 2004) fabricated the membranes by blending Nafion solution with polyvinylidene fluoride (PVDF), this latter is considered as the structural component by virtue of its good methanol resistance as well as its excellent thermal stability. The laminated structure of the blended membrane overcomes the problem, which is poor contact with electrodes in the membrane electrode assembly (MEA) process, and reduces the interfacial resistance of the MEA. Yang and Manthiram studied the methanol crossover and conductivity of Nafion membranes with a thin barrier layer of sulfonated poly(ether ether ketone) (SPEEK). (Yang et al., 2004) Si et al. (Si et al., 2004) also developed trilayer membranes composed of one central methanol barrier layer and two conductive layers to suppress the methanol crossover. Casting non-conductive polymers such as poly(vinyl alcohol) (PVA) onto Nafion membranes can also reduce the methanol crossover. (Shao et al., 2002) However, in all these cases, the proton conductivity also decreased significantly due to the addition of a relatively thick barrier layer.

The latest progress was the deposition of a very thin laminated top from multilayer of poly(diallydimethylammonium chloride) (PDDA, polycation), poly(sodium stryrene sulfonate) (PSSNa, polyanion) and poly(1-(4-(3-carboxy-4-hydroxyphenylazo benzene sulfonamide)-1,2-ethanediyl, sodium salt) (PAZO, polyanion) on the Nafion membrane surface at the anode side via layer-by-layer self-assembling (Jiang et al., 2006) tactic with

the aim of suppressing methanol crossover. The multilayer was anchored to the surface of Nafion through forming ion-pairs with it surface sulfonic groups, which can obstruct methanol effectively. However, such ion-pair binding mechanism disables the surface-pendant sulfonic acid groups for transporting protons, and the surface layer will also be removed after a long contact with aquatic fuel solution.

2.3.2 Sulfonated thermoplastic polymers for proton exchange membranes

While modification of sulfonated perfluoro-polymer PEMs is still a main research direction of the PEM industry, several thermoplastic aromatic polymers including polybenzimidazole (PBI), polyether(ether)ketone (PEEK), polyethersulfone (PES), polyphenylquinoxanline (PPQ), polyimide (PI), poly(4-phenoxybenzoyl-1,4-phenylene) (PPBP), poly(phthalazinones) (PPs), poly(arylene-ether-sulfone) (PSU), and polyphosphazene have been also used as high temperature proton exchange membrane in the recent years due to their excellent chemical resistance, high thermo-oxidative stability, and good mechanical properties. (Misha et al., 2000 and Karlsson et al., 2004) However, it is well known that these pristine polymers have very low conductivity. Therefore, in order to improve proton conductivity, some researchers have impregnated sulfonic groups to the polymers' chains. Sulfonation, a powerful and versatile process, can be used to simultaneously render these polymers proton conductive as well as hydrophilic in nature. Generally, sulfonated polymers are prepared by introducing the sulfonic groups such as free acid ($-SO_3H$), a salt (e.g. $-SO_3^-Na^+$) or an ester ($-SO_3R$) onto the polymer backbone by modification or by polymerizing sulfonated monomers. (Noshay et al., 1976;

Glipa et al., 1997; Roziere et al., 2001; Bae et al., 2002; Smitha et al., 2003 and Xing et al., 2004) Furthermore, Kerres et al. (Kerres, 1999 and 2002) also developed the blends consisting of different sulfonated poly(ethersulfone)s and poly(etherketone)s as well as the blends of sulfonated poly(sulfone)/poly(ether sulfone) and SPEEK/poly(ether sulfone). Although these blends exhibited lower methanol permeability in DMFC tests than Nafion®, clear conclusions could not be drawn as proton conductivity was not measured. Gao et al. (Gao et al., 2003) also studied a novel class of sulfonated polymers (SPPs) including SPPESs, SPPEKs, and SPPESKs and found that highly sulfonated PPs showed proton conductivity about 10^{-2} S/cm at both room temperature and elevated temperature, which is in the range needed for high performance fuel cell PEM. However, it was reported that unsulfonated aromatic polymers were more stable than their sulfonated derivatives under inert and saturated vapor conditions (Kopitzke et al., 2000) and the introduction of sulfonic groups into polymer chains can lead to a decrease in the decomposition temperature. (Gao et al., 2003) Smitha et al. (Smitha et al., 2003) also used the DSC spectra to observe T_g value after sulfonation is reduced from 87 °C to 30 °C. This result is explained by the reason that the structural changes are introduced into the polymer on account of sulfonation, and the higher the degree of substitution, the greater is the free volume of a sulfonated product membrane enabling a change in the state of polymer from more amorphous to more crystalline resulting in the reduction of the glass transition temperature. However, in any case, WAXD studies would be needed to confirm this assumption. In addition, increasing in concentration of sulfonating agents can improve the conductivity of polymers, but can not ensure uniform distribution of sulfonic groups within the polymer matrix, which leads completely membranes of

polymer soluble. McGrath's group applied disulfonated monomer to synthesize sulfonated poly(arylene ether sulfone) copolymers via direct copolymerization in any composition desired. (McGrath et al., 2001 and 2002) These random copolymers displayed a hydrophilic/hydrophobic phase separated morphology that varied depending on the degree of disulfonation. The conductivity and water uptake of this series of copolymers also increased with disufonation. However, once the degree of disulfonation reached 60 mol%, a semicontinuous hydrophilic phase was observed and the membranes swelled dramatically, forming a hydrogel that would not be useful as a proton exchange membrane. Hence, for different high temperature polymers we must control different degree of sulfonation to balance the proton conductivity with the water swelling and mechanical properties of the membrane in these thermoplastic polymers.

2.3.3 Phospohoric acid doped polybenzimidazole (PBI) membranes

Among above these thermoplastic polymers, polybenzimidazole (PBI), poly(2,2'-(m-phenylene)-5,5'-bibenzimidazole), is most promising for high-temperature fuel cells when doped with a strong oxo-acid (phosphoric acid, H_3PO_4) (Wang et al, 1996 and Bozkurt et al., 1997) due to its exceptional thermal and chemical stability (Iwakura et al., 1964 and Choe, 1994). For sulfonation of PBI, the conductivity of PBI membrane with sulfonic acid groups is dependent on the presence of water to solvate the protons of the sulfonic acid groups. Consequently the operational temperature is limited and high water contents must be ensured. A combination of PBI and phosphoric acid is therefore expected to have higher thermal and chemical stability as well as higher conductivity.

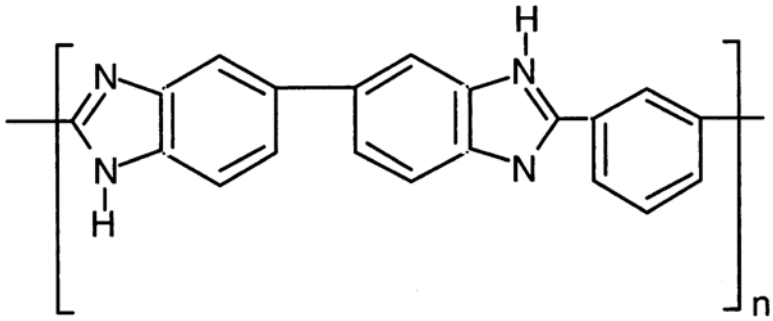

Figure 2.7 Structure of poly(2,2'-(m-phenylene)-5,5'-bibenzimidazole)

Of all PBI systems, phosphoric acid doped PBI membrane has been studied in the greatest detail, but the conductivity mechanism is still unclear phosphoric acid doped PBI membranes were first suggested for fuel cells applications in 1995. (Wainright et al., 1995) During this ten-year, two methods to dope phosphoric acid on PBI membranes have been developed, one is imbedding method and the other is sol-gel method.

(1) Embedding method

There are a lot of reports about H_3PO_4 doped PBI membranes and generally three methods of preparation (Litt et al., 1999): (1) casting form a solution of polymer in NaOH/ ethanol solution under N_2 environment, followed by washing with water until pH=7, then doped by immersion in phosphoric acid solution; (2) casting from a solution of 3-5% polymer in *N, N'*- dimethylacetamide (DMAc), followed by evaporation DMAc, and then doped by immersion in phosphoric acid solution; (3) directly casing from a solution of PBI and H_3PO_4 in a suitable solvent such as trifluoroacetic acid (TFA), followed by evaporation and the film is ready for use. Most of membranes reported in the

literature were prepared by the DMAc method because films cast using them were stronger and have better mechanical properties than those prepared by other two methods.

Table 2.3 Comparison of conductivity at different conditions according different references

	Conductivity (S/cm)	Relative humidity	Doped levels	temperature
Wainringht et al., 1995	2.2×10^{-2}	-	5.01	190 °C
Fontanella et al., 1998	4.5×10^{-5}	0%	6.0	Room temperature
Bouchet et al., 1999	7×10^{-6}	0%	3.05	30 °C
Li et al., 2001	4.6×10^{-2}	80-85%	4.5	165 °C
Ma et al., 2004	4.5×10^{-2}	30%	6.0	140 °C
	2.0×10^{-2}	20%	5.7	110 °C
He et al.,2003	4.0×10^{-2}	10%	5.7	140 °C
	7.9×10^{-2}	5%	5.7	200 °C

In Table 2.3, we need to emphasize that in the above report, conductivity measurements were based on the effect of the water content in both membranes and the atmosphere. On the contrary, in He's paper, (He et al., 2003) special attention was attributed to the relative humidity (RH) in a hydrogen atmosphere. All of the above works were done based on PBI membranes, but the results varied from author to author due to various preparation processes for the membranes and various testing conditions. However, we

can conclude that phosphoric acid doped PBI membranes have higher conductivity at higher H_3PO_4 doping level of PBI membrane.

Despite extensive work on PBI membranes, there are other members of the imidazole family, such as the simpler poly(4-vinylimidazole) (P4VI) and poly(2, 5-benzimidazole) (ABPBI), which are very much worth of attention and study. The synthesis, thermal and conduction properties of blends of poly(4-vinylimidazole) with phosphoric acid have recently been reported by Bozkurt and Meyer. (Bozkurt and Meyer, 2000) P4VI can be dissolved in acidic aqueous solution and then cast P4VI·$x$$H_3PO_4$ membrane, where x is the moles of acid per P4VI repeat unit. The influence of the acid concentration, temperature and pressure on the relative conductance and activation volume of P4VI blended with H_3PO_4 was studied. Moreover, the conductivities of P4VI blended with H_3PO_4 and H_2SO_4 were compared. (Pu et al., 2001) The conductivity of H_3PO_4 blended P4VI was lower than that of H_2SO_4 blended P4VI at the acid concentrations they studied.

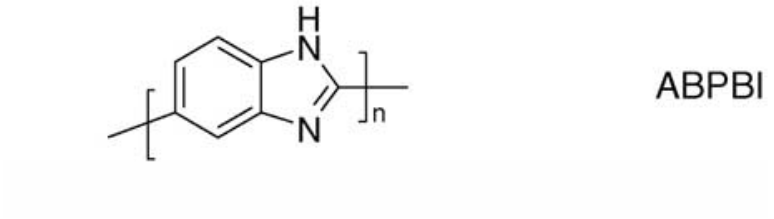

Figure 2.8 Structure of poly (2, 5-benzimidazole)

Poly(2, 5-benzimidazole) (ABPBI) is indeed the simplest among benzimidazole type polymers since it can be prepared easily from a single, inexpensive and commercial monomer (3, 4-diaminobenzoic acid (DABA)) by condensation in polyphosphoric acid (PPA) (Asensio et al., 2002 and 2004a). Furthermore, impregnation of ABPBI with a

given phosphoric acid solution leads to higher acid uptake in comparison with commercial PBI. Litt (Litt et al., 1999) and Wainright (Wainright et al., 2003) have reported that direct acid casting of ABPBI/H_3PO_4, from trifluoroacetic acid (TFA) solutions improved the conductivity on ABPBI/H_3PO_4 and also allowed a better control of the acid content in the resulting membrane. Based on the above reports, Asensio (Asensio et al., 2004b) developed a procedure to prepare the phosphoric acid doped ABPBI membranes for PEMFC by simultaneously doping and casting from an ABPBI/ phosphoric acid/ methanesulfonic acid (MSA) solution. Membranes have been prepared with contents of up to 3.0 H_3PO_4 molecules per ABPBI repeating unit. These membranes achieved a maximum conductivity of 1.5×10^{-2} S/cm at temperatures as high as 180 ^oC in dry conditions. Both sulfonated SABPBI and ABPBI-PMo_{12} membranes have shown an enhanced capacity for phosphoric acid uptake and a consequent increase in conductivity, compared with the non-modificated counterparts. The maximum conductivities measured in dry conditions were 3.5×10^{-2} S/cm at 185 ^oC for SABPBI· 4.6 H_3PO_4 with a degree of sulfonation of 41% and 3.0×10^{-2} S/cm at 185 ^oC for ABPBI-PMo_{12}· x H_3PO_4 membrane with a degree of PMo_{12} of 45%. (Asensio et al., 2004c and Romero et al., 2005)

(2) Sol-gel process

During the last ten years, there have been a lot of reports about H_3PO_4 doped PBI membranes. However, a very high acid doping level may deteriorate the mechanical properties of the acid doped polymer membranes, especially at temperatures above 100 °C. This factor limited improving conductivity at a high temperature, made working

time of fuel cells shorter and decreased mechanical stability of membranes. Recently, Xiao et al. reported a sol-gel process was described to produce phosphoric acid (PA)-doped polybenzimidazole (PBI) (Xiao et al., 2005a) and pyridine-based polybenzimidazole (PPBI) (Xiao et al., 2005b) films that operated as fuel cell membranes above 150 °C for extended periods of time without the need to feed gas humidification. Polymerization to produce PBI or PPBI polymers was carried out using PPA as both the polycondensation agent. After polymerization, the PBI or PPBI solution in PPA was directly cast at approximately 200 to 220 ^{o}C without isolation of redissolution of the polymers. Upon casting, hydrolysis of the PPA to PA introduced a sol-gel transition that produced membranes with a desirable suite of physicochemical properties. The resulting membranes can display high PA doping level and exhibited high ionic conductivities and stable mechanical properties at elevated temperatures. However, for this method, high molecular PBI or PPBI which can be achieved from the strict experiment conditions has to be achieved by forming a piece of membrane for obtaining high mechanical properties.

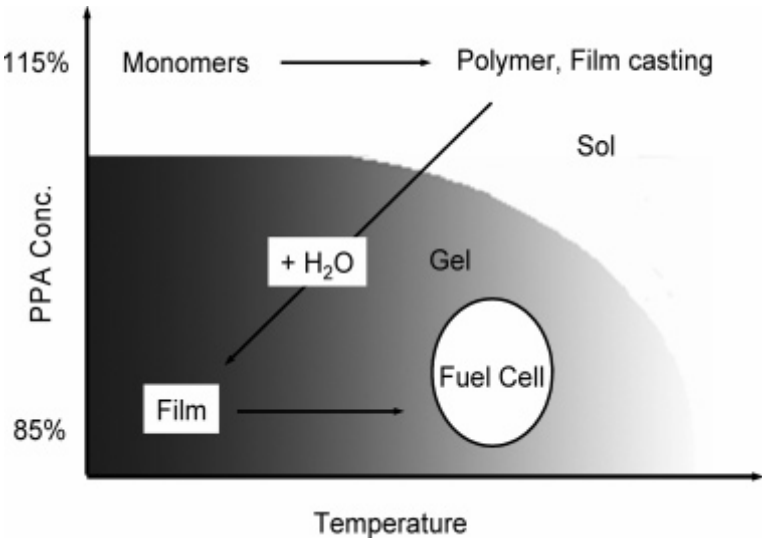

Figure 2.9 State diagram of the PPA sol-gel process (Xiao et al., 2005a)

2.3.4 Polybenzimidazole (PBI) composite membranes

High acid doping levels result in higher conductivity. However, a very high acid doping level may deteriorate the mechanical properties of the acid doped polymers membranes, especially at temperatures above 100°C. In order to overcome this limitation, additional studies also have focused on acid doped composite membranes of PBI with other polymers or inorganic compounds and studies of other derivatives. Introducing single solid proton conductor, e.g. SiO_2, ZrP, PWA or SiWA as inorganic filler, not only improved the mechanical behavior as well as the thermal stability, but also increased the conductivity of the composite membranes (He et al., 2003). A higher conductivity of 9.6×10^{-2} S/cm was observed for the acid doped membranes containing 15 wt.% of ZrP in a PBI membrane at 200 ^{o}C and 5% RH. And homogeneous membranes with good mechanical strength were prepared by introducing PWA (20-30 wt.%) and SiWA(20-30 wt.%) into PBI, and their conductivity were found to be higher than of comparable with that of the PBI membrane at temperatures up to 110 ^{o}C. Moreover, coupling SiWA/SiO_2 inorganic materials have been also applied for hybridization with PBI to get proton conductor membranes. (Staiti et al., 2000a and 2001) The membranes were thermally stable and the conductivity measured on a sample of membrane with 50 % of inorganic proton conductive component gave a value of 1.2×10^{-3} S/cm at 160 ^{o}C and 100 % RH.

Pure PBI has a relatively high cost and performance tests of PBI fuel cells suggest that further optimization is needed. Hence blends of PBI with an inexpensive polymer were synthesized. Sulfonated thermoplastics such as polysulfone (SPSF) have been recently

proposed as possible polymer electrolytes and these PBI-SPSF blends exhibit excellent miscibility characteristics. Deimede and Hasiotis (Deimede et al., 2000; Hasiotis et al., 2001a and 2001b) observed the conductivity of the PBI/SPSF blends possessing different phosphoric acid doping level and different degree of sulfonation and found that the conductivity of blends is dependent on the sulfonation degree of SPSF. Although the blending membrane has a highest conductivity of about 2.1×10^{-1} S/cm, it did not be applied for fuel cell due to its poor mechanical and thermal properties. Kerres (Kerres et al., 2000 and 2001) prepared ionically cross-linked blend membrane by mixing acidic polyaryl membranes such as sulfonated polysulfone (PSU), sulfonated polyether(ether)ketone (SPEEK), and sulfonated polyetherketone (SPEK), with basic membranes such as PBI. The conductivity of the blended membranes depended on the composition and ion exchange capacity (IEC) of the membranes. Also, they applied these membranes in H_2 fuel cells and direct methanol fuel cells (DMFC), and concluded that low methanol-permeability makes this membrane suitable for DMFC even at 110 ^{o}C. Wycisk et al. (Wycisk et al., 2005) developed a series of proton-conducting fuel cell membranes prepared from blends of sulfonated poly[bis(phenoxy)phosphazene] (SPOP) and PBI, where the latter, being a polymer base, was used as a cross-linking component. The resulting membranes had a room temperature proton conductivity in the range 0.005-0.08 S/cm and lower methanol permeability than Nafion® 117, but the DMFC performance of the membranes is not as good as Nafion® 117.

2.3.5 Other polymers for proton exchange membranes

2.3.5.1 Organic-inorganic hybrids

Peled et al. (Peled et al., 2000) developed composite membranes of PVDF filled with nanoparticles, such as silica, zirconium, and aqueous mixtures of acids. These membranes exhibited lower methanol crossover compared to Nafion ®, but due to the use of aqueous acids, corrosion-resistant materials for the fuel cell would be required in the fuel cell assembly. Aparicio et al. (Aparicio et al., 2005) synthesised poly(styrene-co-methacrylate)–silica covalent hybrid membranes using copolymerization of monomers (styrene (STY) and 2-hydroxyethyl methacrylate (HEMA)), with formation of covalent bonds between hydroxyl group from the latter and pre-hydrolyzed tetraethoxysilane. Tungstophosphoric acid hydrate was incorporated to provide proton conductivity for the membranes. The combination of water uptake and water retention properties provided by SiO_2 and tungstophosphoric acid leads to high proton conductivity (maximum values around 1 S/cm) at 120 °C. However, decay in conductivity was observed at higher temperatures, suggesting that dehydration of the membrane occurs. In this paper, it is shown that the rise of conductivity can only be associated with the higher percentage of silica in this membrane.

2.3.5.2 Blending proton exchange membranes

Blending of hydrophilic and hydrophobic polymers is also one of the research areas of PEM. Such a composite structure allows both hydrophilic and hydrophobic domains to fulfill their respective functionalities as a PEM. Chen et al (Chen et al., 2002 and 2004) used a copolymer (PMMA-SSA) formed by styrene sulfonic acid as hydrophilic phase and methyl methacrylate to embed into hydrophobic poly(vinylidene fluoride) (PVDF) to prepare blends of P(MMA-SSA) and PVDF. The blending improved the thermal stability of the SSA and high SSA content can provide higher conductivity. However, because results which the blending membranes became fragile were observed when further increasing content of SSA, these blending membranes can not pursue a satisfied conductivity. Blends of PVA with sulfonic acid containing polymers have also been studied. PVA/PSSA blend membranes were investigated at various PSSA contents and annealing temperatures. (Wu et al., 2002) At 17 wt.% PSSA and annealing temperature of 110 ^{o}C, methanol crossover was half of Nafion®, but proton conductivity was an order of magnitude lower. Similarly, polymer blends of PVA and PSSA-MA were investigated, where introducing maleic acid reduced membrane swelling when compared with pure PSSA. (Kang et al., 2002 and 2005) Blending PVA with PSSA-MA (3:1 mol ratio) in a 1:1 weight ratio yielded proton conductivities as high as 0.095 S/cm and methanol permeabilities an order of magnitude lower than Nafion®. (Kang et al., 2005) In comparison to PVA/PSSA membranes, PVA/PSSA-MA membranes exhibited a 46% increase in proton conductivity and almost a 5-fold decrease in methanol permeability. SAXS results suggest that crosslinked PVA/PSSA-MA membranes possess narrower

ionic channels when compared with Nafion®, which the authors attribute to the decrease in methanol permeability. Some reports investigated PVA/PAMPS blends, where PVA was crosslinked with aldehydes (glutaraldehyde, n-butylaldehyde/terephthalaldehyde, n-hexylaldehyde/terephthalaldehyde, and n-octylaldehyde/terphthalaldehyde). (Qiao et al., 2005b) By using different auxiliary aldehydes, the crosslinking spacer length can be controlled, where an increased crosslinker spacer length resulted in an increase in water sorption. Furthermore, Qiao et al. (Qiao et al., 2005a) introduced poly(vinylpyrrolidone) (PVP) as a stabilizer into the PVA/PAMPS blends . They reported a proton conductivity of 0.088 S/cm (four-electrode) and a methanol permeability of 6.0×10^{-7} cm^2/s.

2.3.5.3 Pore-filling electrolyte membranes

A new membrane concept for fuel cell applications was proposed. Pore-filling membranes are composed of a porous substrate film, whose pores are filled with a polymer electrolyte (Fig. 2.10). Dividing the functions of the membrane into those of a substrate and a filling polymer is expected to induce better performance than can be developed using only single-component membranes. An electrolyte polymer with a proton conductive functional group, such as the sulfonic acid group, used to fill the pores of the substrate, is expected high proton conductivity. A strong and rigid film used as a porous substrate allows the porous substrate matrix to mechanically prevent any excess swelling of the filling polymer.

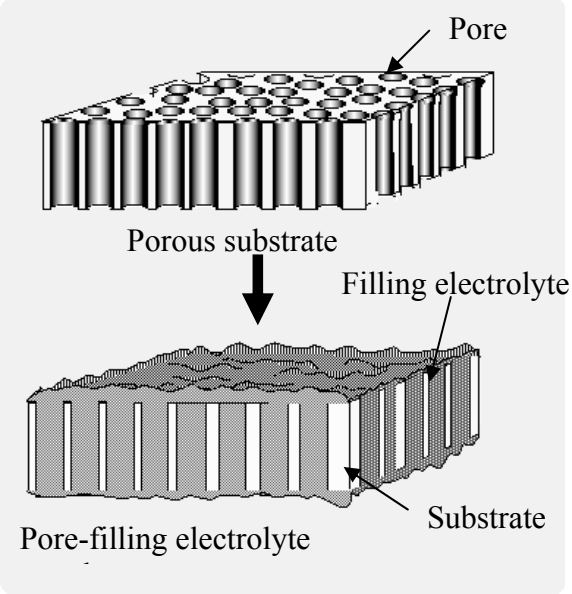

Figure 2.10 Schematic diagram of the concept of a pore-filling electrolyte membrane (Yamaguchi et al., 2003b)

In the earlier report, perfluorosulfonic acid polymers have been used to impregnate porous support membranes. (Penner et al., 1985 and Liu et al., 2001) And further the properties of these ionomers in confined spaces and the effect of the porous material on the behaviour of the membranes have also been studied recently (Rodgers et al., 2008). However, such membrane cannot suppress membrane swelling. Therefore Yamaguchi's groups have focused on this research area to develop this kind of pore-filling electrolyte membranes for a few years. Poly(acrylic acid) (PAA) (Yamaguchi et al., 2003b), poly(vinylsulfonic acid/co-acrylic acid) (PAAVS) (Nishimura and Yamaguchi 2004), poly(acrylamid tert-butyl sulfonic acid) (PATBS) (Nishimura and Yamaguchi 2004; Yamaguchi et al., 2003a), and poly(2-acrylamido-2-methyl-1-propanesulfonic acid) (PAMPS) crosslinked with *N, N'*-methylenebisacrylamide (MBA) (Kanamura et al., 2005) have been used as the filling electrolyte polymers to be introduced into porous silica

(Kanamura et al., 2005), porous poly(tetrafluroroethylene) (PTFE) (Yamaguchi et al., 2003a), porous cross-linked high-density polyethylene (CLPE) (Nishimura and Yamaguchi 2004), polyimide (PI) as the substrate respectively with impregnation polymerization method. For such composite membranes, porous substrates can suppress membrane swelling and then reduce the methanol permeability of membranes. The filling polymer having high sulfonic acid content can show high proton conductivity. The relationship between the proton conductivity and the methanol permeability of a single pore-filling polymer can be controlled by changing the substrate strength and pore-filling ratio. Further this can control the membrane performance for a given fuel cell application.

2.4 Proton transport mechanism

At a molecular level the proton transport mechanism is usually described as the lone proton migration mechanism and proton-carrying mechanisms. (Colomban, 1992) The lone proton migration mechanism (proton translocation or Grotthuss process) is following the process: (a) displacement of H^+ along a hydrogen bond and (b) transport of the H^+ ion form this hydrogen bond to the following one. For the proton-carrying mechanisms (the vehicle mechanism), the proton migrates in one direction as OH_3^+, NH_4^+, etc. bonded to a "vehicle" such as H_2O, NH_3 etc. whereas the "unladen" vehicles move in the opposite direction. For proton exchange membrane, one of the most difficult hurdles facing the development of novel PEM is understanding the proton transport mechanism. Proton conduction in proton exchange membrane is complicated and strongly dependent on humidity, the nature and content of acid as well as temperature.

2.4.1 hydrated acidic polymer membrane

Some polymer membranes containing functional acidic groups have extremely high proton conductivity in the hydrated state. Such membranes combine in one macromolecule the hydrophilic character of terminal acidic functional groups and the hydrophobicity of the polymer backbone. Especially in the presence of water, this leads to some hydrophilic/hydrophobic separation. While this hydrated hydrophilic domain carries the transport of water and protonic charge, the hydrophobic domain gives the material it's morphological. (Kreuer, 2001) The transport properties are determined by the confinement of water within the hydrophilic domain and the interaction with the acidic functional groups. Proton transport in water occurs by long proton migration mechanism and the proton-carrying mechanisms. At low water contents (low humidify), where the number of water/water contacts is significantly reduced compared with bulk water, hydrogen bonds are expected to be tightened. This is expected to lead to a reduced rate of bond breaking and forming processes and then the rate of proton transport is expected to be reduced by water confinement in the hydrophilic domain. Furthermore, the interaction of the water molecules with the acidic functional groups polarizes the protons in the hydrogen bonds towards the acidic anion, i. e. the hydrogen bonds, which are on average symmetrical in bulk water, become biased in this environment which can lead to a decreased activation enthalpy and therefore also to a improved rate of proton mobility. (Tuckerman, et al., 1997 and Kreuer, 2000)

2.4.2 Anhydrous acidic polymer membrane

Anhydrous proton-conducting polymer membranes usually consist of a polymer matrix (base) with an appropriate proton solvent. In particular, composite membranes of strong acids, such as phosphoric acid or sulfuric acid, and basic heterocyclic molecules, such as imidazole and benzimidazole, have been found to show high proton conductivity under anhydrous (low humidity) and intermediate-temperature conditions. The proton transport of an acid – base composite membrane under anhydrous or low-humidity conditions is supposed to occur by a Grotthuss mechanism or proton sweeping mechanism, in which only protons are mobile from site to site without the presence of diffusible water molecules, such as H_3O^+ or $H_5O_2^+$. (Kreuer, 1996) Therefore, the molecular structure of the acid-base composite membrane is crucial for the rate of proton transport. (Goward et al., 2002; Munch et al., 2001 and Hickman et al., 1999) Namely, an existence of a proton conductive pathway in the membrane is one of the most important factors for the high conductivity. Most studies on a random proton-conductive pathway formed by simple mixing of acidic and basic molecules, such as embedding method to prepare H_3PO_4 or H_2SO_4 doping PBI or AB-PBI (Litt et al., 1999 and Wainright et al., 2003). For random proton-conductive pathway, at lower doping levels (x= 0-2, before the maximum protonation is reached,) H_3PO_4 protonates the nitrogen atom of the imino group of the PBI structure (Fig.2.11b). $H_2PO_4^-$ seems to be the predominant anion over the entire acid concentration range with the appearance of HPO_4^{2-} for small values of x (< 0.2) and H_3PO_4 for the highest values of x (> 1.2). Proton exchange mainly happens between protonated and nonprotonated imino nitrogen groups (N-H^+...N-H) (Fig. 2.11b) on

neighboring polymer chains, considering the distance of N atoms in one repeat unit of PBI. The T_g increases with increasing concentration of H_3PO_4 in the polymer. (Glipa et al., 1999 and Bouchet et al., 1999) Membranes with phosphoric acid in the range of doping levels of $0 < x < 2$ have too low a conductivity to be used as electrolytes in fuel cells. After the maximum degree of protonation is reached (x=2), excess acid exists in the membranes. However, for $x < 3$, there is not much excess H_3PO_4, and the average P-P distance is larger than the N-N distance and too large to allow proton jumps between the anions. Therefore, it can be suggested that the proton conductivity in acid-doped PBI in this doping range would rather result from a cooperative motion of two protons along the polymer-anion chain by the Grotthuss mechanism (Fig. 2.11c). With increasing doping level, there is more excess H_3PO_4. Now, protons migrate along the mixed $H_2PO_4^-$ ...H_3PO_4 and N-H^+...$H_2PO_4^-$ anionic chains by successive proton transfer and anion reorientation steps (Fig. 2.11d) For $x > 4.2$, the further addition of H_3PO_4 leads to excess acid in the polymer, which has an NMR spectrum very similar to that given by pure phosphoric acid. Proton migration happens mainly along the acid and anion chain ($H_2PO_4^-$ H^+...$H_2PO_4^-$) (Fig. 2.11d) depending on the water content. Conductivity is increasing with doping level. In this case, the conductivity mechanism is more like that of a concentrated H_3PO_4 solution (Grotthuss mechanism). With these doping levels, the membranes have high conductivity and are most suitable for fuel cells. (Ma et al., 2004)

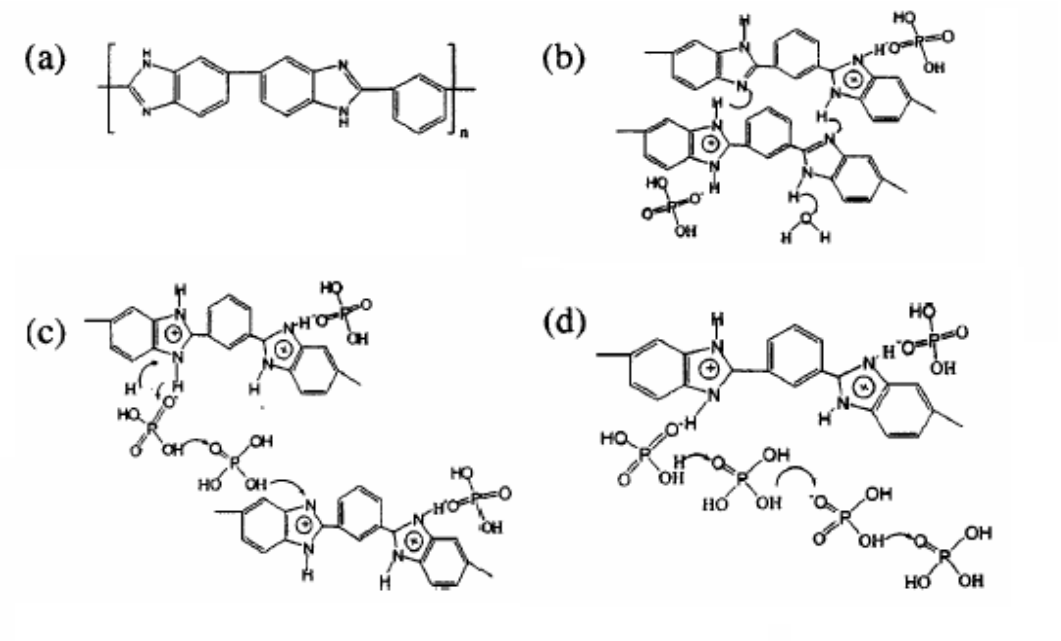

Figure 2.11 Chemical structure of (a) polybenzimidazole (PBI), (b) H_3PO_4 protonated PBI, (c) proton transfer along acid-PBI-acid, (d) proton transfer along acid-acid (Ma et al., 2004)

However, this random proton-conductive pathway does not provide the maximum conductivity that can reached for that acid-base complex. Recently, it has been reported that a self-assembled acid-base complex membrane consisting of acidic and basic molecules. Yamada and Honma (Yamada and Honma, 2004) studied a kind of lamellar composite material with a highly ordered molecular array through the hybridization of acidic surfactant monododecyl phosphate (MDP) and basic surfactant 2-undecylimidzole (UI) molecules (Fig. 2.12). In this case, the transport of the proton can form protonated molecules to nonprotonated molecules. Therefore, the distance between the acidic and basic molecules is important for the formation of an effective proton-conducting pathway in an acid-base composite material.

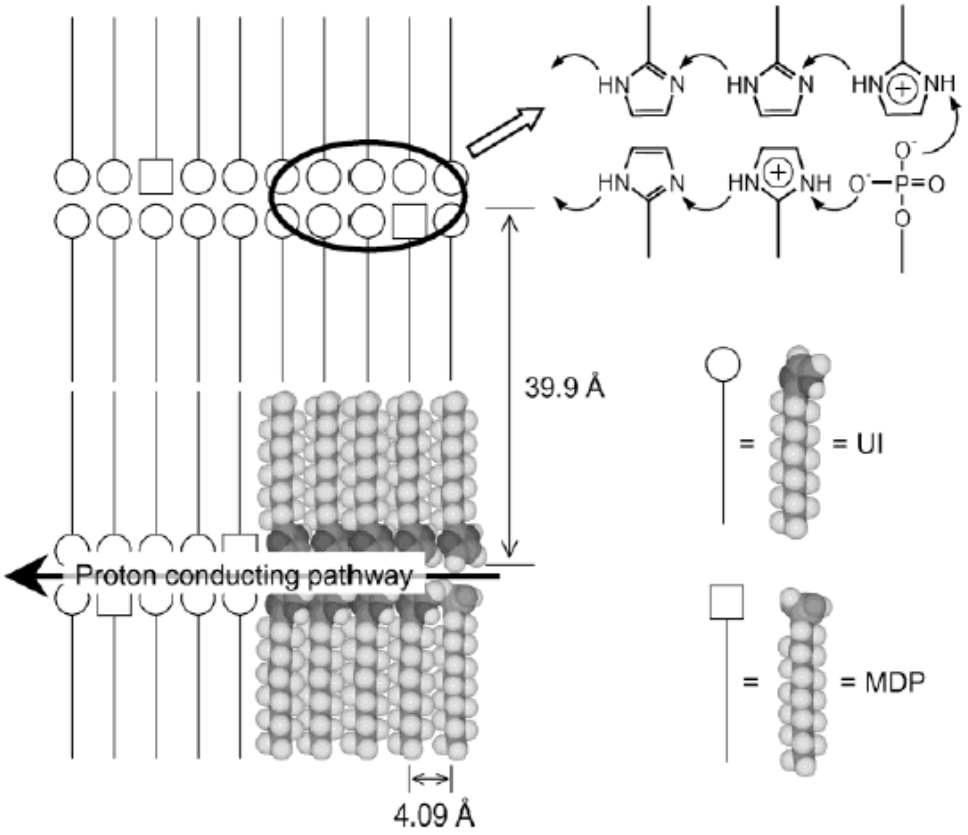

Figure 2.12 Structural model of UI-MDP composite materials. The UI and MDP molecules construct the highly ordered lamellar structure with the proton-conducting pathway. UI and MDP molecules indicate the space-filling and line-drawings models. The insert shows the proton-conducting mechanism in the two-dimensional proton-conducting pathway. (Yamada and Honma, 2004)

The other mechanism has been studied for anhydrous polymer material. Zhang et al. (Zhang et al., 2006) reported that two types of ionic monomers, one sodium 3-sulfopropylacrylate, potassium salt (SPA-K) bearing anionic $-SO_3$ group and the other *N, N'*-methyl-(6-hexylcarbamatoethylmethacrylate) imidazolonium bromide (EMACI) bearing cationic quaternary imidazole group, were grafted to nano silica particles (~7nm) via the heterogeneous ATRP. Grafted particles were then incorporated individually into Nafion membrane and then showed great promoting effect on proton-conductivity of the

membrane in anhydrous state due to noticeable proton-sweeping effect of the copolymeric grafted chains (Fig. 2.13).

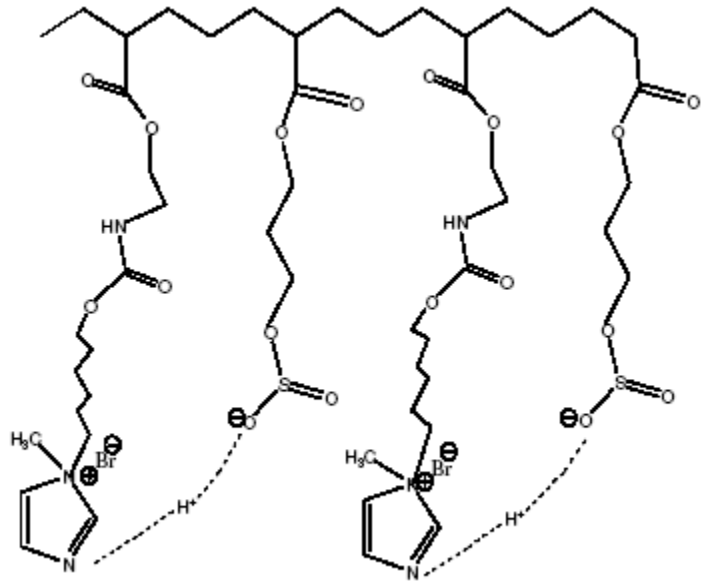

Figure 2.13 Proton sweeping transport scheme (Zhang et al., 2006)

2.4.3 Temperature

The temperature dependence of the conductivity in polymer electrolytes has been taken as an indication for a particular type of conduction mechanism. A distinction is generally made between systems that show the Arrhenius equation and those that present a curvature in log σ versus inverse temperature plots. In the latter case, empirical equations derived from the free volume theory have been used, as for example the Vogel-Tamman-Fulcher (VTF) equation. (Armand, 1983 and Patner, 1987) For a hopping-like conduction mechanism (Grotthuss type mechanism), the conductivity follows the Arrhenius equation,

$$\sigma = \sigma^0 \exp\left(\frac{-E_a}{RT}\right) = \frac{A}{T}\exp\left(\frac{-E_a}{RT}\right) \qquad \text{…… Equation 2.1}$$

Where, σ^0 and A are pre-exponential factors and E_a the activation energy. The VTF behavior is characteristic of the conductivity of amorphous phases or polymer segmental motion and the proton transport could be described as a vehicle mechanism. The equation was originally used to fit the viscosity data in molten glasses.

$$\sigma = \sigma_0 T^{-1/2} \exp\left[\frac{-B}{k(T - T_0)}\right] \qquad \text{…… Equation 2.2}$$

For proton exchange membrane, the conduction mechanism of membrane is, as known, dominated by polymer segmental motion (Vogel-Tamman-Fulcher (VTF) equation) at low water content. At high water content, the proton transport mechanism is much more liquid-like with some polymeric influence and showed an Arrhenius behavior. Therefore, the proton transfer is largely dependent on the water content in the membrane. However, for H_3PO_4 doped PBI membrane, the proton transport is mainly controlled by a "hopping" mechanism rather than by segmental motion at any controlled water content. (Fontanella et al., 1998) The activation energy for acid doped PBI membranes was approximately constant at the acid doping level of 0.2-3.05. (Ma et al., 2004 and He et al., 2003) This is because a correlation between the conductivity and the nature of the predominant anion associated to the polymer is suggested and the conductivity properly originates for the proton hopping the N-H sites of the polymer to the anions of phosphoric acid or vice versa, while the proton hopping from one N-H site to another of the polymer contributes little to the proton conductivity. When increasing doping level

above this range and up to 7, the conductivity and activation energy suggest a quasi-liquid like conduction of proton in the acid doped PBI membranes. For PBI composites with inorganic proton conductors such as ZrP, PWA and SiWA, the proton hopping mechanism still plays a dominant role for proton conduction. (He et al., 2003)

2.5 Characterization of PEM performance

2.5.1 Methanol crossover

To determine the methanol permeability of the membranes, a side-by-side diffusion cell (Fig. 2.14) was used usually, where the PEM is sandwiched between donor (upstream side) and receptor (downstream side) compartments. The donor compartment is charged with methanol (ca. 1-2 M) and the concentration of methanol is measured on the downstream side as a function of time. The permeability can be determined from the slope of the early time data, (Elabd et al., 2003) where a variety of detection methods have been used, including gas chromatography (Lee et al., 2005; Carretta et al., 2000; Yin et al., 2003 and Rhim et al., 2004) refractometry (Li et al., 2003; Shen et al., 2005; and Park et al., 2005), and FTIR-ATR spectroscopy (Elabd et al., 2003 and 2004). From the relationship between the methanol concentration in receptor compartment and the permeation time, methanol permeability, P was calculated by the following equation:

$$V_B \times \frac{dC_{B(t)}}{dt} = (D \times K) \times (C_A - C_B) \times \frac{A}{L} \qquad \ldots\ldots \text{ Equation 2.3}$$

$C_A \rangle\rangle C_{B(t)}$

$$C_{B(t)} = \frac{P \times C_A \times A}{V_B \times L} \times t \text{, where } P = D \times K \qquad \text{…… Equation 2.4}$$

Where C_B is the methanol concentration in the receptor compartment; C_A, the methanol concentration in the donor compartment; D, the diffusion coefficient; K, the partition coefficient between the membrane and the adjacent solution; t, is the permeation time; A, is the exposed area of the membrane; L, the thickness of the membrane, and V_B, the solution volume of the receptor compartment.

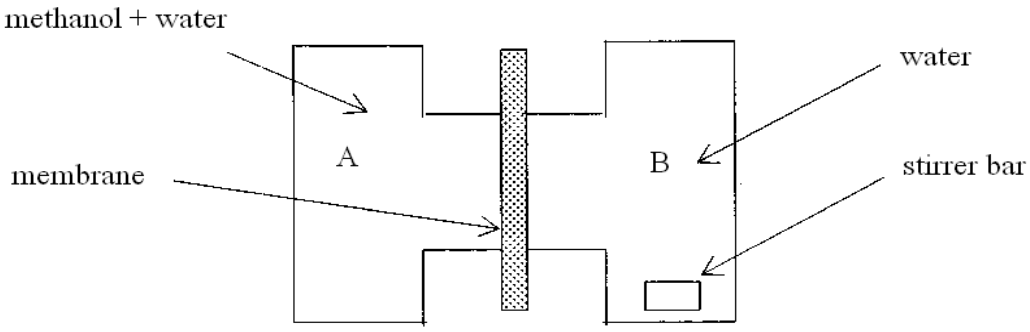

Figure 2.14 Experiment setup for membrane methanol permeability measurement

One of the drawbacks of the diffusion cell is that a potential difference is not applied, and therefore, the permeability of methanol determined may be different to the crossover experienced in the DMFC. Several researchers have developed techniques to determine the methanol permeability in electrochemical cells using a variety of techniques, such as measuring CO_2 formation at the anode (Saarinen et al., 2005) or crossover current. (Ravikumar et al., 1996; Xu et al., 2004 and Ren et al., 2000a) The crossover current can

be extracted from the DMFC potential, where the performance of a DMFC can be modeled as:

$$V_{cell} = E_{cell} - \eta_{an} - \eta_{cat} - \eta_{xover} - \eta_{ohmic} \qquad \text{…… Equation 2.5}$$

V_{cell} is the cell voltage, E_{cell} is the different between the half-cell potentials of the anode and cathode at the reference current density i_0, η_{an} and η_{cat} are the anode and cathode overpotentials, respectively, η_{xover} is the methanol crossover overpotential, and η_{ohmic} is the ohmic overpotential. The crossover overpotential is proportional to the flux of methanol through the membrane, which is governed by methanol concentration, pressure gradient, and electroosmosis:

$$\eta_{xover} = \chi j_2 \qquad \text{…… Equation 2.6}$$

Where χ is a lumped term constant. From this relationship and the following expression, the methanol permeability can be determined experimentally (Shao et al., 2002 and Ren et al., 2000):

$$i_{cross} = i_d \frac{6\xi x_o}{\ln(1 + 6\xi x_o)} \qquad \text{…… Equation 2.7}$$

Where i_d is the limiting methanol permeation current density measured voltammetrically, ξ is the electroosmotic drag coefficient of protons in the membrane, and x_o is the molar

fraction of methanol in the feed stream. The experiment entails exposing the anode side of the MEA to a known concentration of methanol and the cathode side to a humidified nitrogen environment. (Ge et al., 2005) A dynamic potential (ca. 0.1-1 V at 1-2 mV/s) is applied to the cathode side, and the limiting methanol permeation current density is obtained by measuring the limiting current of the methanol electro-oxidation process at the platinum/membrane interface.

2.5.2 Conductivity

The proton conductivity of a polymer intended for the application in an electrochemical device is obviously an important parameter and has been calculated using the following equation by measuring the membrane resistance by direct current (D.C.) impedance and alternating current (A.C.) impedance.

$$\sigma = \frac{L}{RS} \qquad \text{…… Equation 2.8}$$

Where σ, L, R, and S denote the proton conductivity, thickness of membranes, the resistance of the membrane and the cross-sectional area of the membrane, respectively.

The D.C. method provides the most straightforward way for taking ionic conductivity of polymers. With a two-electrode cell, the polymer electrolyte is sandwiched between two metallic electrodes, so that a constant current flows around the circuit and through the cell upon application of a stable D.C. voltage. Despite the simplicity of the D.C. method, the interfacial resistances at the two electrodes are not negligible in comparison with the

bulk resistance of polymer electrolyte, therefore the D.C. method can not give the accurate electrolyte resistance. Although by adding the other two electrodes (four-terminal method) it is possible to eliminate the influence from the electrode/electrolyte interface on the measurement outcome, it is often difficult to obtain sufficiently reversible electrode reactions that remain stable over a wide temperature range. In contrast to the D.C. method, the ions are driven in one direction during the first half of an A.C. cycle and in the opposite direction during the second half-circle and so net build-up and depletion at the electrodes do not occur. Such phenomenon also leads that the cycle time is shorter compared with the diffusion rate of the ions. Moreover, the problems of concentration polarization which complicates D.C. measurement are also largely avoided if an alternating current is used. Therefore, with respect to the known A.C. techniques, the impedance spectroscopy has become the most popular method in the determination of the electrical properties of solid electrolytes. Electrochemical impedance spectroscopy (EIS) applies an A.C. over a broad frequency range, where the resistance of the membrane can be determined from the real impedance data (or the x-intercept of the regression of imaginary vs. real impedance data over a high frequency range). There are two methods for A.C. impedance which are two-electrode method and four-electrode method. Using the two-electrode method for polymer electrolyte membrane with a low resistance, a high frequency is needed to separate membrane resistance for interfacial capacitance. Electrochemical impedance spectroscopy (EIS) analysis of membranes can be performed to provide the impedance plots (Nyquist form) at a frequency range. In the Nyquist impedance plot (Fig. 2.15), the imaginary part (Z") of impedance is plotted as a function of its real component (Z') in the frequency range. (Walls et al., 2003) Using the

four-electrode method, impedance independent of frequency over the frequency range can be observed. This meant the membrane resistance can be separated from interfacial resistance in this frequency region. The resistance of the membrane is obtained from a Cole-Cole plot after checking the frequency region over which the impedance had a constant value. (Sone et al., 1996) Typically, a four-electrode technique is preferred over the two-electrode, because of the significant frequency dependence on impedance at low frequencies due to interfacial impedance for the two-electrode. However, the two-electrode technique measures the membrane impedance in the same direction as methanol transport, which is the direction that is relevant for the DMFC.

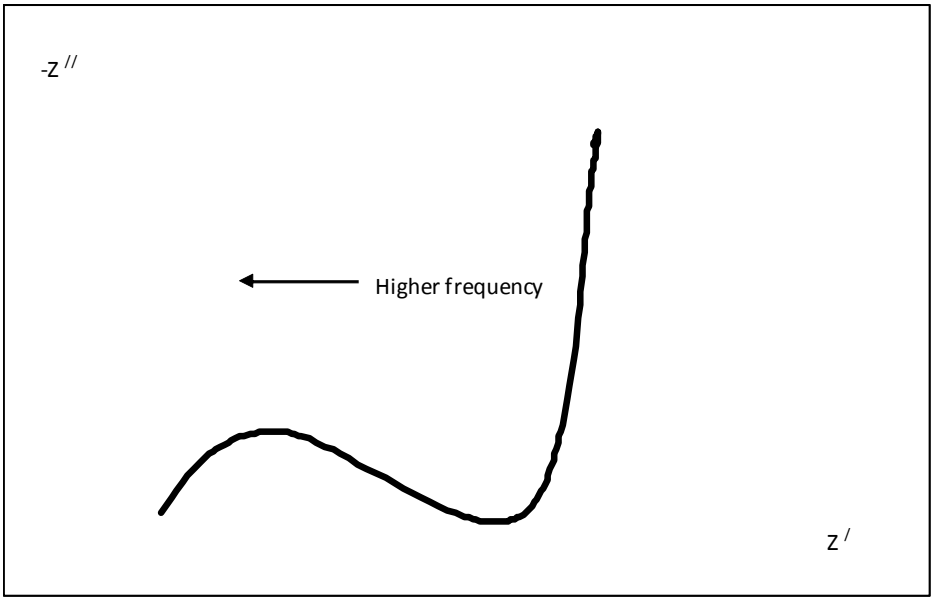

Figure 2.15 Impedance diagram of a typical polymer electrolyte with blocking electrodes

Moreover, it was reported that the proton conductivity for Nafion® 117 shows a 2.5-fold difference in conductivity between the two techniques: 0.067 S/cm and 0.027 S/cm for the four and two-electrode techniques, respectively. (Elabd et al., 2003 and 2004) These

values are similar to other values reported in literature for Nafion® 117 using these two techniques at similar temperatures: 0.067 S/cm, (Gardner and Anantaraman, 1995) 0.061 S/cm, (Fontanella et al., 1993) 0.054-0.082 S/cm, (Tricoli et al., 2000) for the four-electrode technique; and 0.024 S/cm, (Gardner et al., 1995) 0.022 S/cm, (Pourcelly et al., 1990) for the two-electrode technique. Some researchers suggest that the differences are primarily due to the differences in the two techniques, while others suggest that there may be a slight ionic micro-domain orientation during the commercial extrusion process of Nafion® membranes causing this effect. However, the differences between these techniques should be considered more thoroughly when investigating other PEMs. A study by Elabd et al. (Elabd et al., 2003) demonstrates an order of magnitude reduction in proton conductivity, when comparing the two-electrode technique with the four-electrode technique, for sulfonated block copolymer membranes with a lamellar morphology with a preferred orientation in the plane of the membrane. The conductivity difference using the two techniques is about 5-10 times larger than Nafion® 117. Other investigations have demonstrated similar relationships between conductivity and structure in self-assembled oriented polymer systems. Moreover, it is reported that palladium coated Nafion® membranes has a proton conductivity of 0.11 S/cm using the four-electrode technique. However, from other three studies (Li et al., 2003; Kim et al., 2003 and Tang et al., 2005), similar membranes are reported to provide proton conductivities ranging from 0.003 to 0.02 S/cm using the two-electrode technique. These reports highlight the importance of cautiously interpreting conductivity results in this field and stress the importance of critically examining transport data as it relates to polymer structure.

2.5.3 Single cell performance

The performance of a fuel cell device can be summarized with a graph of its current voltage characteristics. (Fig. 2.16) This graph, called a polarization (*i*-V) curve, shows the voltage output of the fuel cell for a given current output. The current has to be normalized by the area of the fuel cell, giving a current density. An ideal fuel cell would supply any amount of current (as long as it is supplied with sufficient fuel) while maintaining a constant voltage determined by thermodynamics. In practice, however, the actual voltage output of a real fuel cell is less than the ideal thermodynamically predicted voltage. There are three major types of fuel cell losses, activation losses (losses due to electrochemical reaction), ohmic losses (losses due to ionic and electronic conduction, and concentration losses (losses due to mass transport), which give a fuel cell *i*-V curve its characteristic shape. Furthermore, the more current that is drawn from a real fuel cell, the lower the voltage output of the cell, limiting the total power that can be delivered. The power (*P*) delivered by a fuel cell is given by the product of current and voltage:

$P = i \times V$ …… Equation 2.9

A fuel cell power density curve (Fig. 2.17), which gives the power density delivered by a fuel cell as a function of the current density, can be constructed from the information in a fuel cell *i*-V curve.

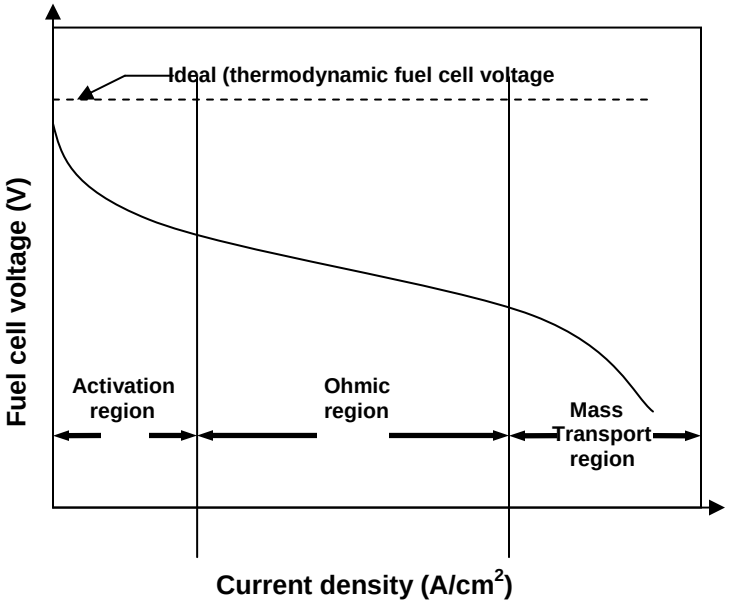

Figure 2.16 Schematic of fuel cell *i*-V curve

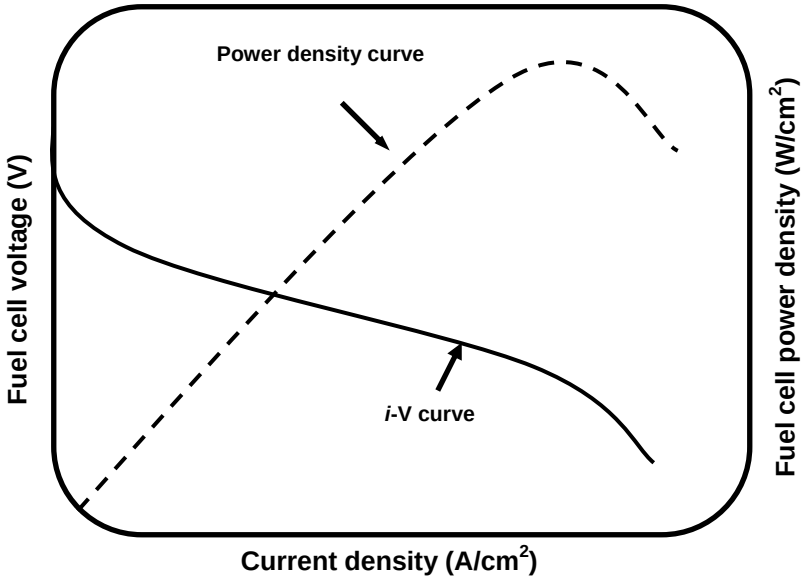

Figure 2.17 Combine fuel cell *i*-V and power density curves

Of these three major types of fuel cell losses, ohmic losses are crucial for evaluating the performance of proton exchange membrane. Fuel cell resistance contributions are additive from a few parts, electrical interconnections, anode electrode, cathode electrode, anode catalyst layer, cathode catalyst layer, electrolyte, and so on. An investigation of the various contributions to fuel cell resistance reveals that the electrolyte component to fuel cell resistance usually dominates. (O'Hayre et al., 2006) Therefore, recently, many reports have introduced single cell test to evaluate performance of their proton exchange membranes. Moreover, good mechanical and thermal properties of membranes are necessary for the fuel cell test, (Harrison et al., 2005 and Xiao et al., 2005a) because the membranes have to bear the pressure charged on the membrane electrode assemblies (MEAs). Besides, the membranes with good mechanical properties can also maintain the performance during a long operation time. In addition, hot pressing of fuel cell electrodes onto the membranes to form membrane electrode assemblies (MEA) has been reported. Such pressing can make the Nafion®-based electrodes to adhere sufficiently well to the membrane to form robust MEAs and improve fuel cell performance. (Wilson, 1993)

CHAPTER 3

INTERFACIAL BEHAVIORS OF DENSELY ANCHORED HYDROPHILIC OLIGOMERIC CHAINS ON SILICA MICROSPHERES

3.1 Introduction

Developing a chemically grafted polymer thin layer at the surface of a solid substrate has paramount technological implications in different combinatorial chemical systems, which include protein separation by adsorption (Coad et al., 2006), electrophoretic deposition (Pallandre et al., 2006), immobilization of bio-molecules (Padeste et al., 2006), and functional additives to various polymer formulations (Rong et al., 2001). Among various chemical means that have been developed to graft functional polymer chains to a solid surface, the atom transfer radical polymerization (ATRP) method is unique because it allows the control of polymer chain length via "living" polymerization mechanism. There is an increasing trend in recent years of performing ATRP on insoluble particles to grow a uniform and dense polymer layer on them; the main vinyl monomers that have been used include styrene, methyl methacrylate, *t*-butylacrylate, 2-hydroxyethylacrylate, 2-(methacryloyloxy)ethyl trimethyl ammonium chloride and so on (Vestal et al., 2002;

Werne et al., 1999 and 2001; Percy et al., 2003; Pyun et al., 2003 and Pantoustier et al., 2003)

The interfacial properties of densely packed oligomeric chains whose one-end are covalently bound to the surface of inorganic particles have not yet received adequate attention to date. This is because the conventional graft polymerization via attaching pre-formed polymer chains to a specific kind of organic anchor on the desired particles or via initiating random radical polymerization by surface-bound peroxide groups which are created by physical means will be normally not able to achieve a dense and uniform grafting polymer layer. (Bhat et al., 2006 and Ikada 1994) In addition, it is even more difficult through the conventional ways to graft di-block copolymer chains to the surface of particles so a copolymer double layer could not be achieved. This is, however, feasible by means of ATRP, which allows the creation of block copolymers not only in solution (Wang et al., 2005; Huang et al., 2005 and Shunmugam et al., 200 5) but also on insoluble substrates (Jia et al., 2005 and Xu et al., 2005). Such synthesized colloid particles are well defined so they can be applied for the studies of interfacial properties and colloidal behaviors.

In this work, trisiloxyl(1, 2-dibromoethyl) groups (≥Si-$CHBrCH_2Br$) are anchored to the surface of silica microspheres as initiating sites where ATRP takes place. The monomers used include an anionic monomer, Sodium 4-styrenesulfonate (SSNa), and a proton-acceptor monomer, 4-vinylpyridine (4VP). Therefore four types of grafting chain structures could be achieved: the homopolymers of SSNa and 4VP, and the block

copolymers in which the PSSNa and P4VP blocks are alternatively used as the interior block being anchored to the silica surface. The particular traits of these core-shell particles include glass transition behaviors of the densely grafted polymer layer, as well as different responses of hydrodynamic volume and ζ potential of the particles to the change of solvating power and pH values of the dispersion media. We also examine how the ionic transport in the designated liquid medium is affected by the solvated particles with a substantially low volume fraction. It is found that the extent of salvation on the inner polymer block affects the stretching of the exterior copolymer blocks, and hence the solvating extents of the copolymer chains in turn reveal different capabilities to channel conduction of ions in the liquid media of interest. On the whole, the interfacial properties can be related to the presence of a thick interfacial polymer layer and the reversed sequences of the PSSNa and P4VP blocks.

3.2 Experimental

3.2.1 Materials

Tetraethyl orthosilicate (TEOS, Fluka, > 98.0%) and Triethoxyvinylsilicane (TEVS, Aldrich, > 97%), Ammonia (Merck, 25%), Cetyltrimethyl ammonium chloride (CTACl, Aldrich, 25% solution in water), Bromine (Mallinckrodt, AR®), Copper (I) bromide (Aldrich, 98%), Sodium 4-styrenesulfonate (SSNa Aldrich) and 4-vinylpyridine (4VP, Aldrich, 95%), 2, 2′-Bipyridyl (Bpy, Fluka, ≥ 99%) were used as received.

3.2.2 Synthesis of 1, 2-di-bromoethyl pendant group on silica microspheres

A given amount of aqueous solution (10 ml, 25%) of cetyltrimethyl ammonium chloride (CTACl), de-ionized water (15 ml) and pure methanol (10 ml) were added into a 100 ml beaker with stirring. After the mixture converted to a homogenous solution, tetraethyl orthosilicate (TEOS, 6 ml, 98%) and triethoxyvinylsilicane (TEVS, 4 ml, 97%) were added into this solution subsequently, which was followed by introduction of ammonia solution (3 ml, 25%) dropwise under vigorous stirring. The resulting solution was stirred for 18 h and kept still at 80 ºC for 3 days for aging the resultant colloidal dispersion. A white vinyl-silica powder was finally obtained after the precipitate was washed twice in a mixed solvent of methanol and hydrochloric acid (HCl) (37%) (v/v =10/1) at 90 ºC. This purifying manipulation with the aim to extract CTACl was repeated twice and each washing lasted 24 h. A whith vinyl-silica powder was obtained after drying, which was identified, according to elemental analysis, to contain pendant vinyl group of 8.3 mmol/g. The given amount of the vinyl-silica powder (0.5 g) was then dispersed in chloroform (5 ml) in a round bottom flask. To the resulting suspension (0-5 ºC) under vigorous stirring, a bromine solution containing Br_2 of 19.5 mmol in chloroform (Br_2:$CHCl_3$=1:5 by volume) was slowly dropped in and the addition reaction was completed within 30 min. The brominated vinyl-silica powder was then purified by washing in pure chloroform three times to remove the adsorbed bromine. The brominated powder displays the characteristic IR absorption peaks of 1, 2-dibromoethyl group at υ_{C-Br} (567 cm^{-1}) and υ_{C-H} (2989 cm^{-1}). According to elemental analysis of 1, 2-dibromoethyl-SiO_2 powder, the equivalent of R-Br group in the resulting powder was 7.1 mmol per gram.

3.2.3 Grafting ionomer chains to 1, 2-di-bromoethyl silica particles through ATRP

In a typical batch of polymerization, the 1, 2-bromoethyl-SiO_2 particles (0.15 g, ca. 1.1 mmol R-Br) was dispersed in a water/methanol mixture (12ml, v/v = 3:1). The monomer SSNa (0.5 g, 2.4 mmol) and 2, 2'-bipyridyl (0.03 g, 0.2 mmol) were then added to this dispersion. The mixture was purged by N_2 for 30 min with continuous stirring at temperature 35-40 °C, and CuBr (0.06 g, 0.4 mmol) was then introduced into the dispersion. The reaction mixture was stirred for 4 h and quenched by air. The blue sediment was then washed in doubly Millipore water and centrifuged at 6000 rpm for 15 min. This purifying procedure was repeated 3 times to clean up the catalyst residues as well as the monomer left from the PSSNa-grafted silica particles. In the case of constructing the pendant di-block P(SSNa-co-4VP)-b copolymer chains, 4VP was added to the ATRP system where SiO_2-P(SSNa)-Br macroinitiator had been formed in advance, and the subsequent polymerization was carried out in the next 4 h. As to the chain composition, a molar ratio of SSNa to 4VP=3/2 in the monomer feed was set. Similarly, the sequence of these two blocks was swapped by introducing 4VP first and then SSNa into ATRP system to obtain the pendant P(4VP-co-SSNa)-b di-block copolymer chains. The samples synthesized are listed in Table 3.1.

3.2.4 Instrumental characterizations

The infrared spectra of the grafted silica powders obtained from the three synthetic stages were recorded on a spectrophotometer (Bio-Rad FTIR model 400). The bromination

extent of vinyl-silica powder was determined by both elemental analysis (PE 2400 Series II CHN analyzer from Perkin-Elmer) and EDX scanning (JGM-6700F from JEOL). The images of core-shell structure of the polyelectrolyte-silica microspheres were taken on a TEM instrument at 200 kV (JEM-2010). The glass transition behaviors of the grafted polymer layer on silica particles were recorded on a DSC set (Mettler Toledo DSC 822e) using heating rate of 10 ^{o}C/min. In order to remove those chain motion barriers left behind by the different thermal histories of sample preparation, all samples were scanned from room temperature to 100 ^{o}C and cooled down to -20 ^{o}C at the same rate, and then subjected to the second scan, of which the energy vs. temperature profiles were recorded, respectively. The influence of pH or the solvent polarity of the dispersion medium on the hydrodynamic dimension of the samples was investigated by dynamic light scattering (DLS, Brookhaven Instruments 90Plus particle size analyzer). The variation of interfacial charge, with the change of pH, due to the presence of the grafted ionomer layer was investigated by Zeta potential measurement (BIC Zetaplus zeta potential analyzer).

3.2.5 Measurement of molecular weight of the grafted polymer chains

The four grafted samples (ca.100 mg) were dispersed in 1ml aqueous HF (5%), and the suspension was stirred at room temperature for 4 h to allow dissolving the silica network. The grafted polymer chains from the disbanded particles became soluble in the HF solution. The resulting polymer solution was then diluted 10 times by water and sent for the measurement of molecular weight by gel permeation chromatography (GPC). The GPC analysis (Waters 1515) used water as eluent (flow rate=1.0 ml/min at 25 ^{o}C) and the

PEG calibration standard for the determining of molecular weight of the polyelectrolyte chains.

3.2.6 Measurement of the ionic conductivity in the colloidal dispersions

The samples of polyelectrolyte-grafted particles (Table 3.1) were dispersed respectively in aqueous solution of HCl (pH=3) with the aid of ultrasonication to form a colloidal dispersion. Each dispersion was designed to have the solid content of 1 mg/ml (equivalent to ca. 0.01 vol. %) and transferred into a curette (1 cm×1 cm×4 cm) installed with two stainless steel electrodes. The electric conductivity of each suspension was measured using the electrochemical analyzer (Autolab Instrument, frequency scanning range 1 Hz ~100 kHz). Similarly, the other set of colloidal suspensions was prepared by using a binary mixture, *N, N'*-dimethyl foramide (DMF) and deionized (DI) water, as the dispersing medium. With respect to a particular powder, the ratio of DMF to water was also varied but the solid content was maintained the same.

3.3 Results and discussions

3.3.1 Implantation of ATRP initiating sites to SiO_2 particle

When the sol-gel reaction of TEOS and TEVS took place together inside microspherical droplets surrounded by surfactant molecules, CTACl, the vinyl-SiO_2 microsphere was generated and its TEM image showed that the particle had a dense core and a rather

porous thick shell wall surrounding the core (Fig. 3.1a, b). The porous shell was generated because it consists primarily of vinylsilane [(-O-)$_3$Si-CH=CH$_2$] units (Fig. 3.1c), which is caused by the discrepancy in the reactivity between TEVS and TEOS, the former being far less reactive than the latter to undertake sol-gel reaction (Brickner and Scherer 1990) and therefore the major portion of TEVS was used to constitute the outer layer of the microsphere.

According to elemental analysis of SiO_2-vinyl particles, the molar ratio of the pendant vinyl group to silicon in SiO_2-vinyl is about 0.4, and about 70% of the vinyl groups were brominated to form 1, 2-dibromoethyl groups according to the EDX surface analysis (Fig. 3.2). For the liquid phase ATRP α-bromoalkyl acetate (AcOCR'Br) is conventionally adopted as the initiator, and some recent reports (Liu et al., 2003 and Mori et al., 2002) showed that the initiator could be anchored to a solid substrate through alkoxylcarbonyl (-OCOCHRBr) linkage and therefore polymer chains could be grown from the surface-fastened α-bromoalkyl acetate groups. Compared with this traditional initiator, the pendant 1, 2-dibromoethyl initiator, which we developed in this work, leads to carbon-carbon bond but rather oxygen-carbon bond linkage between the initiator and the solid substrate. The carbon-carbon linkage is intact in an acidic or alkaline medium.

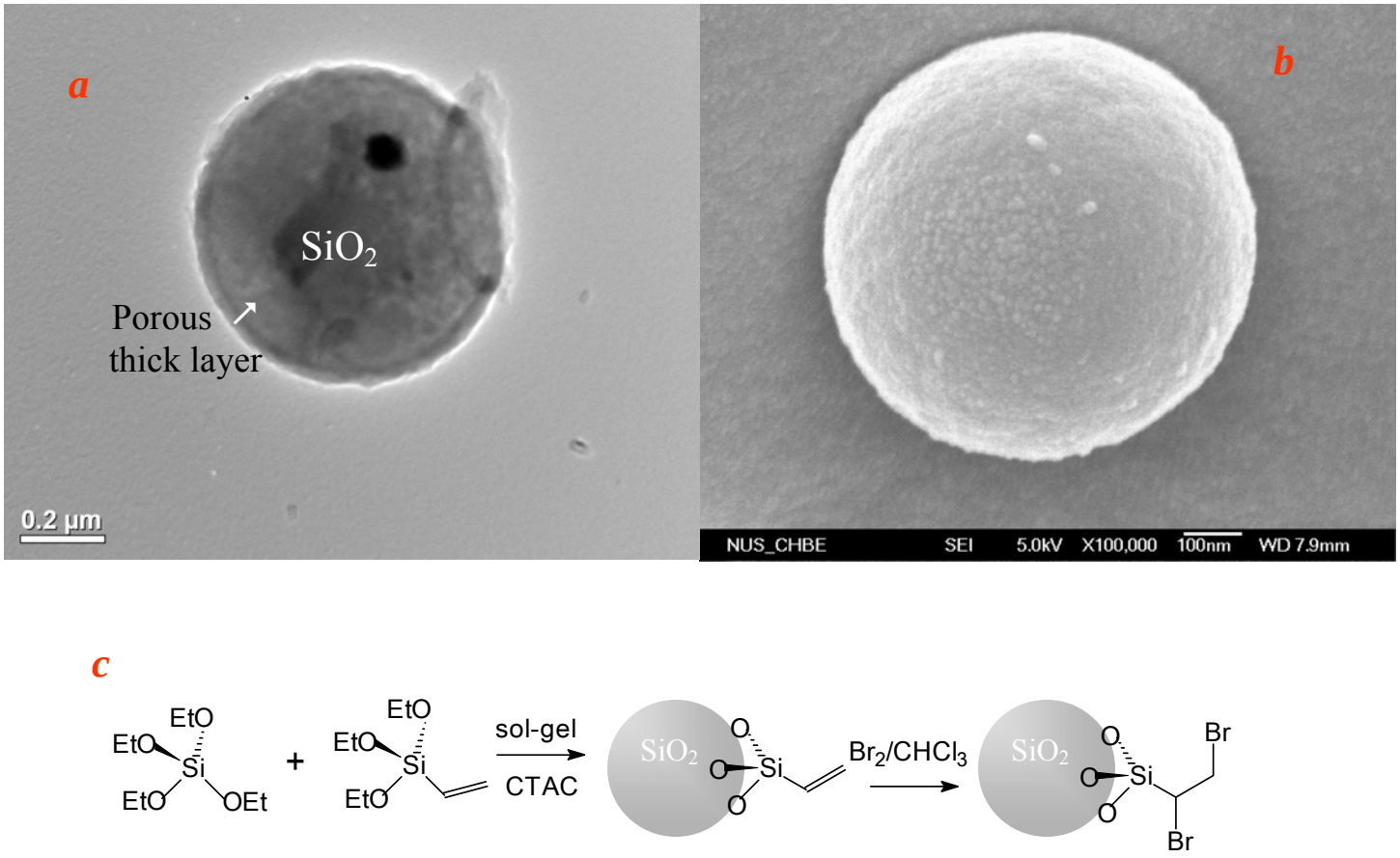

Figure 3.1 *a.* TEM image of vinyl-silica particle; b. FE-SEM image of vinyl-silica particle; c. The schematic of forming 1, 2-dibromoethyl-silica particle

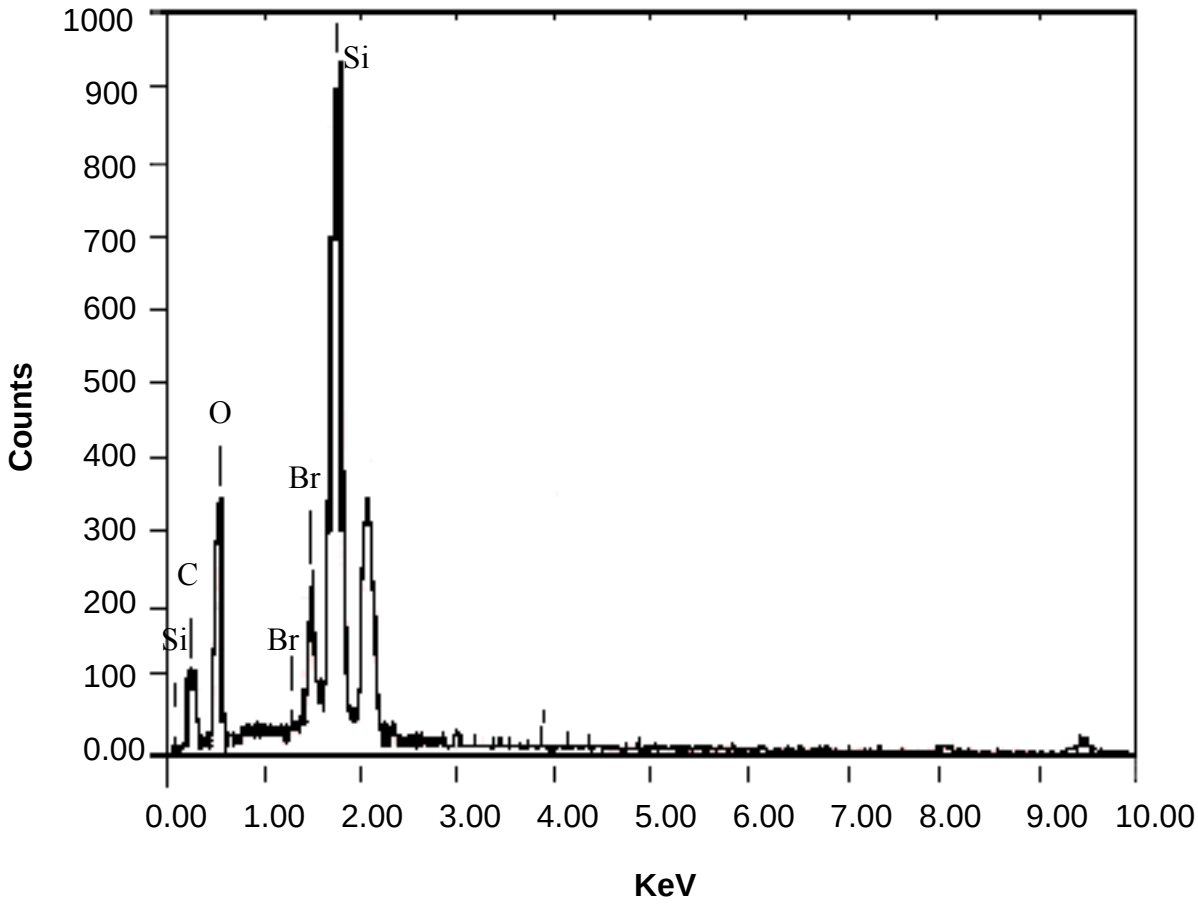

Figure 3.2 EDX spectrum of the brominated silica particles

3.3.2 The structural characteristics of the rigid core-soft shell microsphere

Our study finds that the maximum molar ratio of monomer to the catalyst [Cu(I)] in the feed of ATRP was about 6 and a higher ratio did not help increase the grafted chain length furthermore. Therefore, this ratio was employed to develop both homo-polymer and di-block copolymer chains (Table 3.1).

Table 3.1 The composition of the grafted SiO_2 particles

Sample	Average Molecular Weight	Ratio of Composition SSNa : 4VP
SiO_2-PSSNa	1323 Daltons	-
SiO_2-P(SSNa-co-4VP)-*b*	1015 Daltons	2:9
SiO_2-P(4VP-co-SSNa)-*b*	1050 Daltons	1:3
SiO_2-P4VP	1294 Daltons	-

The generation of short chains was likely due to the entanglement among the growing polymer chains in the porous shell layer of individual SiO_2 microsphere, on which the growing chains were rather cramped with the distending of polymerization. The chain propagating sites became more and more difficult to be accessed by monomers in the liquid phase. The similar phenomenon has also been reported recently (Chen et al., 2003), in which Chen et al. observed that the PSSNa-grafted silica particle has a relatively weak salt dependence that serves as an evidence of the low molecular weight of PSSNa chains. The above inference of oligomerization could be verified by the TEM image of the PSSNa-SiO_2 particle (Fig. 3.3), which exhibits an expanded layer and an irregular core contour in contrast to its precursor as showed in Fig. 3.1a. This morphology can be rationally attributed to the growth of oligomeric PSSNa chains on and underneath the surface of the particle, and as a result, the oligomeric chains expanded the $[(\text{-O-})_3\text{Si-R}]$ shell layer. As noted above, growing di-block copolymer chains on silica microsphere is

the other unique feature of ATRP. In this work two types of di-block copolymer chains, P(SSNa-co-4VP)-b and P(4VP-co-SSNa)-b, were realized, where suffix "-b" stands for the block type of copolymer. The P4VP block bears positive charges in an acidic medium because each 4VP unit is a proton acceptor, while PSSNa block carries negative charges in a neutral and weak alkaline aquatic medium. The IR spectrum of the SiO_2-P(SSNa-co-4VP)-b is taken an example to show the presence of both the 4VP and SSNa units (Fig. 3.4).

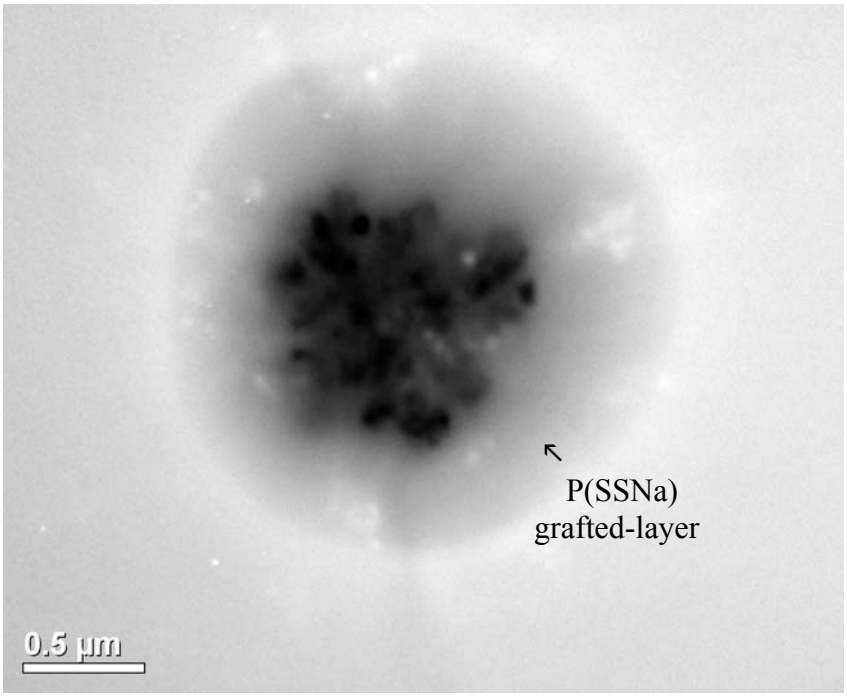

Figure 3.3 Transmission electron micrograph of a PSSNa-grafted silica particle

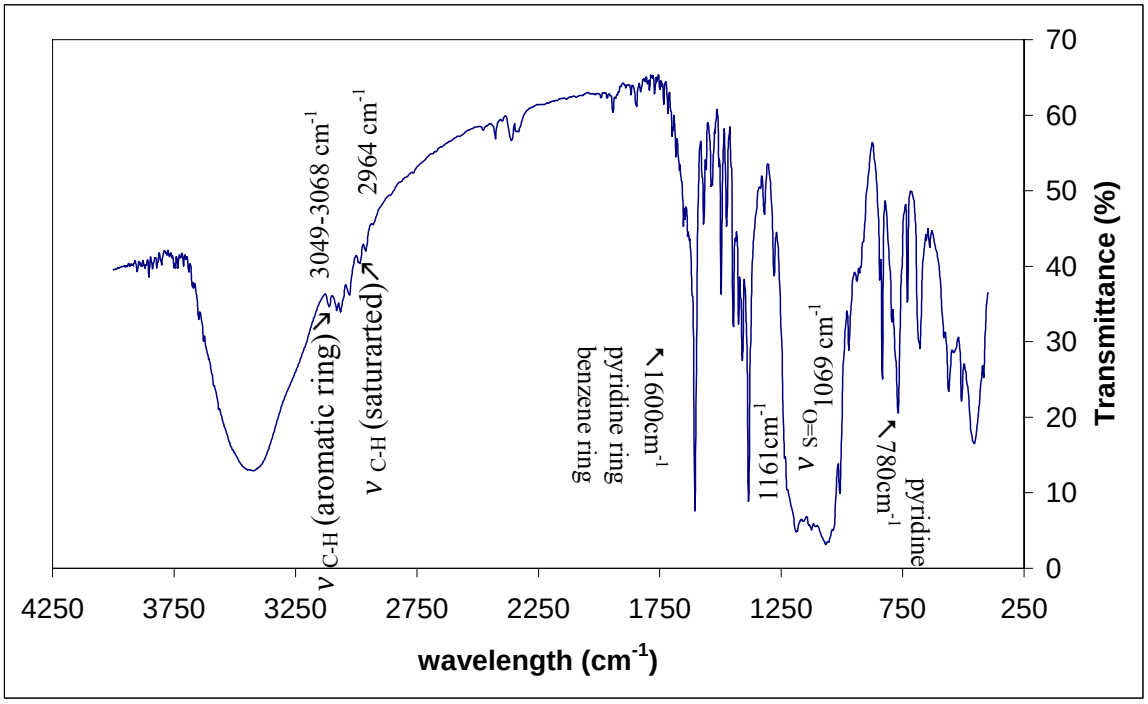

Figure 3.4 FT-IR spectrum of the copolymer-grafted silica particles

3.3.3 The unique response of the pendant polyelectrolyte short chains to thermal stimulus

The thermal analysis of the grafted oligomeric chains is an effective way to probe the particular polymer chain-chain interactions on the surface of SiO_2 beads. On the DSC diagram of SiO_2-vinyl particles an endothermic peak emerged at 138 ^oC (Fig. 3.5); it can be attributed to the creeping of the porous silica network. Besides this reference sample, an unbound homo-polymer sample, PSSNa ($\overline{M}_n \sim 10^4$), was the other reference used, which displays a steep glass transition (T_g) peak consisting of two slopes at 106 ^oC and 153 ^oC, respectively. Compared with the DSC profile of polystyrene, the presence of

para-substituted sulfonate group in benzene ring increases T_g of the segment motions (from ca. 104±2 ^oC to 106-139 ^oC). This strong polar association of sulfonate groups provokes an energy barrier appearing at 153 ^oC.

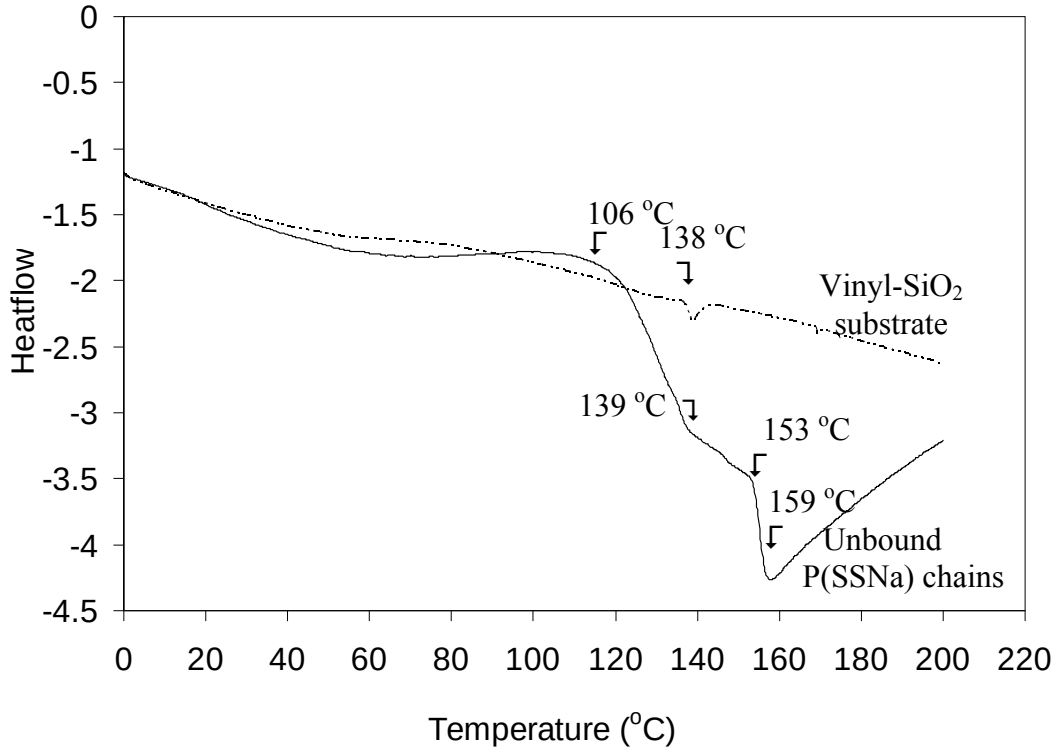

Figure 3.5 Differential scanning calorimetric (DSC) analysis of pure PSSNa and vinyl-silica

Furthermore the bound oligomeric PSSNa chains on silica particles reveal a higher segment motion barrier whose T_g appears at 123 ^oC in contrast to the foregoing 106 ^oC for the unbound PSSNa chains because most of the oligomeric chains are implanted in the rather stiff outer shell network, $[(-O-)_3Si-R]$, and this constraint environment also promotes the sulfonate group association, which shifts the onset of the corresponding glass transition temperature from 153 ^oC to 157 ^oC (Fig. 3.6). Alternatively, in view of the DSC diagram of SiO_2-P4VP, it exhibited an endothermic peak at 138 ^oC and a

shallow glass transition step at 166 ^{o}C, respectively. The first endothermic peak is known as the bulk characteristic of porous silica substrate as found on Fig. 3.5, whose intensity becomes stronger after ATRP, and the glass transition of the bound P4VP is higher than that of the unbound P4VP polymer that has T_g at 154 ^{o}C (Jian et al., 2001).

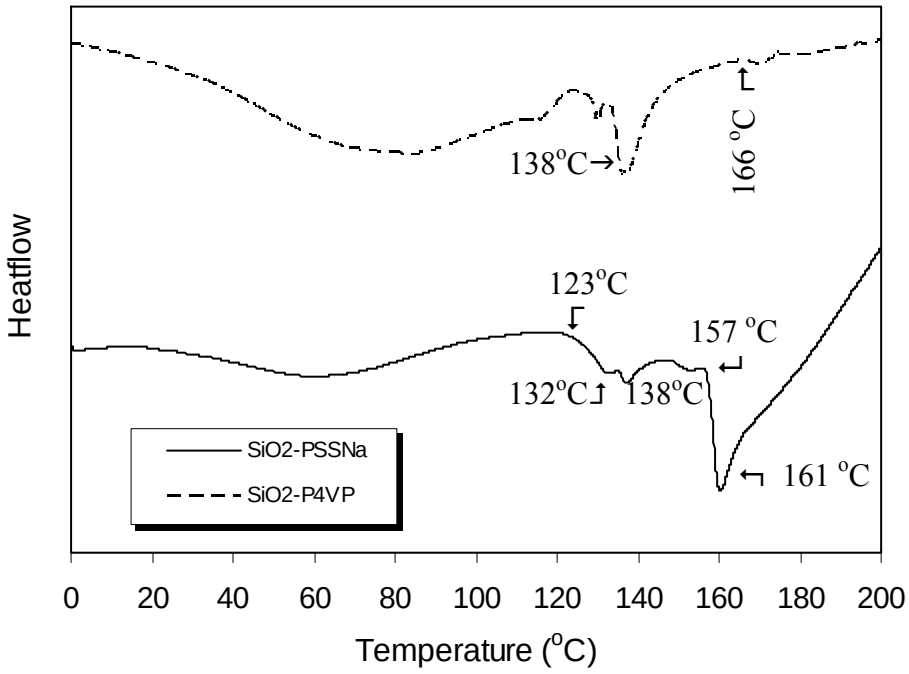

Figure 3.6 DSC analysis of the PSSNa and P4VP grafted silica particles

The glass transition diagrams of the two types of the two pendant di-block copolymer chain structures, SiO_2-P(SSNa-co-4VP)-b and SiO_2-P(4VP-co-SSNa)-b, show very different energy profiles (Fig. 3.7). For the former type, in which the SSNa blocks were fastened to the silica and the 4VP blocks comprise the outer layer, it displays rather analogous profile to SiO_2-P4VP. This phenomenon is due to the external location of the compositionally predominant P4VP blocks. On the contrary, for the latter type, it displays

an intricate T_g profile, of which the first two endothermic peaks (116 ^oC and 127 ^oC) seem to be generated from certain kind of mutual entanglements of the two blocks because they resemble neither of the their homo-polymeric forms. This is the result of the external location of PSSNa blocks and of the longer internal P4VP blocks (Table 3.1). It also deserves to note that a strong exothermic peak appears at 182 ^oC, which we assume is the result of temperature-driven complexation of the pendant 4VP groups with sodium ions, which migrate from the PSSNa blocks to P4VP block when the chain motions gain momentum at this temperature.

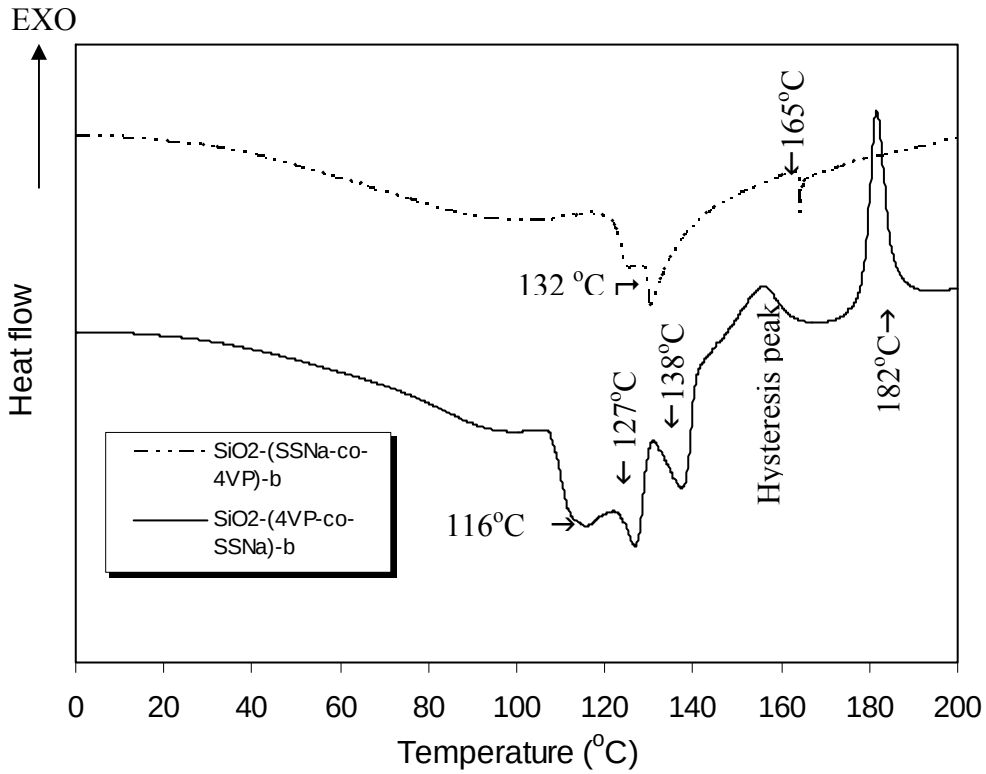

Figure 3.7 DSC analysis of the P(SSNa-co-4VP)-b and P(4VP-co-SSNa)-b grafted silica particles

3.3.4 The impacts of solvating power and pH on the hydrodynamic volume of the hybrid core-shell particles

In this section, we look into how the solvating behavior and surface charge of the hybrid core-shell particles affect their hydrodynamic volume determined by the dynamic light scattering (DLS) and zeta potential methods. Fig. 3.8 shows the mean sizes of the particles in the mixture of (H_2O-CH_3OH), which reflect different solvating extents of the grafted oligomeric chains in the dispersion media. For the two types of homo-polymer grafted particles (inset), SiO_2-P4VP and SiO_2-PSSNa, they exhibit very different response to the increase of methanol mole fraction (x). SiO_2-P4VP particles undergo a quick contraction in the range from pure water to $x = 0.2$, while SiO_2-PSSNa particles undergo a consistent contraction till $x = 0.5$. A certain portion of the pendant 4VP groups may be protonated in water (pH = 6.4) to form pyridinium and therefore the repulsive interactions of positive pyridinium groups sustain the greatest particle sizes of SiO_2-P4VP. But the partially protonated P4VP chains quickly exhibit lyophobic tendency with a slight increase in the content of methanol in the dispersion medium. According to the above comparison, the bound PSSNa chains are better solvated in the binary solvent than the bound P4VP chains due to the strongly hydrophilic sulfonate group. Nevertheless, with inspecting the two copolymers, we found that, in contrast to the exteriorly located PSSNa blocks, the exteriorly located P4VP blocks favored solvating of the polymer layer. This result implies that solvating of the inner blocks could mount the solvating extent of outer blocks. In other words, a lyophilic internal layer could enhance affinity of the external lyophobic blocks to the dispersion medium.

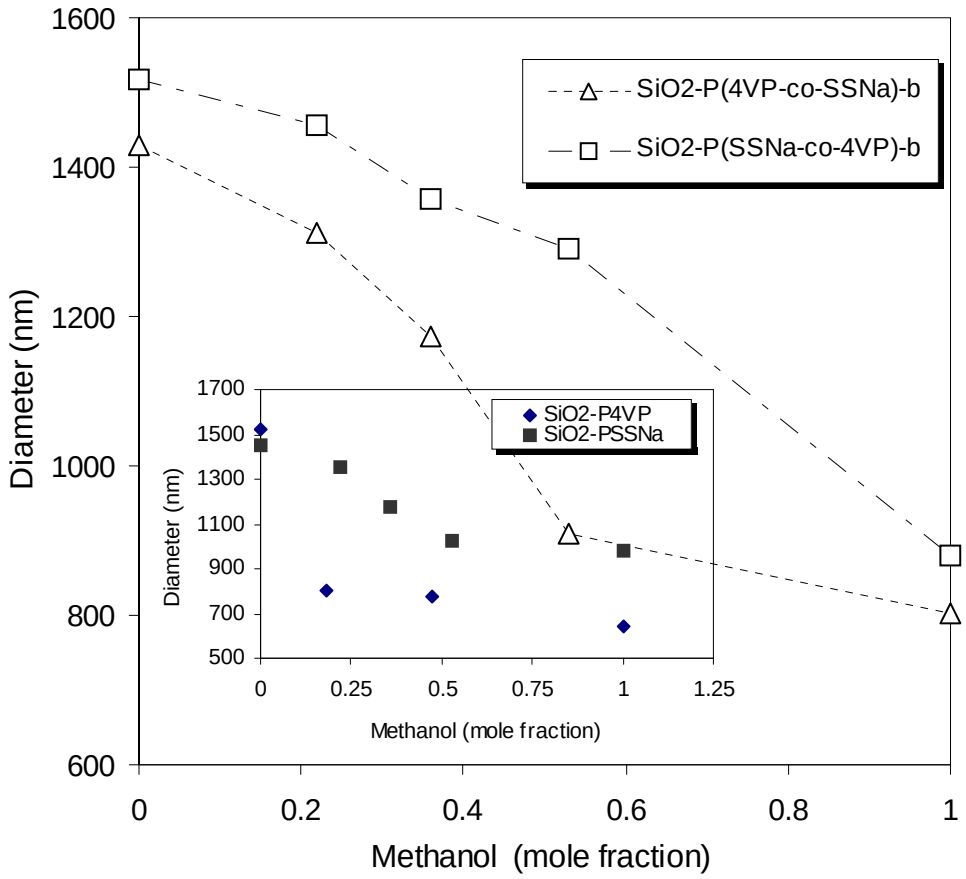

Figure 3.8 Variation of the mean dynamic diameter of P(SSNa-co-4VP)-b and P(4VP-co-SSNa)-b grafted silica particles with the methanol content in the aqueous dispersion medium. Inset represents PSSNa and P4VP grafted silica particles

With respect to the zeta potential measurement of the two homo-polymer-grafted types of particles (Fig. 3.9), as expected, SiO_2-P4VP exhibited positive ζ potential in aqueous medium with pH ≈ 6.4 because of the protonation as aforementioned, whereas the system exhibited negative ζ potential when pH > 6.4, which implies the occurrence of OH^- ion adsorption to the outmost pendant 4VP groups. The adsorption incurs a negatively charged slip plane of fluid (Cao, 2004) that moves as a part with the particle, which was sensed by ζ potential measurement. On the other hand, SiO_2-PSSNa exhibited negative ζ potentials at pH values above its isoelectric point (IEP) that happens at pH =1.3 because the sulfonic acid is strongly acidic. Hence the slip layer of fluid in this case would be

formed by the outmost sulfonate groups and hydrated water molecules. Similar ATRP brush particle systems have been previously investigated by Armes and Advincula (Percy et al., 2003 and Fulghum et al., 2006) In light of the relation of ζ potential vs. pH of the two copolymer-grafted particles, the phenomenon of partial charge neutralization between the two blocks was observed. For SiO_2-P(4VP-co-SSNa)-b particles, despite possessing a negatively charged outer PSSNa layer, its IEP occurs at almost pH=3 and hence its ζ-pH curve located quite above that of SiO_2-PSSNa in Fig. 3.9. On the other hand, SiO_2-P(SSNa-co-4VP)-b particles possess a thick P4VP outer layer and show almost the same IEP as SiO_2-P4VP but its ζ-pH curve still located beneath that of SiO_2-P4VP due to the partial charge neutralization effect of the negatively charged inner layer. The charge neutralization is in principle driven by the softness of chains in the dispersion liquid medium.

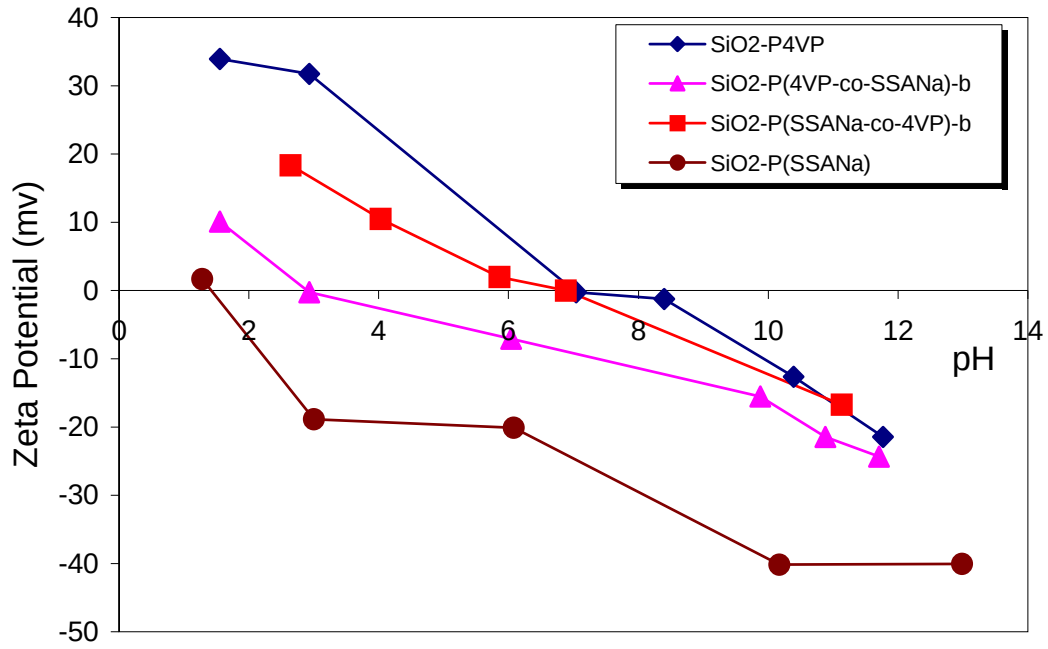

Figure 3.9 Influence of pH on zeta potential of polymer grafted silica particles in aqueous solution

The DLS~pH curve of the dispersion of SiO_2-PSSNa particles in aqueous solution shows that the hydrodynamic volume of the particles decreases with increasing pH (Fig. 3.10) and a steep decrease happens in the range pH = 6.0-6.5. Being a strong polyelectrolyte, as seen from the ζ potential measurement of SiO_2-PSSNa in aqueous solution, the polymer chains bear negatively charged sulfonate groups and the charge density increases with increasing pH. At the same time, the counter-ion layer composed primarily of Na^+ ions becomes thicker correspondingly. The observed reducing trend of hydrodynamic volume could be interpreted as the compressing effect of the counter-ion layer. In comparison with this, P(4VP-co-SSNa)-b particles show relatively slower size-contraction because of the buffering effect of the inner P4VP segments. This is particularly obvious in the basic medium. For instance, the DLS size of P(4VP-co-SSNa)-b is ca. 1350 nm while that of SiO_2-PSSNa is ca. 950 nm at pH = 9 even though the latter has a slightly larger size than the former at pH = 1. The buffering effect as mentioned is deemed to cause by the move of some inner P4VP blocks into the outer PSSNa layer because of their flexibility in hydrated state. Alternatively, SiO_2-P4VP particles also undergo contraction with the increase in pH of the dispersion medium due to the decrease of the pyridinium groups. This mounting effect of inner layer also happens for the P(SSNa-co-4VP)-b particles as presented in Fig. 3.11.

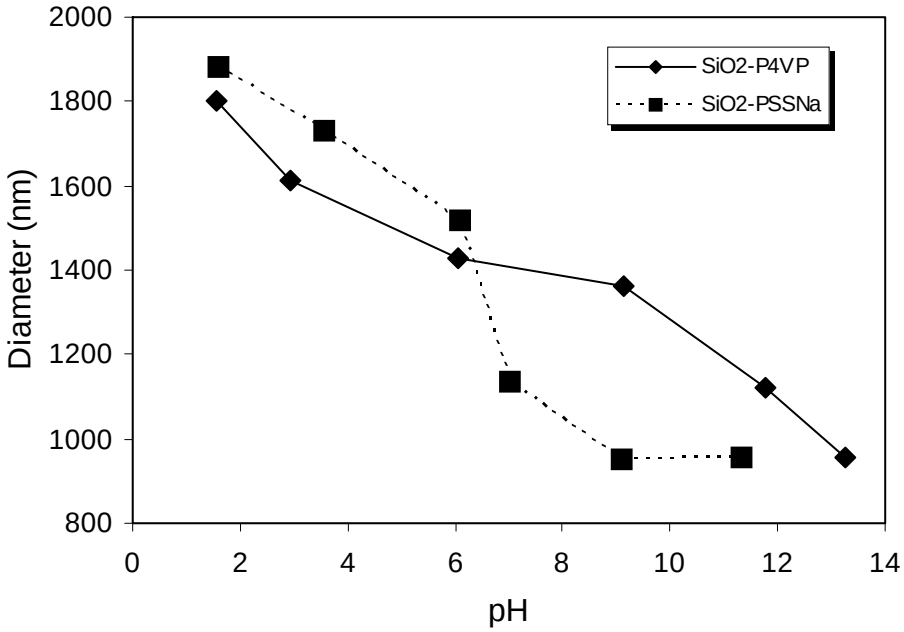

Figure 3.10 Influence of pH on the mean dynamic diameter of PSSNa and P4VPgrafted silica particles

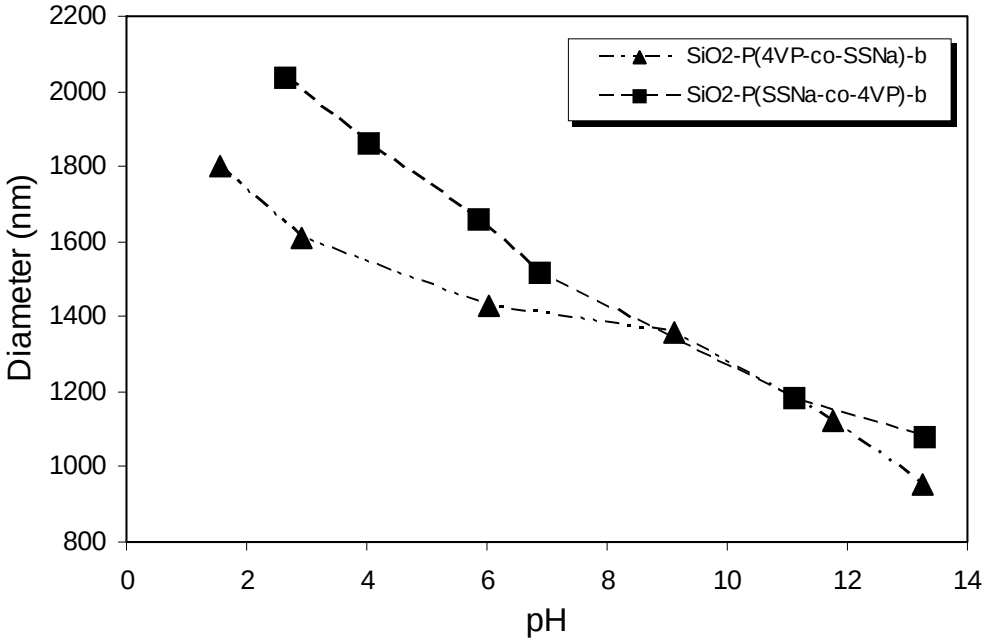

Figure 3.11 Influence of pH on the mean dynamic diameter of P(SSNa-co-4VP)-b and P(4VP-co-SSNa)-b grafted silica particles

3.3.5 The role of the grafted polymer chains in assisting with ion transport

Whether or not and how the polymer chains grafted to SiO_2 microspheres could assist ion transport in a liquid medium where they are dispersed is an appealing problem to study. As indicated in section 3.2.6, the dispersion was designed to have a substantially low volume fraction of the particles (~1.0×10^{-2} %), but this solid content is equivalent to about 10^9 particles moving about in $1cm^3$ liquid dispersion medium, which means on average a particle could be found in per 10^3 μm^3 space. At this low occupancy level we examined how the pendant polymer chains acted on escalating ionic conduction in the liquid phase. Fig. 3.12 displays the proton conductivity of colloidal dispersions of which the dispersion medium is an aqueous solution of HCl (pH=3). The pendant sulfonic acid groups promote proton transport, while the pendant 4VP groups, being an organic base, retard proton conduction. For the copolymer arms, although P(4VP-co-SSNa)-b particles are less expanded (or solvated) than P(SSNa-co-4VP)-b in aqueous solution with pH =3 (Fig. 3.11), the former one revealed stronger role in facilitating proton transport because of their exterior PSSNa blocks. The observation suggests that the surface layers of these floating particles, despite substantially low space occupancy, could confer an alternative proton-conducting channel wherein protons undertake faster hopping than in the bulk phase of solution.

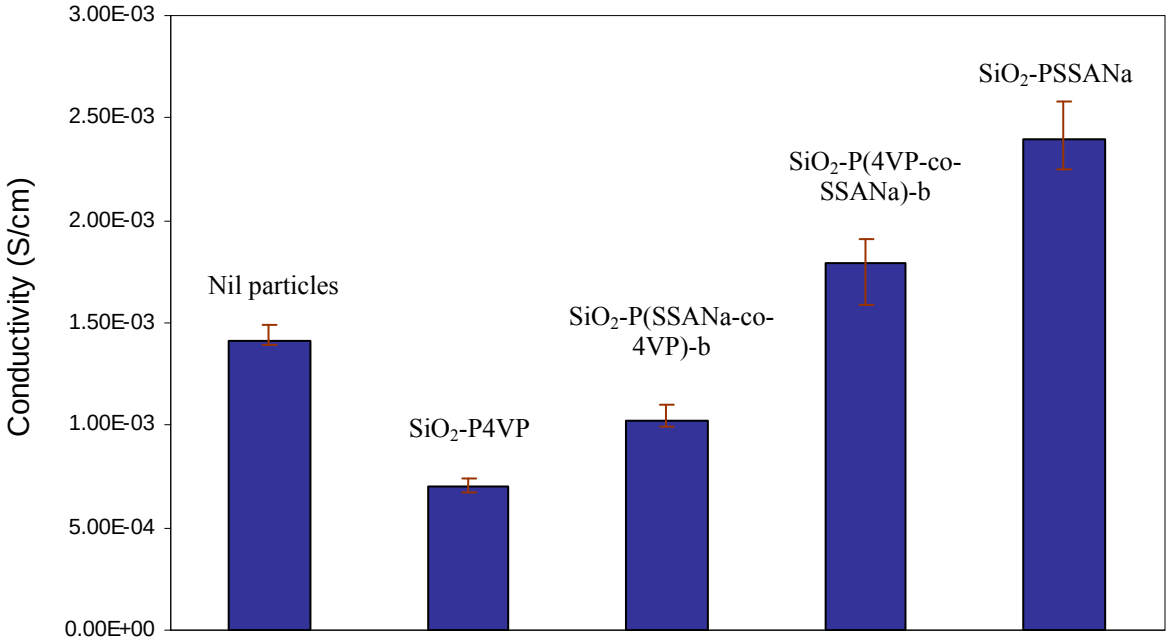

Figure 3.12 Conductivity of the acidified water (pH=3) loading different particles

We further examine the ionic conductivity of the colloidal dispersion formed by dispersing the particles in dimethyl foramide (DMF)-water mixture (Fig. 3.13).This test involved three types of particles containing PSSNa blocks. The concentration of sodium ion, as the major charge carrier, in the resulting colloidal dispersions followed the order: SiO_2-PSSNa > SiO_2-P(4VP-co-SSNa)-b ≈ SiO_2-P(SSNa-co-4VP)-b, because each dispersion system contained the same amount of particles, but each type of the hybrid particles possessed different contents of PSSNa as listed in Table 3.1. The resulting dispersions in DMF-H_2O mixtures were very stable regardless of the ratio of DMF to H_2O. The dispersions of SiO_2-PSSNa exhibit the highest ionic conductivity and the conductivity increases with reducing DMF portion due to its highest Na^+ concentration among the three and the fact that ionization dissociation of the SSNa groups becomes

stronger with increasing of water content. However, it is noteworthy that the unique observation comes from the differences between the two grafted-copolymer types of particles, SiO_2-P(4VP-co-SSNa)-b and SiO_2-P(SSNa-co-4VP)-b. Of the two, the former one contains the exteriorly located PSSNa blocks. Hence it is supposed to be able to reveal higher ionic conductivity than the latter one. The measurement results yet were different from this prediction. The dispersion of the SiO_2-P(SSNa-co-4VP)-b particles showed a clear increasing trend of sodium ion conductivity with increasing of water content in the dispersion medium. We are inclined to consider that the swelling of the P4VP block in DMF-H_2O mixtures as well as the weak association between Na^+ ion and 4VP nitrogen play important roles in channeling transport of Na^+ ions. This association (Gapeev and Dundar, 2003) is regarded to have a weak strength so that the migration of Na^+ ions is not hindered. It deserves to note that the Na^+ conductivity of this system jumps by 5 times from pure DMF to DMF-H_2O (v/v =9), whereas the dispersion of SiO_2-PSSNa conferred only a 3-time increase in Na^+ conductivity in response to the same variation of the water content. The inner PSSNa block functions like a switch, whose hydration triggers a clear ionic conductivity leap. On the contrary, SiO_2-P(4VP-co-SSNa)-b particles displayed only a slim superiority over SiO_2-P(SSNa-co-4VP)-b particles in pure DMF. The outer PSSNa layer, albeit it swells better with increasing water content in the DMF-H_2O mixtures, prevents the P4VP inner layer from acting as effective as the outer P4VP layer for channel transport of sodium ions. In brief, the sequence of the two blocks has a clear impact on sodium ion conduction, namely the inner PSSNa placement is superior over the its outer placement because P4VP blocks take part in shipping Na^+ ions when they are exposed to liquid phase.

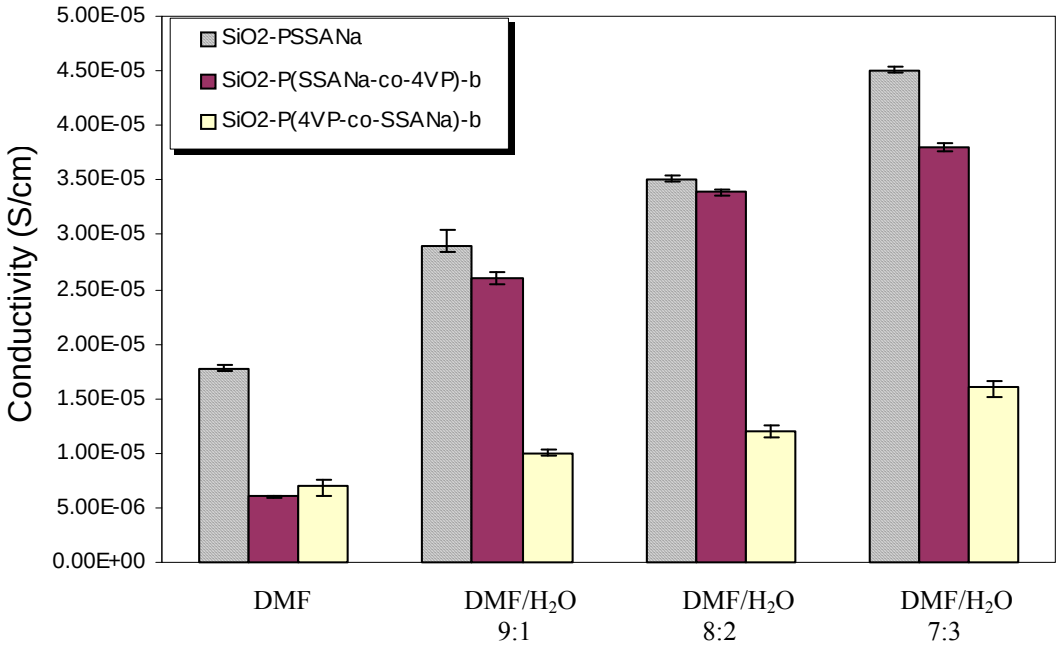

Figure 3.13 Conductivity of different ration DMF and water solution loading different particles

3.4 Conclusions

In this work, a specific structure of microsphere, comprising a silica core and a densely grafted hydrophilic polymer layer with low molecular weights, was synthesized by carrying out the atom transfer radical polymerization (ATRP) of 4-styrenesulfonate (SSNa) and 4-vinylpyridine (4VP). Thus four types of grafted chain structures were achieved: two homopolymers and two block copolymers with inverted block sequence. These four types of hairy microspheres exhibit different solvating volumes (hydrodynamic volumes) in methanol-H_2O mixtures with different ratios of the two components and in aqueous solution with different pH values, respectively. These

variations are governed by solvating extent and charge repulsion or neutralization in the grafted polymer layers. Besides these two factors, the new insight gained from this study is the leverage of the inner blocks of copolymer on the magnitude of surface charge and hydrodynamic volumes of the particles in a dispersion medium. Furthermore, the study also examined whether or not the grafted polymer chains could assist with ion transport in the liquid medium where a substantially low portion of particles is dispersed. In the acidic medium the results showed that the grafted PSSNa chains facilitate but the grafted P4VP chains retard proton transport and the copolymer layer bearing the exterior PSSNa blocks offers a stronger promoting action than that with the PSSNa inner blocks. The investigation was extended to DMF-H_2O dispersion medium, where Na^+ from PSSNa became the major charge carrier. An obvious cooperative action between the inner PSSNa blocks and the outer P4VP blocks to strongly propel Na^+ conduction was observed in DMF-H_2O (v/v =9), while the reversed block sequence did not present such an assisting role in the same dispersion system.

CHAPTER 4

REINFORCING FLUORINATED POLYMER PEM BY "HAIRY" SILICA NANOPARTICLES AND IMPROVING TEMPERATURE AND METHANOL TOLERANCE

4.1 Introduction

Perfluoro-polymers bearing sulfonic acid groups at the terminal position of their side chains have become a very important type of cation-exchange resin, which have applications in electrochemical cells used in the large scale industrial production of NaOH, KOH, and Cl_2 as a permselective membrane separator as well as in proton exchange membrane (PEM) fuel cells as solid electrolyte. Nafion® (with the perfluoroethylene polymer main chain) and Dow XUS 13204.10 (with the fluorinated-styrenic polymer main chain) are commercial products. Although Dow® PEM exhibits superior performance over Nafion PEM in PEMFC, it has been less used because of the high cost in comparison with Nafion PEM.

The main drawback of Nafion PEM lies in its a weak capability of preserving matrix-water at temperatures above 80°C and an intrinsically high diffusivity of low- molecular-weight alcohols. As a result, Nafion PEM cannot be used in a H_2-FC operated at an

elevated temperature in order to promote electrode-catalytic efficiency because of a significant loss of proton conductivity caused by the reducing of humidity level in the membrane matrix. On the other hand, replacing H_2 with methanol to power portable mini fuel cells (DMFC) has a promising commercial prospective, and Nafion PEM is inappropriate to this cell due to severe crossover of methanol through it, which results in the lowering of cell efficiency.

Many strategies have been proposed to improve the high temperature performance and methanol rejection of Nafion PEM. Modified Nafion membranes containing inorganic fillers (SiO_2, TiO_2, ZrO_2, and ZrP) have been reported. (Adjemian et al., 2002; Sacca et al., 2005; Xu et al., 2005; Jalani et al., 2005 and Jiang et al., 2006) However, these inorganic oxide particles are too large to disperse in the Nafion polymer matrix very well. On the other hand, due to the fact that these inorganic oxides have very low proton conductivity, introducing them can not always lead to a desired improvement in the performance of the membrane electrode assembly (MEA). In chapter 3, we introduced a special polymerization, heterogeneous ATRP to develop a special type of microsphere that comprise a silica core and a densely grafted hydrophilic polymer layer. Therefore, in the present write-up, we continue to apply this method to modify silica nano-particles with a thin layer of grafted ionomer chains, known as the "hairy" layer and then bring into the Nafion matrix a low content of resulting hairy-silica nano-particles. Such hairy-silica nanoparticles present in the Nafion matrix exhibit an obvious role in enhancing the proton-conductivity at high temperature, and as a result, this unique type of composite PEM gives rise to superior electrochemical performances (cell voltage at higher current

density and power output) over the native Nafion PEM in the single cell driven by H_2 and methanol, respectively. In conclusion, these miniature hairy particles help holding matrix bound water as well as blocking permeation of methanol through Nafion matrix.

4.2 Experimental

4.2.1 Materials

Fume silica powder (average particle sizes 7 nm, Aldrich), triethoxyvinylsilicane (TEVS, 98%, Aldrich), triethyl amine (Et_3N, Merck), bromine(Mallinckrodt, AR®), copper(I) bromide (99%, Aldrich), 2, 2'-Bipyridyl (Bpy, ≥ 99%, Fluka), 3-sulfopropyl acrylate potassium salt ($H_2C{=}CHCO_2(CH_2)_3SO_3K$, SPA-K, Aldrich), and Nafion® resin (Aldrich) was used as received.

4.2.2 Synthesis of PSPA-SiO_2 particles through grafting polymerization

As a typical synthetic procedure, the entire preparation includes the following four synthetic steps:

Step 1: *Silanization to prepare vinyl-silica nanoparticles*

SiO_2 (500 mg) and TEVS (1 ml) were added in toluene of 50 ml together with Et_3N (0.15 ml) as the catalyst of silanization. The resulting mixture was stirred at room temperature under argon atmosphere for 24 h. The vinyl-SiO_2 powder was recovered as

wet slurry after centrifuging the reaction mixture at 8000 rpm for 15 min. The slurry was washed with THF, re-dispersed in THF and re-centrifuged several times to remove the excess of TEVS. The slurry was dried at 60 ºC in a vacuum oven for 72 h.

Step 2: *Bromination of the grafted vinyl group to form 1, 2-dibromoethyl group*

The vinyl-SiO_2 powder from the first step was then added into a round bottom flask holding chloroform (~5 ml). To this stirred suspension a chloroform solution of bromine (19.5 mmol) was slowly added in at temperature 0-5 ºC. After stirring for 30 min, the resulting 1, 2-dibromoethyl-silica powders were then purified by washing three times in pure chloroform. 1, 2-dibromoethyl groups on silica particles were created as the bound initiator for the grafting polymerization of SPA-K in the following step.

Step 3: *Grafting SPA-K oligimer chains to 1,2-dibromoethyl-silica particles*

The oligomer chains of SPA-K were grafted to silica nano-particles by the atom transfer radical polymerization (ATRP) method under the controlled conditions. The initiator-grafted silica particles (0.15 g) were dispersed in a water-methanol mixture (3:1 v/v, 12 ml) with the aid of ultrasonic mixing. Monomer SPA-K and catalyst-ligand, bpy, were then added into this suspension system. The mixture was degassed using nitrogen purge for 30mins with continuous stirring at temperature 35-40 °C. Copper (I) bromide (0.06 g) was then added into the flask and then the mixture was stirred for 4 h under the same conditions. The polymerization was terminated by exposing the mixture to air. The reaction mixture was finally centrifuged at the rate of 6000 rpm for 15 min. The supernatant was decanted and the centrifugation tube was charged with doubly distilled

DI water to wash the blue ATRP catalyst-contaminated sediment, and the washing was assisted with ultrasonic agitation. Such centrifugation-cleaning cycle was repeated three times to obtain purified PSPA-K-grafted silica particles.

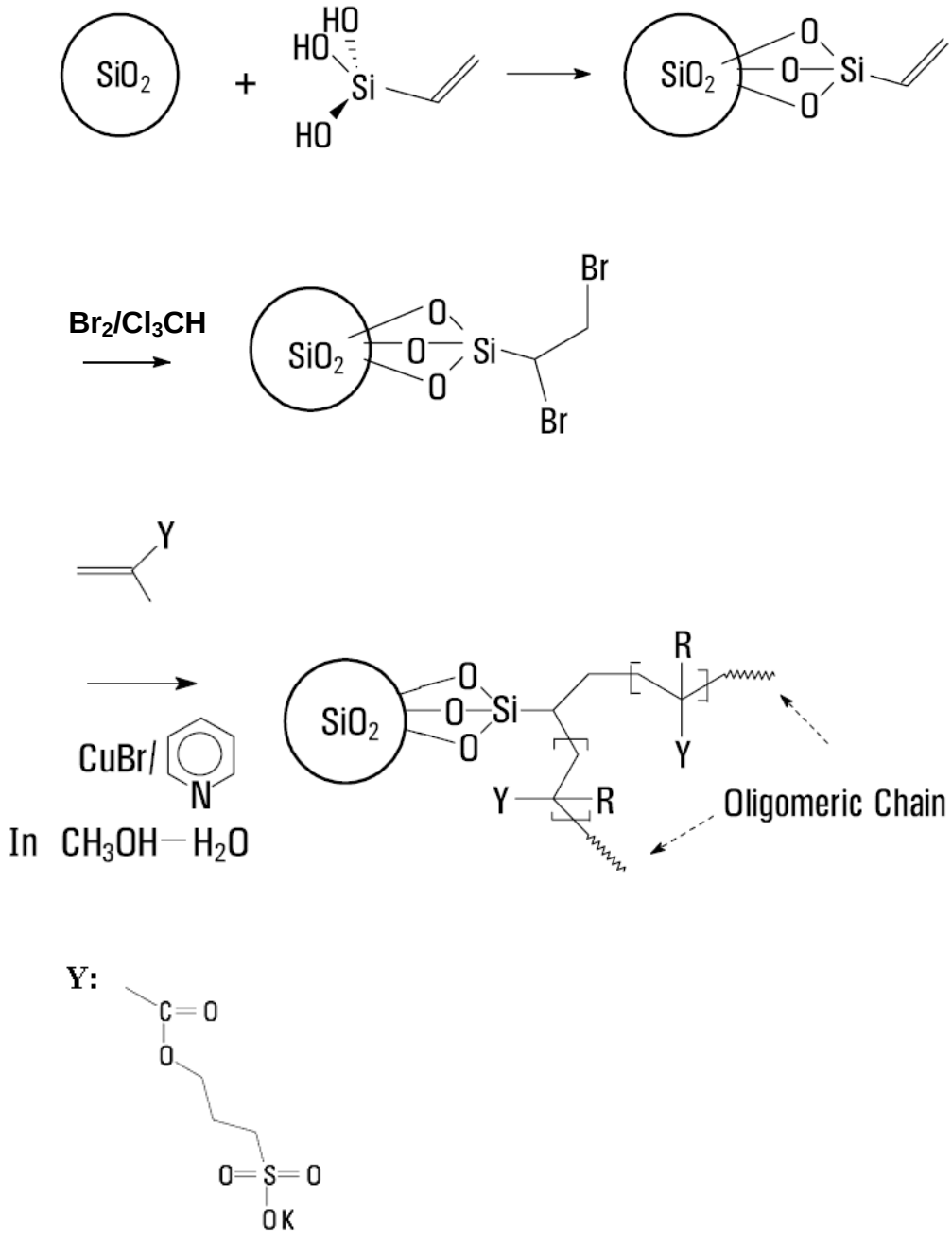

Scheme 4.1 The schematic of forming PSPA-K-grafted silica particles

Step 4. *Ion-exchange of PSPA-K-SiO_2 to PSPA-SiO_2*

The PSPA-K-SiO_2 obtained from the previous step was introduced into an aquatic solution of sulfuric acid (30%) and the mixture was mildly stirred at room temperature for 6 h to convert the salt form $–SO_3K$ to its acid form $–SO_3H$. After that, the acidified sample was washed with DI water and centrifuged at 6,000 rpm for 15 min for separating the powder from the liquid phase. This process was replicated two more times for cleaning up the attached residual acid. The PSPA-SiO_2 powder was subjected to vacuum drying and stored for further use.

4.2.3 Fabrication of the Nafion/PSPA-SiO_2 composite membranes

A 2-ml Nafion solution (5-10 wt.% in H_2O-alcohol-DMF mixture) was mixed with a given amount of PSPA-SiO_2 powder (2 wt.%, 4 wt.% and 6 wt.% of the dry Nafion resin, respectively), and the resulting blend was cast in a Petri dish (d = 3 cm) and placed in an oven (at 80 ºC) for 30 mins to remove the solvent and cure the film left behind. The composite film was then de-molded from the Petri dish after soaking in DI water and dried at room temperature.

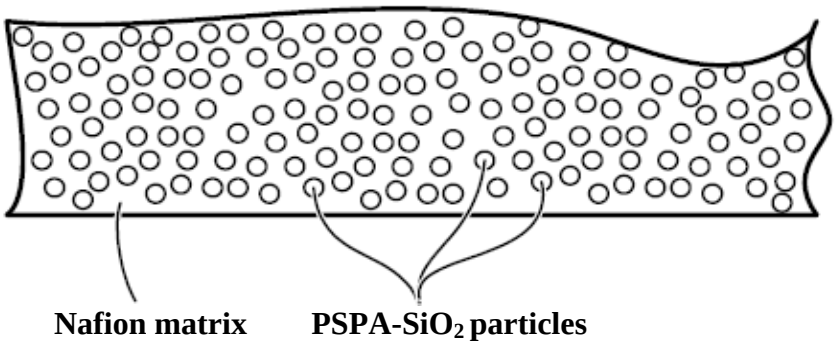

Scheme 4.2 The structure representation of PSPA-grafted silica particles in Nafion matrix

4.2.4 Instrumental Characterizations of the Materials Synthesized

FT-IR spectra of the products from the different steps of synthesis of PSPA-SiO_2 powder were recorded in air on a Bio-Rad FTIR model 400 spectrophotometer by accumulating 16 scans. The particle images and cross-sectional matrix morphology of the membranes were investigated using FESEM (JGM-6700F from JEOL). Glass transition behaviors of the membranes were detected by DSC (Mettler Toledo DSC 822e), and the corresponding thermal stabilities and degradation behaviors were detected on a TGA Instrument (TA Instruments 2050 Thermogravimetric Analyzer) to obtain the TGA themograms under N_2 at 100 ml/min with rate of 10 ^oC/min. For silica powders, the thermogrames were obtained from room temperature to 600 ^oC; for the membrane samples, the thermogrames were obtained from room temperature to 800 ^oC.

4.2.5 Electrochemical Evaluations of the PSPA-SiO_2/Nafion Composite Membranes

The assessment of proton conductivity of the composite membranes at different temperatures were carried out by the AC impedance spectroscopic method using the frequency scanning range from 0.01 Hz to 1 MHz, an AC perturbation voltage of 10 mV and a DC rest voltage of 0.0 V on an electrochemical analyzer (Autolab Model). A circular shape of membrane (1.3 cm in diameter) was sandwiched and tightened by two smooth stainless steel discs (electrodes) in a Teflon sample holder, which was then

immersed in a water-bath with different temperatures. The proton conductivity of the membranes was calculated using the following equation:

$$\sigma = \frac{L}{RS}$$

where σ, L, R, and S denote the proton conductivity (S/cm), thickness of membranes (cm), the resistance of the membrane (Ω) and the cross-sectional area of the membrane (cm^2), respectively.

The MEA (membrane electrode assembly) was made by compressing a sample membrane in between an anode sheet and a cathode sheet. For the DMFC test, the anode sheet was a carbon paper (SGL, Germany) with a carbon-supported Pt or Pt-Ru catalyst layer. The cathode sheet was a carbon paper with a carbon-supported 40 wt.% Pt catalyst layer supplied by E-TEK. The average platinum loadings in the anode and cathode were 3 and 2 mg/cm^2, respectively, and the effective electrode area was 5 cm^2. The fuel was 2 M CH_3OH aqueous solution delivered at 2 ml/min by a micro-pump, and an oxygen flow rate of 500 cm^3/min was regulated to purge the cathode side. For the H_2-FC test, , The MEA was operated under 1 bar for both H_2 and O_2 without humidification using Arbin Electronic load and PC with MITS software. The anode and cathode sheet were a carbon paper (SGL, Germany) with carbon-supported 20 wt.% Pt catalyst layer supplied by E-TEK, Natick, MA. The catalyst loadings at the anode and cathode were 2 mg/cm^2, thus, Pt loadings at the anode and cathode were 0.4 mg/cm^2. The effective electrode area was 5 cm^2. The gas flow rate was kept at a fixed stoichiometry (1.15 times stoichiometric for H_2 and 2 times stoichiometric for O_2) at 1 A/cm^2 current density.

4.3 Results and discussions

4.3.1 The structural characteristics of PSPA-K-SiO_2 particles made by means of ATRP

The FT-IR spectrum of the PSPA-K-SiO_2 (Fig. 4.1) displays the main structural features of the grafted PSPA-K chains including the S=O stretching vibration absorption of sulfonate group occurring at around 1120 cm^{-1}, the C-H stretching vibration absorption of $–CH_2CO-O-$ group and CH_2 group (hydrocarbon backbone) at 3047 cm^{-1} and 2985 cm^{-1}, the C=O stretching vibration absorption band of the ester group at approximate 1734 cm^{-1}, and the C-H bending vibration absorption of the hydrocarbon backbone at 1420 cm^{-1}. These absorptions show that PSPA groups are grafted on the silica particles.

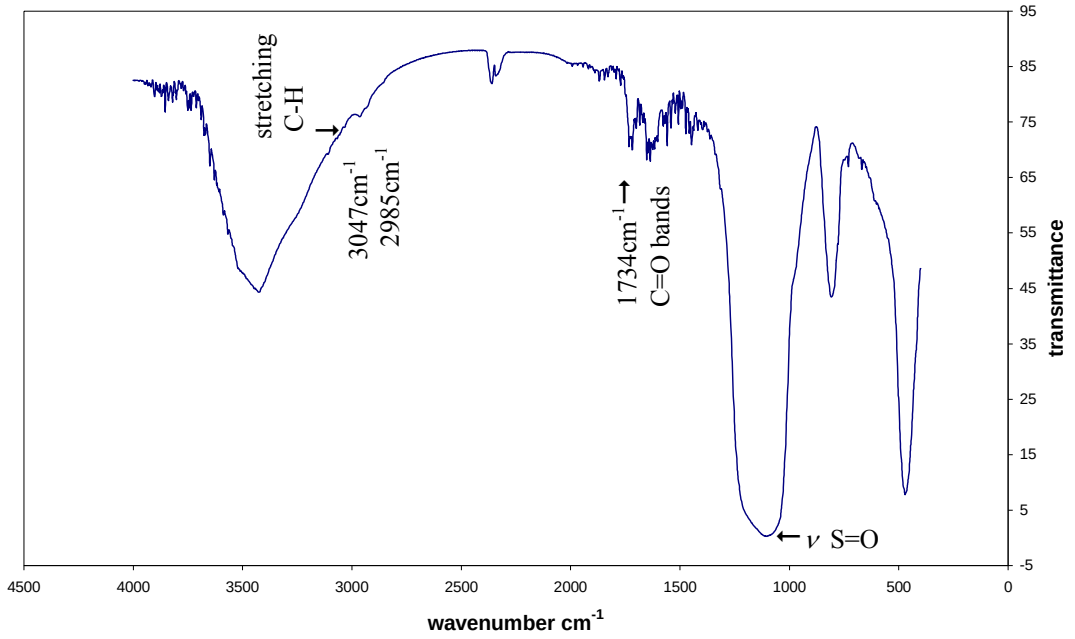

Figure 4.1 FT-IR spectra of PSPA-K- SiO_2

Furthermore, by comparing Fig. 4.2b and TEM image of pure silica particles, we observed that the image of the ionomer-grafted particles shows light agglomeration among the particles was occurred. Such morphology change of particles may be caused by grafting of the soft PSPA-K (ionomer) chains to SiO_2.

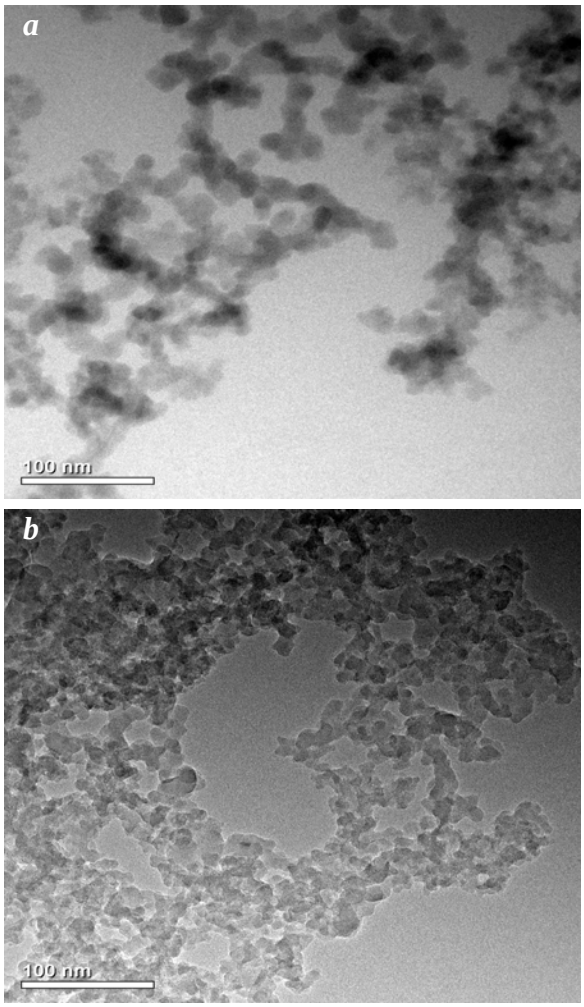

Figure 4.2 TEM of (a) SiO_2 particles, (b) PSPA-K- SiO_2

The TGA curves of the pure SiO_2, vinyl-SiO_2 and PSPA-K-SiO_2 are shown in Fig. 4.3. The pure fumed silica showed negligible mass loss over the temperature range under investigation, while vinyl-SiO_2 powder showed a mass-loss stage (210-260 ^oC, labeled by two arrows) indicating the decomposition of vinyl groups that is anchored to SiO_2 particles via silanization of TEVS. Regarding PSPA-K-SiO_2, there was dehumidifying mass-loss in the range below 100 ^oC, and a slight mass-loss stage (~ 2%) happening in the range of 160-260 ^oC. These two mass-losses could be due to the removal of moisture trapped in the silica cores. A strong mass loss gradient occurred from 260 ^oC and leveled off at about 600 ^oC. It was ascribed to the elimination of the grafted PSPA-K chains, which accounted for about 18% of mass in PSPA-K-SiO_2 sample. In addition, this analytical result shows that PSPA-K-SiO_2 is stable at temperatures below 160 ^oC.

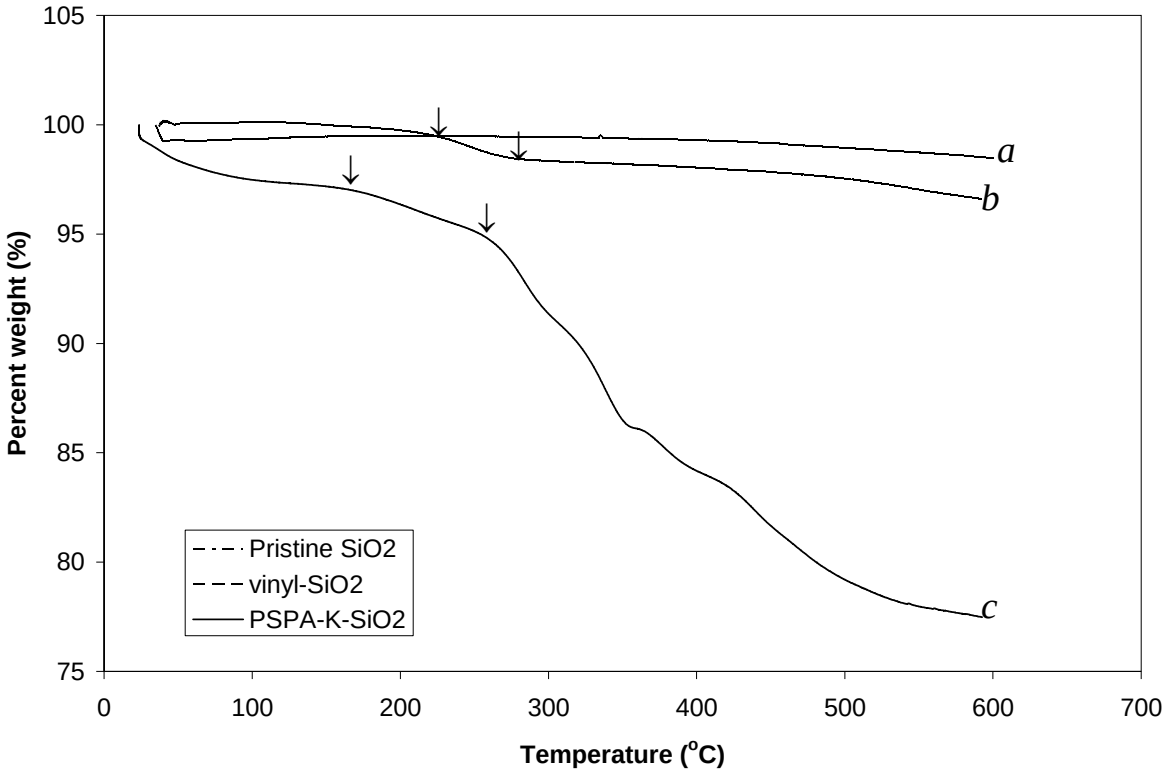

Figure 4.3 TGA profiles of the (*a*) pristine silica; (*b*) vinyl-SiO_2; and (*c*) PSPA-K-SiO_2

4.3.2 Characterization of Nafion/PSPA-SiO_2 composite membranes

The TGA thermogram (Fig. 4.4) shows that both pure Nafion membrane and composite membrane [Nafion/PSPA-SiO_2 (4 wt.%)] retained more than 90% of total membrane weight up to a temperature of about 300 ^{o}C. The mass discarded before this temperature point is mainly caused by the vaporizing of small solvent molecules such as water, methanol and ethanol. Moreover, the mass loss of the two membrane samples occurred in the range from 300 to 600 ^{o}C. The results appear to confirm that the presence of the low content of PSPA-SiO_2 in the Nafion matrix does not noticeably lower the thermal stability of Nafion matrix.

The compatibility between the host polymer matrix (Nafion, in this case) and the powder filler influences the thermal, mechanical and electrical properties of the membrane. The agglomerates of pristine nano-silica particles formed could be clearly spotted in the cross-section of the membrane, Nafion/SiO_2, which was prepared by fracturing in liquid nitrogen (Fig. 4.5a). This morphology may account for spontaneous aggregation of silica particles in the Nafion matrix. In contrast, Fig. 4.5b shows no significant agglomerates of the PSPA-SiO_2 particles were observable in the cross-section of membrane Nafion/PSPA-SiO_2, and no embedded granules could be distinguished from the cross-section image. This obvious difference of pure silica and PSPA-SiO_2 particles distribution in the Nafion matrix indicates that the PSPA ionomer chains grafted onto fume silica nano-particles play a key role in boosting the dispersion extent of the silica particles in the Nafion matrix.

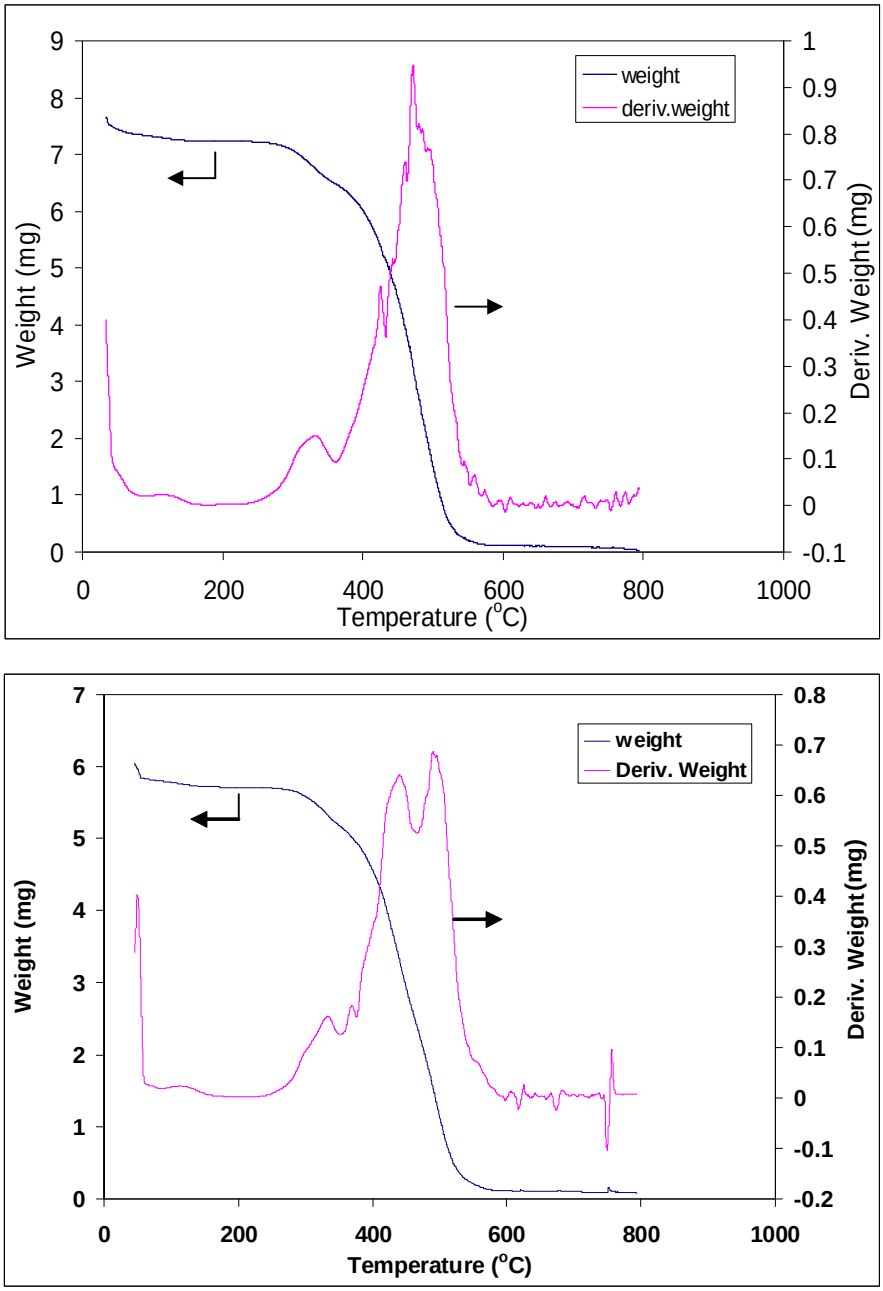

Figure 4.4 TGA thermograms for *a*. Pure Nafion membrane and *b*. Nafion/PSPA-SiO_2 (4 wt.%)

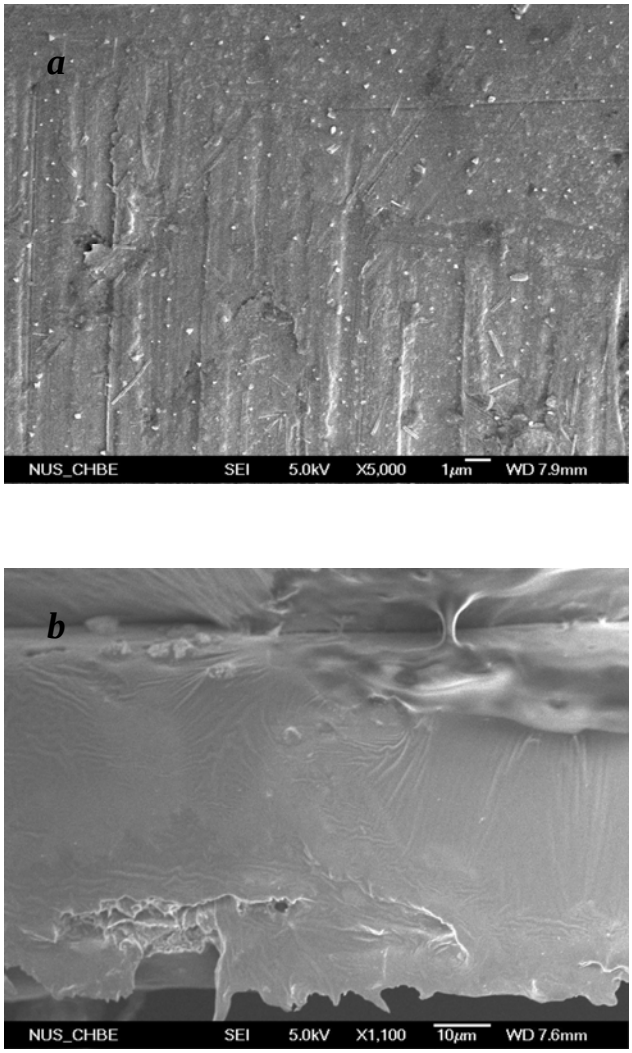

Figure 4.5 Field emission scanning electron micrographs of: (*a*) the cross-section of Nafion/SiO_2 composite membrane and (*b*) the cross-section of Nafion/PSPA-SiO_2 membrane

4.3.3 Investigation of proton conductivity of the composite membranes

The dispersion extent of silica (pristine and modified) in the Nafion matrix was investigated from the perspective of the dispersing effect on proton conductivity at different temperatures (Fig. 4.6). We selected four membrane samples to study, which were native Nafion membrane, Nafion/SiO_2 (2 wt.%) and Nafion/SiO_2-PSPA (2 wt.% and 4 wt.%) composite membranes. For all membrane samples, with increasing temperature, the proton conductivity values increased. This is probably because high temperatures improve the motion of polymer chains and provides more free volume for sulfonic groups, and hence it is easy to transport proton in the membranes. However, after reaching maximum values their proton conductivities started to decrease with further increasing temperature, as shown in the Fig. 4.6. This is probably because higher temperature reduces water uptake of the membranes without controlling humidity in this experiment. On the other hand, Fig. 4.6 also shows the Nafion membrane doped with 2 wt.% of pristine fume silica had lower proton conductivity than pure Nafion membrane in the temperature range of 50 to 80 ^{o}C and this difference is due to non-conductive property of pure silica particles as well as their agglomerated distribution in the Nafion matrix. In contrast, SiO_2-PSPA particles in Nafion matrix at a low loading could apparently boost the proton conductivity of the membrane. This result manifests the crucial role of the SiO_2 surface-grafted PSPA layer in facilitating H^+ transport across the Nafion matrix. Further, it is noticeable that the two Nafion/SiO_2-PSPA (2 wt.% and 4 wt.%) membranes displayed superior proton conductivity over the native Nafion in the temperature range greater than 70 ^{o}C. This result strongly suggests that the SiO_2 surface-

grafted PSPA layer not only has the crucial role of facilitating H^+ transport across Nafion matrix, but also preserves the matrix humidity.

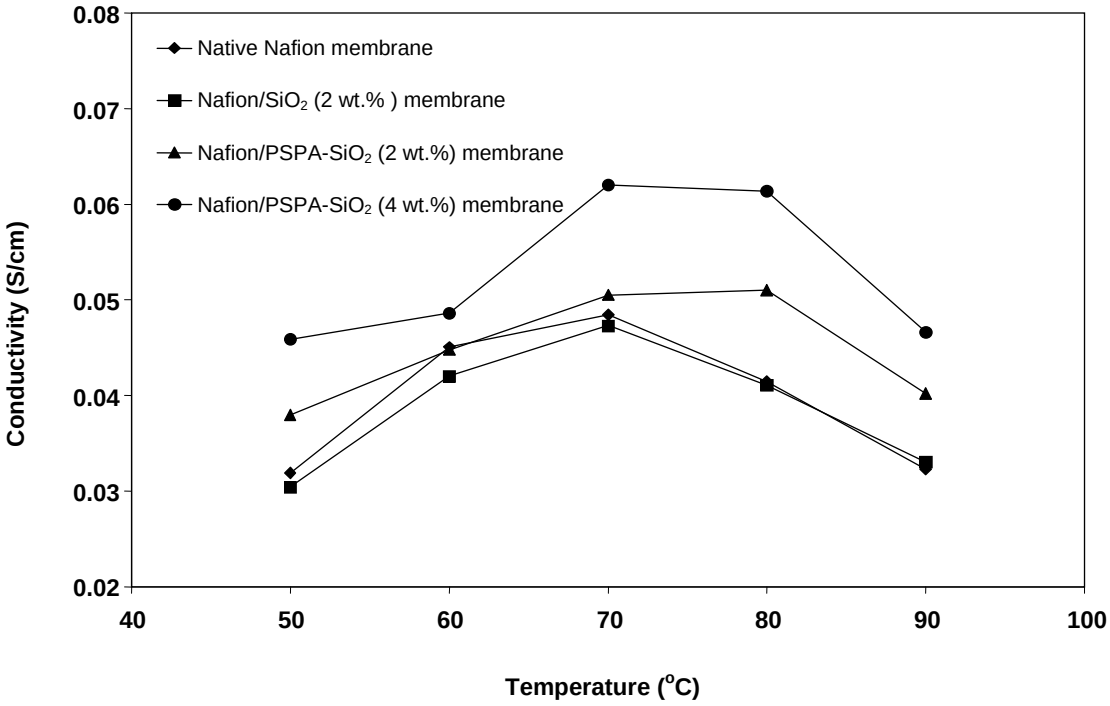

Figure 4.6 Influence of temperature on the conductivity of various membranes under investigation

4.3.4 Single-cell performance of the composite membranes

This part of the study aimed at unveiling the improved electrochemical performance of the composite membranes Nafion/PSPA-SiO_2 relative to the native Nafion membrane in the two types of proton-exchange membrane fuel cells (PEMFC), of which one used 2 M-methanol (DMFC) and the other used hydrogen (H_2-FC) as fuel.

- The DMFC was operated at 50 ^{o}C and 80 ^{o}C (Fig. 4.7)

The results (power density and cell voltage) showed that when DMFC was operated at 50 ^{o}C (Fig. 4.7a), the membranes Nafion/PSPA-SiO_2 had obviously better performances than Nafion, and the average increased with the loading of filler. The maximum open circuit voltage (OCV = c.a. 0.58 V) and powder density output (22.4 mW/cm^2) were achieved with the use of PSPA-SiO_2 of 6 wt.%. The difference between the two high loading membranes (4 wt.% and 6 wt.%) diminished quickly with the increase of current density. When the operation temperature was raised to 80 ^{o}C, the composite membranes though still showed better electrochemical cell performance than Nafion and the loading effect followed the trend observed previously at 50 ^{o}C. And the excess of the two cell parameters gained by the use of PSPA-SiO_2 was reduced. This outcome implies that the swelling of Nafion matrix by methanol aqueous solution at the higher operation temperature become an important factor, which allows proton to pass through the matrix water channels.

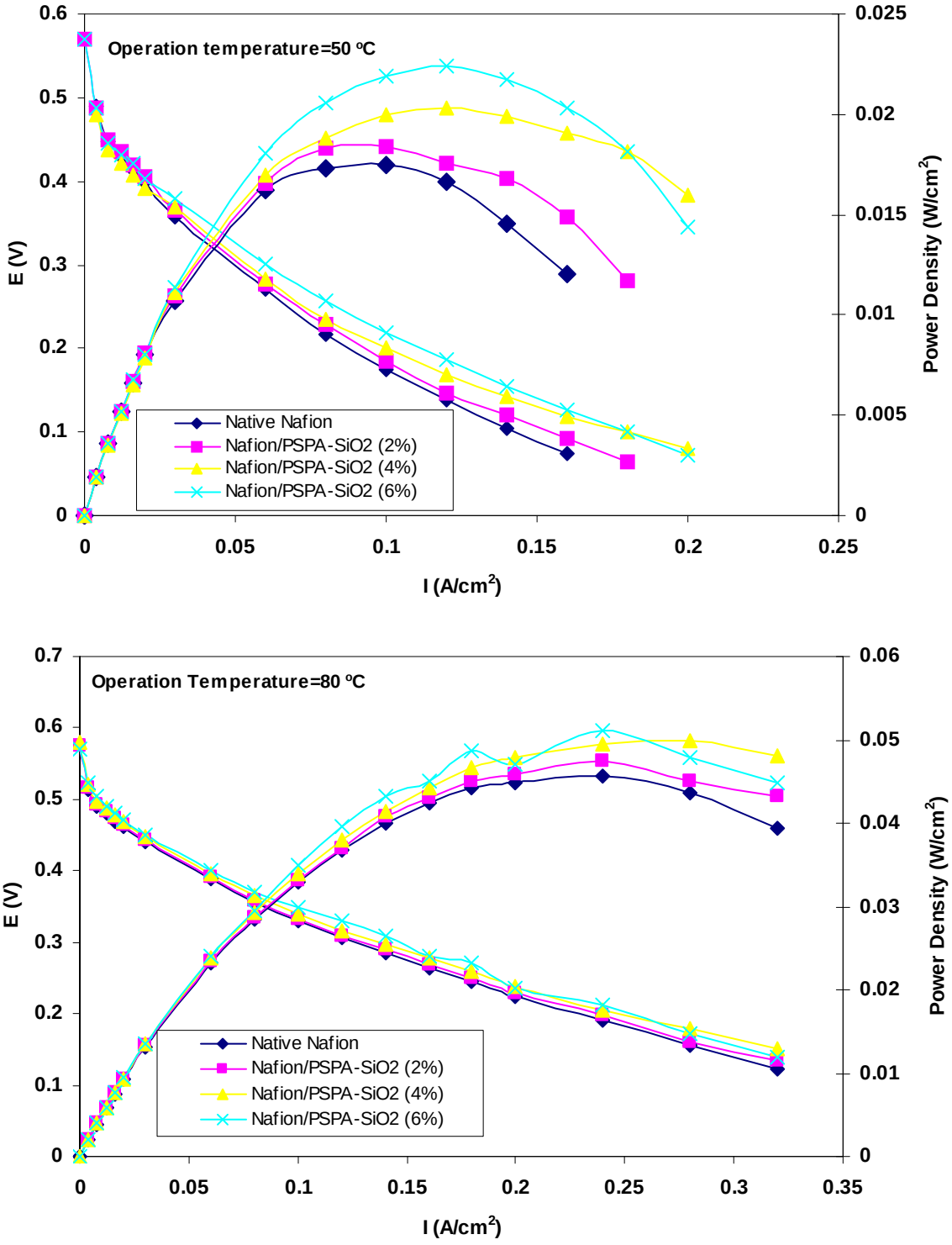

Figure 4.7 The electrochemical performances of the four membranes respectively in a single direct methanol fuel cell operated at 50 °C and 80 °C

- The H_2-FC was operated at 23 ^oC and 80 ^oC (Fig. 4.8)

Compared with DMFC, the cell assessment under lower humidity condition demonstrated more explicitly the advantage of the presence of PSPA-SiO_2 nano-particles in the Nafion matrix. The composite membrane loaded with PSPA-SiO_2 of 6 wt.% gives rise to the maximal OCV (0.96 V) and the power density of 19.6 mW/cm^2 at the ambient temperature, which were the best output among the membranes examined. In contrast to their performance in DMFC at high temperature, the composite membranes manifested even better cell performance than the native Nafion at 80 ^oC; this is because of the two factors: firstly, the proton conductivity of the native Nafion membrane declined more rapidly with the increase of temperature (Fig. 4.6); and secondly, the composite membranes could still offer a continuous improvement, namely maintaining the similar maximal OCV at a higher current density setting. Taking the composite membrane (6 wt.%) for example, it retained OCV of 0.95 V at the current density of ca. 3 mA/cm^2, and had accordingly the highest maximal power density (21.9 mW/cm^2) at 80 ^oC

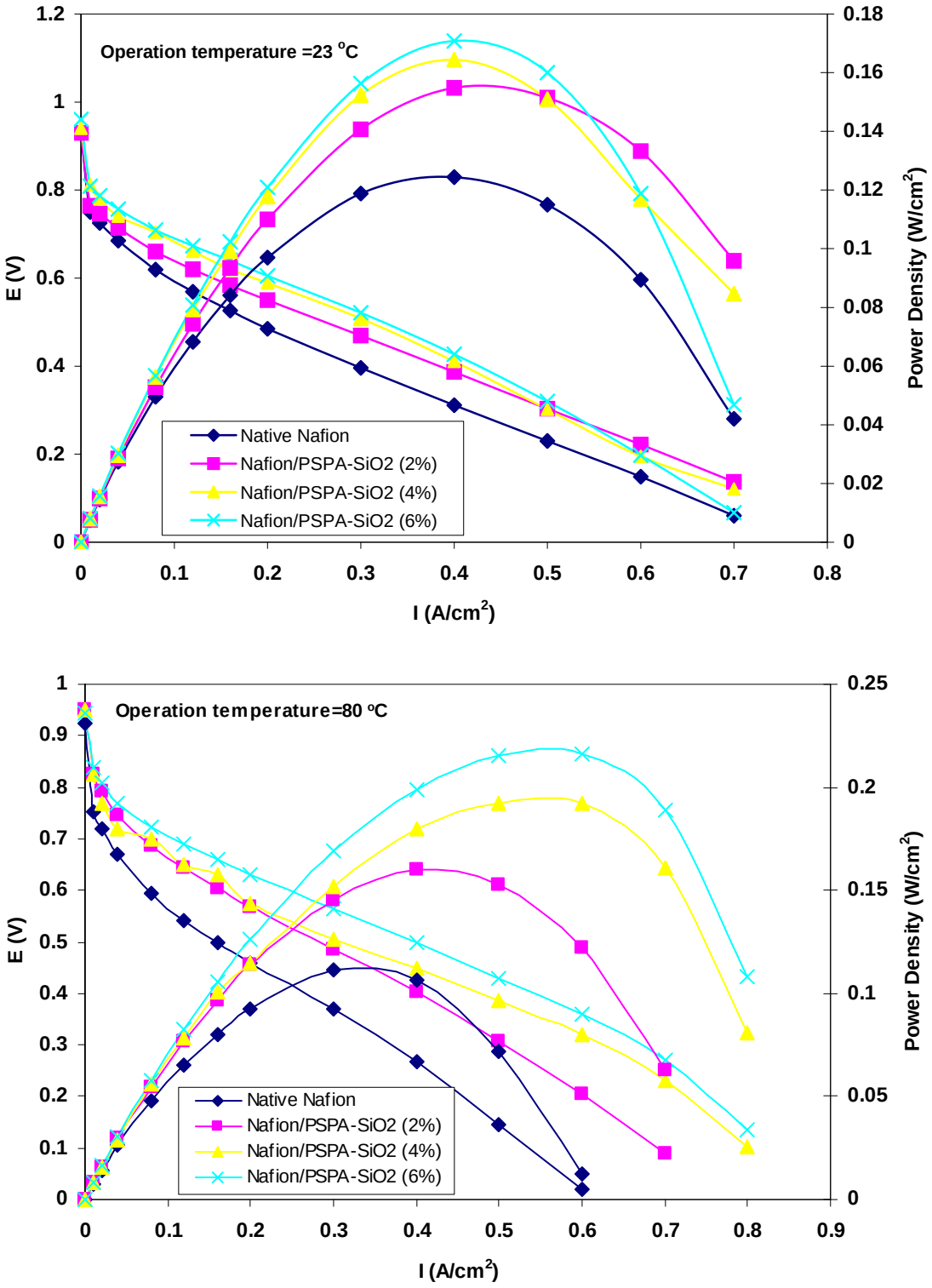

Figure 4.8 The electrochemical performance of the four membranes respectively in a hydrogen-driven single fuel cell at the two elevated temperatures

4.4 Conclusions

In conclusion, the presence of ionomer-grafted silica nano particles, PSPA-SiO_2, in the membrane matrix of Nafion enhances its performance in PEMFC through boosting the flux of protons and facilitating their transport. The boosting role comes from the fact that each PSPA-SiO_2 particle bear a high density of sulfonic acid groups, and the facilitating role is attributed to the hydrophilic interactions between PSPA-SiO_2 particles and the sulfonic acid groups of Nafion chains. The composite membranes with different ratio of PSPA-SiO_2 loading have better conductivity than the pristine Nafion membrane and Nafion/silica in the experiment temperature range. And the composite membrane with optimal PSPA-SiO_2 (6 wt.%) has higher performance than pure Nafion membrane at 50 ^{o}C and 80 ^{o}C operating temperature for DMFC and H_2-FC.

CHAPTER 5

REFORMATTING NAFION MATRIX VIA *IN-SITU* GENERATED POLYPOSS BLOCKS TO PROMOTE ITS PERFORMANCE IN DIRECT METHANOL FUEL CELL

5.1 Introduction

In recent years, the development of direct methanol fuel cells (DMFCs) for powering small electronic devices has received increasing attention (Surampudi et al., 1994; Ren et al., 1996; Aramata et al., 1992; Arico et al., 1994; Wang et al., 1995 and Wasmus et al., 1999) since storage of aqueous methanol solution is much easier than hydrogen. However, Nafion becomes unsuccessful for the application in DMFC as its matrix permits a methanol-diffusivity of 10^{-6} ($cm^{-2}\cdot s^{-1}$) at room temperature. It has been found that over 40% of methanol can be lost due to excessive swelling of Nafion in methanol solution (Heinzel and Barragan 1999). Besides this, the permeation of methanol through the membrane also results in a mixed potential at the cathode, and leads to lowering the voltage and electrochemical efficiency of DMFC (Chu et al., 1994; Surampudi et al., 1994; Scott et al., 1999; Ren et al., 2000a and 2000b). It is thus meaningful for exploring effective solutions to this intrinsic drawback of Nafion. A variety of approaches has been attempted to modify Nafion matrix in order to cut down methanol permeability (Hong et

al., 1999; Kim et al., 2004; Adjemian et al., 2002; Staiti et al., 2001b and Jalani et al., 2005). In general, there is a trade-off between proton conductivity and methanol diffusivity. For instance, inclusion of nano silica particles in Nafion matrix manifested a noticeable reduction in methanol crossover at the cost of proton conductivity because of using a rather high content (e.g., 20 wt.%) of SiO_2. (Miyake et al., 2001)

It is important to understand how the microstructure of Nafion matrix undergoes change upon adding nanoparticles. Nafion has a very hydrophobic poly (tetrafluoroethylene) main chain (~ 87 mol%) and short side chains terminated by sulfonic acid groups. The molecular weight of Nafion is known to fall into the range of 10^5-10^6 a.u., and on average each segment length of about 1440 a.u. contains one sulfonic acid group (Mauritz and Moore 2004). It is therefore rational to view Nafion as an anionic polymer surfactant. According to the previous studies on the microstructure of Nafion that were highlighted in the review article of Mauritz and Moore, negatively charged pendant sulfonic acid groups undergo association in the hydrophobic perfluoro matrix with the increase of water content and finally form numerous hydrophilic channels, which can be ideally envisioned as worm-like hydrophilic channels. It could be projected that this hydrophilic assembling process is to be deeply disturbed with including of pristine inorganic oxide nanoparticles or ionomer modified nanoparticles into the matrix as shown in the chapter 4 because the oxide particles are adsorbent of sulfonic acid groups due to their hydrophilic surface predominated with –O- and –OH sites. As a result, methanol molecules are not easy to enter into the interface between particles and sulfonic acids, and protons transport along the interface between particles and sulfonic acid besides along the native

hydrophilic channels. It can be rationalized that the adsorption extent affects both proton conductivity and methanol diffusivity. Such composite matrix often forgoes some part of proton conductivity and mechanical strength of Nafion for the exchange of depressing methanol permeation.

In contrast to these metal oxide nanoparticles, polyhedral oligomeric silsesquioxane (POSS) is a delicate molecule that could also be regarded as a hybrid nanoparticle since it has well-defined cube-octameric siloxane skeleton (about 1-3 nm in size) with eight organic vertex groups, one or more of which are reactive or polymerizable. (Lichtenhan et al., 1993 and 1995; Mantz et al., 1996; Haddad et al., 1996; Feher et al., 1999a and 1999b) These particular structural features render POSS be a versatile additive for acquiring enhanced themomechanical properties, better thermal stability, (Huang et al., 2003; Choi et al., 2003a and 2003b) atom oxygen resistance, abrasion resistance and low water uptake (Tsai et al., 2001 and Wright et al., 2003). In these applications precise control of nanoarchitecture of POSS derivatives in the host matrix is crucial to attain the desired features. (Zhao et al., 2005) POSS molecules have also been incorporated into a variety of polymer materials by means of blending, grafting or copolymerization with vinyl monomers in pursuit of nano-structured polymeric materials that possess the hybrid properties of organic polymer and ceramics. (Marcolli et al., 1999)

This chapter advances the existing Nafion membrane modification strategies, as aforementioned, through introducing into the host matrix the hydrophobic 1, 3, 5, 7, 9, 11, 13, 15- octakis (dimethylviylsiloxy) pentacycloc octasiloxane ($Q_8M_8^V$) molecules into the

host matrix. These molecules are polymerizable due to the presence of eight pendant vinyl groups (Fig 5.1). Naturally, these particulate molecules, $Q_8M_8^V$, do not behave like hydrophilic SiO_2 nanoparticles as an adsorbent of pendant sulfonic acid groups when introduced into Nafion matrix. $Q_8M_8^V$ could be very uniformly distributed in perfluorocarbon matrix via recasting because they are not only small but also compatible with perfluorocarbon backbone of Nafion molecules. Upon subjected to *in-situ* polymerization, these particulate molecules are converted to rigid blocks (Fig. 5.2), $P(Q_8M_8^V)$, each of which consists of a certain number of $Q_8M_8^V$ cubes depending upon the content designated. The blocks generated restrict, due to their geometric boundary effect, random extension and interconnections of hydrophilic proton-conducting channels (PCCs) composed of the sulfonic acid groups of Nafion molecules. As a result, the entire Nafion matrix will become less hydrophilic and PCC will also become more localized with increasing $P(Q_8M_8^V)$ loading. Our experimental data showed that such change in PCC distribution lead to a series of variations of properties, typically, a clear reduction in methanol permeability, a sharp decrease in the activation energy of proton conduction, and an obvious increase in cell voltage and power density of single DMFC. This work attempts to offer an understanding of the relations between the microstructure of the $P(Q_8M_8^V)$-Nafion composite membrane and its unique properties on the basis of various instrumental characterizations.

5.2 Experimental

5.2.1 Materials

Tetraethylorthosilicate (TEOS, ≥ 98%, Fluka), tetramethylammonium hydroxide pentahydrate (≥ 97%, Sigma), chlorodimethylvinyl-silane (CDMVS, 97%, Aldrich), Nafion® perfluorinated ion exchange resin 5 wt. % soln in lower aliphatic alcohols/H_2O mix (Aldrich), methanol (Merck), tetrahydrofuran (THF, Merck), *N, N'*-dimethyl formide (DMF, Merck) and *N*, *N'*-dimethylacetamide (DMAc) (99%, Aldrich) were used as received.

5.2.2 Synthesis of 1, 3, 5, 7, 9, 11, 13, 15- octakis (dimethylviylsiloxy) pentacycloc octasiloxane (VinylMe$_2$-SiOSiO$_{1.5}$)$_8$ ($Q_8M_8^V$)

This compound was prepared following the Isao Hasegawa's procedure (Hasegawa and Motojima 1992). The first step was the preparation of tetramethylammonium silicate (TMAS) methanolic solution (20 ml): 4.48 ml of TEOS was mixed with tetramethylammonium hydroxide pentahydrate methanol solution (10 ml) and water (1.8 ml) by stirring, and methanol was then added into the mixture to bring the total volume to 20 ml. The solution was then vigorously stirred at room temperature for one day to allow formation of tetramethyl- ammonium silicate solution, in which cubic octamer $Si_8O_{20}^{8-}$ was the main product.

In the second step, CDMVS (8.5ml) was mixed with THF (16.5 ml) by stirring for 5 min to form an extractant of silicate acids. Then a 5-ml portion of the methanol solution of TMAS was added dropwise into this 25-ml extractant solution. The mixture was stirred for 1 h at room temperature. As the boundary between organic and aqueous phases of the mixture was unclear after the reaction, de-ionized and hexane were then added respectively into the reaction mixture to obtain two clear phase layers. The organic phase was transferred to a round bottom flask, and the organic solvent was removed via low-pressure evaporation. After that, the residue was re-crystallized in a small amount of THF to generate cubic octamer particles, and subsequently the product was dried to obtain a white powder. The chemical shifts (ppm) of the product on ^{1}H NMR spectrum are: 5.80-6.20 (m, 18H, vinyl-Hs) (Fig. 5.1), and on ^{29}Si NMR spectrum are: 100.4 (SiO_4), 8.58 and 9.026 (CH_2=$CHMe_2OSi$).

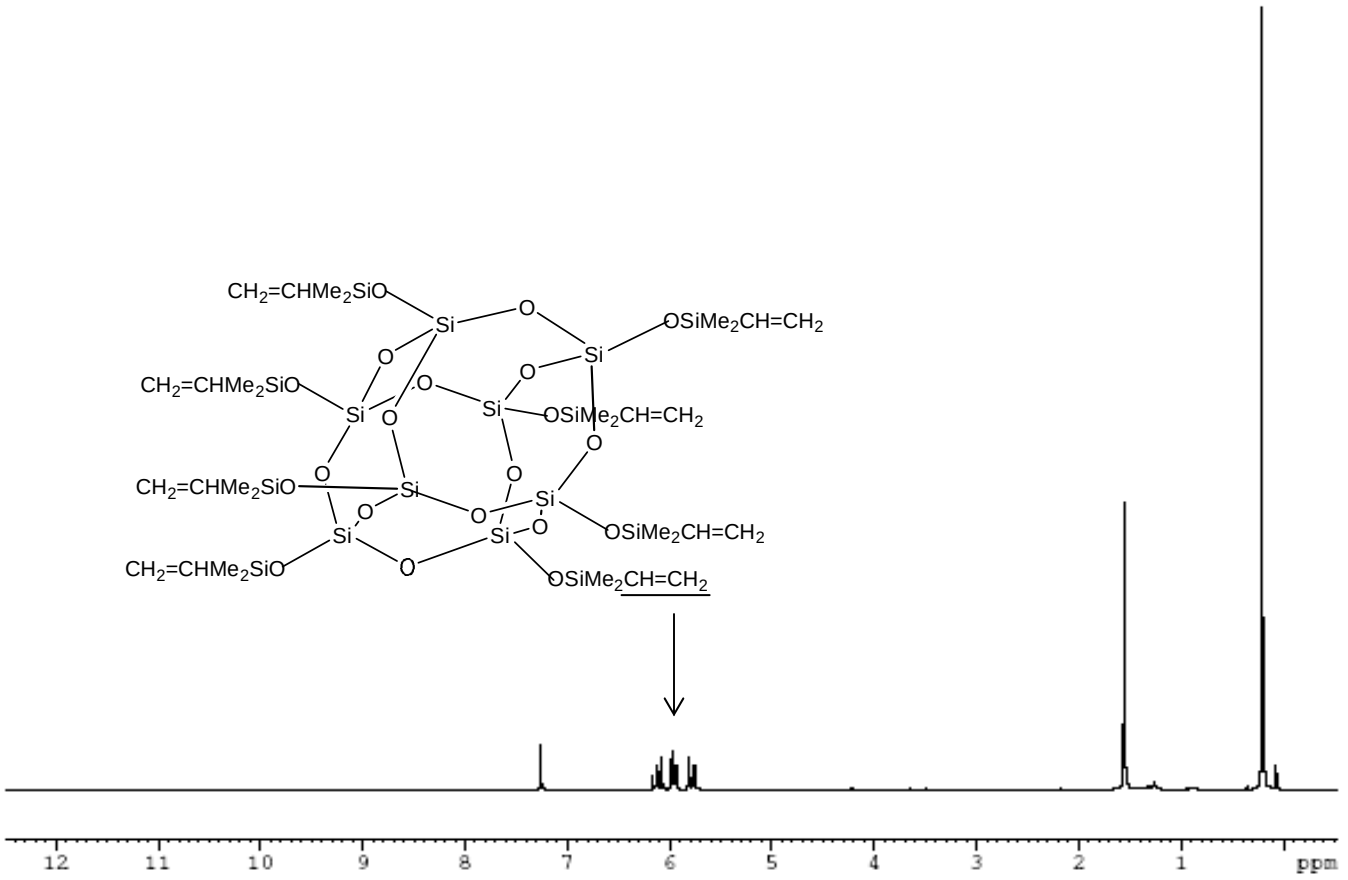

Figure 5.1 ^{1}H-NMR of 1, 3, 5, 7, 9, 11, 13, 15-octakis (dimethylviylsiloxy) pentacycloc octasiloxane (VinylMe$_2$-SiOSiO$_{1.5}$)$_8$ ($Q_8M_8^V$)

5.2.3 *In-situ* polymerization of $Q_8M_8^V$ in the Nafion matrix

Nafion® solution (5 wt.%, 100 ml) in a crystallization dish was subjected to evaporation at 50 ^oC in a ventilation hood to remove the solvent (iso-propanol, *n*-propanol and water). The solid Nafion resin obtained was re-dissolved in *N*, *N*'- dimethylacetamide (DMAc) to prepare a 5 wt.%-solution. Different amounts of $Q_8M_8^V$ compound were introduced into the solution respectively and the resulting suspensions were thoroughly mixed in an ultrasonic bath until a clear solution was formed. Then α,α-dimethylol propionic acid (DMPA), a polymerization initiator, was added into the solution with a $Q_8M_8^V$/DMPA ratio of 100:1 (w/w). The composite membranes were prepared by casting the solutions in separate Petri-dishes. Each dish was kept inside an oven at 60 ^oC for 3 h, and then baked at 120 ^oC for another 3 h. In this heating course polymerization of $Q_8M_8^V$ took place partially in accompanying with evaporation of DMAc and finally the polymerization of $Q_8M_8^V$ was completed in the Nafion matrix by placing the membrane in an UV oven (SpectroLinker UV Cross Linker, XL-1500) for 2 h. For recasting pure Nafion membrane, the same procedure was applied except UV baking.

5.2.4 Characterizations of structures and properties

5.2.4.1 Spectroscopy analysis

^{1}H and ^{29}Si NMR spectra of $Q_8M_8^V$ were recorded on a Bruker ultrashield 400 spectrometer, using chloroform-*d* as solvent and tetramethylsilane internal standard. Fourier transform infrared spectroscopy-attenuated total reflectance (FTIR-ATR) spectra of the membrane samples were obtained on a BioRad spectrometer (resolution 2 cm^{-1}). A ZnSe crystal was used as the ATR plate with an angle of incidence of 45°. The cross-section morphological images of the membrane samples were taken on a field emission scanning electron microscope (FESEM, JEOL-JSM-6700).

5.2.4.2 Thermal analysis

The thermal stability of the prepared membranes was evaluated by thermogravimetric analysis (TGA) using a TA Instruments 2050 Thermogravimetric Analyzer. The heating rate was 10 ^{o}C/min and the sample was under a dry nitrogen purge (100 ml/min) through the entire heating process. The glass transition behaviors of the membrane samples were measured on a Mettler Toledo DSC 822e equipped with a pressure DSC Cell. The scanning rate of 10 ^{o}C/min was set and the first scan (from rt. to 100 ^{o}C) was intended to remove different thermal history of the samples. The results from the second scan were recorded. The dynamic mechanical analysis (DMA) was performed on a TA Instruments (DMA 2980) using a heating rate of 3 ^{o}C/min from room temperature to 200 ^{o}C and a vibration frequency of 1 Hz.

5.2.4.3 Solvent-matrix interactions analysis

Methanol permeability measurement was conducted using a glass diffusion cell. One compartment of the cell (V_A =50 ml) was filled with 2 M methanol solution (8 vol.%, typical concentration used in current DMFC), and the other compartment (V_B =50 ml) was filled with deionized water. The membrane (wetted area = 4.90 cm^2) after fully hydrated with deionized water for 24 h was fastened between the two compartments where the two solutions were kept stirred throughout measurement. The concentration-driven diffusion of methanol from compartment A to B across the membrane was measured against time using a Shimadzu GC2010 gas chromatograph (GC) equipped with a HP-Plot Q column (30 m×0.32 mm×20 μm) and a flame ionization detector. 1-butanol was the internal standard for the GC analysis. The solvent-swelling of the membrane samples in a binary THF-DMF solution at room temperature was determined by gravimetric approach. The membrane samples were vacuum dried at 70 ^oC for 24 h in prior of measurement. Swelling degree (%) was evaluated using the following formula:

$$\text{Swelling percentage (\%)} = \frac{W_{wet} - W_{dry}}{W_{dry}} \times 100\% \quad \text{…… Equation 5.1}$$

5.2.4.4 Ionic exchange capacity (IEC)

Each dry membrane was soaked in 10 ml 0.05 M sodium chloride aqueous solution for 24 h to allow exchange of protons with sodium ions. The ion-exchanged solution (containing hydrogen chloride) was titrated to pH 7.0 using a standard 0.05 M sodium hydroxide aqueous solution and the end-point of titration was indicated by a pH meter (HORIBA).

Each exchanged NaCl solution was titrated twice and the mean titrate volume was used for the IEC calculation.

5.2.4.5 Electrochemical analysis

The proton conductivity, σ (S/cm), of membranes was gauged by AC impedance method on an Autolab electrochemical analyzer using a frequency scanning range of 0.01 Hz to 1 MHz, AC perturbation of 10 mV and DC rest voltage of 0.0 V. A sample of the membrane (1.3 cm in diameter) was sandwiched by two stainless steel disk electrodes of the same diameter and fastened in a Teflon holder, and the holder was immersed in a heating bath with a setting temperature. The membrane electrode assembly (MEA) for the direct methanol fuel cell evaluation was made by sandwiching a membrane with an anode sheet and a cathode sheet. The anode sheet was a carbon paper (SGL, Germany) coated with a Pt-Ru/C catalyst layer and the cathode sheet was a carbon paper coated with a layer of carbon-supported 40 wt.% Pt catalyst supplied by E-TEK. The catalyst slurries were prepared by mixing de-ionized water, Nafion® solution (Aldrich), and 40 wt.% Pt/C for cathode ink and 40 wt.% Pt-Ru/C for anode ink. The average platinum loadings at the anode and cathode were 3 and 2 mg/cm^2, respectively, and the effective electrode area was 5 cm^2. The fuel used was 2 M CH_3OH delivered at 2 ml/min by a micropump, and the oxygen flow (500 cm^3/min) was regulated by a flowmeter.

5.3 Results and discussions

5.3.1 Structural characteristics of Nafion-P($Q_8M_8^V$) composite membrane

As a $Q_8M_8^V$ cubic molecule bears eight vinyl groups, the free radical chain growth would be very localized because the polymerization medium (i.e. the cast Nafion solution in DMAc) is tranquil and the simultaneous three-dimensional growth would undergo quickly to generate rigid P($Q_8M_8^V$) blocks as shown in Fig. 5.2. Consequently, nano-blocks generated from the *in-situ* polymerization are distributed uniformly in Nafion matrix, and each of them interlocks a certain number of polytetrafluoroethylene (PTFE) backbones of Nafion due to the *in-situ* polymerization scenario. Furthermore, it is rational to consider that the Nafion molecules physically anchored to P($Q_8M_8^V$) blocks will trigger formation of domains through the association of the sulfonic acid groups at the end of their side chains with those of the unbound Nafion molecules surrounded by the P($Q_8M_8^V$) blocks as illustrated in Fig. 5.3. As a result of this boundary regulating effect, PCCs are formed primarily through assembling of the Nafion molecules in respective domains. To prove the happening of this domain-predominant matrix, thermal analyses (TGA, DMA and DSC) were employed to probe changes in thermal stability of the pendant sulfonic acid groups and, more importantly, in dynamic response of segment motions to increase of temperature.

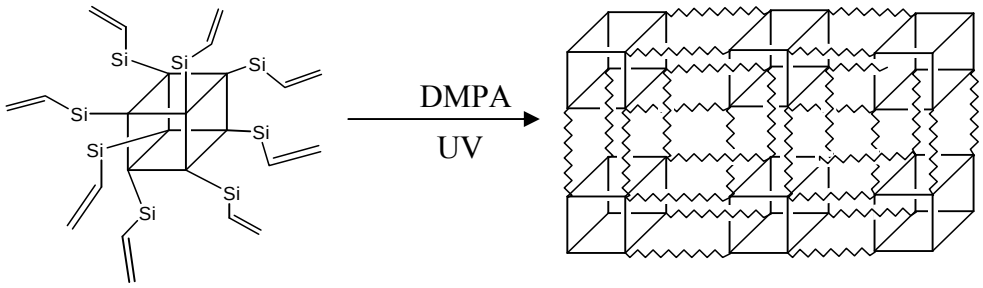

Figure 5.2 Synthesis of poly($Q_8M_8^V$) fragments from $Q_8M_8^V$ monomers

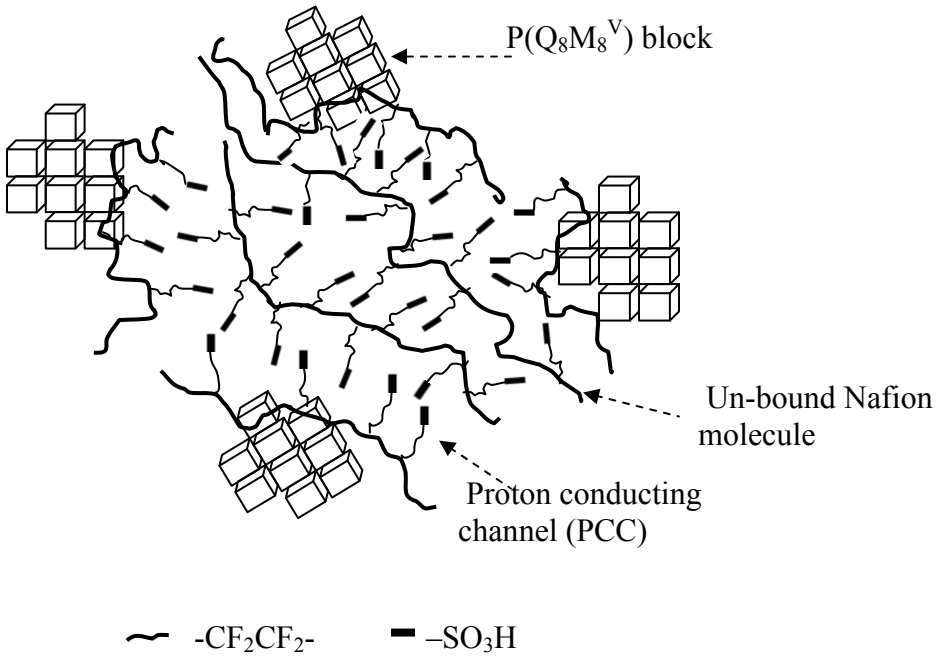

Figure 5.3 Schematic representation of the domain formation due to induction of the embedded $P(Q_8M_8^V)$ blocks

The TGA weight-loss profiles (Fig. 5.4) show no difference in the onset temperature (~355 ^oC) of the 1st weight loss slope, which is attributed to the degradation of sulfonic acid groups, between the pristine Nafion matrix and the composite membranes. But the first weight-loss plateau of the composite membranes is located below that of the pristine membrane, this phenomenon implies that the composite membranes are thermally more vulnerable, in particular the 15-wt.% membrane. It is contemplated that the unbound Nafion molecules in the composite membrane could undertake thermal motions to a greater magnitude than those in the pristine membrane because each individual Nafion molecule in the latter scenario takes part in more PCC branches and is therefore more strongly tightened. As to the viewpoint that a part of perfluoro-chains of Nafion was hung

on to P($Q_8M_8^V$) blocks via physical interlocking, the variation of storage modulus of the composite membranes (Fig. 5.5) suggests the presence of such dispersed physical crosslinking sites over the bulk of membrane. With the increase in the content of P($Q_8M_8^V$) blocks, more Nafion molecules are physically anchored to these blocks, which brings about reinforcing effect on the membrane because the affixed molecules interact with the other molecules via the association of their respective sulfonic acid groups as portrayed in Fig. 5.3. Hence macroscopically the storage modulus of the composite membranes shows a clear dependence upon the P($Q_8M_8^V$) content.

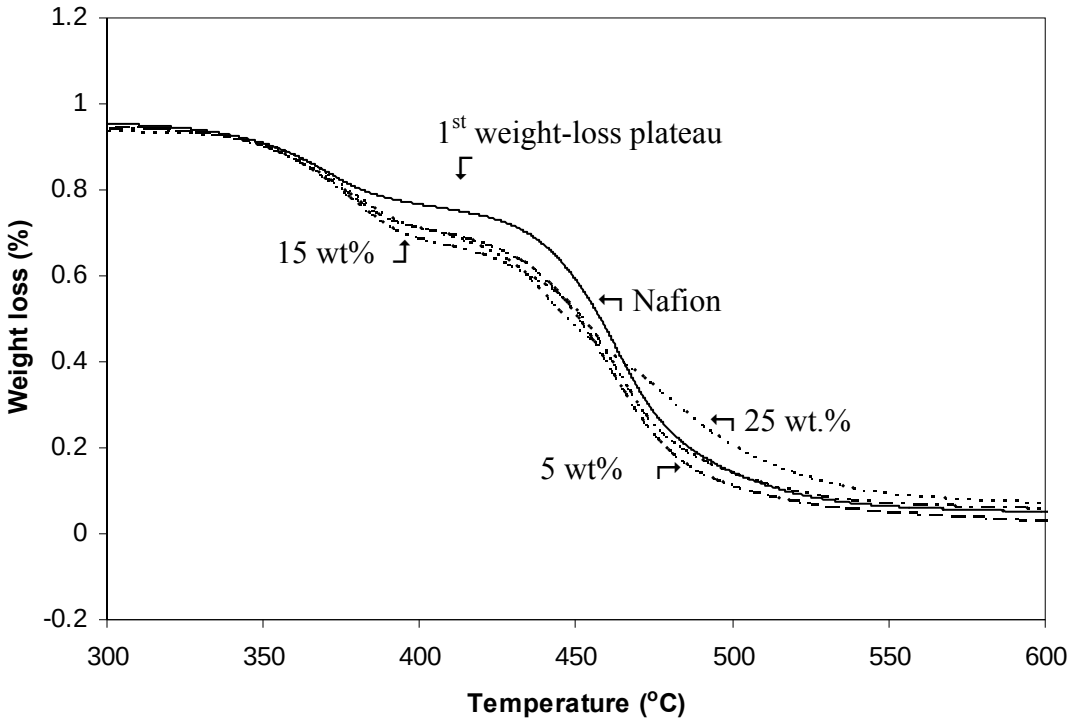

Figure 5.4 TGA data for recast Nafion and composite membranes with 5 wt.%, 15 wt.% and 25 wt.% poly($Q_8M_8^V$) loading

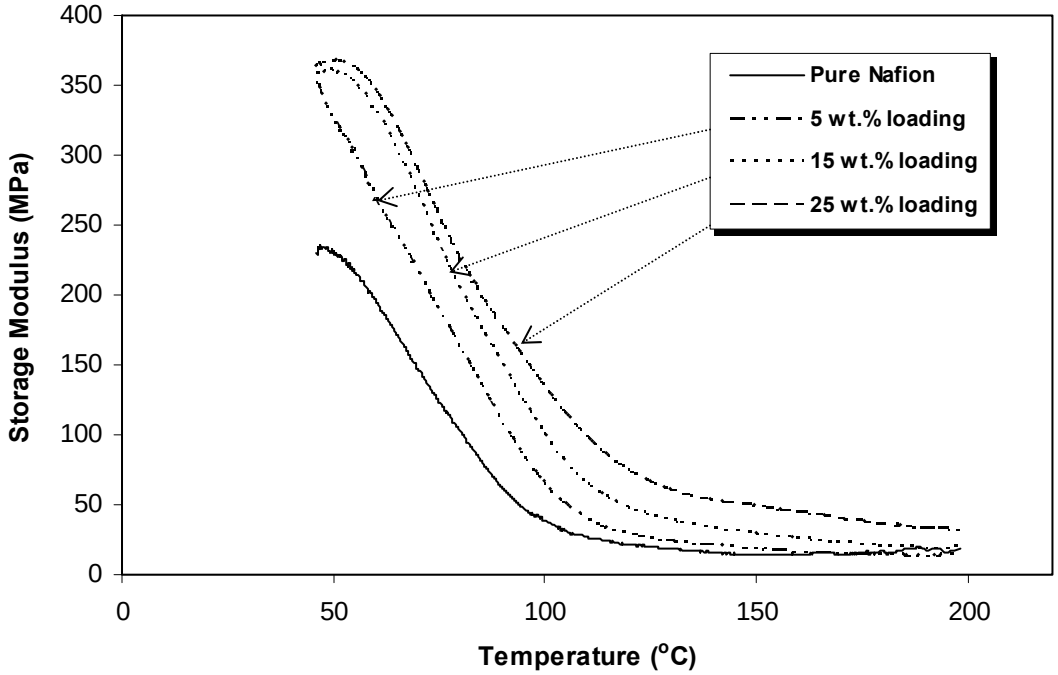

Figure 5.5 The dynamic mechanical properties (real part) of the four recasting membrane

The DSC experiment shows an appealing phenomenon: the glass transition step of composite membrane shifted toward low temperature direction with increasing the $P(Q_8M_8{}^V)$ content in it as displayed in Fig 5.6. We have also identified, on the basis of the small angle X-ray scattering (SAXS) result, that nil crystallization of Nafion molecules occured in the recast pristine membrane and composite ones. Therefore the crystallization effect on the polymer chain motions is beyond the scope of consideration. In the Nafion membrane the energy barrier of the glass transition is affirmed to originate from strong attractive interactions of the pendant sulfonic acid groups in PCC. In this context rolling down of T_g implies that this cohesive interaction becomes weakened, and it is known from the above discussion that the $P(Q_8M_8{}^V)$ blocks curb interconnecting

extents of PCC, or an individual Nafion molecule is involved in fewer PCC branches than it behaves in the pristine Nafion matrix. Consequently, segment motions of the Nafion molecules are needed to overcome weaker binding caused by the associations of the pendant sulfonic acid groups. When the $P(Q_8M_8^V)$ content reaches 25 wt.%, the highest content in the three composite membranes, a broad and shallow endothermic bow appears on its DSC profile, which can be attributed to segment motions of unbound Nafion chains. Compared with the other two composite membranes, the strongest partitioning action of $P(Q_8M_8^V)$ blocks exists in this membrane. Consequently the unbound Nafion molecules involve the least extent of inter-chain connections and have highest degree of freedom of chains motions. This rubbery behavior can also be spot from the infrared absorption spectra of the Nafion-$P(Q_8M_8^V)$ composite membranes. According to the reflective IR spectrum of Nafion, three absorption bands at the wave-number of 806 cm^{-1}, 972-984 cm^{-1}, and 1053 cm^{-1} are normally known as the finger prints of perfluorocarbon chain, in which the lowest energy band (806 cm^{-1}) is generated from the carbon skeleton vibration modes (Fig. 5.7). It is found that this absorption band becomes broader and shift slightly to low frequency direction with the increase in $P(Q_8M_8^V)$ loading, in particular from 5 wt.% to higher ones. This phenomenon can be interpreted as the relaxation of a portion of perfluorocarbon chains. On the other hand, the ν(S=O) scissor peak of the pendant sulfonic acid group becomes flatter with increasing of the content of $P(Q_8M_8^V)$ because the latter one has a very strong and broad absorption peak, ν(Si-O), appearing almost at the same frequency range as the ν(S=O). As a result, the ν(S=O) vibration peak is shielded by the ν(Si-O) peak.

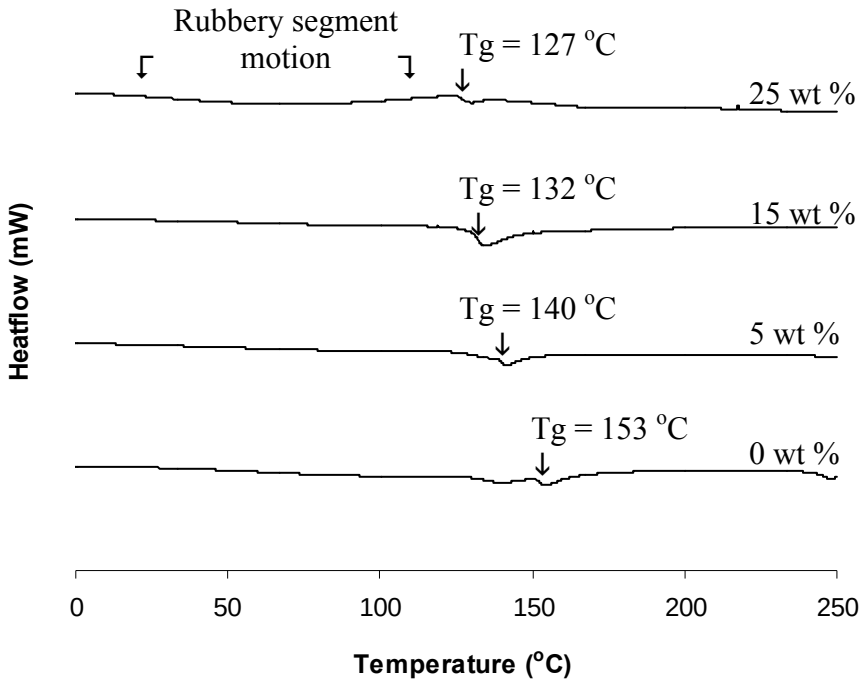

Figure 5.6 DSC data for recast Nafion and composite membranes with 5 wt.%, 15 wt.% and 25 wt.% poly($Q_8M_8^V$) loading

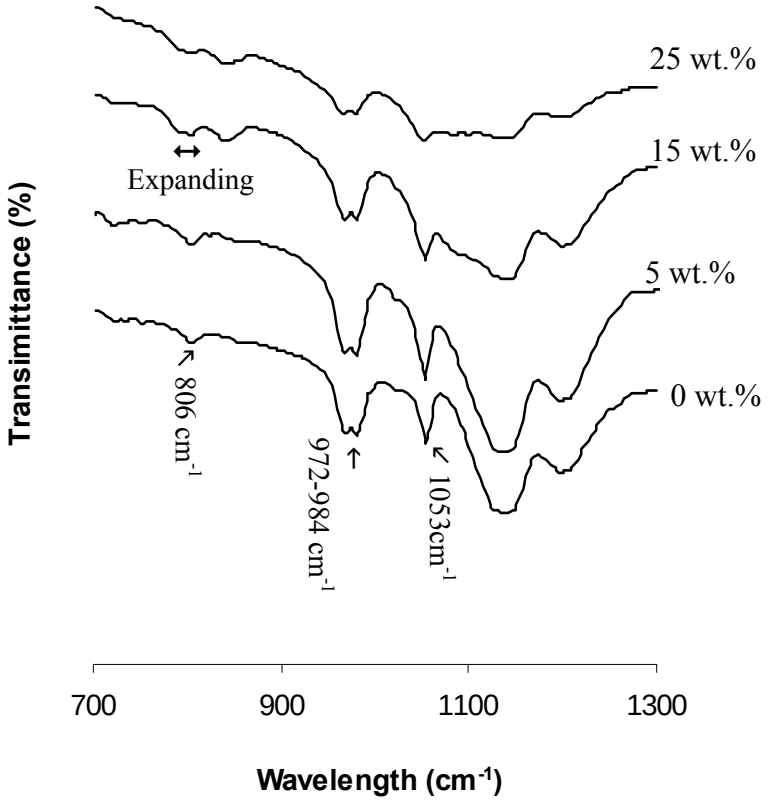

Figure 5.7 FTIR-ATR spectra of recast Nafion and composite membrane with 5 wt.%, 15 wt.% and 25 wt.% P($Q_8M_8^V$) loading

The cryo-fractured cross-sectional surfaces of the composite membranes were examined by FESEM (Fig. 5.8). As they were recast using the dipolar aprotonic organic solvent (DMAc) as aforementioned, this particular solvent (Jiang et al., 2006) possesses affinity with both perfluorocarbon backbone and pendant sulfonic acid groups, hence resulting in a matrix without a clear pattern (Fig. 5.8a). In contrast, a ribbon-like dense fractured surface (Fig. 5.8b) was obtained from the membrane developed by directly casting Nafion-117 solution (alcohols/water) because Nafion molecules undergo association to form rodlike aggregates in this very hydrophilic solvent environment (Mauritz and Moore 2004). In Fig. 5.8c, a lamina-like fractured surface was observed because of the presence of 5 wt.%–P($Q_8M_8^V$) in the Nafion matrix. The further increase in the P($Q_8M_8^V$) content to 15 wt.% gave rise to a step-like matrix morphology. As per the preceding discussion, these two particular bulk phase morphologies are generated from the two types of chain packing manners as illustrated in (Fig. 5.9): the 5 wt.%-loading was only enough to induce laminar domains but 15 wt.%-loading could narrower down domains in 3-D assembly. Increasing the loading to 25 wt.% caused a bulk phase that is lack of a long range pattern. Obviously, a too crowded P($Q_8M_8^V$) content is responsible for this randomness.

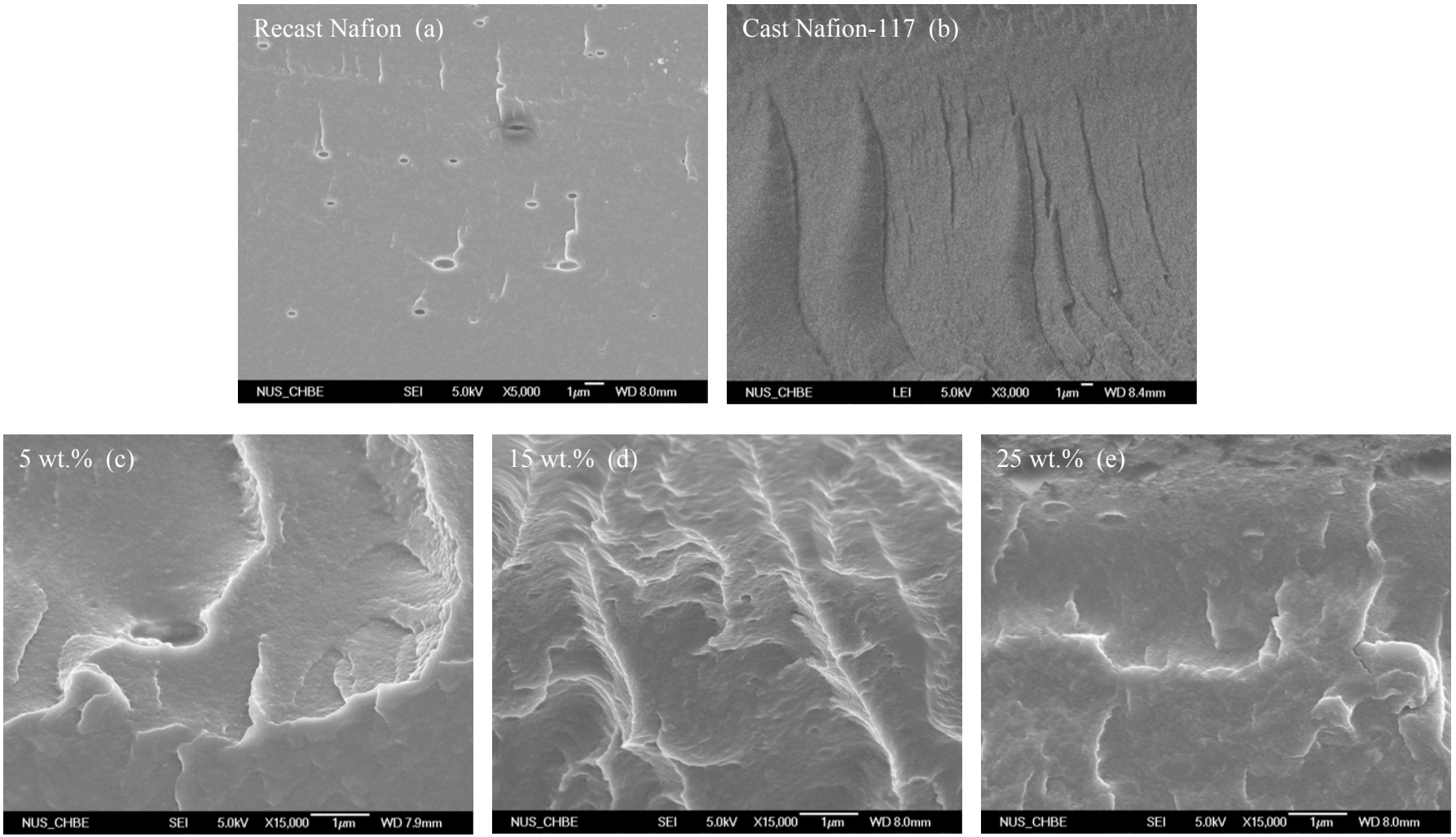

Figure 5.8 FESEM cross-section micrographs of composite membrane with (a) recast Nafion, (b) cast Nafion-117, (c) 5 wt.%, (d) 15 wt.% and (e) 25 wt.% poly($Q_8M_8^V$) loading

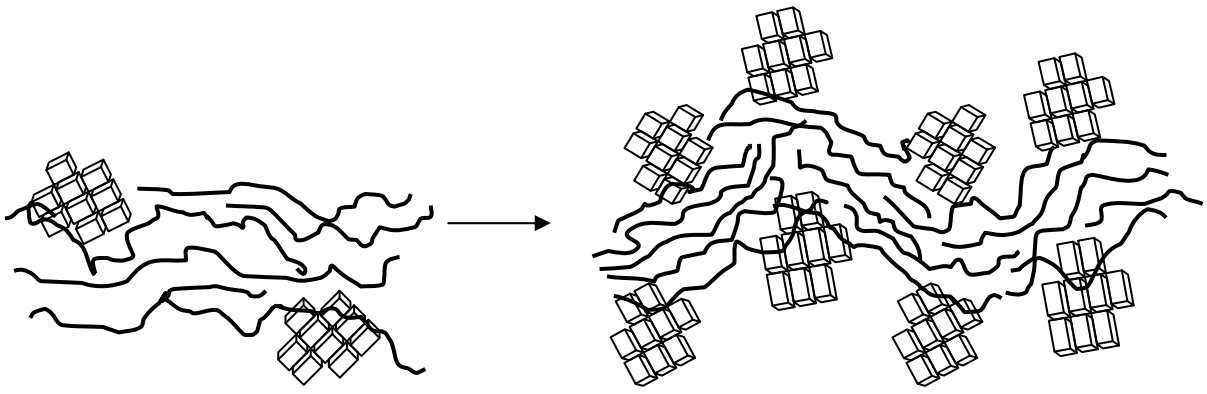

Scale-like chain packing

Wave-like chain packing

Figure 5.9 Schematic representation of the two types of chain-packing domains

5.3.2 An investigation of membrane-solvent interactions

From the above discussion, the presence of $P(Q_8M_8^V)$ blocks in Nafion matrix caused a reduction in the interconnecting extent of PCC, as a result, the composite matrixes can be more easily accessed by less polar solvents, for instance, tetrahydrofurane (THF) is less hydrophilic than *N, N'*-dimethylformide (DMF). The higher swelling extents of the three recast composite membranes in pure THF proved this estimation (Fig. 5.10). With adding a small amount of DMF (0.05 w/w) into THF, the pure Nafion membrane underwent a greater increase in swelling degree than the composite membranes. As a result, the discrepancy in swelling extent between the pristine Nafion membrane and the composite membranes was narrowed down. It seems that the inclusion of such a substantially small amount of DMF in THF triggered out swelling of the pristine Nafion matrix, which verifies the preceding inference that the pristine Nafion matrix contains a greater extent

of randomly interconnected PCC and thus is more hydrophilic. Thermodynamically, this prompt increase in swelling extent is also driven by the infinite partial molar properties (e.g. solvating enthalpy) of DMF in Nafion matrix. On the other hand, the three composite membranes displayed very close swelling extents in pure THF, namely the $P(Q_8M_8^V)$ content affected insignificantly swelling of composite matrix in THF. However these congested swelling degrees in THF became differentiated with the introduction of a small amount of DMF into THF. This phenomenon could be interpreted as the DMF penetration through the interface between Nafion matrix and $P(Q_8M_8^V)$. It was also observed that the further increase in DMF concentration up to 0.18 w/w (equivalent to 25 vol. %) enhanced only slightly swelling degrees of the three composite membranes and did not alter their sequence as well. It is likely that there was a swelling saturation limit in each composite membrane in the concentration range of DMF-THF solvent and the existing of swelling limit was due to the presence of $P(Q_8M_8^V)$ "grid" in the Nafion matrix. In contrast, the pristine Nafion membrane underwent more perceptible swelling with the increase of DMF concentration.

How the content of $P(Q_8M_8^V)$ in Nafion matrix affects methanol permeability is the key issue to understand. In the permeability measurement, the commercial Nafion-117 ® membrane (made by extrusion) was chosen as the control sample to benchmark the four recast membranes and the results are shown in Fig. 5.11. Firstly, it is clear that the methanol permeability of the commercial Nafion-117 membrane at room temperature is about double as much as that of the recast Nafion-117 membrane. This discrepancy can be attributed to the existence of an ordered and extensively distributed PCC network in

the former than in the latter membrane since methanol molecules permeate through PCC only. However, among the composite membranes the 15 wt.%-loading one exhibited the lowest methanol permeability (4.09×10^{-7} cm^2/s), which is about 30% of the permeability of the recast pristine membrane. After passing this lowest point, a slightly higher permeability (5.55×10^{-7} cm^2/s) was given by the membrane with the loading of 25 wt.%. A similar trend was also observed from the variation of ion exchange capacity (IEC) of the four membranes (Table 5.1), in which the 15 wt.% membrane showed the lowest IEC value while the 25 wt.% membrane displayed a higher IEC than the pristine Nafion on the equal Nafion mass basis. As described above, the 25 wt.% membrane contains randomly oriented PCC and the highest interfacial area between Nafion and $P(Q_8M_8{}^V)$ blocks. These two factors make PCC be most easily accessible by sodium ions in the membranes of interest. It is comprehensible that implantation of $P(Q_8M_8{}^V)$ blocks in Nafion matrix restricts random spread of PCC, and hence discourages diffusion of methanol molecules in the composite membranes. It is noteworthy that the ordered chain packing manner (refer to Fig. 5.9) also plays a favorable role in restricting methanol permeation.

Table 5.1 The ion-exchange capacity of the four membranes

Membrane sample	Nafion	Poly ($Q_8M_8{}^V$)-Nafion composite membranes		
		5 wt.%	15 wt.%	25 wt.%
Ion exchange capacity (meq/g)*	0.705±0.005	0.700±0.003	0.656±0.005	0.746±0.005

* meq/g represents milli-equivalent per gram of pristine Nafion.

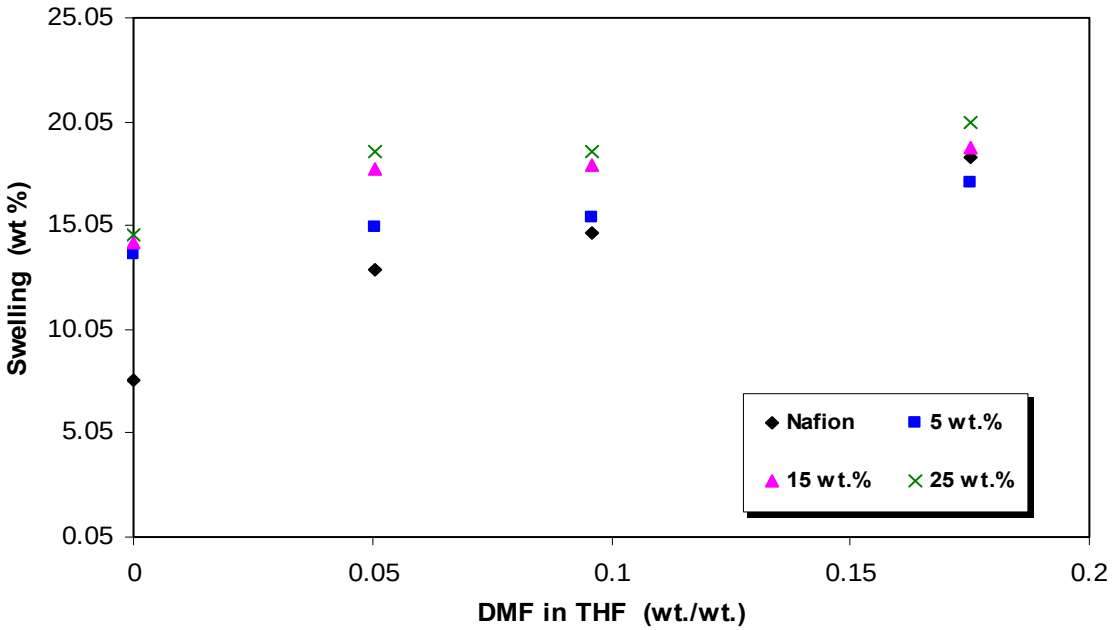

Figure 5.10 Solvent-swelling test for recast Nafion and composite membrane with 5 wt.%, 15 wt.% and 25 wt.% poly($Q_8M_8^V$) loading

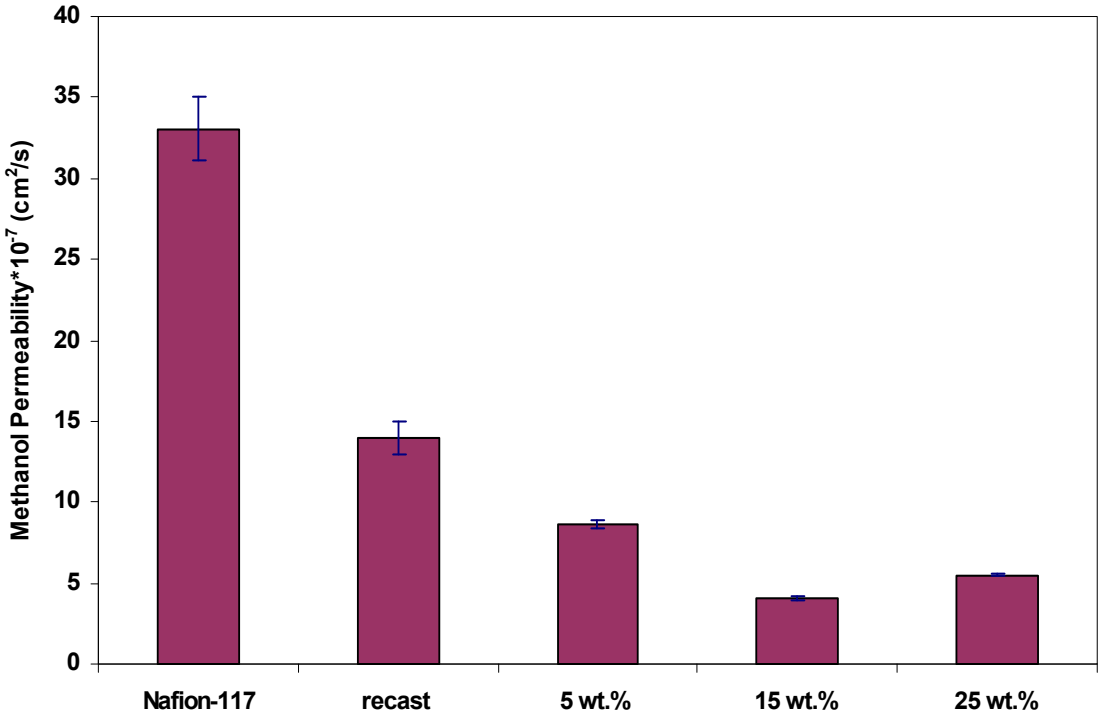

Figure 5.11 Methanol permeability of commercial Nafion-117, recast Nafion and composite membrane with 5 wt.%, 15 wt.% and 25 wt.% poly($Q_8M_8^V$) loading

5.3.3 Electrochemical Evaluations

The proton conducting traits of the four recast membranes were evaluated by their particular Arrhenius plots, from which we find that the inclusion of 5 wt.% $P(Q_8M_8^V)$ into Nafion matrix reduced about a half of its proton conduction activation energy, but the further increase in $P(Q_8M_8^V)$ loading led to insignificant reduction of this kinetic energy barrier (Fig. 5.12). This outcome is deemed to have a direct relation with the PCC distribution in the bulk phase. Among the four membranes, PCC could achieve maximal extension in the matrix of pristine Nafion because each individual Nafion molecule in DMAc solvent is fully random and could therefore take part in forming the largest possible number of PCC during drying process. Also because of this greater extent of interconnection, PCC generated should contain relatively dilute sulfonic acid groups. A high interconnecting extent of PCC is an encouraging factor for proton transport but a low density of pendant sulfonic acid groups and tortuous channel structure will offset to a certain extent the advantage. Indeed, its high activation energy implies that proton transport relies on matrix water molecules as hopping sites since hydrogen bonding needs thermal energy to overcome it. (Ye et al., 2007) The high water uptake is an essential result of the large interconnecting extent of PCC. On the contrary, the laminar domains were induced upon *in-situ* formation of $P(Q_8M_8^V)$ blocks in the recast Nafion matrix as shown in Fig. 5.8, which confined PCC formation primarily within individual lamina. This change would increase the density of sulfonic acid groups in PCC with sacrificing the interconnecting extent of PCC, which benefits cutting down water uptake and hence methanol diffusion as it has been examined above. Indeed, compared with the pristine

Nafion membrane, the fact that the 5 wt.%-membrane showed obviously lower activation energy means that proton transport through pendant sulfonic acid groups became significant. When the loading was raised to 15 wt.%, the membrane exhibited highest proton conductivity of the four over the temperature range of study. In this case, although the PCC interconnecting extent was farther decreased with narrowing down the laminar domains, which has been observed in IEC testing result (Table 5.1), they were likely more straightforward and less twisted, which can be inferred from its anisotropic matrix shown in Fig. 5.8d. In addition, with the increase of $P(Q_8M_8^V)$ loading from 5 wt.% to 15 wt.%, only a small decrease in the activation energy of proton migration implies that the density of sulfonic acid groups in PCC of the 5 wt.%-membrane already reached percolation of proton conduction that takes place through hopping over the pendant sulfonic acid groups. In pursuit of the loading up to 25 wt.%, it yielded a counter-productive effect, namely the membrane exhibited the lowest proton conductivity of the four. It is rational to suggest that PCC were twisted by the random matrix resulted. This factor plus the minimum extent of interconnection of PCC in this particular membrane are responsible for lowest proton conductivity in the temperature span of study.

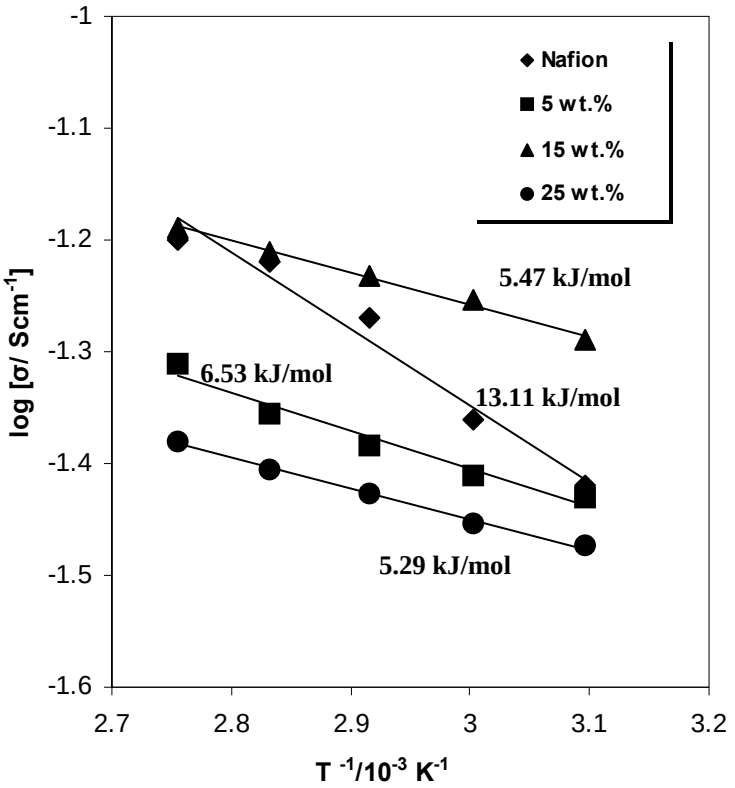

Figure 5.12 Arrhenius plots of conductance vs. temperature for recast Nafion and composite membrane with 5 wt.%, 15 wt.% and 25 wt.% poly($Q_8M_8^V$) loading

The above four recast membranes were evaluated in the single DMFC at room temperature and 50 ^oC, respectively (Fig. 5.13). Theoretically, the slow kinetics of the electrode-oxidation of methanol at the anode as well as the oxidation of methanol at the cathode generated detrimental impact on the cell performance of the DMFC (O'Hayre et al., 2006). Besides these two potential losses, the degree of ohmic loss is directly affected by the structure of PCC which sustains the flux of proton through the membrane. At ambient temperature (20 ^oC), the overall potential loss of the four membranes followed the order: recast Nafion > 25 wt.% > 5 wt.% > 15 wt.%, in which the position of Nafion dropped to the bottom from the 2nd rank in the order of proton conductivity. This flipping-over of order could be attributed to the methanol crossover from anode to

cathode through the membrane and the low efficiency of PCC due to their torturous structures in the pristine Nafion as concluded above. The methanol permeation measurement (Fig. 5.11) truly reflects the methanol crossover when the membrane is used in the DMFC environment, but the conductivity measurement only represents the situation when a substantially low proton transport flux going across the membrane. In the single cell assessment, the ohmic loss over the pristine Nafion membrane is an indication that its PCC do not possess adequate capability to sustain a high proton flux, or current density. Consequently, the membranes with different $P(Q_8M_8^V)$ contents lead to very different power density output in the single DMFC loaded up with them respectively. For example, the maximum of the power density upheld by the 15 wt.%-membrane was 13.92 $mWcm^{-2}$, while the pristine Nafion membrane was merely 4.62 $mWcm^{-2}$.

When the testing temperature of the DMFC cell was raised to 50 ^{o}C, the 5 wt.%-membrane exhibited slightly better cell performance than the 15 wt.% one (Fig. 5.13b), which is reversed to their room-temperature performances. In light of the structure of PCC, rising of temperature would accelerate proton migration but also thermal motions of the pendant sulfonic acid groups; the latter factor will be a negative factor affecting transport of protons because of increasing chaotic collisions. Hence, there should be an optimal density of sulfonic acid groups in PCC that balances these two factors. From this perspective, proton transport in the 5 wt.% membrane is less affected by thermal motions of the pendant sulfonic acid groups than in the 15 wt.% membrane, because sulfonic acid groups in the former membrane are in general not as tight as those in the latter one as we know from the previous discussion.

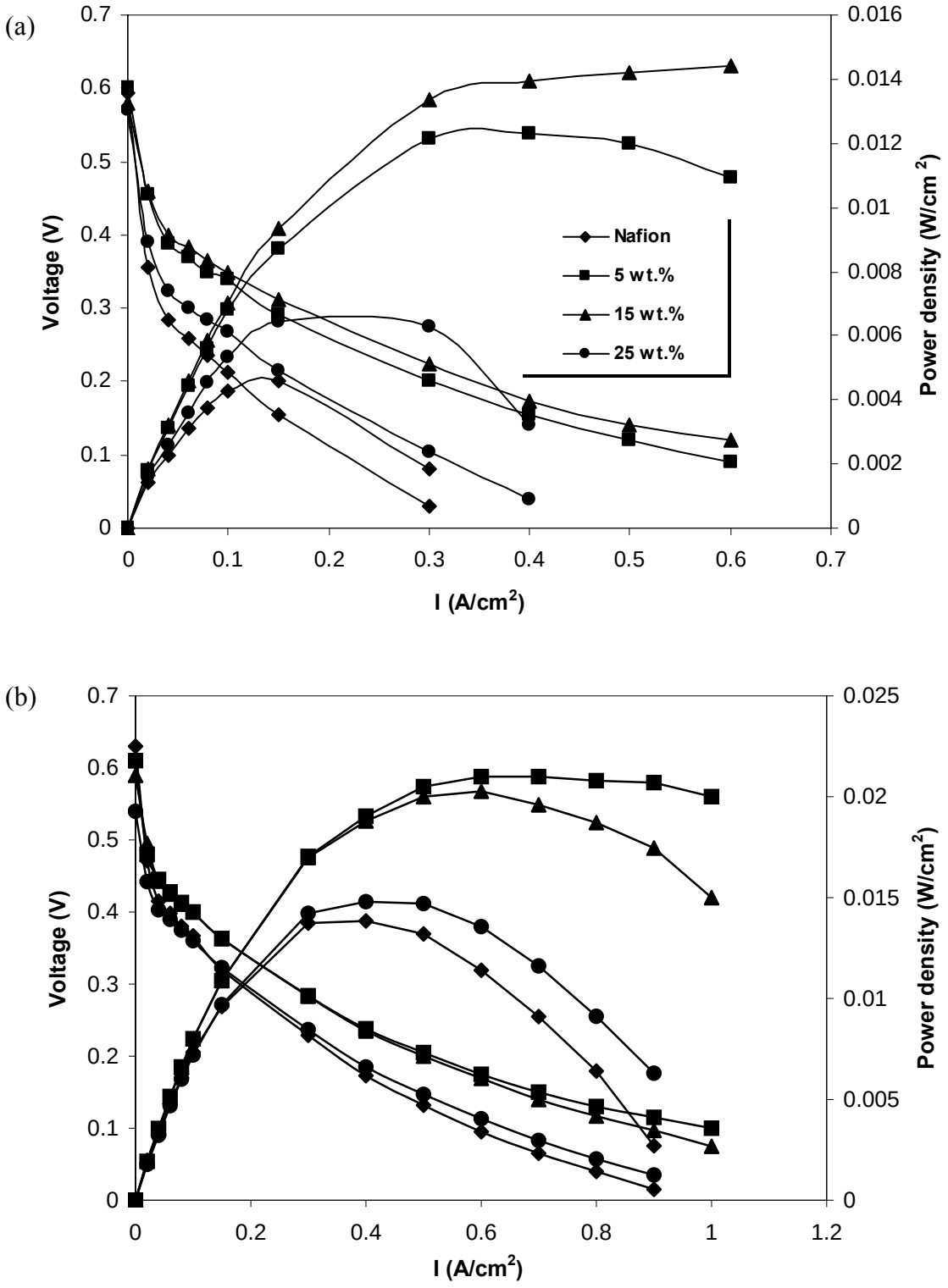

Figure 5.13 Polarization curves and power output of a DMFC using recast Nafion membrane and composite membrane with 5 wt.%, 15 wt.% and 25 wt.% poly($Q_8M_8^V$) loading measured at (a) 20 °C; (b) 50 °C

5.4 Conclusions

This work develops a special nano filler P($Q_8M_8^V$) to enhance inherent traits of Nafion membrane for the use in direct methanol fuel cell (DMFC). The inclusion of the particles into the host matrix was carried out via polymerizing cubic octasiloxane molecules, $Q_8M_8^V$, inside the recast Nafion membrane. It is important to note that the P($Q_8M_8^V$) blocks do not draw adsorption of sulfonic acid groups of Nafion molecules due to their intrinsic hydrophobicity, but rather, the *in-situ* polymerization renders P($Q_8M_8^V$) blocks interlock perfluorocarbon backbones of Nafion molecules on them. As a result of the implantation of such rigid blocks in the Nafion matrix, the interconnecting extent of proton conducting channels (PCC) was confined and, in contrast to the pristine host matrix, the assembling of Nafion molecules displayed a long-range pattern depending upon the P($Q_8M_8^V$) content. The understanding of the aforementioned structural characteristics was established on the basis of the thermal property, matrix morphology, solvating behavior, and kinetics of proton transport of the composite membranes. It is because of the unique matrix-formatting role of P($Q_8M_8^V$) blocks, the composite membranes containing the filler of 5 wt.% to 15 wt.% impart apparently lower methanol permeation coefficients and far greater power density output of single DMFC than the pristine Nafion membrane.

CHAPTER 6

RESTRUCTURING PROTON CONDUCTING CHANNELS BY EMBEDDING STARBURST POSS-g-ACRYLONITRILE OLIGOMER IN NAFION®

6.1 Introduction

From the earlier chapter, it was reported that polymerizing vinyl-overhung octasiloxane ($Q_8M_8^V$) cubic molecules in the Nafion recasting process yields an impact on formatting the Nafion matrix. As a result, compared with the pristine Nafion membrane, the resultant composite membranes containing P($Q_8M_8^V$) of 5 ~ 15 wt.% manifested obvious improvement on both repressing methanol permeability and raising power density output of the single direct methanol fuel cell (DMFC).

In this work, we continue to attempt to decrease methanol permeation level through the Nafion membrane by mean of incorporating another type of hybrid POSS nano-particles, composed of a pendant polymer outer layer and an inorganic core, into the matrix of Nafion. The starburst oligomeric structure, *sb*-POSS, is considered as a suitable candidate of the hybrid nanoparticles for this aim. The *sb*-POSS particle has a unique structure that is characterized by the anchoring of eight oligomeric polyacrylonitrile chains to cubic

polyhedral oligomeric silsesquioxane (POSS) core (Fig. 6.1). The atom transfer radical polymerization (ATRP) method was employed to synthesize the *sb*-POSS structure. Pyun et al. have investigated the kinetics of surface-initiated ATRP and morphology of the resultant hybrid particles. (Pyun et al., 2003a and 2003b) It is important to note that ATRP on a POSS core results in only oligomeric (short) polymer chains. As a result, the particles generated could still remain in the nano sizes range (< 20 nm) due to no chain entanglements.

We observed via thermal analysis an appealing phenomenon: the *sb*-POSS particles, when dispersed in the Nafion matrix, caused restructuring of the hydrophilic proton conducting channels (PCCs) that are composed of the pendant sulfonic acid groups. Further investigations showed that this restructuring effect is sensitive to the *sb*-POSS (as filler) content. Indeed, the power output (in mW/cm^2) of a single DMFC loaded with the *sb*-POSS/Nafion composite membrane was clearly affected by the *sb*-POSS content. The composite membrane containing 5 wt.% *sb*-POSS particle gave rise to the largest power output with a maximum power of 44.2 mW/cm^2. In contrast, the Nafion membrane (e.g. the host matrix alone) conferred only a power density of 19.9 mW/cm^2. Therefore, this work focused on elucidating the interactions between *sb*-POSS particles and Nafion molecules using the structural characterization results, and understanding the key factors responsible for the boost of fuel cell performance.

6.2 Experimental

6.2.1 Synthesis of starburst POSS-g-acrylonitrile oligomer (*sb*-POSS)

The POSS (POSS-methacryl substituted cage mixture, Aldrich) was brominated in the chloroform solution at temperature 0-5 ºC for 30 min. The brominated POSS was then purified by washing in pure chloroform for three times. A typical procedure for the synthesis of *sb*-POSS by ATRP is as follows: Ethylene carbonate (5 g) (EC, Aldrich) and Dimethylformamide (1 ml) (DMF, Aldrich) as the co-solvent of reaction were added into a 25 ml round bottom flask, and acrylonitrile (6 ml) (+99%, Aldrich, inhibitor removed), the brominated POSS (0.073 g) and 2, 2'-bipyridyl (90.75 mg) (Bpy, Fluka) were introduced into the flask. The reaction flask was immersed in an oil heating bath (70 ^{o}C-80 ^{o}C). After 30 minute, a calculated amount of CuBr (27.9 mg) (> 98%, Aldrich) was added into the flask sealed and charged with argon gas. Samples were withdrawn from the reaction mixture by a syringe and dropped into a methanol water mixture (v:v=1:1) to form white *sb*-POSS precipitation for GPC measurement. In addition, the molecular structure of the *sb*-POSS was determined by ^{1}H NMR in DMSO-d^{6} (Fig. 6.1).

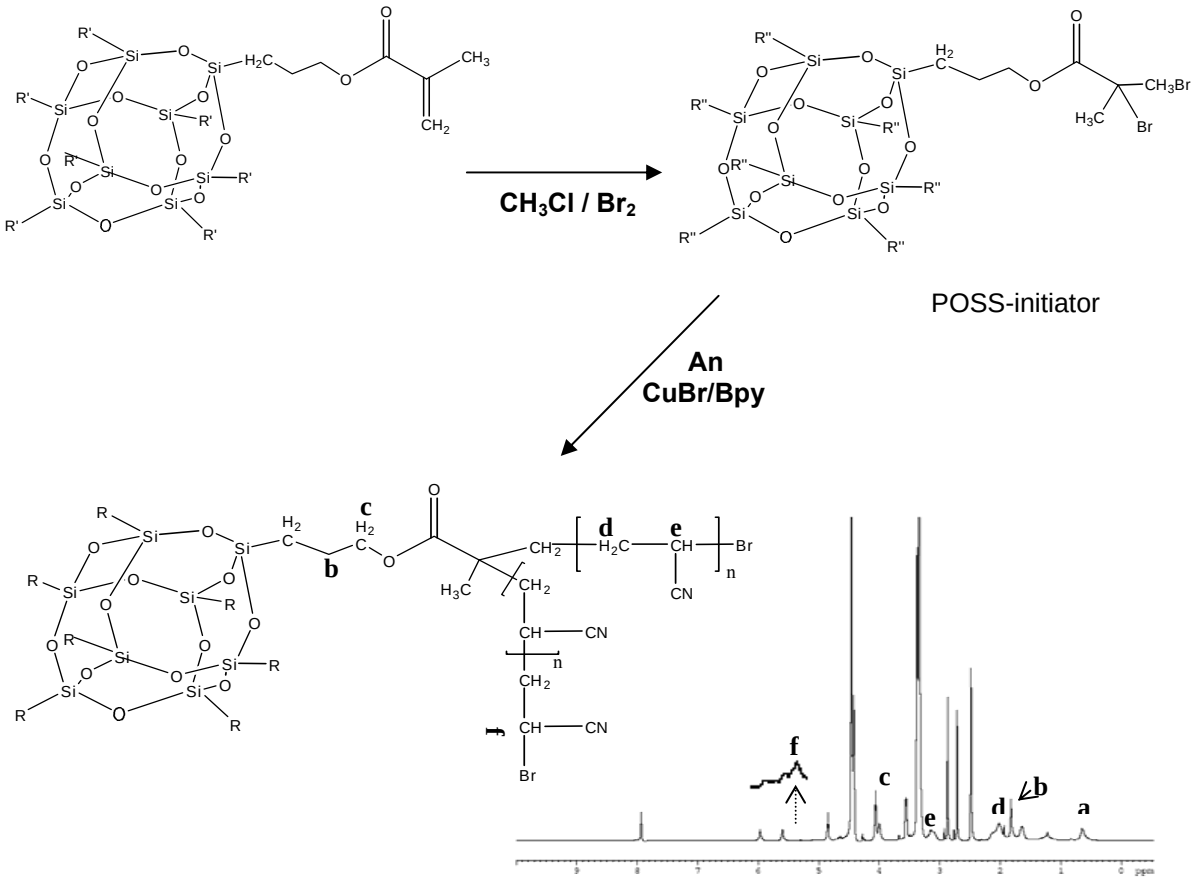

Figure 6.1 Growing oligomeric PAn chains on POSS by atom transfer radical polymerization (ATRP) method; ^{1}H-NMR spectrum of *sb*-POSS synthesized with [CuBr]/[Bpy]/[An]=1:3:600 for reaction time 6 h

6.2.2 Fabrication of *sb*-POSS/Nafion composite membranes

Nafion® perfluorinated resin solution (5 wt.%, Aldrich) was placed in an ventilation hood at 50 ^{o}C to remove the solvent (iso-propanol, n-propanol and water). The solid Nafion gained was re-dissolved in *N, N'*-dimethylacetamide (DMAc) (99%, Aldrich) solvent to formulate a 5 wt.% solution. A calculated amount of *sb*-POSS obtained from the ATRP synthesis was introduced into the solution (5 ml) and mixed uniformly with the aid of ultrasonication. The resulting solution was cast in a Petri-dish (d = 6 cm). The dish was kept inside an oven at 60 ^{o}C for 3 h, and then the temperature was increased to 120 ^{o}C for additional 3 h to generate the composite membrane. The pristine Nafion membrane was also prepared using the same procedure. All membrane samples were around 60 μm thick.

6.2.3 Instrumental characterizations

6.2.3.1 Molecular weight distribution analysis of sb-POSS nanoparticles

Gel permeation chromatography (GPC) analysis was carried out at 25 ^{o}C on Waters 1515 using DMF as eluent at a flow rate of 1.0 ml min^{-1}. PEG standards were employed to calibrate retention times.

6.2.3.2 Intrinsic viscosity measurement of the Nafion-PAn mixtures

The intrinsic viscosity values of the four Nafion ($\overline{M} \approx 10^5$ g mol^{-1}) [26] and polyacrylonitrile ($\overline{M}$ = 50,500 g mol^{-1}) mixtures in DMF were measured using Ubbeldohe capillary viscometer that was immersed in a water bath with fixed temperature (20 ^{o}C). The mass ratios of PAn to Nafion of these four mixtures were varied from 0.05 to 0.3. For the measurement of an intrinsic viscosity value, different concentrations (in the range from 0.1 g l^{-1} to 0.5 g l^{-1}) of one of the above mixtures in DMF were used to obtain the linear $\eta_{SP} / c \sim c$ relation (where η_{SP} is the specific viscosity and c is concentration). The intrinsic viscosity of the each mixture was determined by extrapolating the relation to zero concentration.

6.2.3.3 Spectroscopy analysis

^{1}H nuclear magnetic resonance (NMR) spectrum of *sb*-POSS was recorded on a Bruker Ultrashield-400 spectrometer using DMSO-d^6 as the solvent. The fourier transform infrared (FT-IR) analysis was carried out on Bio-Rad FT-IR 400 spectrophotometer. The samples with exactly the same amount were ground together with KBr before pellets were pressed. Spectra of the samples were recorded in the range from 400 to 4000 cm^{-1} using 64 cumulative scans. The images of *sb*-POSS particles in Nafion membranes were observed and recorded using both a transmission electron microscope (TEM, JEM 2010F JEOL) and a field emission scanning electron microscope (FE-SEM, JEOL-JSM-6700). For the TEM analysis, a carbon-coated copper grid was dipped in a dilute solution of a composite membrane in DMF (~ 0.05 % by weight), and a very thin liquid film developed was then dried. For the FE-SEM analysis, a cross section of the composite

membrane was prepared using the cryofixation method, e.g., the sample was ruptured in liquid nitrogen. Since the examined composite membrane is non-conductive, the cryo cross section was sputtered with a layer of Pt for 30 s at 10 mA.

6.2.3.4 The analysis of thermal properties

The thermal properties of the hybrid membranes were measured on a differential scanning calorimeter (Mettler Toledo DSC 822e). The analysis was performed using a two-scan mode, in which the first scan (25 ^{o}C$\rightarrow$100 ^{o}C$\rightarrow$0 ^{o}C) was designed to clean up discrepant thermal histories of the samples and the second one (0 ^{o}C$\rightarrow$250 ^{o}C) for collating data. The same ramp (10 ^{o}C min^{-1}) was set for running both heating and cooling courses.

6.2.3.5 Measurement of proton conductivity

The proton conductivity of the composite membranes at various temperatures was measured using an AC impedance spectroscopy (Autolab Instrument) over the frequency range from 0.01 Hz to 1 MHz, an AC perturbation of 10 mV and a DC rest voltage of 0.01 V. The membrane (1.3 cm in diameter) was soaked in 1 M H_2SO_4 solution for 12 h and sandwiched in two smooth stainless steel disk electrodes in a cylindrical Teflon holder. The holder was then enclosed in a silicon rubber pouch, and it was immersed in an oil heating bath with a setting temperature to conduct the measurement.

6.2.3.6 Methanol permeability measurements

Methanol permeability measurement was conducted in a cylindrical glass diffusion cell. One compartment of the cell (V_A=50 ml) was filled with 2 M methanol solution (the typical concentration used in a DMFC), and the other compartment (V_B=50 ml) was filled with deionized water. The membrane, after being soaked in deionized water for 24 h, was fastened between the two compartments, where the two solutions were stirred continuously throughout the measurement. The concentration-driven diffusion of methanol from compartment A to B across the membrane (area=4.90 cm^2) was monitored as a function of time, using a Shimadzu GC2010 gas chromatography (GC), a HP-Plot Q column (30 m×0.32 mm×20 μm) and a flame ionization detector. 1-Butanol was employed as the internal standard.

6.2.3.7 Setting up of single DMFC cell

The membrane electrode assembly (MEA) for the direct methanol fuel cell evaluation was made by sandwiching a membrane with an anode sheet and a cathode sheet. The anode sheet was a piece of carbon paper (SGL, Germany) coated with a layer of carbon-supported Pt-Ru (40% by weight) catalyst and the cathode sheet was a piece of the same type of carbon paper coated with a layer of carbon-supported Pt (40% by weight) catalyst supplied by E-TEK. The two catalyst slurries were prepared respectively by mixing de-ionized water, Nafion® solution (Aldrich), and the catalyst powder to form an ink, which was then applied on the carbon paper. The average platinum loadings at the anode and

cathode were 3 and 2 mg cm^{-2}, respectively, and the effective electrode area was 5 cm^2. The fuel used was 2 M CH_3OH delivered at 2 ml min^{-1} by a micropump, and the oxygen flow (500 cm^3 min^{-1}) was regulated by a flowmeter.

6.3 Results and Discussions

6.3.1 Interactions between *sb*-POSS particles and Nafion molecules

The *sb*-POSS particles were synthesized by grafting polyacrylonitrile (PAn) oligomeric chains to eight corners of cubic POSS molecules using the ATRP approach (Zhao et al., 2005 and Costa et al., 2001) (Fig. 6.1). In the reaction of growing PAn chains on cubic POSS, although the PAn chain length could be varied by adjusting the molar ratio of monomer/catalyst (An/CuBr), the effective range is actually rather narrow. Of the three molar ratios designed, the 400 and 600 could produce molecular weights much greater than the 200 according to GPC analysis (Table 6.1). However a further increase in the ratio does not increase the molecular weight of PAn but lowers the polymerization rate instead. It seems that oligomerization is the trait of ATRP when it takes place on pendant initiators, similar phenomenon has been reported by Laine and coworkers, (Costa et al., 2001) in their work cross-star coupling of PMMA chains were observed. The grafting of PAn to POSS and the different PAn chain-lengths were characterized by FT-IR spectroscopy (Fig. 6.2). The -CH_3 vibration (2990 and 2964 cm^{-1}) and –C=O vibration (1730 cm^{-1}) of the POSS-initiator became weaker with increasing PAn chain length, and *sb*-POSS-6 showed stronger –C≡N vibration (2254 cm^{-1}) than *sb*-POSS-2 (see details of

these two sample names in Table 6.1). The GPC analysis also displayed that the molecular weight distribution ($\overline{M}_w / \overline{M}_n$) of *sb*-POSS increased slightly with the increase in molecular weight.

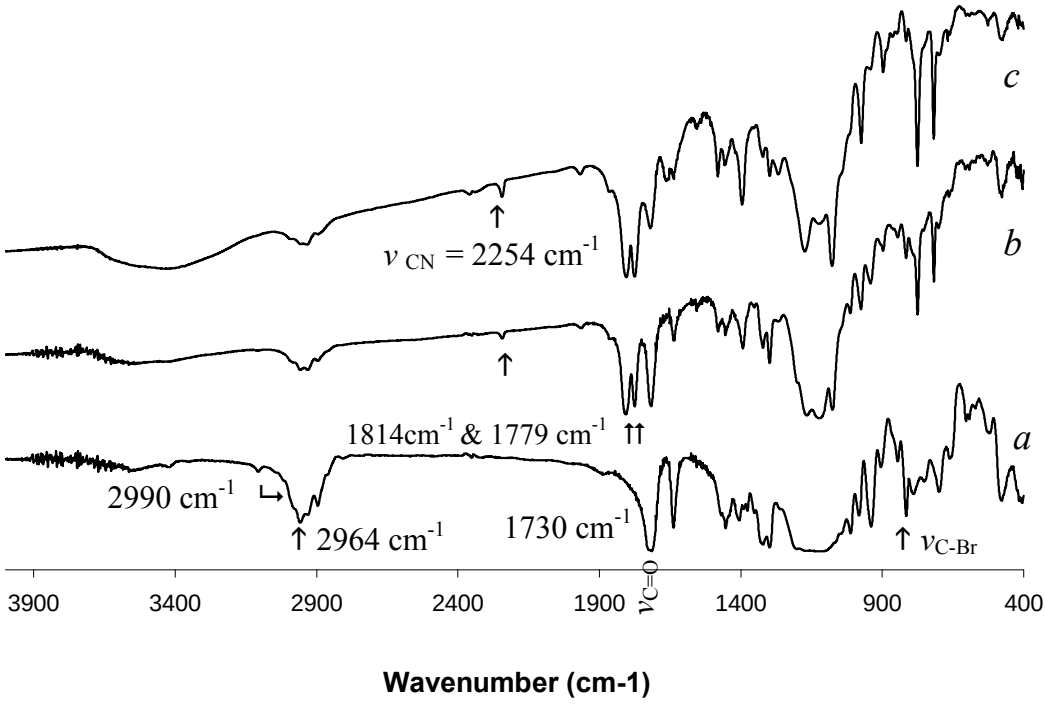

Figure 6.2 FT-IR spectra of *a*, vinyl-POSS, *b*, *sb*-POSS-2; *c*, *sb*-POSS-6, whose synthetic conditions are listed in Table 6.1

Synthesis of this branched cubic structure is based on the anticipation that it would trigger both repulsive and attractive interactions when dispersed in the Nafion matrix. The repulsive interactions exist between the grafted PAn and the perfluorocarbon chains of Nafion (Drobny, 2001) because they are thermodynamically incompatible, a high Flory-Huggins interaction parameter χ is incurred between them. (Pimbert et al., 2002) As to the attractive interactions, the nitrile groups of the PAn chains possess intrinsic

affinity with the sulfonic acid groups of Nafion molecules because both functional groups can be associated via hydrogen bonding and dipole moment interactions (Fig. 6.3a). In a comparison of the infrared vibration frequency of C≡N bond of pure PAn to that of PAn distributed in Nafion matrix (by 15 wt.%), an increase in the bond strength by a few wavenumbers can be discerned (Fig. 6.3b). Such enhancement in bond strength is thought of to be the result of the formation of a six-membrane ring complex as illustrated in Figure 6.3a. Such an association between Nafion and PAn molecules could also be detected by their chain expansion extents in DMF via the measurement of intrinsic viscosity (Section 6.2.3.2). Figure 6.4 shows that the intrinsic viscosity of the binary solution varies with the mass ratio of PAn to Nafion. With the increase in the mass ratio from 0 to 0.1, the intrinsic viscosity of this binary polymer mixture reveals a fast decreasing trend, but after that a gradual rise of intrinsic viscosity is observed. The steep reduction of the intrinsic viscosity in the initial range is the result of contraction of Nafion molecules due to crosslinking with PAn molecules via sulfonic-nitrile group interactions. However when an excess of PAn molecules, which are free of interactions with Nafion molecules, is present, the intrinsic viscosity of the mixture increases since the PAn sample has a greater intrinsic viscosity than Nafion in DMF. It may also be noted that the POSS core of *sb*-POSS is incompatible with both the perfluorocarbon backbone and the sulfonic acid groups of Nafion.

Table 6.1 Effect of the monomer/catalyst ratio of ATRP on the size of *sb*-POSS particles

Sb-POSS	POSS-initiator [a] (mmol)	Mol ratio ligand/CuBr	Mol ratio AN/ CuBr	$\overline{M}_n$ [b] g/mol	$\overline{M}_w / \overline{M}_n$
Sb-POSS-2	0.024	3	200	11352	1.07
Sb-POSS-4	0.024	3	400	32442	1.21
Sb-POSS-6	0.024	3	600	33746	1.38

[a] The molecular weight of POSS-initiator is 5175 by GPC measurement.

[b] The reaction time to achieve the $\overline{M}_n$ listed is 6 h, and a further extension of reaction time to 20 h brings about less than 10% increase in molecular weight.

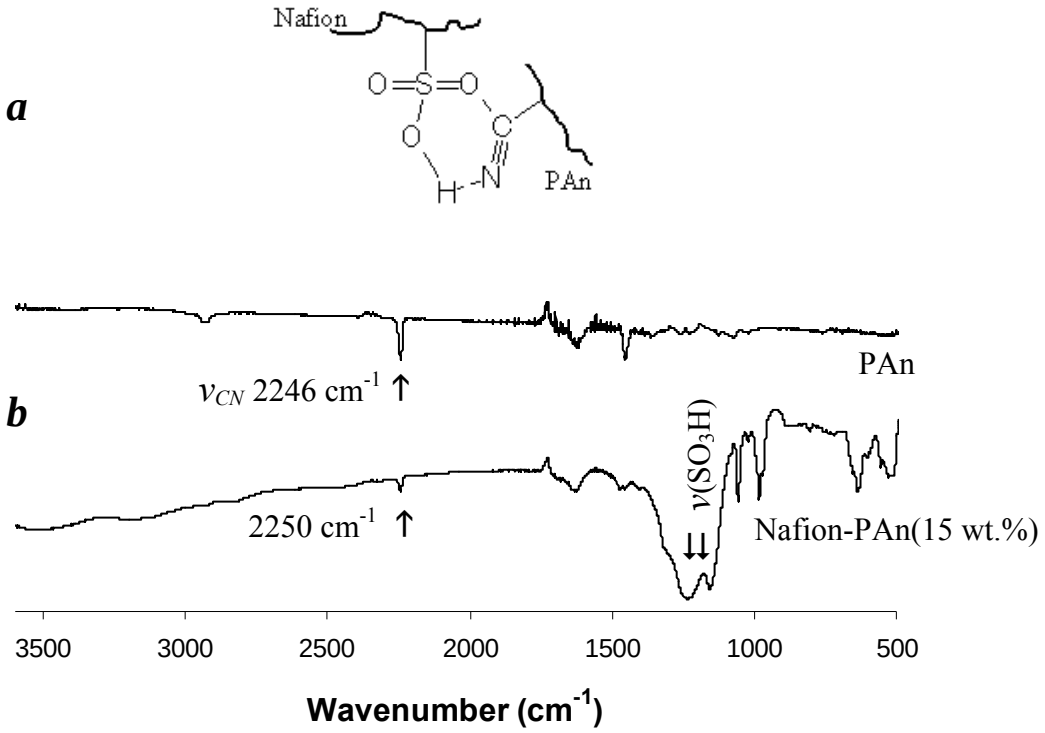

Figure 6.3 *a*. Schematic representation of the hydrogen bonding and polar interaction between sulfonic acid group and nitrile groups; *b*. Infrared spectra of the two membrane samples that show vibration band of nitrile group at different frequencies

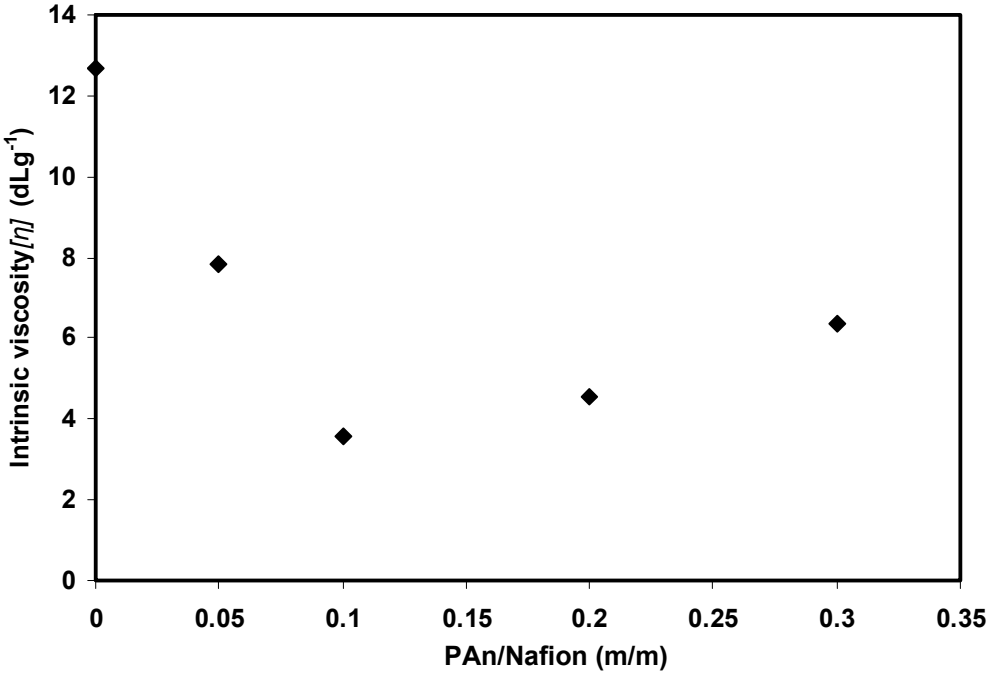

Figure 6.4. The composition-dependence of the intrinsic viscosity of the Nafion-PAn binary mixture.

The *sb*-POSS particles can be dissolved in the DMAc solution of Nafion, and their agglomeration (< 100 nm) could hardly be spotted in the dry matrix of the composite membrane formed at the content of 5 wt.% (Fig. 6.5a). The aggregation of *sb*-POSS in Nafion matrix became noticeable at 15 wt.%. At this point, the membranes became slightly translucent. The attractive interaction between the pendant nitrile groups and the sulfonic acid groups plays a key role in maintaining a low aggregating extent of *sb*-POSS particles in the range of low particle content. In spite of this, the composite matrix containing 25 wt.% of *sb*-POSS (Fig. 6.5b) exhibits a high concentration of *sb*-POSS agglomerations. Furthermore, the TEM image was obtained from the sample made by casting a substantially dilute solution of the composite membrane (5 wt. % *sb*-POSS) in DMF. The image displays discrete *sb*-POSS particles with particulate dimension below 10 nm (Fig. 6.5c). Meanwhile, we were not able to detect individual particles of the pure *sb*-POSS alone under TEM. This result may retrospectively suggest that the associations of Nafion molecular chains with the PAn chains of *sb*-POSS assist in creating a clear boundary of *sb*-POSS particles as shown in Fig. 6.5c.

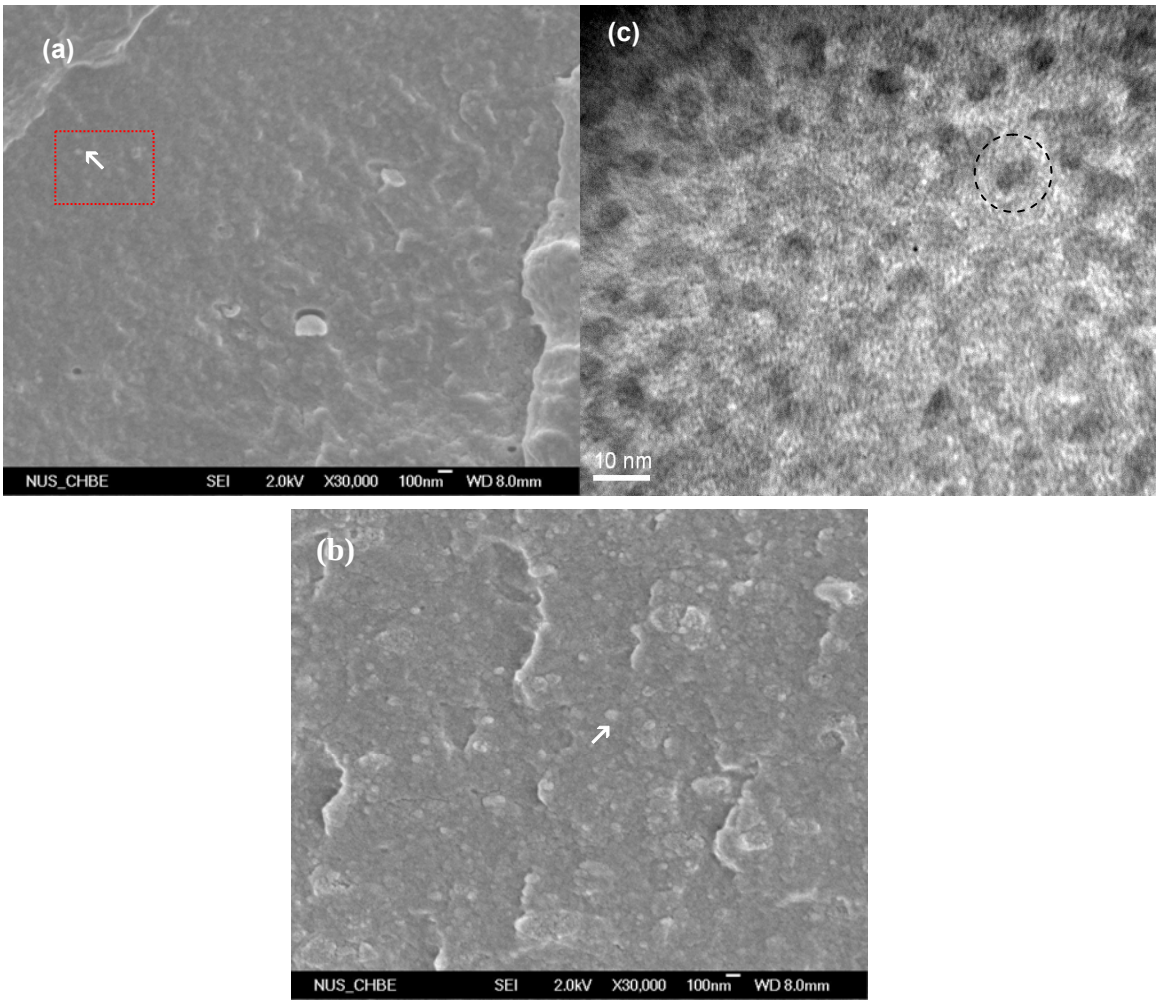

Figure 6.5 (a) Field emission scanning electron microscopic (FE-SEM) image of composite membrane with 5 wt.% *sb*-POSS-6; (b) FE-SEM image of composite membrane with 25 wt.% *sb*-POSS-6; (c) Transmission electron microscope (TEM) image of *sb*-POSS-6 with Nafion as a background

6.3.2 The leverage of *sb*-POSS particles on PCC structure of composite membrane

DSC analysis is an apt approach to study effects of *sb*-POSS particles on the PCC in the Nafion matrix. The DSC charts of *sb*-POSS-6/Nafion composite membranes were carefully investigated (Fig. 6.6). As the reference, the pure Nafion matrix reveals two shadowy glass transition steps (at 133 ^{o}C and 155 ^{o}C respectively), and the major slope is

the latter one that describes the energy barrier due to hydrogen bonding and polar association of the pendant $-SO_3H$ groups. This glass transition attribute undergoes a profound change when *sb*-POSS is incorporated into the Nafion matrix. The inclusion of *sb*-POSS-6 of 2 wt.% into Nafion matrix rolls down the major T_g step to ca. 140 ^oC, while the further increase in *sb*-POSS-6 loading to 5 wt.% leads to the two distinct T_g steps, of which the higher one occurred almost at the same temperature as that of the pure Nafion but extended farther to the high temperature direction and the lower one slides to ca. 125 ^oC. A further increase in the loading from 5 to 15 wt.% brings down the higher T_g step by ca. 5 ^oC. Finally, with the increase in the loading to 25 wt.% the previous two T_g steps merge at the temperature point close to that appearing on the 2 wt.% curve. Another unique phenomenon is that the glass transitions of the *sb*-POSS-6/Nafion membranes all reveal greater specific heat values (ΔH_{Tg}) than that of the pure Nafion. Accompanying the rise of *sb*-POSS-6 loading in the Nafion matrix, the variation of glass transition and energy signifies the structural change of PCC and will be stipulated in the following paragraph.

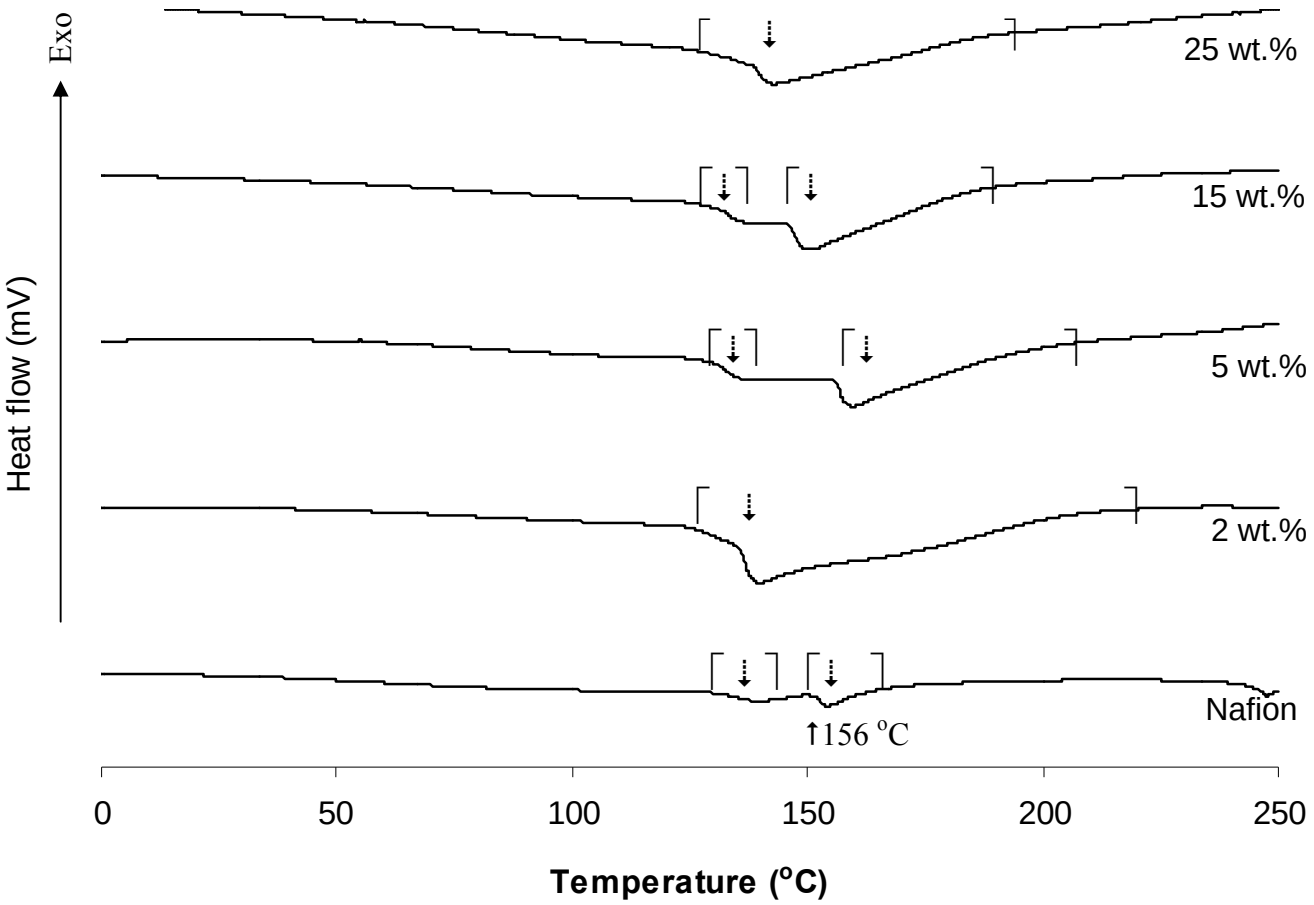

Figure 6.6 Differential scanning calorimeter (DSC) data for composite membranes with different weight percentage *sb*-POSS-6 loading in the Nafion matrix

The above observed glass transition behaviors of the pendant $–SO_3H$ groups can be attributed to the competition of the two types of interactions as stated in section 6.3.1. In the membrane containing 2 wt.% *sb*-POSS-6, the association of $–SO_3H$ groups in PCC is thawed due to the wedging of nitrile groups into them, which results in a downward shift of the T_g step. By raising the content of *sb*-POSS-6 to 5 wt.%, the coalescing trend of the particles lessens the participation of PAn segments in PCC, which thereby leads to the two kinds of PCC structures, the perturbed and unperturbed ones, represented by the two T_g steps, respectively. The unperturbed PCC are those involving segmental motions with higher energy barriers compared with the pure Nafion because of no involvement of nitrile groups. Although the 15 wt.% membrane still displays two T_g steps, the higher-temperature one has already been below its counterpart in the 5 wt.% membrane by 5 ^oC, indicating the participation of PAn units into a part of prior unperturbed PCC and the generated perturbed PCC thus became stabilized. Lastly, increasing the loading of *sb*-POSS-6 up to 25 wt.% allows greater involvement of nitrile groups in the PCC, which is evidenced by the fusing of the previous two glass transition steps and the display of a rather similar T_g location and energy absorption to those appearing on the DSC profile of the 2 wt.% membrane. In order to estimate the portion of unperturbed PCC component in the different composite membranes, an area covering the major glass transition bowl (152-167 ^oC) of the pure Nafion membrane was used as the reference for comparison, in which 156 ^oC is the temperature point at the dip of the endothermic bowl. The corresponding area of a composite membrane in its glass transition bowl could then be found and divided by the reference defined above. The ratios obtained from the four different membranes are listed in Table 6.2. As the respective area stands for the specific

heat of glass transition, the ratio thus represents the contribution of those segmental motions which takes place at temperatures above the upper T_g of the pure Nafion. It could be then concluded that among the four *sb*-POSS-6/Nafion composite membranes, the 5 wt.% membrane contains the greatest portion of unperturbed PCC. From the viewpoint that the unperturbed PCC involve segmental motions with higher energy barriers, it is thus rational to deem that these channels comprise densely packed sulfonic acid groups due to the compression action of Nafion matrix. The origin of such matrix compressive action could be attributed to the formation of *sb*-POSS-6 agglomerations since the polar rejection and size exclusion between the perfluorocarbon matrix and these small granules cause the matrix compression as portrayed in Figure 6.7. In addition, it is noteworthy that this compression effect is size sensitive. The larger *sb*-POSS-6 particles function more intensely than the smaller *sb*-POSS-4 ones to cramp the unperturbed PCC. This feature is reflected by the rather different two ratios (22.9 vs. 17.3 in Table 6.2) between the two samples containing 5 wt.% *sb*-POSS supports the above inference.

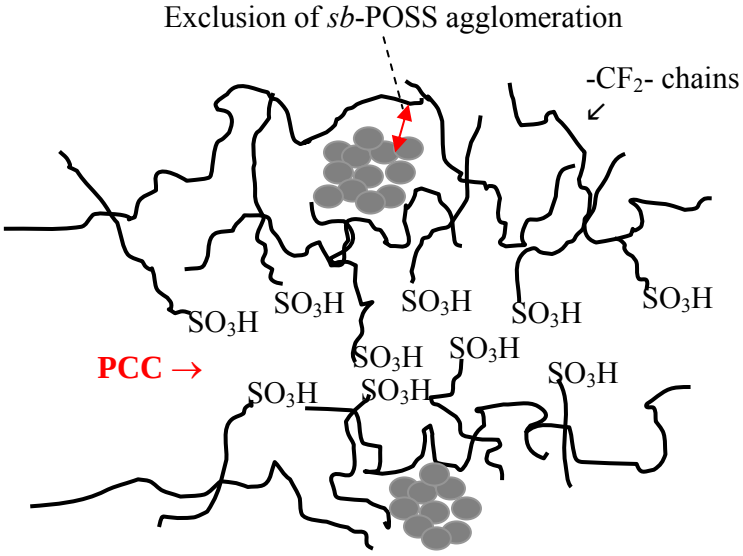

Figure 6.7 Illustrative representation of the matrix compressing effect on PCC

Table 6.2 The specific energy barriers of the glass transition ascribed to the unperturbed PCC in the composite membranes [a.]

Filler type and dose	*Sb*-POSS-6 (2 wt.%)	*Sb*-POSS-6 (5 wt.%)	*Sb*-POSS-6 (15 wt.%)	*Sb*-POSS-6 (25 wt.%)	*Sb*-POSS-4 (5 wt.%)	*Sb*-POSS-4 (25 wt.%)
$\Delta H_{T_g} / \Delta H_{T_g}(Nafion)$ [b.]	15.2	22.9	10.6	10.4	17.3	8.6

a. Determined by the area (with T > 156 ^{o}C) of the larger glass transition step in each T_g curve. The samples for this measurement were controlled to have the same mass.

b. the relative specific energy value of the composite membranes.

It is now rational to examine how the *sb*-POSS particles in Nafion matrix affect proton conduction. The Arrhenius-plots [$\log\sigma(T) = \log\sigma_0 - (E_a / 2.3RT)$] of the three selected membranes (Fig. 6.8) show that the two composite membranes displayed better linearity than the pure Nafion membrane because the pure one could no longer maintain its prior $\log\sigma$-$(1/T)$ relation when testing temperature reached 80 ^{o}C. It has been known that Nafion starts to lose its matrix water starting at 70 ^{o}C. This comparison means that the proton transport in the two composite membranes is less dependent on the matrix water content as compared to that of the pure Nafion membrane. The average activation energies (E_a) followed the order: the pure Nafion > *sb*-POSS-4 (5 wt.%)/Nafion > *sb*-POSS-6 (5 wt.%)/Nafion. The E_a of Nafion is quite close to the lower limit of the range defined by the Grotthuss mechanism (14 – 40 kJ mol^{-1}). According to this mechanism, protons are transported through a succession of breaking and forming of hydrogen bonds with water molecules. (Ye et al., 2007) Apparently, the activation energies of the two composite membranes are below the lower E_a bound of this range, which implies that proton transport is relatively independent of the water molecules in PCC, and therefore the close-packed sulfonic acid groups in PCC would function as the main hopping sites for proton transport in these two composite membrane matrices. It is worth noting that despite the highest proton conductivity given by the Nafion membrane at 80 ^{o}C, this does not indicate that that Nafion membrane has better capability to transport protons in a DMFC since the proton conductivity measurement entails only a substantially low proton flux.

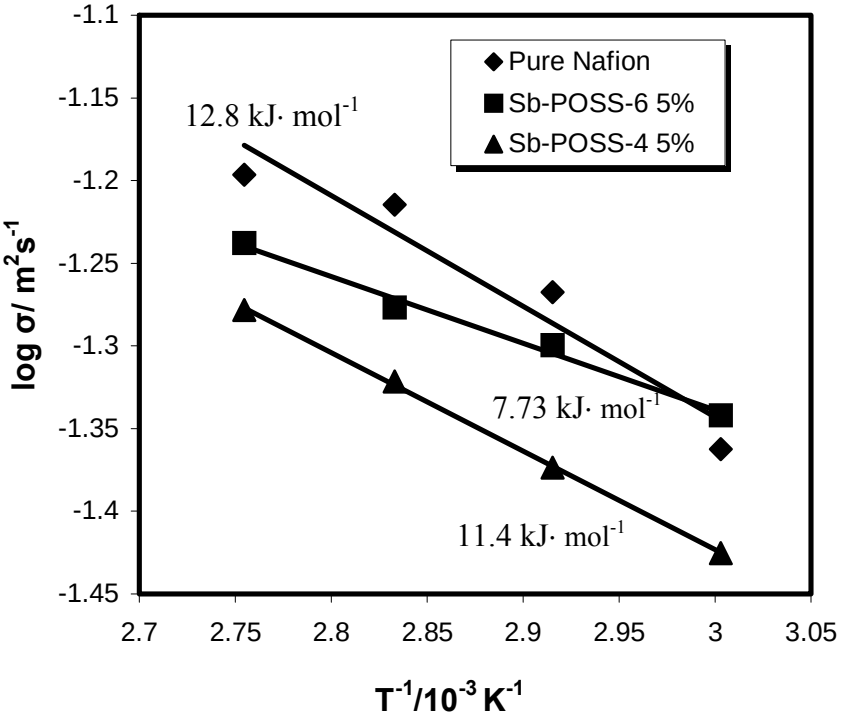

Figure 6.8 The Arrhenius plot of proton conduction

6.3.3 The blocking effect to methanol crossover and single DMFC evaluation

The methanol permeability measurement at ambient temperature (Fig. 6.9), using 2 M CH_3OH aquatic solution as feed, showed that the diffusion coefficient ($\text{in} 10^{-7} cm^2 \cdot s^{-1}$) reduced from 10 in the pure Nafion membrane to 5 in the 2 wt.% composite membrane. This outcome is consistent with the PCC structures that are classified above, namely, the reduction in permeation of methanol is due to the involvement of nitrile groups into PCC, which results in an increase in their hydrophobicity. For the higher contents of *sb*-POSS-6 in the Nafion matrix, the membranes showed slightly lower permeability values to

around 4. This further decrease in permeability could be due to the unperturbed PCC because of the crowded sulfonic acid groups. Moreover, the methanol blocking effect was also observed in the composite membranes containing *sb*-POSS-4 that exhibited similar permeability.

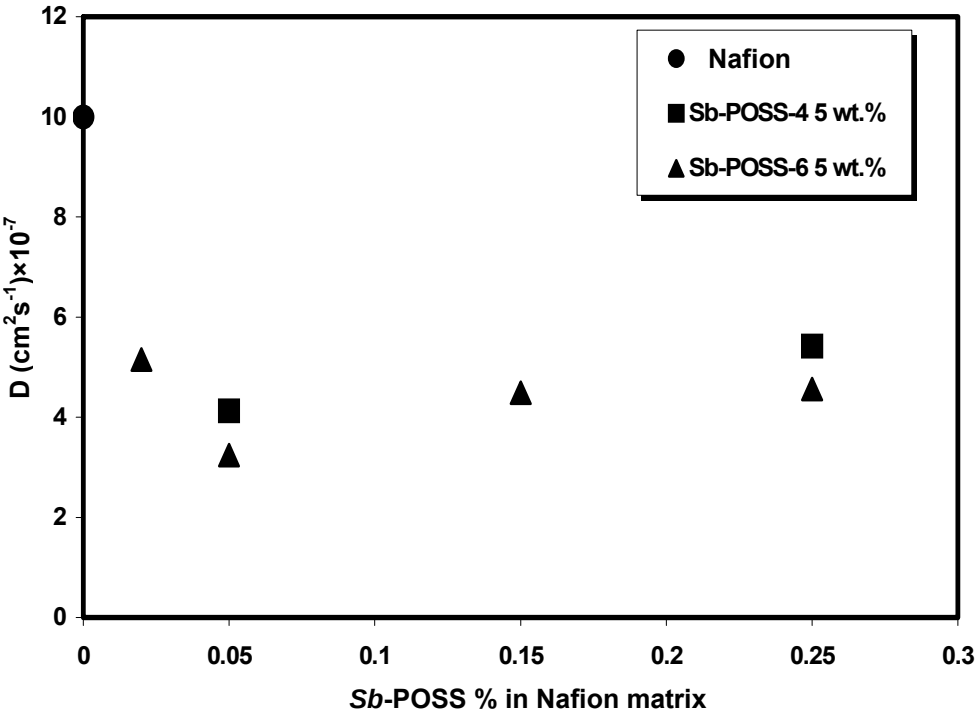

Figure 6.9 The measurement of methanol diffusivity in the *sb*-POSS-Nafion composite membranes driven by concentration difference across the membrane: 2 M CH_3OH solution vs. pure water.

When evaluated in the single DMFC cell, among the four *sb*-POSS-6/Nafion composite membranes, the 5 wt.% membrane demonstrated exceptionally well performance at 80 ^oC in contrast to the pure Nafion membrane and the other composite membranes (Fig. 6.10). This particular membrane exhibited the maximum power output of 44.2 mW cm^{-2} as compared to the 19.9 mW cm^{-2} of pure Nafion membrane at the identical current density

of 0.18 A cm^{-2}. The outcome is deemed to the contribution of the unperturbed PCC structure, which the 5 wt.% membrane exhibits the largest portion among the four composite membranes (Table 6.2). The compact sulfonic acid groups in PCC would facilitate fast protons hopping along them because of their proximity to each other, and hence the electrochemical polarization phenomenon caused by slow kinetics of proton transport could be effectively alleviated. On the contrary, as to the perturbed PCC, the association of nitrile groups with the pendant sulfonic groups in PCC not only lowers down the methanol permeability but also the proton transport efficiency especially when the flux of proton across the membrane rises. On the other hand, although the other three hybrid composite membranes (2 wt.%, 15 wt.% and 25 wt.%) contained certain portions of unperturbed PCC as summarized in Table 6.2, the perturbed PCC were prevalent in these three membranes and thus they displayed inferior cell performance than the pure Nafion membrane. The same single DMFC evaluation was also carried out at 50 ^{o}C (Fig. 6.11). It turned out that with respect to the 5 wt. % membrane this decrease in operation temperature (from 80 ^{o}C to 50 ^{o}C) led to a 2/3 lost in powder output owing to the drop in current density (i.e. proton flux). The similar trend was also observed in the composite membranes using *sb*-POSS-4 particles as filler, in which the 5 wt.% membrane also offered the best cell performance, whose maximum power output was 34.6 mW cm^{-2} occurring also at the same current density value of 0.18 A cm^{-2} as those used to evaluate the previous set of composite membranes. Compared with *sb*-POSS-6, the shorter grafted PAn chains of *sb*-POSS-4 are likely responsible for its weaker effect to augment the cell performance of membrane.

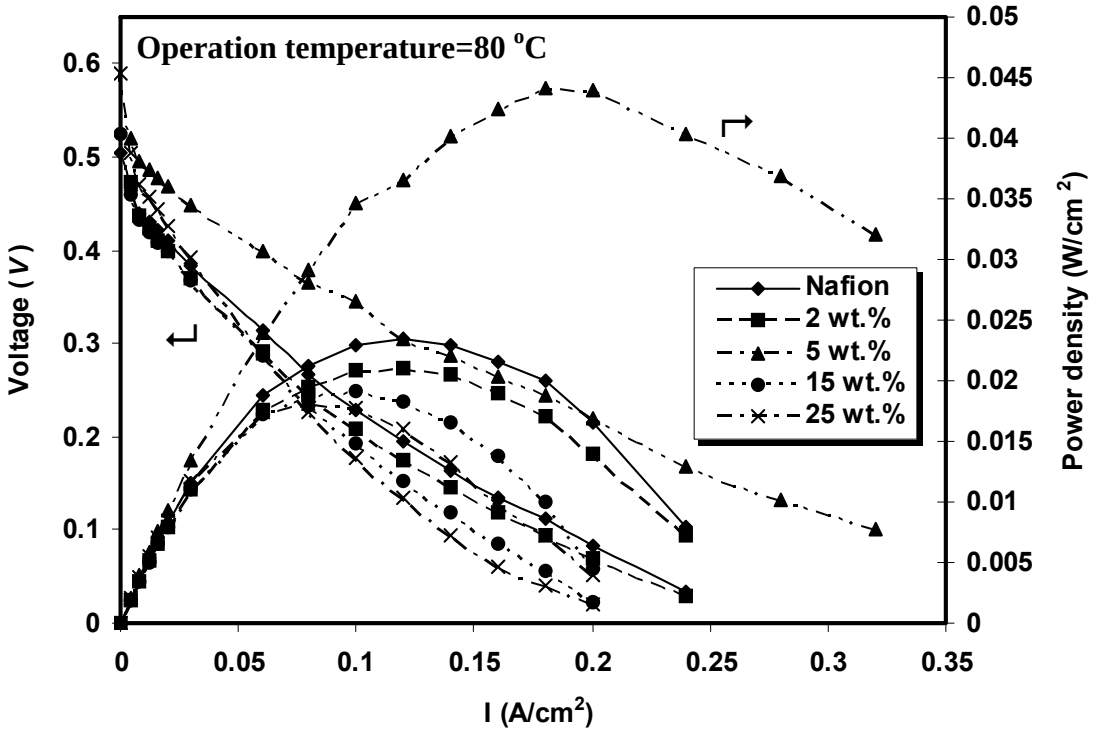

Figure 6.10 The effect *sb*-POSS-6 content in Nafion membrane on the polarization curve and power output of the single DMFC at 80 °C

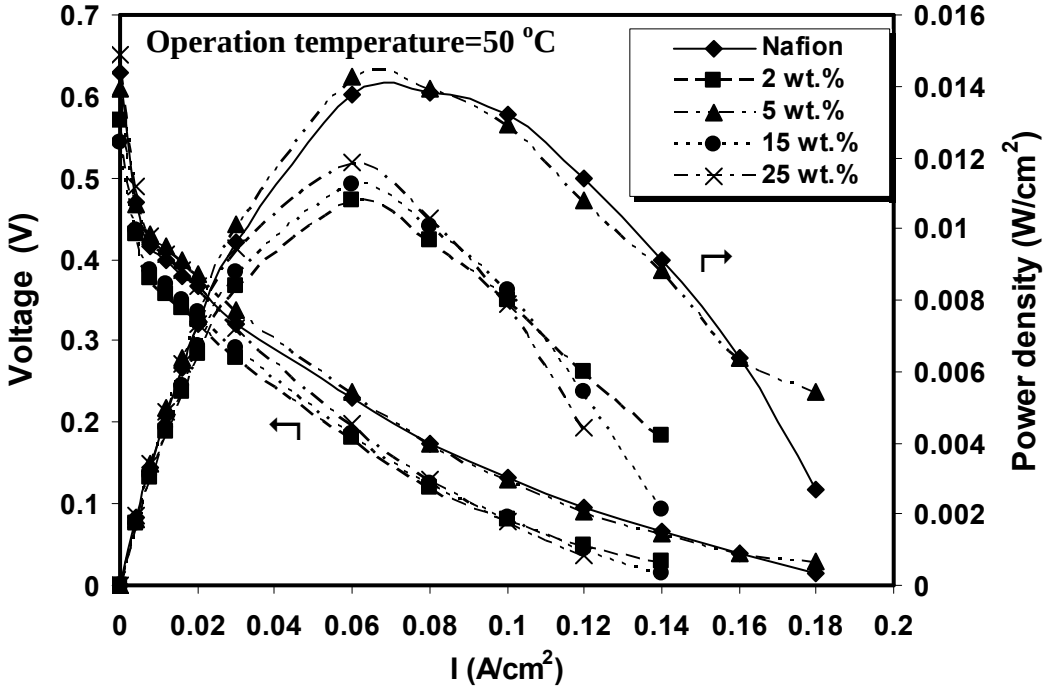

Figure 6.11 The effect *sb*-POSS-6 content in Nafion membrane on the polarization curve and power output of the single DMFC at 50 °C

6.4 Conclusions

This work synthesized a novel type of highly branched nanoparticles (*sb*-POSS) by grafting polyacrylonitrile (PAn) short chains to POSS, a cubic silicone molecule. The starburst architecture of *sb*-POSS particles and the strong polar nitrile groups of the grafted PAn oligomeric chains are the key structural traits that assist dispersion of the particles in the sulfonic perfluoro polymer matrix. There are two opposite effects affecting the dispersion states of *sb*-POSS particles in the matrix, namely, the association of the pendant sulfonic acid groups with nitrile groups of the PAn chains and the rejection of the particles by the perfluorocarbon chains. Consequently, the proton conducting channels (PCCs) of the pure Nafion undertake restructuring to form the perturbed and unperturbed PCC, coexisting in all the four composite membranes formed. In the former type of PCC, the participation of nitrile groups impedes methanol permeation as well as proton transport. On the contrary, for the unperturbed PCC, the close packing of sulfonic acid groups due to matrix compression on PCC, caused by the aforementioned repulsive action, allows faster proton hopping over them. It was identified through DSC characterization that the *sb*-POSS-6 content of 5 wt.% conferred the highest portion of the unperturbed PCC in the composite membrane, and as a result, the composite membrane displayed superior single DMFC performance over the pure Nafion and the other composite membranes. In addition, the length of PAn chains tethered to *sb*-POSS particles is the other key factor affecting the portion of unperturbed PCC in the composite membrane. The maximal PAn chain-length that could be realized

by the grafting method employed (i.e., ATRP) offered the best cell performance result.

CHAPTER 7

REINFORCING H_3PO_4-DOPED POLYBENZIMIDAZOLE PROTON-EXCHANGE MEMBRANE BY INCORPORATING UNSATURATED POLYESTER MACROMER AS CROSSLINKER

7.1 Introduction

From the earlier chapters, we have introduced three different hybrid structure nano-particles, nano-particles with dense oligomeric ionomer layer, starburst oligomeric molecules and rigid molecular fragments to modify Nafion® PEMs. It was found that the presence of these nano particles in the membrane matrixes of Nafion can improve their performances in DMFC and low-temperature H_2-FC significantly. However, currently there has also been an increasing interest in making use of PEMs for high temperature H_2-FC (> 120 °C) applications due to the fact that lifting operation temperature of PEMFC will not only largely promote CO-tolerance of the anode, but also be of benefit to electrode kinetics and the catalytic activity for a better cell output. Many studies on phosphoric acid (H_3PO_4, PA) doped polybenzimidazole (PBI) membrane as the most promising one of these PEMs, have been published over the past decade (Fontanella et al., 1998; Bouchet et al., 1999; Li et al., 2001; He et al., 2003and Ma et al., 2004). It has been

realized, nevertheless, a high H_3PO_4 doping level (> 10), though is needed to target designated proton conductivity, will thwart the structure of membrane, especially at temperatures above 100 °C, and therefore severely shortens the operation life of membrane at high temperatures. Recently, Xiao et al. (Xiao et al., 2005) reported a sol-gel process to fabricate the H_3PO_4-doped PBI membrane and it can be operated in the H_2-FC at above 150 °C for an extended period of time without the need for feed gas humidification. It is interesting to note that a high PA doping level was reached in this PBI membrane, which exhibited high ionic conductivity and stable mechanical properties in the temperature range from 150-200 ^oC. Unlike the conventional H_3PO_4 doping process, the sol-gel way innovatively made polymerization that produces PBI macromolecular chains take place in pristine polyphosphoric acid (PPA) medium, which was followed by hydrolysis of PPA *in-situ*. It is deemed that the units of PBI chains have achieved to the maximum and special contact with PA molecules and should possess a semi-gel matrix. However, with this method, only if a series of strict polymerization conditions is satisfied, can the meaningful average molecular weight of PBI be achieved. These strict synthetic conditions of PBI include, in principle, highly pure monomers of PBI, anhydrous solvent for polymerization, and a high monomer conversion.

In this work, we attempt to weave a network comprising PBI blocks and unsaturated polyester (UP) macromer crosslinker. This modifying measure alleviates the demand on the polymerization conditions and would be greatly beneficial to the industrial fabrication of this unique type of gel-matrix membrane. As far as the effect of modification is

concerned, the crosslinking not only reinforces the membrane and also promotes the complexation of PA with the polymer phase.

7.2 Experimental

7.2.1 Materials

Isophthalic acid (99%), 3, 3'-diaminobenzidine tetrahydrochloride dehydrate (97%), and polyphosphoric acid (PPA, 115%) were purchased from Sigma-Aldrich. Unsaturated polyester (UP) resins, consisting of maleic anhydride, phthalic acid and propylene glycol, were obtained from Talton Technology Co.

7.2.2 Preparation of PA doped PBI-unsaturated polyester (UP) membrane

The general procedure for the preparation of PA-doped PBI-UP membrane (scheme 7.1) is described as follows: 3, 3'-diaminobenzidine tetrahydrochloride dehydrate (97%) (4.60 g, 11.6 mmol) was added in a three-neck reaction flask with polyphosphoric acid (PPA) of 90 g. The mixture was stirred at 140 ^{o}C for 1 h to remove hydrochloride from the amine. After that, isophthalic acid (1.922 g, 11.6 mmol) was introduced into the flask and the reaction mixture was stirred using a mechanical overhead stirrer under the purge of a slow stream of nitrogen. The polymerization was maneuvered to proceed in the range of 170-190 ^{o}C for 24 h. Through this course, the reaction mixture became more viscous and developed a dark brown color, which was the characteristic of forming the pre-PBI in

PPA. UP (2 wt.% of total reaction monomers) was introduced into the pre-PBI PPA solution and the polymerization reaction was continued for additional 12 h at 150-200 ^{o}C to allow generation of a loose crosslinking network consisting of rigid PBI blocks and UP chains. A small amount of specimen was withdrawn from the viscous solution and added into water to form a solid specimen, and then it was soaked in a dilute $NaHCO_3$ solution for overnight, finally the specimen was washed thoroughly with water and methanol respectively, and dried in the vacuum oven for thermal and spectroscopy analysis.

A membrane was developed by casting the hot PBI-UP PPA solution directly on a flat glass panel using a film applicator with a gate thickness of 150 μm. The cast membrane was allowed to cool down from reaction temperature to 60-70 ^{o}C, over which the hydrolysis of PPA to PA took place at the same time. After that, the membrane formed was transferred to a chamber where the relative humidity and temperature were controlled at 25±5% and 60 ^{o}C, respectively, for 24 h. In the final step the membrane was cured at 200 ^{o}C for 2 h and subsequently enclosed in a dry container to isolate it from moisture because the membrane would otherwise quickly absorb moisture from air and causes loss of mechanical properties and proton conductivity.

For the comparison purpose, PA-doped PBI membrane was fabricated by applying the usual embedding method: The PBI powder separated from the polymerization system in PPA was dissolved in *N, N'*-dimethylacetamide (DMAc) at 150 ^{o}C under stirring to prepare a 5 wt.%-solution. Afterwards, the PBI solution was cast on a glass Petri dish and the solvent was slowly evaporated at 120 ^{o}C for a period of 20 h. The membrane was

further soaked in concentrated H_3PO_4 solution (85 wt.%) for a few days at room temperature. The doped PBI membrane was dried in a vacuum oven at 100 ^oC to conduct dehydration before the doping level of PA in the membrane was determined.

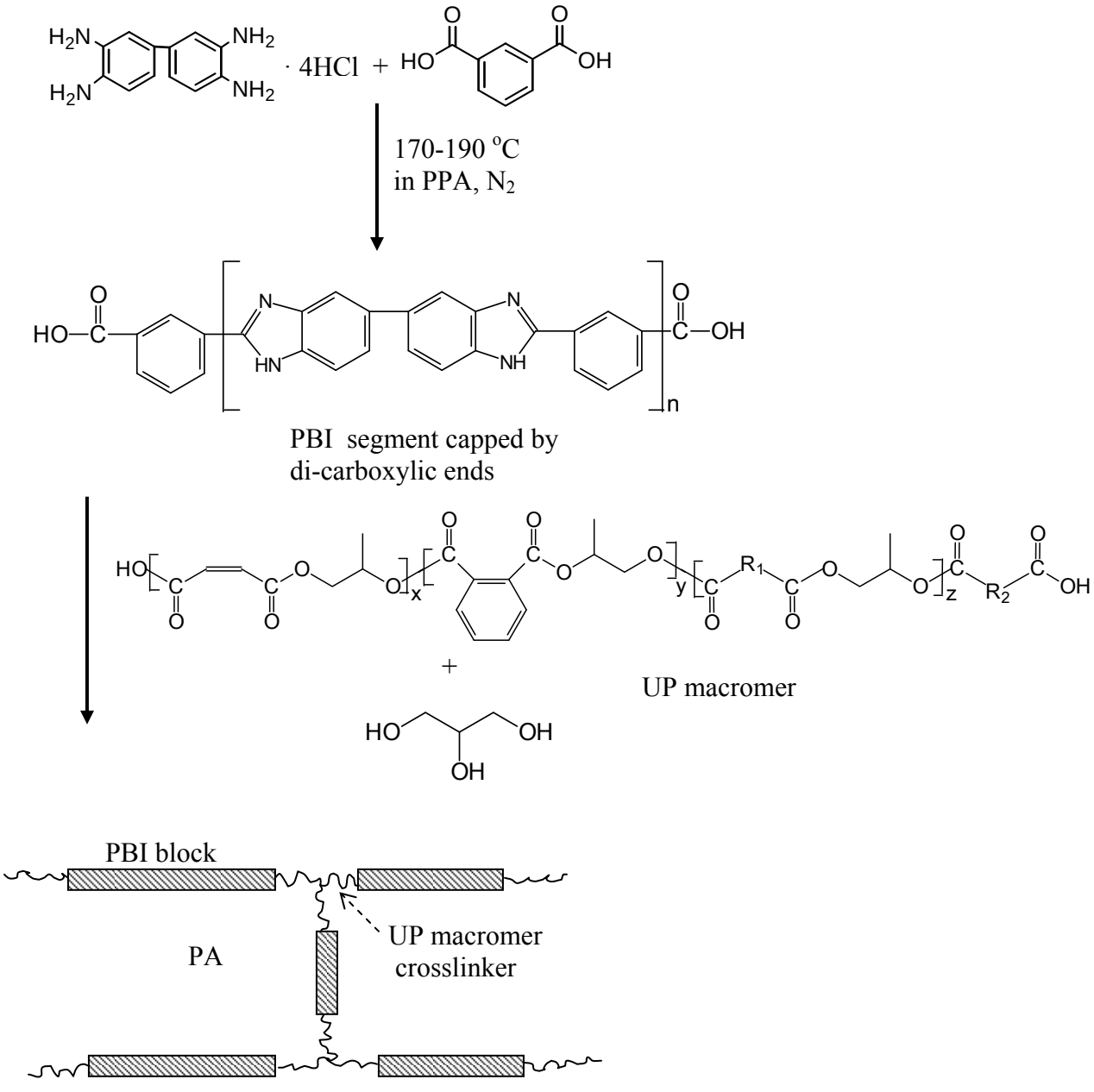

Scheme 7.1 *In-situ* synthesis of PBI-UP in PPA

7.2.3 Characterizations of structure and properties

7.2.3.1 Doping level

The PA-doping level of membrane was determined by the titration method. A pre-weighed piece of membrane sample was immersed in a sodium hydroxide solution (0.1 M) for a few hours. The sample was then washed with water and dried in a vacuum oven at 100 °C for overnight to obtain the dry weight of polymer. The acid-doping levels X, expressed as moles of phosphoric acid per mole of PBI repeat unit were calculated from the equation:

$$X = (V_{NaOH} \times C_{NaOH})/(W_{dry}/M_w) \quad \text{…… Equation 7.1}$$

where, V_{NaOH} and C_{NaOH} are the volume and the molarity of the sodium hydroxide titer, while W_{dry} is the dry polymer weight and M_w is the formula weight of the repeating unit, respectively.

7.2.3.2 Inherent viscosity

Inherent viscosity (η_i) of a polymer solution depends on concentration and size of the dissolved polymer molecules. A polymer sample was dissolved in the concentrated sulfuric acid (96%) to make a solution of 0.2 g/dL and its η_i was measured using a

viscometer (Brookfield, DV-II+Pro). Let η_0 be the viscosity of the pure solvent and η the viscosity of the solution in this solvent.

1. Relative viscosity

$$\eta_r = \frac{\eta}{\eta_0} \qquad \text{…… Equation 7.2}$$

2. Inherent Viscosity

$$\eta_i = \frac{\ln \eta_r}{c} \qquad \text{…… Equation 7.3}$$

7.2.3.3 Thermal and mechanical properties of the membrane

The thermal stability of the samples was measured by on a High Resolution Thermogravimetric Analyzer (TA Instruments 2950) using a sample of 5 to 15 mg. The weight-loss was recorded in the range from 25 ^oC to 800 ^oC using a constant heating rate of 10 ^oC/min and N_2 purge of 100 ml/min. The polymer segment motion behaviors of membrane were measured using a differential scanning calorimeter (DSC, Mettler Toledo DSC 822e) equipped with a pressure DSC cell. The temperature scanning range from 25 ^oC to 160 ^oC was set for the first scan to erase the thermal history of a sample caused by particular preparation conditions. After the sample was cooled down to -50 ^oC, the second scan was followed and up to 160 ^oC as well, and the energy-temperature profile was recorded from this scan. Both heating and cooling rates were fixed at 10 ^oC/min in

the above two scans. The mechanical properties of membrane were tested on the instrument (Instron 5569) using a 10 N load cell.

7.2.3.4 Proton Conductivity

The proton conductivity of the membrane was measured using the normal four-point probe technique (Sone et al., 1996). The sample holder made from Teflon consists of two flat stainless steel ribbon as the outer current-carrying electrodes (2 cm apart) and two Au wire as the inner potential-sensing electrodes (1 cm apart). Membrane in 1 cm wide and 2 cm long was mounted on the holder. The impedance was determined using the electrochemical analyzer (Autolab Instrument) at galvanostatic mode with an AC current amplitude of 0.1 mA and the frequency scanning range was from 1 MHz to 50 Hz. On the Bode plot there is a frequency range over which the impedance had a constant value, and the resistance corresponding to this frequency range could then be obtained from the Nyquist plot of this sample. The proton conductivity (σ) is calculated according to the following expression:

$$\sigma = \frac{L}{RWd} \qquad \text{…… Equation 7.4}$$

where, R is the resistance of membrane specimen obtained, L is the distance between potential-sensing electrodes, $W{\cdot}d$ is the cross section area of the specimen. The cell was placed in a programmable furnace to control the temperature. The conductivity of the specimen was measured from 330K to 450K. Before the measurements at each set temperature point, the sample was held at constant temperature for at least 30 min.

7.2.3.5 Fuel cell test

For the polarization measurements, a single cell was operated at 95, 115 and 150 ^{o}C and the pressure of both H_2 and O_2 streams was 1 bar without humidification. The measurement was carried out using Arbin Electronic loaded with MITS system. The anode and cathode sheet were a carbon paper (SGL, Germany) that is coated with a layer of carbon-supported Pt (20 wt.%) catalyst, which was supplied by E-TEK, Natick, MA. The Pt catalyst loadings at the anode and cathode were 2-3 mg/cm^2, repectively. The effective electrode area was 5 cm^2. The gas flow rate was kept at a fixed stoichiometry (the molar ratio of H_2 to O_2 was 1.15/2) at the current density of 1 A/cm^2.

7.3 Results and discussions

7.3.1 Membrane formation and doping level

Carrying out polymerization of 3, 3'-diaminobenzidine tetrahydrochloride dehydrate and isophthalic acid in PPA is a unique system because PPA is both polar solvent and the precursor of PA, an acid dopant. We have confirmed that the PBI synthesized in PPA could often reach only a low level of average molecular weight according to its η_i value (0.8 dL/g) in 96% sulfuric acid at 20 ^{o}C although occasionally higher molecular weight (~1.0-1.1 dL/g) could obtained be obtained. The low molecular weight PBI in PPA could hardly be converted to an integrity membrane through the casting procedure. In order to surmount this hurdle, UP macromer (2 wt.% of PBI) was incorporated into the

polymerization process with the aim of connecting individual PBI short segments together to form a loosely crosslinked structure. Experimentally, 2 wt.% UP is the highest possible dose that could be charged to PBI polymerization system in PPA, over which the casting cannot be proceeded due to a too viscous gum (PBI-UP in PAA) is resulted. The inherent viscosity measurement indeed showed that the PBI-UP polymer made has a greater η_i value (1.378 dL/g) than PBI alone, and an integrity membrane was obtained after hydrolysis of PPA and curing (Table 7.1).

Table 7.1 Effect of inherent viscosity on membrane development

Sample	η_i / (dL/g)	Membrane formation process	
		After hydrolysis	After curing
PBI	0.802	No membrane formed	
PBI-UP	1.378	Mechanically week membrane	Mechanically strong membrane

The doping level of PBI-UP membrane was found not to be affected by thermal curing after the hydrolysis of PPA (Table 7.2). The PBI-UP network and PA molecules constitute a uniform semi-gel structure, which is characterized by a large doping extent and therefore expectedly maintained by the two layers of interactions: (1) the electrostatic interaction between protonated imidazole ring and dihydrogen phosphate anions as well as the hydrogen bonding between the PA molecules and oxygen-containing segments of

UP; and (2) the interaction between the PA molecules of the first layer and the rest PA molecules.

Table 7.2 A comparison of H_3PO_4 doping levels in PBI matrix

Doping method	PA-doped PBI via immersion	PA-doped PBI-UP via sol-gel	
		After hydrolysis	After curing
PA Doping level	9	24	23

7.3.2 Thermal and mechanical properties of the membrane

In the Figure 7.1 different thermal responsibilities of the PA-doped PBI-UP membrane and the PBI-UP powder are compared. Over the temperature range of investigation, the PA-doped PBI-UP membrane exhibited four weight loss slope (Fig. 7.1). The first slope (with peak value at 80 ^{o}C) reports a mass loss of 35 wt.%, which comprises mainly water due to the hygroscopic nature of PA and those PA molecules that are in the bulk of the trapped PA phase. The removal of the strongly bound PA took place in the range from 160 ^{o}C to above 300 ^{o}C; this amount accounts for about 7 wt.% of mass loss, which is above the normal boiling point of absolute PA (at 158 ^{o}C), implying the effect of attractive interactions between PA and the polymer matrix. The last three mass loss slopes represent the decomposition of the matrix. On the contrary, for the PBI-UP powder, there were two weight loss-slopes below 800 ^{o}C. A small dehydration peak appeared at near 100 ^{o}C and the decomposition of PBI matrix started at 490 ^{o}C. It

deserves to note that the PA-doped PBI-UP matrix displayed a far stiffer matrix disassociation slope than that of the dry matrix. This difference reflects the effect of thermal curing treatment, which is the crucial step to complete the formation of crosslinked network. The higher the crosslinked extent of a network, the stronger will be the tendency that it shatters coincidently at its decomposition point.

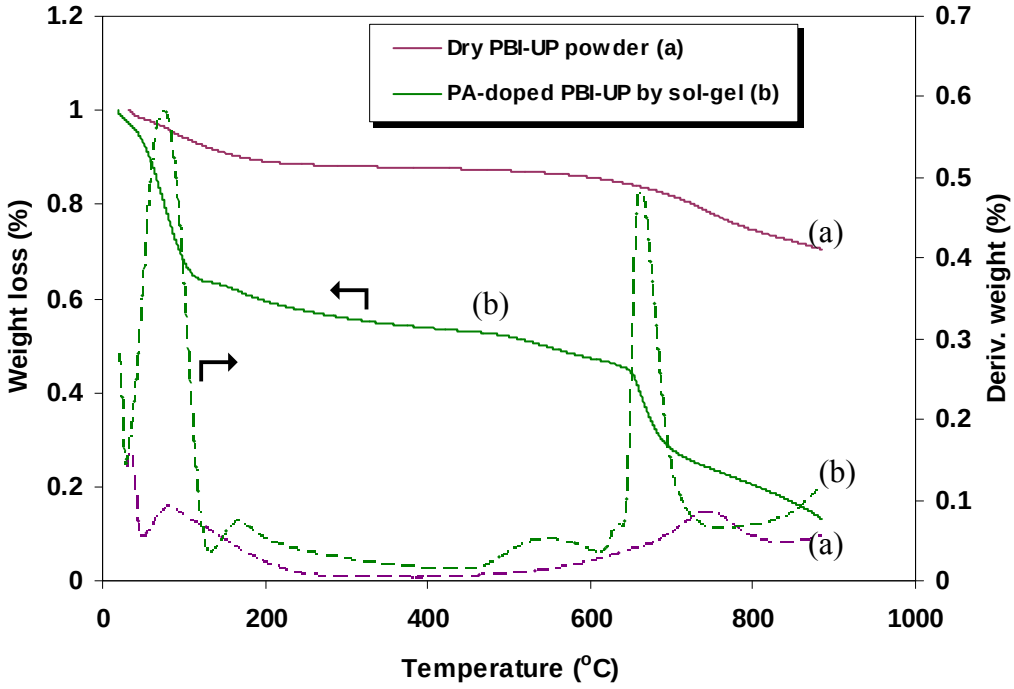

Figure 7.1 TGA of PBI-polymer powder and PA-doped PBI-UP membrane

In the Figure 7.2, the PA-doped PBI membrane developed via impregnation method and the dry PBI powder are compared. After the elimination of liquid component, the PA-doped PBI membrane displays a similar TGA profile to that of PBI powder. However, compared with PA-doped PBI membrane the PA-doped PBI membrane has much better thermal stability. This observation is consistent with the above inference that increasing crosslinking extent leads to a faster decomposition rate.

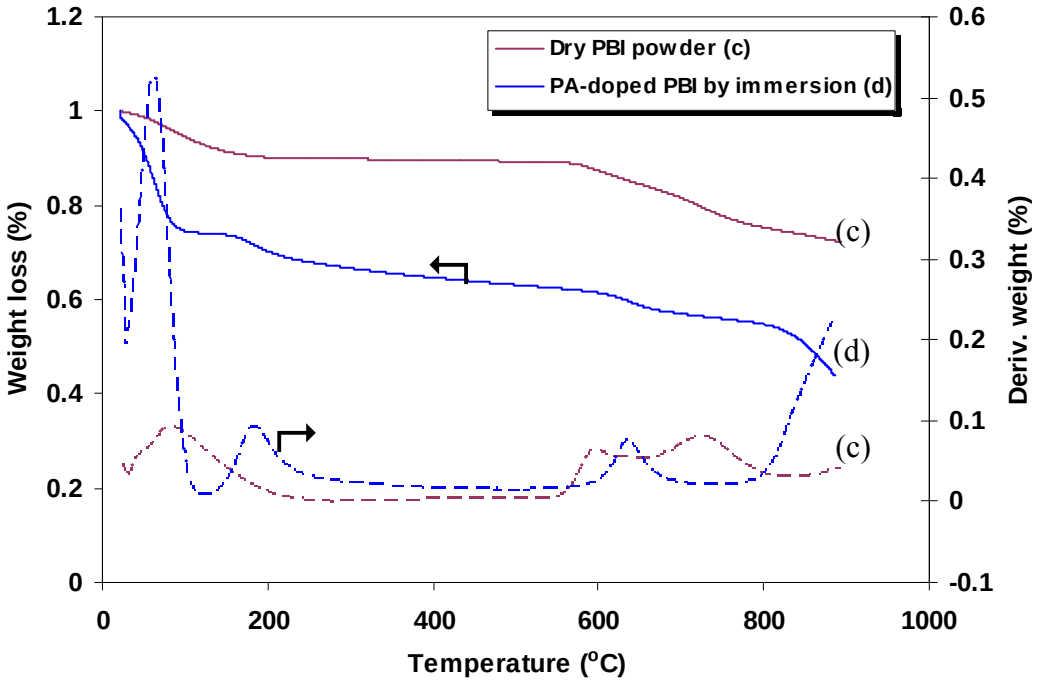

Figure 7.2 TGA of PBI polymer powder and PA-doped PBI membrane from embedding method

From the DSC analysis (Fig. 7.3) of PBI powder and PBI-UP powder, it can be observed that the PBI-UP polymer displayed slightly higher glass transition temperature (T_g) than PBI powder. This result indicates that crosslinking extent in PBI-UP was mild before thermal curing. Namely there is only a low extent of crosslinking that takes place during the polymerization process.

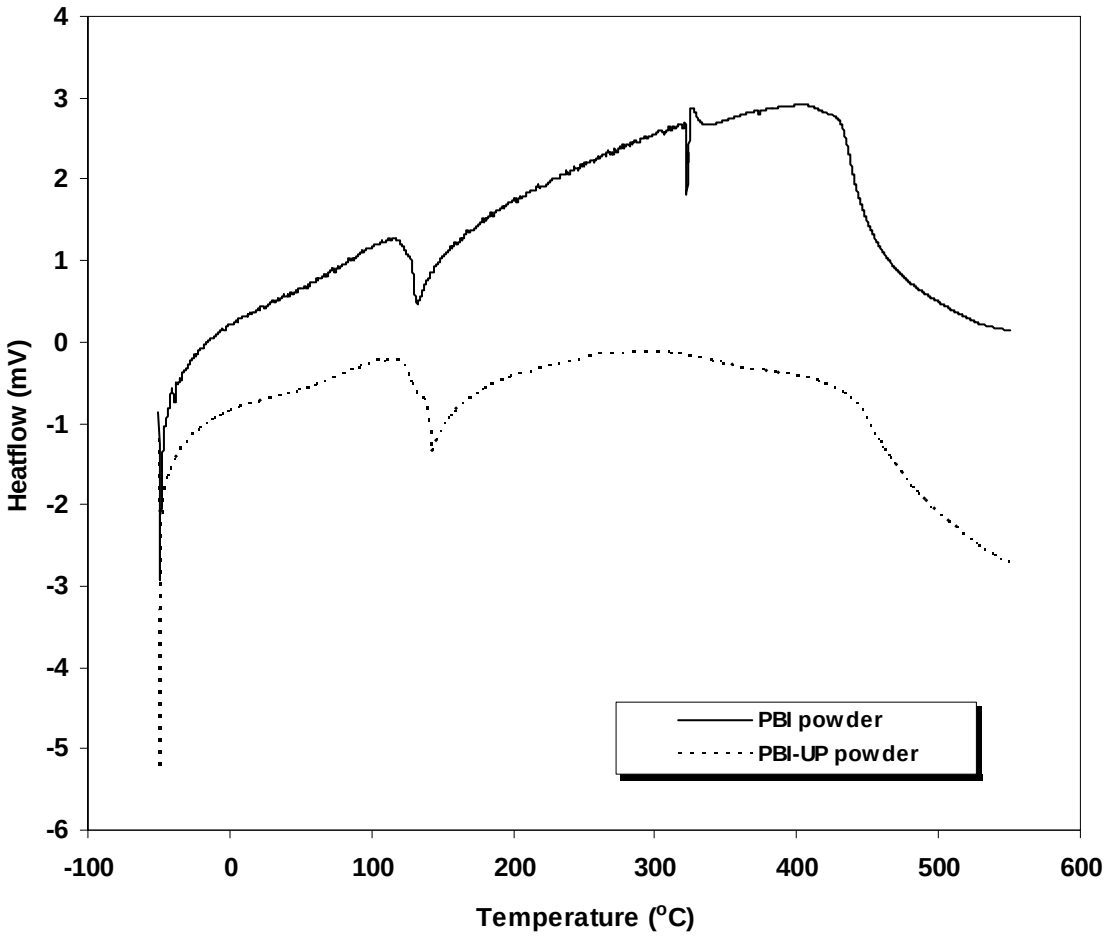

Figure 7.3 DSC of PBI polymer powder and PBI-UP polymer powder

Furthermore, regarding how the curing treatment augments the PBI-UP network, the two samples from PA-doped PBI-UP before and after curing were analyzed by DSC, respectively. (Fig. 7.4) A two-scan scheme was set to carry out the analysis. For each sample (with the identical mass), the first scan (from rt. to 160 ^{o}C) removed moisture and weakly held PA molecules from the sample and the second scan (from rt. to 550 ^{o}C) was recorded for the study. Both DSC diagrams revealed a broad endothermic transition peak

that spans from 150 ^{o}C to 360 ^{o}C. On the basis of the TGA profile of the cured PA-doped PBI-UP membrane presented in Fig. 7.1, the endothermic response of DSC describes the evaporation of PA molecules from the PBI-UP network. The PA-doped PBI-UP membrane without being cured in prior exhibited a stronger endothermic downturn (or specific heat) than its cured counterpart below 200^{o}C, but the later one showed that a greater portion (ca. 6/7) of specific endothermic heat occurs in the upper temperature range (200 - 360^{o}C) than then the former. Besides this difference, the cured sample displayed a more symmetric endothermic contour than the the un-cured sample. The above outcomes clearly suggest that the cured PBI-UP network be a better lodger for the PA molecules in terms of holding affinity and uniformity of network distribution.

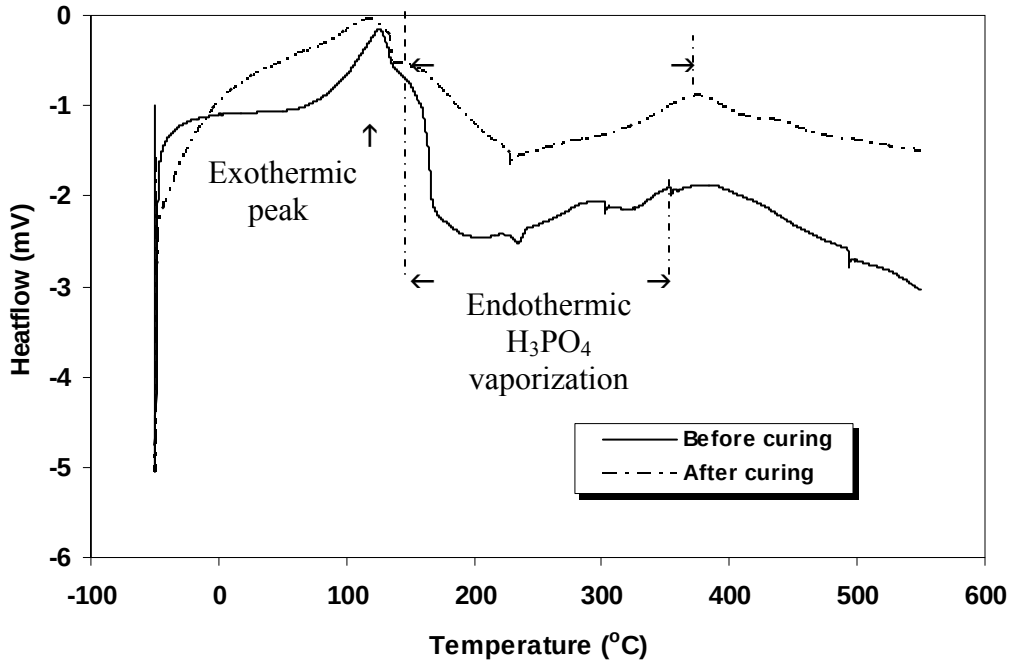

Figure 7.4 DSC of PA-doped PBI-UP membranes

From the above discussion, it has been established that two types of freestanding membranes have been prepared by means of the in-situ sol-gel polymerization method (i.e. PA-doped PBI-UP) and the post polymerization impregnating method (i.e. PA-doped PBI), respectively. The former membrane exhibited an yield strength of approximately 1.7 MPa at the yield strain of 9.11% and an ultimate tensile strength of about 10.05 MPa at the elongation of 146.7%. As shown in Fig. 7.5, this membrane, because of its viscoelastic network structure, owns a far greater strength at breaking point and strain than the PA-doped PBI membrane (Fig. 7.5). The tensile stress and Young's modulus data of these two membranes are given in Table 7.3. Regarding the PA-doped PBI membrane, it showed poorer mechanical properties primarily because all the PBI molecular segments are not interconnected by chemical bonding as aforementioned. Hence weaker H-bonding as well as van der Waals forces between PBI segments and between PBI and PA was not able to offer desired mechanical properties.

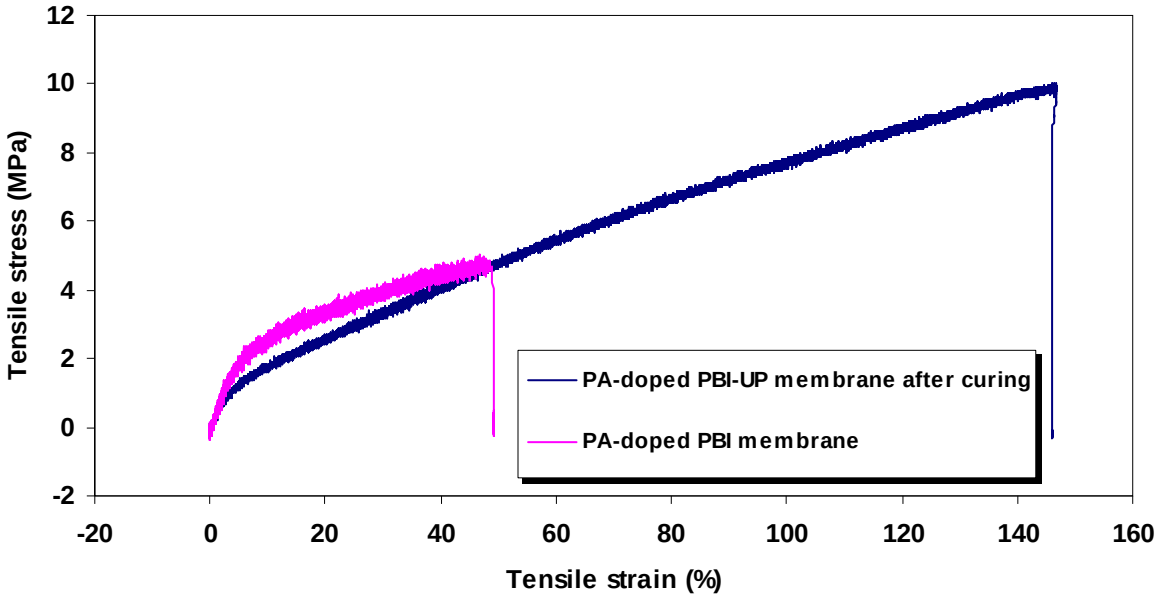

Figure 7.5 Mechanical strength of PA-doped PBI-UP membrane after densing and PA doped PBI from embedding method

Table 7.3 Mechanical properties of the two types of PA-doped PBI

Sample	Load at Max. tensile stress (N)	Tensile Modulus (GPa)	Yield stress (MPa)	Yield strain (%)	Max. tensile stress (MPa)	Strain (%)
PA-doped PBI-UP after curing	5.75	33.70 (±1.33) $\times 10^{-3}$	1.70	9.11	10.05	146.7
PA-doped PBI via immersion	1.53	50.11 (±0.41) $\times 10^{-3}$	2.41	8.18	5.01	49.0

7.3.3 Proton conductivity and single fuel cell performance

The most valuable trait of PBI-based membranes lies in its humidity-independent proton conductivity in the temperature range from 120 ^{o}C to 150 ^{o}C. To assess the proton conductivity of these two particular membranes (as discussed in Fig. 7.5), the membrane samples were kept in an oven to maintain their anhydrous matrixes before measurement. Their temperature-dependent proton conducting behaviors, obtained by using the 4-probe method and under nil humidity circumstance, are concluded in Fig 7.6. The PA-doped PBI membrane provided maximum conductivity of 0.025 S/cm at just 110 ^{o}C. In contrast, the PA-doped PBI-UP membrane showed 0.072 S/cm at 60 ^{o}C and reached as high as 0.125 S/cm at 160 ^{o}C followed by decrease in conductivity with increasing temperature. The key factor responsible for the superiority of the PA-doped PBI-UP membrane over the PA-doped PBI membrane was their largely different PA doping levels (Table 7.2), which according to previous discussion is supported by visoelastic network.

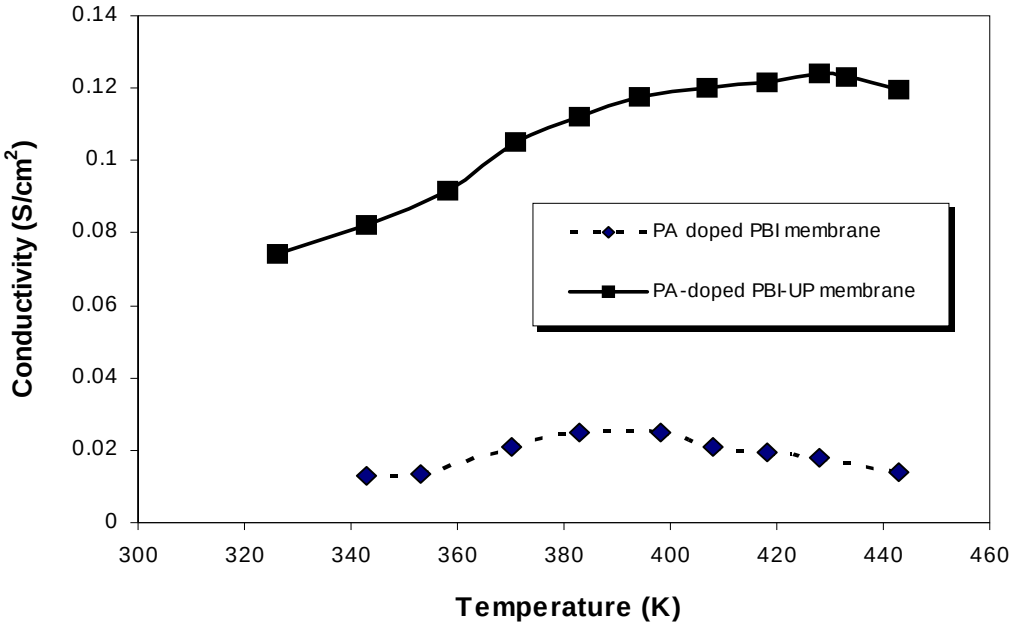

Figure 7.6 Influence of temperature on the conductivity of various membranes under investigation

On the basis of conductivity measurement, only the PA-doped PBI-UP membrane has significance of being assessed to determine its fuel cell performance. Figure 7.7 displays the polarization curves of this membrane in a single H_2-PEMFC without humidifying either electrode. The membrane was evaluated at three temperature points and the power density is increased with increasing of temperature. At 150^{o}C and the current density of 0.9 A/cm^2 the highest power output (0.3W/cm^2) of the cell was achieved. This outcome confirms that the PA molecules constitute a continuous phase in the PBI-UP network, which permits transport of protons across the anhydrous membrane. For this conducting mechanism an operation temperature in the range of 150-200^{o}C is imperative in order to achieve a high power output.

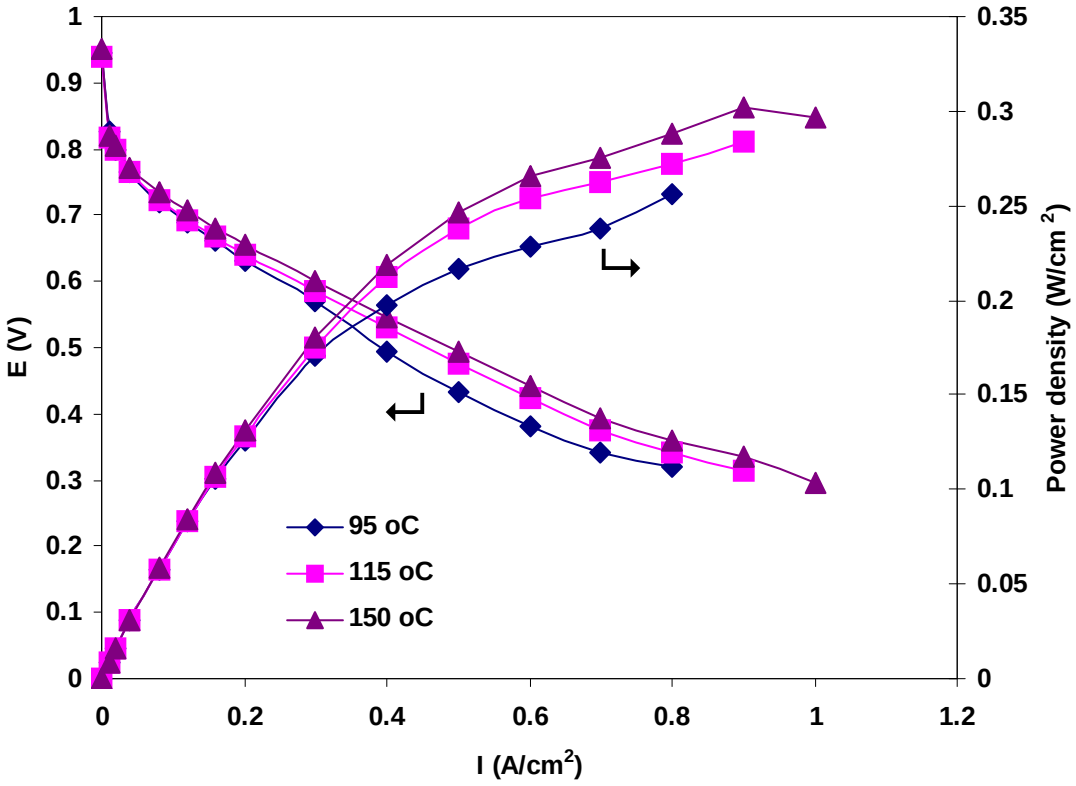

Figure 7.7 The electrochemical performance of PA-doped PBI-UP membrane after densing in a hydrogen-driven single fuel cell at the three elevated temperatures

7.4 Conclusions

This work proposes an effective measure to conquer the problem caused by difficult control over the reaction conditions for fabricating H_3PO_4-doped polybenzimidazole (PBI) membrane in the *in-situ* sol-gel polymerization system. The measure is simply to include an unsaturated polyester (UP) macromer into the PBI polymerization system to form a crosslinked network. Sustained by this particular network, the resulting membrane scored a much higher H_3PO_4-doping level than the H_3PO_4-doped PBI membrane made by the conventional impregnating method, and such a high H_3PO_4 doping level brings about a proton conductivity of 10^{-1} S/cm at 160 ^oC and with zero matrix humidity. Furthermore, a promising performance of the membrane in a single H_2 fuel cell was accomplished at 150 ^oC without humidifying either electrode. Besides possessing the desired high-temperature proton conductivity, the H_3PO_4-doped PBI-UP membrane also exhibited sound mechanical properties and thermal stability.

CHAPTER 8

CONCLUSIONS AND RECOMMENDATIONS

8.1 Conclusions

This thesis focuses on fabrication and study of proton exchange polymer membranes (PEMs) which suit the applications for the fuel cells that are required to operate at high temperatures (80-150 ^{o}C) or use CH_3OH instead of H_2 as fuel. Three appealing types of hybrid sulfonic perfluoropolymer (SPFP) membranes have been fabricated through incorporating unique nano-particles, which have dense oligomeric ionomer outer layer, are starburst super-molecules, or own rigid 3-D architecture, into SPFP (e.g. Nafion) matrix. Besides these, the success in crosslinking polybenzimidazole by unsaturated polyester macromer to form a H_3PO_4-impregnated matrix, which is a promising high-temperature and non-humidified PEM, was achieved. All of these resulting composite membranes were characterized using pertinent instrumental methods with the aim to understand the fundamental interactions between filler (or macromer) and host matrix as well as the effects, generated due to formation of composite, on the proton conduction, electrochemical polarization in fuel cell, methanol diffusion, and mechanical properties. Of the preceding investigations, how a modification design alters or restructures hydrophilic proton conducting channels so as to benefit conveying a high flux of protons across membrane is the center issue to

explore. It is anticipated that these fundamental studies offer useful knowledge for the future researches attempting to revamp or synthesize PEMs to meet requirements of high-performance PEMFCs. The main triumph of this thesis work is the augmenting of membrane capacity to sustain a higher proton flux, consequently, the membranes achieved manifest superior single cell performances over their respective native membranes. The important findings of this work are summarized as follows:

(1) A core-shell microspheric structure was constructed by growing the polymer chains on the surface of silica microspheres using the atom transfer radical polymerization (ATRP), which comprises the homo-polymer or the block-copolymer chains of sodium 4-styrenesulfonate (SSNa) and 4-vinylpyridine (4VP). Firstly, it was observed that the molecular weights of the grafted chains fell into the range of a dozen hundred Daltons. This result shows that such an oligomerization outcome is the characteristic of ATRP on an insoluble substrate. Further, the physical responses and colloidal behaviors of the resulting microspheres were also studied in this work. It was found that the grafted homo-oligomeric layers displays stronger chain-chain interactions than their unbound counterparts, and the more interesting observation was that the two mutually inverted sequences of copolymer block produce rather different impacts on the chain association pattern. Moreover, it was found that the functional group type and the sequence of the grafted copolymer blocks influenced the hydrodynamic volume of the particles in dispersing liquid solutions with different pH or polarity. This effect is mainly due to the leverage of the inner blocks of copolymer

on the magnitude of surface charge and hydrodynamic volumes of the particles, besides the known factors including solvating extent and charge repulsion /neutralization. In the final part of this work, electrochemical properties of the four types of grafted oligomeric chains were investigated in very dilute colloidal dispersion in HCl (pH=3) and DMF-H_2O medium respectively. It was found that the two grafted copolymer sequences exhibited very different roles in mediating ion (H^+ or Na^+) transport in a liquid medium where substantially dilute microspheres were present. The solvating extent of the inner polymer block affects stretching of the copolymer chains, which in turn display different capabilities to sweep ions in the liquid media of interest. From this study, such core-shell particles with polyelectrolyte chains can be considered as valuable materials to be used to modify Nafion® matrix in the next section.

(2) Modification of Nafion membrane with ionomer-grafted silica nano particles, PSPA-SiO_2 was investigated. PSPA-SiO_2 was synthesized by carrying out atom transfer radical polymerization (ATRP) of 3-sulfopropyl acrylate potassium salt (SPA-K) on nano silica particles. The composite Nafion membranes with different ratio of PSPA-SiO_2 loading had higher conductivity than Nafion membrane and Nafion/silica in the experiment temperature range of 50 ^oC to 90 ^oC. Furthermore, it was found that the presence of ionomer-grafted silica nano particles, PSPA-SiO_2, in the membrane matrix of Nafion improved its performance in PEMFC significantly, which is due to the fact that PSPA-SiO_2 particles can boost the flux of protons and

facilitate their transport. The boosting role comes from the fact that each PSPA-SiO_2 particle bears a high density of sulfonic acid groups, and the facilitating role is attributed to the hydrophilic interactions between PSPA-SiO_2 particles and the sulfonic acid group of Nafion chains.

(3) Poly($Q_8M_8^V$) fragments were incorporated into Nafion polymer matrix during embedded polymerization. It was found that these fragments can restrict, due to their geometric boundary effect, random extension and crosslinking of hydrophilic proton-conducting channels (PCC) composed of the sulfonic acid groups of Nafion molecules. Therefore, the whole Nafion matrix became less hydrophilic and PCC also became more localized with increasing P($Q_8M_8^V$) loading. Such change in the PCC distribution led to the following results: the composite membranes containing the filler of 5 wt.% and 15 wt.% imparted apparently lower methanol permeation coefficients and far greater power density output of single DMFC than the pristine Nafion membrane. These results shows that introduction of poly($Q_8M_8^V$) in the SPFP matrix is a potentially effective technique to minimize the methanol-crossover problem in DMFCs and further achieve a significant enhancement in the performance of DMFCs. However, in this work, we also observed that higher poly($Q_8M_8^V$) loading did not provide better cell performance of DMFCs owing to negative effect for original Nafion structure. Therefore poly($Q_8M_8^V$) loading for composite membranes need to be optimized.

(4) A novel type of highly branched nanoparticles (*sb*-POSS) was synthesized by grafting polyacrylonitrile (PAn) short chains to POSS, a cubic silicone molecule with atom transfer radical polymerization (ATRP) method. In this study, it was found that the proton conducting channels (PCCs) of the native Nafion undertake restructuring to form the perturbed and unperturbed PCCs which can coexist in the all composite membranes formed. This coexistence may be attributed to the fact that the starburst architecture of *sb*-POSS particles and the strong polar nitrile groups of the grafted PAn oligomeric chains are the key structural traits that assist dispersion of the particles in the Nafion membrane matrix. In addition, the performance of Nafion membrane with different content of *sb*-POSS particles in a direct methanol fuel cell (DMFC) was also evaluated. The single DMFC assessment showed that the composite membrane containing *sb*-POSS ($\overline{M}_n$=33746) of 5 wt.% had more than double the power density output of the native Nafion membrane. This may be explained using the DSC characterization result that the *sb*-POSS content of 5 wt.% confers the highest portion of the unperturbed PCC in the composite membrane. Furthermore, the length of PAn chains grafted on *sb*-POSS particles was the other key factor affecting the portion of unperturbed PCC in the composite membrane. As a result, the maximal PAn chain-length that could be achieved by employing the present grafting method (ATRP) offers the best result in improving DMFC performance.

(5) In the final part of this study, a PBI-Unsaturated polyester blending system was synthesized from 3, 3'-diaminobenzidine tetrahydrochloride dehydrate and

Isophthalic acid with unsaturated polyester (UP) macromer as crosslink agent in PPA solvent and subsequently high PA doped PBI-UP membrane (about 24 mol of PA per PBI repeat unit) was cast and polycondensed from this PBI-UP blending system with the hydrolysis of PPA to PA. It was observed that the resulting membrane scored a much higher H_3PO_4-doping level than the H_3PO_4-doped PBI membrane made by the conventional impregnating method, and also achieved higher mechanical strength. As a result, it was found that the membrane provided a higher conductivity at higher temperature (e.g. 0.125 S/cm at 160 ^oC) than the PA-doped PBI membrane obtained with conventional impregnating method (e.g. 0.025 S/cm at 110 ^oC). Single fuel cell performances of the membrane at different operated temperature 95 ^oC, 115 ^oC and 150 ^oC without external humidification of the gases supplied to either electrode were also evaluated. The highest power density at operation pressure was about 30.24 mW/cm^2 at 0.9 A/cm^2 at 150 ^oC.

8.2 Recommendations

On the basis of the above results of study, the following recommendations are considered relevant to the further research on the development of composite PEMs.

(1) We have prepared a kind of core-shell silica nanoparticles bearing graft ionomer with pendant sulfonic acid groups to modify the Nafion matrix. This type of hybrid nanoparticles is used, for the first time, to modify Nafion membrane. However, other

vinyl monomers carrying sulfonic acid groups, such as 4-styrenesulfonate (SSNa), 2-acrylamido-2-methyl propanesulfonic acid (AMPS), and 3-sulfropopyl methacrylate, potassium salt (SMP-K) have not been investigated yet in the previous work. Therefore, it is worth, in the future study, to graft these monomers to the particle surface via the living radical polymerization method. Moreover, in this study, we chose SiO_2 nanoparticles as precursors of ATRP because it is the most popular inorganic oxide filler that supplies the composite membranes with a good mechanical and thermal resistance. Besides SiO_2 particles, other types of inorganic oxides (e.g. TiO_2 and ZrO_2) may be employed to substitute SiO_2. And these synthesized core-shell particles can also be studied to examine their effect on the Nafion membrane structure and performance.

(2) As a novel hybrid precursor, polyhedral oligomeric silsesquioxane (POSS) can be extended by a variety of organic functional groups from its corner silicone atoms. We have selectively derived two kinds of functional groups, polyacryonitrile short chains and 2-methyl-vinyl, from cubic POSS to form two kinds of molecular particles and studied different effects of these hybrid particles on proton transport in the membranes in the Chapter 3 and 4. The aim of introducing these functionalized POSS into Nafion is to reduce methanol crossover of Nafion matrix and thus to improve the performance of membrane in DMFC. Some other functionalized POSS molecules can be further explored to modify Nafion matrix. For example, POSS could be grafted by vinyl monomers carrying sulfonic groups using ATRP method. It will be interesting

to understand whether or not and to what magnitude this specific type of oligomeric molecular particles could bring about to enhance proton transport traits of the resulting composite Nafion membranes.

(3) PA doped PBI-UP membrane has been synthesized in the final part of this work. From the study, high mechanical strength and doping level have been achieved at the same time. These properties are significant because they not only increase the conductivity of the membrane to higher level, but also allow the membrane to be applied in the high temperature fuel cell under the condition of zero humidity. However, explanations for proton transport in the membrane are limited in this study due to complexity of the composite membrane internal structure. Therefore, as a potentially valuable extension of this work, physical and chemical interaction between polymer chains and phosphoric acid molecules should be investigated by solid state NMR and simulation method. Besides, both chemical stability and mechanical durability of the membrane are also very important for PEM commercialization. Because the fuel cells are required to demonstrate durability of about 5000 h for automotive applications and 10,000-40,000 h for stationary application. Therefore, the decomposition issues of the membrane should be studied from a stress-cycle experiment in the future. And at the same time, durability issues of the membrane should also be investigated by accelerated experiment and durability evaluation.

REFERENCES

Adjemian, K.T., Lee, S.J., Srinivasan, S., Benziger, J., Bocarsly, A.B., Silicon oxide Nafion composite membranes for proton-exchange membrane fuel cell operation at 80-140 ^{o}C, J. Electrochem. Soc., 149, pp.A256-A261, 2002.

Alberti, G., Casciola, M., Massinelli, L., Bauer, B., Polymeric proton conducting membranes for medium temperature fuel cells (110-160 ^{o}C), J. Membr. Sci., 185, pp.73-81, 2001.

Aramata, A., Toyoshima, I., Enyo, M., Study of methanol electrooxidation on Rh-Sn oxide, Pt-Sn oxide, and Ir-Sn oxide in comparison with that on the Pt metals, Electrochim. Acta., 37, pp.1317-1320, 1992.

Arico, A.S., Kim, H., Shukla, A.K., Ravikumar, M.K., Antonucci, V., Giordano, N., Methanol oxidation on carbon-supported Pt-Sn electrodes in silicotungstic acid, Electrochim. Acta., 39, pp.691-700, 1994.

Armand, M.B., Polymer solid electrolytes-an overview, Solid State Ionics, 9-10, pp.745-754, 1983.

styrene-co-methacrylate-silica sol-gel membranes containing tungstophosphoric acid, Solid State Ionics, 176, pp.333-340, 2005.

Asensio, J.A., Borros, S., Gomez-Romero, P., Polymer electrolyte fuel cells based on phosphoric acid-impregnated poly(2,5-benzimidazole) membranes, J. Electrochem. Soc., 151, pp.A304-A310, 2004a.

Asensio, J.A., Borros, S., Gomez-Romero, P., Proton-conducting polymers based on benzimidazoles and sulfonated benzimidazoles, J. Polym. Sci. Part A: Polym. Chem., 40, pp.3703-3710, 2002

Asensio, J.A., Borros, S., Gomez-Romeroa, P., Proton-conducting membranes based on poly(2,5-benzimidazole) (ABPBI) and phosphoric acid prepared by direct acid casting, J. Membr. Sci., 241, pp.89-93, 2004b.

Asensio, J.A., Borros, S., Gomez-Romeroa, P., Sulfonated poly(2,5-benzimidazole (SABPBI) impregnated with phosphoric acid as proton conducting membranes for polymer electrolyte fuel cells, Electrochim. Acta, 49, pp.4461-4466, 2004c.

Bae, J.M., Honma, I., M. Murata, Yamamoto, T., Rikukawa, M., Ogata, N., Properties of selected sulfonated polymers as proon-conducting electroytes for polymer electrolyte fuel cells, Solid State Ionics, 147, pp.189-194, 2002.

Bauerl, F., Willert-Porada1, M., Comparison between Nafion® and a Nafion® zirconium phosphate nano-composite in fuel cell applications, Fuel Cells, 3-4, pp.261-269, 2006.

Basu, S., Recent trends in fuel cell science and technology, Springer, New York, 2007.

Bhat, R.R., Tomlinson, M.R., Wu, T., Genzer, J., Surface-grafted polymer gradients: formation, characterization, and applications, Adv. Polym. Sci., 198, pp.51-124, 2006.

Boddeker, K.W., Peinemann, K.V., Nunes, S.P., Membranes in fuel cells, J. Membr. Sci., 185, pp.1, 2001.

Borup, R., Vanderborgh, N., Design and testing criteria for bipolar plate materials for PEM fuel cell applications, Mater. Res. Soc. Symp. Proc., 393, pp.151-155, 1995.

Bouchet, R., Siebert, E., Proton conduction in acid doped polybenzimidazole, Solid State Ionics, 118, pp.287-299, 1999.

Bozkurt, A., Ise, M., Kreuer, K.D., Meyer, W.H., Wegner, G., Proton-conducting polymer electrolytes based on phosphoric acid, Solid State Ionics, 125, pp.225-233, 1999.

Bozkurt, A., Meyer, W.H., Proton conducting blends of poly(4-vinylimidazole) with phosphoric acid, Solid State Ionics, 138, pp.259-265, 2001.

Brickner, C.J., Scherer, G., in Sol-gel science: the physics and chemistry of sol-gel processing, Academic Press, San Diego, pp.135-139, 1990.

Burstein, G.T., Barnett, C.J., Kucernak, A.R., Williams, K.R., Aspects of the anodic oxidation of methanol, Catal. Today, 38, pp.425-437, 1998.

Cao, G., Nanostructures & Nanomaterials: synthesis, properties & applications, Imperial College Press, pp153, 2004.

Carretta, N., Tricoli, V., Picchioni, F., Ionomeric membranes based on partially sulfonated poly(styrene): synthesis, proton conduction and methanol permeation, J. Membr. Sci., 166, pp.189-197, 2000.

Chang, H.Y., Thangamuthu, R., Lin, C.W., Structure-property relationships in PEG/SiO2 based proton conducting hybrid membranes- A ^{29}Si CP/MAS solid-state NMR study, J. Membr. Sci., 228, pp.217-226, 2004.

Choi, J.W., A.F., Yee, Laine, R.M., Organic/inorganic hybrid composites from cubic silsesquioxanes: epoxy resins of octa (dimethylsiloxyethylcyclohexylepoxide) silsequioxane, Macromolecules, 36, pp.5666-5682, 2003a.

Choi, J.W., Tamaki, R., Kim, S.G., Laine, R.M., Organic/inorganic imide nanocomposites form aminophenylsilsesquixanes, Chem. Mater., 15, pp.3365-3375, 2003b.

Chu, D., Gilman, S., The influence of methanol on O_2 electroreduction at a rotating Pt disk electrode in acid electrolyte, J. Electrochem. Soc., 141, pp.1770-1773, 1994.

Chen, N., Hong, L., Proton-conducting membrane composed of sulfonated polystyrene microspheres, poly(vinylpyrrolidone) and poly(vinylidene fluoride), Solid State Ionics, 146, pp.377-385, 2002.

Chen, N., Hong, L., Embedding poly(styrene sulfonic acid) into PVDF matrix—a new type of proton electrolyte membrane, Polymer, 45, pp.2403-2411, 2004.

Chen, X.Y., Randall, D.P., Perruchot, C., Watts, J.F., Patten, T.E., Werne, T., Armes, S.P., Synthesis and aqueous solution properties of polyelectrolyte-grafted silica particles prepared by surface-initiated atom transfer radical polymerization, J. Colloid Interface Sci., 257, pp.56-64, 2003.

Choe, E-W., Catalysts for the preparation of polybenzimidazoles, J. Appl. Polym. Sci., 53, pp.497-506, 1994.

Coad, B.R., Steels, B.M., Kizhakkedathu, J.N., Brooks, D.E., Haynes, C.A., The influence of grafted polymer architecture and fluid hydrodynamics on protein separation by entropic interaction chromatography, Biotechnol. Bioeng., 97, pp. 574-587, 2006.

Colomban, P., Proton conductors: solids, membranes, and gels-materials and devices, Cambridge University Press, New York, 1992.

Costa, R.O.R., Vasconcelos, W.L., Tamaki, R., Laine, R.M., Organic/inorganic nanocomposite star polymers via atom transfer radical polymerization of methyl methacrylate using octafunctional silsesquioxane cores, Macromolecules, 34, pp.5398-5407, 2001.

Daiko, Y., Klein, L.C., Kasuga, T., Nogamia, M., Hygroscopic-oxides/Nafion® hybrid electrolyte for direct methanol fuel cells, J. Membr. Sci., 281, pp.619-625, 2006.

Datta, B.K., Velayutham, G., Groud, A.P., Fuel cell power source for a cold region, J. Power Sources, 106, pp.370-376, 2002.

Deimede, V., Voyiatzis, G.A., Kallitsis, J. K., Li, Q., Bjerrum, N.J., Miscibility behaviour of polybenzimidazole/sulfonated polysulfone blends for use in fuel cell applications, Macromolecules, 33, pp.7609-7617, 2000.

Donoso, P., Gorecki, W., Berthier, C., NMR, Conductivity and neutron scattering investigation of ionic dynamics in the anhydrous polymer protonic conductor $PEO(H_3PO_4)_x$, Solid State Ionics, 28-30, pp.969-974. 1988.

Drobny, J.G., Blends and composites based on fluoropolymers**,** Macromol. Symp., 170, pp.149-156, 2001.

Elabd, Y.A., Walker, C.W., Beyer, F.L., Triblock copolymer ionomer membranes: Part II. Structure characterization and its effects on transport properties and direct methanol fuel cell performance, J. Membr. Sci., 231, pp.181-188, 2004.

Elabd, Y.A., Napadensky, E., Sloan, J.M., Crawford, D.M., Walker, C.W., Triblock copolymer ionomer membranes: Part I. Methanol and proton transport, J. Membr. Sci., 217, pp.227-242, 2003.

Elsman, G.A., The application of Dow Chemical's perfluorinated membranes in proton-exchange membrane fuel cells, J. Power Sources, 29, pp.389-398. 1990.

Feher, F.J., Wyndham, K.D., Baldwin, R.K., Soulivong, D., Lichtenhan, J.D., Ziller, J.W., Methods for effecting monofunctionalization of $(CH_2=CH_2)_8Si_8O_{12}$, Chem. Commun., 1289-1290, 1999a.

Feher, F.J., Wyndham, K.D., Soulivong, D., Nguyen, F.J., Syntheses of highly functionalized cube-octameric polyhedral oligosilsesquioxanes, Dalton Trans., 1491-1497, 1999b.

Fontanella, J.J., Wintersgill, M.C., Wainright, J.S., Savinell, R.F., Litt, M., High pressure electrical conductivity studies of acid doped polybenzimidazole, Electrochim. Acta., 43, pp.1289-1294, 1998.

Fontanella, J.J., McLin, M.G., Wintersgill, M.C., Calame, J.P., Greenbaum, S.G., Electrical impedance studies of acid form NAFION® membranes, Solid State Ionics, 66, pp.1-4, 1993.

Fulghum, T.M., Patton, D.L., Advincula, R.C., Fuzzy ternary particle systems by surface-initiated atom transfer radical polymerization from layer-by-layer colloidal core-shell macroinitiator particles, Langmuir, 22, pp.8397, 2006.

Gao, Y., Robertson, G.P., Guiver, M.D., Jian, X., Mikhailenko, S.D., Wang, K., Kaliaguine, S., Sulfonation of poly(phthalazinones) with fuming sulfuric acid mixtures for proton exchange membrane materials, J. Membr. Sci., 227, pp.39-50, 2003.

Gapeev, A., Dunbar, R.C., Na^+ affinities of gas-phase amino acids by ligand exchange equilibrium, Int. J. Mass Spectrom., 228, pp.825-839, 2003.

Gardner, C.L., Anantaraman, A.V., Measurement of membrane conductivities using an open-ended coaxial probe, J. Electroanal. Chem., 395, pp.67-73, 1995.

Ge, J., Liu, H.J., Experimental studies of a direct methanol fuel cell, J. Power Sources, 142, pp.56-69, 2005.

Glipa, X., Haddad, M.E., Jones, D.J., Roziere, J., Synthesis and characterization of sulfonated polybenzimidazole: a highly conducting proton exchange polymer, Solid State Ionics, 97, pp.323-331, 1997.

Glipa, X., Bonnet, B., Jones, D.J., Roziere, J., Investigation of the conduction properties of phosphoric and sulfuric acid doped polybenzimidazole, J. Mater. Chem., 9, pp.3045-3049, 1999.

Goward, G.R., Schuster, M.F.H., Sebastiani, D., Schnell, I., Spiess, W., High-resolution solid-state NMR studies of imidazole-based proton conductors: structure motifs and chemical exchange from ^{1}H NMR, J. Phys. Chem. B, 106, pp.9322-9334, 2002.

Gottesfeld, S., Zawodzinski, T.A., Alkire, R.C., Gerischer, H., Kolb D.M., Tobias (Eds), Advances in Electrochemical Science and Engineering, Vol 5, Wieley VCH, Weinheim, pp.195, 1997,

Grot, W.G., Rajendran, G., Membranes containing inorganic fillers and membrane and electrode assemblies and electrochemical cells employing same, US Patent 5919583, 1999.

Haddad, T.S., Lichtenhan, J.D., Hybrid organic-inorganic thermoplastics: styryl-based polyhedral oligomeric silsesquioxane polymers, Macromolecules, 29, pp.7302-7304, 1996.

Harrison, W.L., Hickner, M.A., Kim, Y.S., McGrath, J.E., Poly(arylene ether sulfone) copolymers and related systems from disulfonated monomer building blocks: synthesis, characterization, and performance-A topical review, Fuel Cells, 5, pp.201-212, 2005.

Hasegawa, I., Motojima, S., Dimethylvinykilylation of $Si_8O_{20}^{8-}$ silicate anion in methanol solutions of tetramethylammonium silicate, J. Organometallic Chem., 441, pp.373-380, 1992.

Hasiotis, C., Li, Q., Deimede, V., Kallitsis, J.K., Kontoyannis, C.G., Bjerrum, N.J., Development and characterization of acid-doped polybenzimidazole/sulfonated polysulfone blend polymer electrolytes for fuel cells, J. Electrochem. Soc., 148, pp.A513-A519, 2001a.

Hasiotis, C., Deimede, V., Kontoyannis, C.G., New polymer electrolytes based on blends of sulfonated polysulfones with polybenzimidazole, Electrochim. Acta, 46, pp.2401-2406, 2001b.

Heinzel, A., Barragan, V.M., A review of the state-of-the-art of the methanol crossover in direct methanol fuel cells, J. Power Sources, 84, pp.70-74,1999.

He, R., Li, Q., Xiao, G., Bjerrum, N.J., Proton conductivity of phosphoric acid doped polybenzimidazole and its composites with inorganic proton conductors, J. Membr. Sci., 226, pp.169-184, 2003.

Hickman, B.S., Mascal, M., Titman, J.J., Wood, I.G., Protonic conduction in imidazole: A solid-state ^{15}N NMR study, J. Am. Chem. Soc., 121, pp.11486-11490, 1999.

Holmberg, S., Lehtinen, T., Näsman, J., Ostrovskii, D., Paronan, M., Serimaa, R., Sungholm, F., Sundholm, G., Torell, L., Torkkeli, M., Structure and properties of sulfonated poly[(vinylidene fluoride)-g-styrene] porous membranes, J. Mater. Chem., 6, pp.1309-1317, 1996.

Hong, L., Zhou, Y.; Chen, N., Li, K., Association of Nafion with polypyrrole nanoparticles in a hydrophilic polymer network: effects on proton transport, J. Colloid Interface Sci., 218, pp.233-242, 1999.

Hsu, W.Y., Gierke, T.D., Ion transport and clustering in Nafion perfluorinated membranes, J. Membr. Sci., 13, pp.307-326, 1983.

Huang, C.F., Kuo, S.W., Chen, J.K., Chang, F.C., Sythesis and characterization of polymerstyrene-b-poly(4-vinyl pyridine) block copolymers by atom transfer radical polymerization, J. Polym. Res., 12, pp.449-456, 2005.

Huang, J.C., He, C.B., Xiao, Y., Mya, K.Y., Dai, J., Siow ,Y.P., Polyimide/POSS nanocomposites: interfacial interaction, thermal properties and mechanical properties, Polymer, 44, pp.4491-4499, 2003.

Ikada, Y., Surface modification of polymers for medical applications. Biomaterials, 15, pp.725-736, 1994.

Iwakuha, Y., Uno, K., Imai, Y., Polyphenylenebenzimidazoles, J. Polym. Sci., Part A: Polym. Chem., 2, pp.2605-2615, 1964.

Jalani, N.H., Dunn, K., Datta, R., Synthesis and characterization of Nafion®-MO_2 (M = Zr, Si, Ti) nanocomposite membranes for higher temperature PEM fuel cells, Electrochim. Acta, 51, pp.553-560, 2005.

Jiang, R., Kunz, H.R., Fenton, J.M., Composite silica/Nafion® membranes prepared by tetrathylorthosilicate sol-gel reaction and solution casting for direct methanol fuel cells, J. Membr. Sci., 272, pp.116-124, 2006.

Jiang, S.P., Liu, Z., Tian, Z.Q., Layer-by-layer self-assembly of composite polyelectrolyte-Nafion membranes for direct methanol fuel cells , Adv. Mater., 18, pp.1068-1072, 2006.

Jesus, M.C., Weiss, R.A., Hahn, S.F., Synthesis of conductive nanocomposites by selective *in situ* polymerization of pyrrole within the lamellar microdomains of a block copolymer, Macromolecules, 31, pp.2230-2235, 1998.

Jia, Z., Zhou, Y., Yan, D., Amphiphilic star-block copolymers based on a hyperbranced core: synthesis and supramolecular self-assembly, J. Polym. Sci., Part A: Polym. Chem., 43, pp.6534-6544, 2005.

Jian, W., Cheung, M.K., Mia, Y., Miscibility in blends of poly(4-vinylpyridine)/poly(4-vinylphenol) as studied by ^{13}C solid-state NMR, Polymer, 42, pp.3087-3093, 2001.

Kanamura, K., Mitsui, T., Munakata, H., Preparation of composite membrane between a uniform porous silica matrix and injected proton conductive Gel Polymer, Chem. Mater., 17, pp.4845-4851, 2005

Kang, M.S., Kim, J.H., Won, J., Moon, S.H., Kang, Y.S., Highly charged proton exchange membranes prepared by using water soluble polymer blends for fuel cells, J. Membr. Sci., 247, pp.127-135, 2005.

Kang, M.S., Choi, Y.J., Moon, S.H., Water-swollen cation-exchange membranes prepared using poly(vinyl alcohol) (PVA)/poly(styrene sulfonic acid-co-maleic acid) (PSSA-MA), J. Membr. Sci., 207, pp.157-170, 2002.

Karlsson, L.E., Jannasch, P., Polysulfone ionomers for proton-conducting fuel cell membranes: sulfoalkylated polysulfones, J. Membr. Sci., 230, pp.61-73, 2004.

Kerres, J., Zhang, W., Jorissen, L., Gogel, V., Application of different types of polyaryl-blend-membranes in DMFC, J. New Mater. Electrochem. Syst., 5, pp.97-107, 2002.

Kerres, J., Ullrich, A., Haring, T., Preidel, W., Baldauf, M., Gebhardt, U., Preparation, characterization and fuel cell application of new acid–base blend membranes, J. New Mater. Electrochem. Syst., 3, pp.229-239, 2000.

Kerres, J.A., Development of ionomer membranes for fuel cells, J. Membr. Sci., 185, pp.3-27, 2001.

Kerres, J.A., Ullrich, A., Meier, F., Haring, T., Synthesis and characterization of novel acid–base polymer blends for application in membrane fuel cells, Solid State Ionics, 125, pp.243-249, 1999.

Kim, Y.M., Park, K.W., Choi, J.H., Park, I.S., Sung, Y.E., A Pd-impregnated nanocomposite Nafion membrane for use in high-concentration methanol fuel in DMFC, Electrochem. Commun., 5, pp.571-574, 2003.

Kim, H.J., Shul, Y.G., Han, H.S. Nafion-Nafion/polyvinylidene fluoride-Nafion laminated polymer membrane for direct methanol fuel cells, J. Power Sources, 135, pp.66-71, 2004.

Kopitzke, R.W., A.Linkous. C., Nelson, G.L., Thermal stability of high temperature polymers and their sulfonated derivatives under inert and saturated vapor conditions, Polym. Degrad. Stab., 67, pp.335-344, 2000.

Kreuer, K.D., Weppner, W., Rabenau, A., Vehicle mechanism; a new model for the interpretation of the conductivity of fast proton conductors, Angew. Chem. Int. Ed. Engl, 21, pp.208–209, 1982.

Kreuer, K.D., Proton conductivity: materials and applications, Chem. Mater., 8, pp.610-641, 1996.

Kreuer, K.D., On the complexity of proton conduction phenomena, Solid State Ionics, 136–137, pp.149-160, 2000.

Kreuer, K.D., On the development of proton conducting polymer membranes for hydrogen and methanol fuel cells, J. Membr. Sci., 185, pp.29-39, 2001.

Kreuer, K.D., On the development of proton conducting materials for technological applications, Solid State Ionics, 97, pp.1-15, 1997.

Lee, P.C., Meisel, D., Luminescence quenching in the cluster network of perfluorosulfonate membrane., J. Am. Chem. Soc., 102, pp.5477-5481, 1980.

Lee, K., Nam, J.H., Lee, J.H., Lee, Y., Cho, S.M., Jung, C.H., Choi, H.G., Chang, Y.Y., Kwon, Y.U., Nam, J.D., Methanol and proton transport control by using layered double hydroxide nanoplatelets for direct methanol fuel cell, Electrochem. Commun., 7, pp.113-118, 2005.

Litt, M., Ameri, R., Wang, Y., Savinell, R., and Wainright, J., Polybenzimidazoles/ phosphoric acid solid polymer electrolytes: mechanical and electical properties, Mater. Res. Soc. Symp. Proc., 548, pp.313, 1999.

Li, L., Zhang, J., Wang, Y., Sulfonated poly(ether ether ketone) membranes for direct methanol fuel cell, J. Membr. Sci., 226, pp.159-167, 2003.

Li, Q., Hjuler, H.A., Bjerrum, N.J., Phosphoric acid doped polybenzimidazole membranes: physiochemical characterization and fuel cell applications, J. Appl. Electrochem., 31, pp.773-779, 2001.

Li, Q., He, R., Jensen, J.O., Bjerrum, N.J., Approaches and recent development of polymer electrolyte membranes for fuel cells operating above 100 ^{o}C, Chem. Mater., 15, pp.4896-4915, 2003.

Lichtenhan, J.D., Vu, N.Q., Carter, J.A., Gilman, J.W., Feher, F.J., Silsesquioxane-siloxane copolymers from polyhedral silsesquioxanes, Macromolecules, 26, pp.2141-2142, 1993.

Lichtenhan, J.D., Otonari, Y.A., Carr, M.J., Linear hybrid polymer building blocks: methacrylate-functionalized polyhedral oligomeric silsesquixane monomers and polymers, Macromolecules, 28, pp.8435-8437, 1995.

Liu, W., Ruth, K., Rusch, G., Membrane durability in PEM fuel cells, J. New Mater. Electrochem. Syst., 4, pp.227-231, 2001.

Liu, T.Q., Jia, S.J., Kowalewski, T., Matyjaszewski, K., Casado-Portilla, R., Belmont, J., Grafting poly(n-butyl acrylate) from a functionalized carbon black surface by atom transfer radical polymerization, Langmuir, 19, pp.6342-6345, 2003.

Ma, Y.L., Wainright, J.S., Litt, M., Savinella, R.F., Conductivity of PBI membranes for high-temperature polymer electrolyte fuel cells, J. Electrochem. Soc., 151, pp.A8-A16, 2004.

Maki-Ontto, R., Moel, K., Polushkin, E., Ekenstein, G.A., Brinke, G., Ikkala, O., tridirectional protonic conductivity in soft materials, Adv. Mater., 14, pp.357-361, 2002.

Malhotra, S., Datta, R., Membrane-supported nonvolatile acidic electrolytes allow higher temperature operation of proton-exchange membrane fuel cells, J. Electrochem. Soc., 144 pp.L23-L26, 1997.

Mantz, R.A., Jones, P.F., Chaffee, K.P., Lichtenhan, J.D., Gilman, J.W., Ismail, I.M.K., Burmeister, M.J., Thermolysis of polyheral oligomeric silsesquioxane (POSS) macromers and POSS-siloxane copolymer, Chem. Mater., 8, pp.1250-1259, 1996.

Marcolli, C., Calzaferri, G., Monosubstituted octasilasesquioxanes, Appl. Organomet. Chem., 13, pp.213-226, 1999.

Masanori, Y., Itaru, H., Anhydrous protonic conductivity of a self-assembled acid-base composite material J. Phys. Chem .B, 108, pp.5522-5526, 2004.

Mauritz, K.A., Moore, R.B., State of understanding of Nafion, Chem. Rev., 104, pp.4535-4585, 2004.

Mehta, V., Cooper, J.S., Review and analysis of PEM fuel cell design and manufacturing, J. Power Sources, 114, pp.32-53, 2003.

Misha, R., Tripathy, S.P., Sinha, D., Dwivedi, K.K., Ghosh, S., Khating, D.T., Muller, M., Fink, D., Chung, W.H., Optical and electrical properties of some electron and proton irradiated polymers, Nucl. Instrum. Methods Phys. Res. Sect. B, 168, pp.59-64, 2000.

Miyake, N., Wainright, J.S., Savinell, R.F., , Evaluation of a sol-gel derived Nafion/ Silica Hybrid Membrane for Polymer Electrolyte Membrane Fuel Cell Applications, J. Electrochem. Soc., 148, pp.A905-A909, 2001.

Mori, H., Seng, D.C., Zhang, M.F., Muller, A.H.E., Hybrid nanoparticles with hyperbranched polymer shells via self-condensing atom transfer radical polymerization from silica surfaces, Langmuir, 18, pp.3682-3693, 2002.

Munch, W., Kreuer, K.D., Silvestri, W., Maier, J., Seifert, G., The diffusion mechanism of an excess proton in imidazole molecule chains: first results of an ab initio molecular dynamics study, Solid State Ionics, 145, pp.437-443, 2001.

Nishimura, H., Yamaguchi, T., Performance of a pore-filling electrolyte membrane in hydrogen-oxygen PEFC, Electrochem. Solid State Lett., 7, pp.A385-A388, 2004.

Noshay, A., Robenson, L.M., Sulfonated polysulfone, J. Appl. Polym. Sci., 20, pp.1885-1903, 1976.

O'Hayre, R., Cha, S-W., Colella, W., Prinz, F.B., Fuel cell fundamentals, John Wiley & Sons, New York, 2006.

Pallandre A., Lambert B., Attia R., Jonas A.M., Viovy J.L., Surface treatment and characterization: Perspectives to electrophoresis and lab-on-chips, Electrophoresis, 27, pp. 584-610, 2006.

Pantoustier N., Moins S., Wautier M., Degee P., Dubois P., Solvent-free synthesis and purification of poly[2-(dimethylamino)ethyl methacrylate] by atom transfer radical polymerization, Chem. Commun., pp.340-341, 2003.

Park, H., Kim, Y., Hong, W.H., Choi, Y.S., Lee, H., Influence of morphology on the transport properties of perfluorosulfonate ionmers/polypyrrole composite membrane, Macromolecules, 38, pp.2289-2295, 2005.

Padeste C. , Farquet P., Potzner C., Solak H.H. , Nanostructured bio-functional polymer brushes, J. Biomater. Sci., Polym. Ed., 17, pp.1285-1300, 2006.

Peled, E., Duvdevani, T., Aharon, A., Melman, A., A direct methanol fuel cell based on a novel low-cost nanoporous proton-conducting membrane, Electrochem. Solid State Lett., 3, pp.525-528, 2000.

Peneri, M., Eisenberg, A., Structure and properties of ionomers, NATO ASI Series 198, Reidel Publishing Co., Dordrecht, The Netherlands, 1987.

Penner, R.M., Martin, C.R., Ion transporting composite membranes, J. Electrochem. Soc., 132, pp.514-515, 1985.

Percy M.J., Michailidou V., Armes S.P., Synthesis of vinyl polymer-silica colloidal nanocomposites via aqueous dispersion polymerization, Langmuir, 19, pp.2072-2079, 2003.

Pietrogrande, P., Bezzecheri, M., Fuel cell systems, Plenum Press, New York, pp.121, 1993.

Pimbert, S., Avignon-Poquillon, L., Levesque, G., Calorimetric study of fluorinated methacrylic and vinyl polymer blends: part 2: correlation between miscibility, chemical structure and χ_{12} interaction parameter in binary systems, Polymer, 43, pp.3295-3302, 2002.

Pourcelly, G., Oikonomous, A., Gavach, C., Hurwitz, H. D., Influence of the water content on the kinetics of counter-ion transport in perfluorosulphonic membranes, J. Electroanal. Chem., 287, pp.43-59, 1990.

Pu, C., Huang, W., Ley, K.L., Smotkin, E.S., A methanol impermeable proton conducting composite electrolyte system, J. Electrochem. Soc., 142, pp.119-120, 1995.

Pu, H., Meyer, W.H., Wegner, G., Proton conductivity in acid-blended poly(4-vinylimidazole), Macromol. Chem. Phys., 202, pp.1478-1482, 2001.

Pu, H., Studies on polybenzimidazole/poly (4-vinylpyridine) blends and their proton conductivity after doping with acid, Polym Int., 52, pp.1540-1545, 2003.

Pyun J., Jia S.J., Kowalewski T., Patterson G.D., Matyjaszewski K., Sythesis and characterization of organic/ inorganic hybrid nanoparticles: kinetic of surface- initiated atom transfer radical polymerization and morphology of hybrid nanoparticle ultrathin films, Macromolecules, 36, pp.5094-5104, 2003.

Qiao, J., Hamaya, T., Okada, T., New highly proton-conducting membrane poly(vinylpyrrolidone)(PVP) modified poly(vinyl alcohol)/2-acrylamido-2-methyl-1-propanesulfonic acid (PVA–PAMPS) for low temperature direct methanol fuel cells (DMFCs), Polymer, 46, pp.10809-10816, 2005a.

Qiao, J., Hamaya, T., Okada, T., Chemically modified poly(vinyl alcohol)-poly(2-acrylamido-2-methyl-1-propanesulfonic acid) as a novel proton-conducting fuel cell membrane, Chem. Mater., 17, pp.2413-2421, 2005b.

Ramani, V., Kunz, H.R., Fenton, J.M., Investigation of Nafion®/HPA composite membranes for high temperature/low relative humidity PEMFC operation, J. Membr. Sci., 232, pp.31-44, 2004.

Ratner, M.A., in: Polymer Electrolyte Review, Mac-Callum, J.R., Vincent, C.A., Eds., Elsevier Applied Science press, New York, pp.173, 1987.

Ravikumar, M.K., Shukla, A.K., Effect of methanol crossover in a liquid-feed polymer-electrolyte direct methanol fuel cell, J. Electrochem. Soc., 143, pp.2601-2606, 1996.

Ren, X., Wilson, M.S., Gottesfeld, S., High performance direct methanol polymer electrolyte fuel cells, J. Electrochem. Soc., 143, pp.L12-L15, 1996.

Ren, X., Springer, T.E., Gottesfeld, S., Water and Methanol Uptakes in Nafion Membranes and Membrane Effects on Direct Methanol Cell Performance, J. Electrochem. Soc., 147, pp.92-98, 2000a.

Ren, X., Springer, T.E., Zawodzinski, T.A., Gottesfeld, S., Methanol transport through Nafion membranes electro-osmotic drag effects on potential step measurements, J. Electrochem. Soc., 147, pp.466-474, 2000b.

Rhee, C.H., Kim, Y., Lee, J.S., Kim, H.K., Chang, H., Nanocoposite membranes of surface-sulfonated titanate and Nafion® for direct methanol fuel cells, J. Power Sources, 159, pp.1015-1024, 2006.

Rhim, J.W., Park, H.B., Lee, C.S., Jun, J.H., Kim, D.S.. Lee, Y.M., Crosslinked poly(vinyl alcohol) membranes containing sulfonic acid group: proton and methanol transport through membranes, J. Membr. Sci., 238, pp.143-151, 2004.

Rodgers, M.P., Berring, J., Holdcroft, S., Shi, Z., The effect of spatial confinement of Nafion® in porous membranes on macroscopic properties of the membrane, J. Membr. Sci., 321, pp.100-113, 2008.

Rodriguez, D., Jegat, C., Trinquet, O., Grondin, J., Lassegues, J.C., Proton conduction in poly(acrylamide)-acid blends, Solid State Ionics, 61, pp.195-202, 1993.

Romero, P.G., Asensio, J.A., Borros, S., Hybrid proton-conducting membranes for polymer electrolyte fuel cells phosphomolybdic acid doped ploy (2, 5-benzimidazole)-(ABPBI-$H_3PMo_{12}O_{40}$), Electrochim. Acta, 50, pp.4715-4720, 2005.

Rong, M.Z., Zhang, M.Q., Zheng, Y.X., Zeng, H.M., Walter, R., Friedrich, K., Structure–property relationships of irradiation grafted nano-inorganic particle filled polypropylene composites, Polymer, 42, pp.167-183, 2001.

Roziere, J., Jones, D.J., Marrony, M., Glipa, X., Mula, B., On the doping of sulfonated polybenzimidazole with strong bases, Solid State Ionics, 145, pp.61-68, 2001.

Saarinen, V., Kallio, T., Paronen, M., Tikkanen, P., Rauhala, E., Kontturi, K., New ETFE-based membrane for direct methanol fuel cell, Electrochim. Acta, 50, pp.3453-2460, 2005.

Sacca, A., Carbone, A., Passalacqua, E., Epifanio, A.D., Licoccia, S., Traversa, E., Sala, E., Traini, F., Ornelas, R., Nafion-TiO_2 hybrid membranes for medium temperature polymer electrolye fuel cells (PEFCs), J. Power Sources, 152, pp.16-21, 2005.

Samms, S.R., Wasmus, S., Savinell, R.F. Thermal stability of Nafion® in simulated fuel cell environments, J. Electrochem. Soc., 143, pp.1498-1504, 1996.

Savinell, R., Yeager, E., Tryk, D., Landau, U., Wainright, J., Weng, D., Lux, K., Litt, M., Rogers, C., A polymer electrolyte for operation at temperature up to 200 ^oC, J. Electrochem. Soc., 141, pp.L46-L48, 1994.

Scott, K., Taama, W.M., Argyropoulos, P., Sundmacher, K., The impact of mass transport and methanol crossover on the direct methanol fuel cell, J. Power Sources, 83, pp.204-216, 1999.

Shao, Z.G., Wang, X., Hsing, I.M., Composite Nafion/polyvinyl alcohol membranes for the direct methanol fuel cell, J. Membrane Sci., 210, pp.147-153, 2002.

Shao, Z.G., Joghee, P., Hsing, I.M., Preparation and characterization of hybrid Nafion-silica membrane doped with phosphotungstic acid from high temperature operation of proton exchange membrane fuel cells, J. Membr. Sci., 229, pp.43-51, 2004.

Shen, M., Roy, S., Kuhlmann, J.W., Scott, K., Lovell, K., Horsfall, J.A., Grafted polymer electrolyte membrane for direct methanol fuel cells, J. Membr. Sci., 251, pp.121-130, 2005.

Shunmugam, R., Tew, G.N., Efficient route to well- characterized homo, block, and statistical polymers containing terpyridine in the side chain, J. Polym. Sci., Part A: Polym. Chem., 43, pp.5831-5843, 2005.

Si, Y., Lin, J.C., Kunz, H.R., Fenton, J.M., Trilayer membranes with a methanol-barrier layer for DMFCs, J. Electrochem. Soc., 151, pp.A463-A469, 2004.

Smitha, B., Sridhar, S., Khan, A.A., Sythesis and characterization of proton conducting polymer membranes for fuel cells, J. Membr. Sci., 225, pp.63-76, 2003.

Sone, Y., Ekdunge, P., Simonsson, D., Proton conductivily of Nafion 117 as measured by a four-electrode AC impedance method, J. Electrochem. Soc., 143, pp.1254-1259, 1996.

Staiti, P., Minutoli, M., Hocevar, S., Membranes based on phosphotungstic acid and polybenzimidazole for fuel cell application, J. Power Sources, 90, pp.231-235, 2000.

Staiti, P., Lufrano, F., Arico, A.S., Passalacqua, E., Antonucci, V., Sulfonated polybenzimidazole membranes: preparation and physico-chemical characterization, J. Membr. Sci., 188, pp.71-78, 2001a.

Staiti, P., Arico, A.S., Baglio, V., Lufrano, F., Passalacqua, E., Antonucci, V., Hybrid Nafion-silica membranes doped with heteropolyacids for application in direct methanol fuel cells, Solid State Ionics, 145, pp.101-107, 2001b.

Surampudi, S., Narayanan, S.R., Vamos, E., Frank, H., Halpert, G., Laconti, A., Kosek, J.,. Prakash, G.K.S., Olah, G.A., Advances in direct oxidation methanol fuel cells, J. Power Sources, 47, pp.377-385, 1994.

Tang, H., Pan, M., Jiang, S., Wan, Z., Yuan, R., Self-assembling multi-layer Pd nanoparticles onto Nafion™ membrane to reduce methanol crossover, Colloids Surfs., A: Physicochem. Eng. Aspects, 262, pp.65-70, 2005.

Tricoli, V., Carretta, N., Bartolozzi, M., Comparative investigation of proton and methanol transport in fluorinated ionomeric membranes, J. Electrochem. Soc., 147, pp.1286-1290, 2000.

Tuckerman, M.E., Marx, D., Klein, M.L., Parrinello, M., On the quantum nature of the shared proton in hydrogen bonds, Science, 275, pp.817-820, 1997.

Vestal, C.R., Zhang, Z.J., Atom transfer radical polymerization synthesis and magnetic characterization of $MnFe_2O_4$/polystyrene core/shell nanoparticles, J. Am. Chem. Soc., 124, pp.14312-14313, 2002.

Wainright, J.S., Litt, M., Savinell, R.F., High temperature membranes, in: Fuel Cell Handbook, 2003.

Wainright, J.S., Wang, J.T., Weng, D., Savinell, R.F., Litt, M., Acid-doped polybenzimidazoles: a new polymer electrolyte, J. Electrochem. Soc., 142, pp.L121-L123, 1995.

Walls, H.J., Riley, M.W., Fedkiw, P.S., Spontak, R.J., Baker, G.L., Khan, S.A., Composite electrolytes from self-assembled colloidal networks, Electrochim. Acta, 48, pp.2071-2077, 2003.

Wang, D., Wainright, J.S., Landau, I., Savinell, R.F., Electro-osmotic drag coefficient of water and methanol in polymer electrolytes at elevated temperatures, J. Electrochem. Soc., 143, pp.1260-1263, 1996.

Wang, F., Hickner, M., Ji, Q., Harrison, W., Mecham, J., Zawodzinski, T.A., McGrath, J.E., Synthesis of highly sulfonated poly(arylene ether sulfone) random (statistical) copolymer via direct polymerization, Macromol. Symp., 175, pp.387-396, 2001.

Wang, F., Hickner, M., Kim, Y.S., Zawodzinski, T.A., McGrath, J.E., Direct polymerization of sulfonated poly(arylene ether sulfone) random (statistical) copolymers: candidates for new proton exchange membranes, J. Membr. Sci., 197, pp.231-242, 2002.

Wang, J., Wasmus, S., Savinell, R.F., Evalution of ethanol, 1-propanol, and 2-propanol in a direct oxidation polymer- electrolyte fuel cell, J. Electrochem. Soc., 142, pp.4218-4224, 1995.

Wang, T.L., Liu, Y.Z., Jeng, B.C., Cai, Y.C., The effect of initiators and reaction condictions on the polymer syntheses by atom transfer radical polymerization, J. Polym. Res., 12, pp.76-75, 2005.

Wasmus, S., Kuver, A., Methanol oxidation and direct methanol fuel cells: a selective review, J. Electroanal. Chem., 461, pp.14-31, 1999.

Werne, T., Patten, T.E., Preparation of structurally well-defined polymer-nanoparticle hybrids with controlled/ living radical polymerizations, J. Am. Chem. Soc., 121, pp.7409-7410, 1999.

Werne, T., Patten, T.E., Preparation of structurally well-defined polymer-nanoparticle hybrids with controlled/ living radical polymerizations, J. Am. Chem. Soc., 121, pp.409-7410, 1999.

Wilson, M.S., Busick , D.N., Composite bipolar plate for electrochemical cells, US Patent 6248467, 2001.

Won, J., Park, H.H., Kim, Y.J., Choi, S.W., Ha, H.Y., Oh, I.H., Kim, H.S., Kang, Y.S., Ihn, K.J., Fixation of nanosized proton transport channels in membrane, Macromolecules, 36, pp.3228-3234, 2003.

Woo, Y., Oh, S.Y., Kang, Y.S, Jung, B., Synthesis and characterization of sulfonated polyimide membranes for direct methanol fuel cell, J. Membr. Sci., 220, pp.31–45, 2003.

Wright, M.E., Schorzman, D.A., Feher, F.J., Jin, R.Z., Synthesis and thermal curing of aryl-ethynyl-terminated coPOSS imide oligomers: new inorganic/organic hybrid resins, Chem. Mater., 15, pp.264-268, 2003.

Wu, H., Wang, Y., Wang, S., A methanol barrier polymer electrolyte membrane in direct methanol fuel cells, J. New Mater. Electrochem. Sys., 5, pp.251-254, 2002.

Wycisk, R., Lee, J.K., Pintauro, P.N., Sulfonated polyphosphazene-polybenzimidazole membranes for DMFCs, J. Electrochem. Soc., 152, pp.A892-A898, 2005,

Xiao, L., Zhang, H., Scanlon, E., Ramanathan, L.S., Choe, E-W., Rogers, D., Apple, T., Benicewicz, B.C., High-temperature polybenzimidazole fuel cell membranes via a sol-gel process, Chem. Mater., 17, pp.5328-5333, 2005a.

Xiao, L., Zhang, H., Scanlon. E., Chen, R., Choe, E-W., Ramanathan, L.S., Yu, S., Benicewicz, B.C., Synthesis and characterization of pyridine-based polybenzimidazoles for high temperature polymer electrolyte membrane fuel cell applications, Fuel Cells, 5, pp.288-295, 2005b.

Xing, P., Robertson, G.P., Guiver, M.D., Mikhailenko, S.D., Wang, K., Kaliaguine, S., Synthesis and characterization of sulfonated poly(ether ether ketone) for proton exchange membranes, J. Membr. Sci., 229, pp.95-106, 2004.

Xu, W., Liu, C., Xue, X., Su, Y., Lv, Y., Xing, W., Lu, T., New proton exchange membranes based on poly(vinyl alcohol) for DMFCs, Solid State Ionics, 171, pp.121-127, 2004.

Xu, W., Lu, T., Liu, C., Xing, W., Low methanol permeable composite Nafion/silica/PWA membranes for low temperature direct methanol fuel cells, Electrochim. Acta, 50, pp.3280-3285, 2005.

Xu, C., Wu, T., Mei, Y., Drain, C.M., Batteas, J.D., Beers, K.L., Sythesis and characterization of tapered copolymer brushes via surface-initiated atom transfer radical copolymerization, Langmuir, 21, pp.11136-11140, 2005.

Yamada. M., Honma. I., Anhydrous protonic conductivity of a self-assembled acidbase composite material, J. Phys. Chem. B., 108, pp.5522-5526, 2004.

Yamaguchi, T., Miyata, F., Nakao, S., Polymer electrolyte membranes with a pore-filling structure for a direct methanol fuel cell, Adv. Mater., 15, pp.1198-1201, 2003a.

Yamaguchi, T., Miyata, F., Nakao, S, Pore-filling type polymer electrolyte membranes for a direct methanol fuel cell, J. Membr. Sci., 214, pp.283-292, 2003b.

Yamaguchi, T., Ibe, M., Nair, B.N., Nakao, S., A pore-filling electrolyte membrane-electrode integrated system for a direct methanol fuel cell application, J. Electrochem. Soc., 149, pp.A1448-A1453, 2002.

Yang, C., Costamagna, P., Srinivasan, S., Benziger, J., Bocarsly, A.B., Approaches and technical challenges to high temperature operation of proton exchange fuel cells, J. Power Sources, 103, pp.1-9, 2001.

Yang. B., Manthiram. A., Multilayered membranes with suppressed fuel crossover for direct methanol fuel cells, Electrochem. Commun., 6, pp.231-236, 2004.

Ye, G., Hayden, C.A., Goward, G.R., Proton dynamics of Nafion and Nafion/SiO_2 composites by solid state NMR and pulse field gradient NMR, Macromolecules, 40, pp.1529-1537, 2007.

Yin, Y., Fang, J., Cui, Y., Tanaka, K., Kita, H., Okamoto, K., Synthesis, proton conductivity and methanol permeability of a novel sulfonated polyimide from 3-(2′,4′-diaminophenoxy)propane sulfonic acid, Polymer, 44, pp.4509-4518, 2003.

Young, S.K., Mauritz, K.A., Nafion®/[organically-modified silicate]nanocomposites via polymer-*in situ* sol-gel reactions: mechanical tensile properties, J. Polym. Sci., Part B: Polym. Phys., 40, pp.2237-2247, 2002.

Yoshida, H., Kishimoto, N., Kataoko, T., Adsorption of strong acid on polyaminated highly porous chitosan –equilibria, Ind. & Eng. Chem. Res., 33, pp.854-859. 1994.

Zhang, X., Hong, L., Liu, Z., Proton-sweeping role of oligomeric electrolyte chains grown on silica nanospheres, Mater. Res. Soc. Symp. Proc., 923, 0923-V05-08.

Zhai. Y., Zhang. H., Hu. J., Yi. B., Preparation and characterization of sulfated zirconia (SO_4^{2-}/ZrO_2)/Nafion composite membranes for PEMFC operation at high temperature/low humidity, J. Membr. Sci., 280, pp.148-155, 2006.

Zhao, Y., Schiraldi, D.A., Thermal and mechanical properties of polyhedral oligomeric silsesquioxane (POSS)/polycarbonate composites, Polymer, 46, pp.11640-11647, 2005.

LIST OF PUBLICATIONS

1. Zhang, X., Hong, L., Liu, Z., Proton-sweeping role of oligomeric electrolyte chains grown on silica nanospheres, Mater. Res. Soc. Symp. Proc. Vol. 923, 0923-V05-08.
2. Zhang, X, Hong, L., Liu, Z., Interfacial behaviors of densely anchored hydrophilic oligomeric chains on silica microspheres, Colloid. Polym. Sci., in press.
3. Zhang, X, Hong, L., Liu, Z., Restructuring proton conducting channels by embedding starburst POSS-g-acrylonitrile oligomer in Nafion® membrane, Submitted to J. Membr. Sci..
4. Tay, S.W., Zhang, X, Hong, L., Liu, Z., Chan, S.H., Composite Nafion® membrane embedded with hybrid nanofillers for promoting direct methanol fuel cell performance, J. Membr. Sci., 321, pp.139-145, 2008.
5. Zhang, X, Tay, S.W., Hong, L., Liu, Z., Chan, S.H., Reformating Nafion® matrix via *in-situ* generated polyPOSS blocks to promote its performance in direct methanol fuel cell, Submitted to J. Membr. Sci., 320, pp.310-318, 2008.